



HAL
open science

Ciliogenesis Control Mechanisms in Cerebellar Neuron Progenitors

Marco Zanini

► **To cite this version:**

Marco Zanini. Ciliogenesis Control Mechanisms in Cerebellar Neuron Progenitors. Subcellular Processes [q-bio.SC]. Université Paris-Saclay, 2019. English. NNT : 2019SACLS475 . tel-02410263

HAL Id: tel-02410263

<https://theses.hal.science/tel-02410263>

Submitted on 13 Dec 2019

HAL is a multi-disciplinary open access archive for the deposit and dissemination of scientific research documents, whether they are published or not. The documents may come from teaching and research institutions in France or abroad, or from public or private research centers.

L'archive ouverte pluridisciplinaire **HAL**, est destinée au dépôt et à la diffusion de documents scientifiques de niveau recherche, publiés ou non, émanant des établissements d'enseignement et de recherche français ou étrangers, des laboratoires publics ou privés.

Ciliogenesis control mechanisms in cerebellar neuron progenitors

Thèse de doctorat de l'Université Paris-Saclay
préparée à l'Université Paris Sud

École doctorale n°582 *Cancérologie : biologie, médecine, santé*
Spécialité de doctorat : Aspects moléculaires et cellulaires de la biologie

Thèse présentée et soutenue à Orsay, le 5 Décembre 2019, par

Marco Zanini

Composition du Jury :

Simon Saule PR1, Institut Curie, Orsay (CNRS UMR3347, Inserm U1021)	Président
Julie Gavard DR2, Centre de Recherche en Cancérologie et Immunologie Nantes – Angers, Nantes (CNRS UMR6299, Inserm U892)	Rapporteur
Frédéric Charron Associate Professor, Department of Medicine, Institut de Recherches Cliniques de Montréal, Montréal	Rapporteur
Lucia Di Marcotullio PR, Department of Molecular Medicine, Rome	Examinatrice
Olivier Ayrault DR2, Institut Curie, Orsay (CNRS UMR3347, Inserm U1021)	Directeur de thèse

Acknowledgements

The first person I wish to acknowledge is my chief and PhD supervisor, Olivier. I wish to thank him for having hired me as a Master intern more than four years ago and for having renewed his trust one year later, when I became a PhD student. I am immensely grateful for his mentoring and teaching activities, which enabled me to learn a lot about different aspects of science, not only the technical-related ones. I am thankful because he has always granted me with trust, liberty and independence, hence allowing me to explore my strengths, but also my weaknesses. Many thanks also for having been patient, when for various personal reasons I was perhaps not performing well at work.

I am very grateful to Dr. Julie Gavard and Dr. Frédéric Charron for having accepted to be members of my PhD defense jury and review my manuscript. I am also really thankful to Pr. Lucia Di Marcotullio and Pr. Simon Saule for being part of my PhD committee.

I would like also to express my gratitude to Chia-Hsiang Chang and Pr. Jin-Wu Tsai for their great work and for the successful collaboration we set up and carried on together in the context of this project.

An enormous thanks goes to all the people of the lab, past and present members, who were directly involved in this study: Hamasseh Shirvani for having started and managed the project before my arrival; Hua Yu, for having trained me during my Master and for having being extremely kind and willing to help me in every situation, not only at work. Audrey Mercier, for her continuous support and for having been always available to hear me and advise me, whatever it was the matter, science or personal life; Antoine Forget, because even though he has never directly supervised me, he was a milestone for me in the lab and I learnt a lot from him; Sara Maria Cigna for her help and tips during my Master.

A big thanks also to the people of the technical support staff of the Institute Curie in Orsay: Claire Lovo for her great help with microscopy, Sophie Leboucher for her always punctual

work on the tissue IHC, Charlène Lasgi for the assistance with the FACS, and the whole team of the animal facilities, in particular Christophe Alberti, Elodie Belloir and Adlin Thadal.

I wish also to thank a lot other present members of the lab for their support throughout various phases of my PhD: Julie Talbot, for her extreme kindness and for having (maybe without even realizing it) pushed me to start to speak French; Emilie Indersie for all her advice and the amusing time spent all together in the lab; Gabriele Cancila for his enthusiasm that in part contributed to relight my passion for research in the last months.

Even without being involved the project, some can be equally (if not more) important for its success, just by providing love and support to who is in charge of managing it.

I am immensely grateful to my friend Benedetta, for all the company and the moral help she has always given me in any circumstances along these last four years. She was always there when I needed to stay or talk with someone, and I thank her a lot for this.

An enormous *dzięki* goes to Maria for having been so patient in the last months, when I could not be as present as both of us wished. Thank you for having always stayed on my side, provided massive support and love, shared good and bad moments and always understood my needs.

I am also very grateful to Flavia, who was actually a colleague of mine at the time of the project, but I prefer to thank her here, in this section, because the firm friendship we developed is now a stronghold on which I can always count. Thank you for everything.

Similarly, I wish to thank Ludovica, as I really enjoyed the evenings spent all together in Paris this year.

A great thanks then goes to all the big group of Italian friends in Paris for the great moments shared together in these years and for making me feeling home also here, abroad.

Un grand merci également à Romain, Grégoire et Kanok du labo Ghysdael pour les bons moments passés ensemble.

Thanks to all the people of the Domain 1 for the good and relaxing time spent during the Happy Fridays and the ReSiPis.

E infine, anche se dovrei metterli per primi, il più grosso ringraziamento tra tutti va alla mia famiglia, in particolare ai miei genitori perché nella buona e nella cattiva sorte, loro ci sono sempre stati e hanno rappresentato un punto fermo su cui fare stabile affidamento per qualunque cosa.

Table of Contents

ACKNOWLEDGEMENTS	3
TABLE OF CONTENTS	5
ABBREVIATIONS.....	9
TABLE OF FIGURES.....	15
INTRODUCTION	17
I.1 THE CEREBELLUM	19
<i>I.1.1 ANATOMY OF THE CEREBELLUM.....</i>	19
<i>I.1.2 MAIN FUNCTIONS OF THE CEREBELLUM.....</i>	21
I.1.2.1 Functional compartmentalization of the cerebellum.....	21
<i>I.1.3 MICROANATOMY OF THE CEREBELLAR CORTEX.....</i>	23
I.1.3.1 Cells of the cerebellar cortex	23
I.1.3.2 Major cerebellar circuits.....	24
I.2 DEVELOPMENT OF GRANULE NEURONS	27
<i>I.2.1 EARLY SPECIFICATION AND PATTERNING OF THE CEREBELLUM</i>	27
I.2.1.1 Regionalization of the neural tube	27
I.2.1.2 Specification of cerebellar territories in rhombomere 1	29
<i>I.2.2 EARLY HISTOGENESIS IN THE CEREBELLAR ANLAGE.....</i>	30
I.2.2.1 Temporal origin of uRL derivatives.....	32
<i>I.2.3 GNPs: TANGENTIAL MIGRATION FROM THE uRL TO THE EGL</i>	34
<i>I.2.4 GNPs: FROM PROLIFERATION TO TERMINAL DIFFERENTIATION.....</i>	36
I.2.4.1 Brief overview of the whole process	36
I.2.4.2 Proliferation and differentiation of GNPs at the histological level.....	36
I.2.4.3 Discovery of SHH as the main mitogen for GNPs.....	38
I.2.4.4 SHH boosts GNPs expansion by acting on the cell cycle machinery	39
I.2.4.4 Synergy and interplay with SHH during GNPs expansion	40
I.2.4.4.1 SDF-1α	40
I.2.4.4.2 Igf-II	41
I.2.4.4.3 Heparan sulfate proteoglycans.....	42
I.2.4.4.4 Laminin-integrin signaling	42
I.2.4.4.5 Notch2-Hes1 signaling	43
I.2.4.5 Mechanisms controlling cell cycle exit and differentiation of GNPs	44
I.2.4.5.1 Non canonical Wnt3 signaling.....	45
I.2.4.5.2 BMP2 and BMP4 signaling.....	45

1.2.4.5.3 <i>Mycn</i> protein degradation at mitosis	45
1.2.4.5.4 Ubiquitin ligases.....	46
1.2.4.5.5 Vitronectin	47
1.2.4.6 Tangential migration and onset of parallel fibers formation	47
1.2.4.7 Terminal radial migration toward the IGL.....	48
1.3 MEDULLOBLASTOMA.....	51
1.3.1 EPIDEMIOLOGY OF MEDULLOBLASTOMA	51
1.3.1.1 Risk factors associated to medulloblastoma	52
1.3.2 CLINICOPATHOLOGICAL FEATURES OF MEDULLOBLASTOMA.....	53
1.3.2.1 Histological characteristics	53
1.3.2.2 Metastases and recurrence of medulloblastoma	54
1.3.3 MOLECULAR CLASSIFICATION OF MEDULLOBLASTOMA	55
1.3.3.1 WNT-medulloblastoma	57
1.3.3.2 Group3-medulloblastoma	58
1.3.3.3 Group4-medulloblastoma	59
1.3.3.4 SHH-medulloblastoma	60
1.3.3.4.1 <i>SHH</i> -medulloblastoma intertumoral heterogeneity	61
1.3.3.4.2 Mouse models of <i>SHH</i> -medulloblastoma	63
1.3.3.4.3 Discovery of GNP as the cell-of-origin of <i>SHH</i> -MB	64
1.3.4 STANDARD OF CARE, LIMITATIONS AND FUTURE DIRECTIONS	65
1.3.4.1 Targeted therapies in <i>SHH</i> -Medulloblastoma	67
1.4 THE PRIMARY CILIUM.....	69
1.4.1 DIFFERENT TYPES OF CILIA EXIST IN NATURE.....	69
1.4.2 STRUCTURE OF CILIA.....	70
1.4.2.1 The ciliary shaft	70
1.4.2.2 The basal body	72
1.4.2.3 The transition zone.....	73
1.4.2.4 The ciliary pocket and the periciliary membrane	74
1.4.3 TRAFFICKING OF CILIARY PROTEINS	74
1.4.3.1 The intraflagellar transport.....	76
1.4.3.1.1 <i>IFT</i> motors	76
1.4.3.1.2 <i>IFT</i> particles	77
1.4.3.1.3 The <i>BB</i> some.....	78
1.4.3.2 Ciliary import, transport and export of <i>IFT</i> cargoes	79
1.4.3.2.1 Transport of ciliary membrane proteins	80
1.4.4 CILIOGENESIS IS ENTANGLED TO CELL CYCLE PROGRESSION	81
1.4.4.1 Biogenesis of primary cilia	82
1.4.4.2 Disassembly of primary cilia	83
1.4.5 PRIMARY CILIA ARE SIGNALING CENTERS IN VERTEBRATES.....	84
1.4.5.1 Overview of the Hedgehog signaling.....	85
1.4.5.2 Major components of the Hedgehog signaling	86
1.4.5.2.1 Hedgehog proteins.....	86
1.4.5.2.2 <i>Patched</i> is the <i>HH</i> receptor	88
1.4.5.2.3 <i>Smoothed</i> is repressed by <i>Patched</i>	88
1.4.5.2.4 The <i>Gli</i> transcription factors	90
1.4.5.3 Mechanisms of vertebrate <i>HH</i> signaling through the primary cilium	92

1.4.5.3.1 <i>HH pathway OFF</i>	92
1.4.5.3.2 <i>HH pathway ON</i>	94
1.4.5.4 Roles of primary cilia in normal GNs development	96
1.4.5.5 Roles of primary cilia in SHH-MB tumorigenesis	97
1.5 CENTRIOLAR SATELLITES	99
<i>1.5.1 COMPOSITION OF CENTRIOLAR SATELLITES</i>	99
1.5.1.1 Pericentriolar material 1 is the major component of CS	99
1.5.1.2 CS are mainly composed by centrosomal proteins	100
<i>1.5.2 CENTRIOLAR SATELLITES INTEGRITY AND LOCALIZATION</i>	101
1.5.2.1 The trafficking of CS depends on microtubules	102
1.5.2.2 CS integrity and localization depends on many integral components	102
1.5.2.3 Post-translational modifications contribute at shaping CS	103
1.5.2.4 Cell cycle dependent regulation of CS localization and integrity	104
<i>1.5.3 FUNCTIONS OF CENTRIOLAR SATELLITES</i>	105
1.5.3.1 CS are required for numerous centrosome functions	105
1.5.3.2 CS are regulators of ciliogenesis	106
1.6 ATOH1	111
<i>1.6.1 ROLES OF bHLH TRANSCRIPTION FACTORS IN NEUROGENESIS</i>	111
<i>1.6.2 STRUCTURE AND EXPRESSION OF ATOH1</i>	113
1.6.2.1 Structure of Atonal/Atoh1 proteins	113
1.6.2.2 Atoh1 is expressed in many tissues, besides the cerebellum	114
1.6.2.2.1 <i>Atoh1 in the hindbrain</i>	114
1.6.2.2.2 <i>Atoh1 in the dorsal neural tube</i>	115
1.6.2.2.3 <i>Atoh1 in the inner ear</i>	115
1.6.2.2.5 <i>Atoh1 in the intestine</i>	116
1.6.2.2.6 <i>Atoh1 in Merkel cells</i>	116
1.6.2.2.7 <i>Concluding remarks</i>	117
1.6.2.3 Atoh1 expression is highly regulated in the GN lineage	117
1.6.2.3.1 <i>Transcriptional control of Atoh1 gene in the cerebellum</i>	117
1.6.2.3.2 <i>Post-translational control of Atoh1 protein expression in the cerebellum</i>	120
<i>1.6.3 FUNCTIONS OF ATOH1 IN THE GRANULE NEURON LINEAGE</i>	121
1.6.3.1 Functions of Atoh1 during normal GNs development	121
1.6.3.2 Functions of Atoh1 during SHH-MB formation and expansion	122
1.7 OBJECTIVES OF THE STUDY	125
RESULTS	127
ARTICLE AND MAIN FIGURES	129
SUPPLEMENTAL INFORMATION	173

DISCUSSION 197

D.1 Highlights of our findings and take-home messages 198
D.2 Atoh1 may control cell cycle and timing of neurogenesis, by regulating ciliogenesis 199
D.3 Possible consequences of loss or gain of Cep131 on centrosome duplication 201
D.4 Role of CS in neurogenesis and consequences of their absence in post mitotic GNs 202
D.5 Contribution of Atoh1 to SHH signaling 203
D.6 Atoh1 collaborates with the SHH pathway at multiple steps. 205
D.7 Dual and opposite roles of Atoh1 in GNs development 207

BIBLIOGRAPHY 211

ANNEX 253

RÉSUMÉ EN FRANÇAIS 255

Abbreviations

ACVR2A/B: Activin receptor 2A/B
APC/C: Anaphase promoting complex/cyclosome
APC: Adenomatous polyposis cancer
Arf4: ADP-ribosylation factor 4
Arl13b: ADP-ribosylation factor-like protein 13b
Ascl1: Achaete-scute homolog 1
AtEAM: Atoh1 E-box associated motif
Atoh1: Atonal homolog 1
ATP: Adenosine triphosphate
Aurka: Aurora A kinase
Barhl1: BarH-like 1 homeobox protein
BBIP10: BBSome Interacting Protein 10
BBS: Bardet-Biedl syndrome
BCC: Basal cell carcinoma
bHLH: Basic helix-loop-helix
Bmi1: B cell-specific Moloney murine leukemia virus integration site 1
BMP2/4/7: Bone morphogenetic protein 2/4/7
BDNF: Brain-derived neurotrophic factor
Boc: Brother of Cdo
BRCA2: Breast cancer 2
BrdU: 5-bromo-2'-deoxyuridine
Ccdc14: Coiled-coil domain containing protein 14
Ccnd1/2: Cyclin D1/2
Cdc25b: Cell division cycle 25B
CDK1/4/6: Cyclin-dependent kinase 1/4/6
Cdkn1b: Cyclin-dependent kinase inhibitor 1b
Cdkn2a/c: Cyclin-dependent kinase inhibitor 2a/c
Cdo: Cell adhesion molecule-related/down-regulated by oncogenes
Cep72/83/97/110/131/152/164/290: Centrosomal protein of 72/83/97/110/131/152/164/290 kDa
ChIP-seq: Chromatin-immunoprecipitation sequencing
Ci: *Cubitus interruptus*
CKI δ : Casein kinase I δ
cKO: Conditional knockout
CLS: Cilium-localization signals
CMP: Ciliary membrane protein
CNS: Central nervous system

COPI/II: Coat protein I/II
CP110: Centriolar colic-coil protein of 110kDa
Crcx4: C-X-C chemokine receptor type 4
CRD: Cystein-rich domain
CREB: Cyclic AMP-responsive element-binding protein
CS: Centriolar satellites
CSF: Cerebrospinal fluid
CSI: Craniospinal irradiation
CT: Chemotherapy
Cyld: Cyldromatosis
D/N: Desmoplastic/nodular
DCI: Dorsal commissural interneuron
DCN: Deep cerebellar nuclei
DDX3X: DEAD-box helicase 3 X-linked
Dhh: Desert Hedgehog
DRG: Dynein regulatory complex
E: Embryonic day
ECM: Extracellular matrix
EdU: 5-ethynyl-2'-deoxyuridine
Egf: Epidermal growth factor
En1/2: Engrailed 1/2
EphB2: Ephrin type-B receptor 2
ERBB4: Erb-b2 receptor tyrosine kinase 4
Evc: Ellis van Creveld protein
EZH2: Enhancer of zeste homolog 2
Fgf8: Fibroblast growth factor 8
FOP: FGFR1 oncogene partner
For20: FOP-related protein of 20 kDa
FoxM1: Forkhead box M1
GABA: Gamma-Aminobutyric acid
Gas1: Growth arrest specific1
Gbx2: Gastrulation brain homeobox 2
GEF: Guanine nucleotide exchange factor
Gfap: Glial fibrillary acidic protein
GFI1: Growth factor independent 1
GFP: Green fluorescent protein
Gli1/2/3: Glioma-associated oncogene 1/2/3
Gli^{A/FL/R}: Gli activator/full-length/repressor form
GN: Granule neuron
GNP: Granule neuron progenitor
GPCR: G-protein coupled receptor

Gpr161: G-protein-coupled receptor 161
Gprk2: G-protein-coupled receptor kinase 2
GSK-3 β : Glycogen synthase kinase-3 β
GTP: Guanosine triphosphate
HC: Hair cell
HDAC1/6: Histone deacetylase 1/6
Hes1/5: Enhancer of split 1/5
HH: Hedgehog
Hhip1: Hedgehog-interacting protein 1
Hic1: Hypermethylated in cancer 1
Hoxa2: Homeobox A2
Hrs: hours
HSPGs: Heparan sulfate proteoglycans
Huwe1: HECT, UBA and WWE domain containing E3 ubiquitin protein ligase 1
Id2: Inhibitor of DNA-binding/differentiation 2
IDH1: Isocitrate Dehydrogenase 1
iEGL: Inner external granular layer
IFT: Intraflagellar transport
Ift20/88/172: Intraflagellar transport protein 20/88/172
Igf2: Insulin-like growth factor 2
IGL: Internal granular layer
Ihh: Indian Hedgehog
ILK: Integrin linked kinase
IsO: Isthmic organizer
Itch: Itchy homolog
JBTS: Jubert syndromes
JNK: c-Jun N-terminal kinase
Kap3: Kinesin-associated protein 3
KBTBD4: Kelch repeat and BTB domain containing 4
KDM6A: Lysine demethylase 6A
Kif3a/3b/3c/7/17/24: Kinesin family member 3a/3b/3c/7/17/24
KMT2C: Lysine methyltransferase 2C
KO: Knockout
Lh2A/B: LIM/homeobox protein A/B
Lmx1a/b: LIM homeobox transcription factor 1, alpha/beta
LOH: Loss of heterozygosity
IRL: Lower rhombic lip
MAPK: Mitogen-activated protein kinases
MB: Medulloblastoma
MBEN: Extensive nodularity
MDM4: Murine double minute 4

MEP: Multipotent epithelial progenitor
MHB: Midbrain-hindbrain boundary
Mib1: Mindbomb 1
MKS: Meckel syndrome
ML: Molecular layer
MRI: Magnetic resonance imaging
MTOC: Microtubule organizing center
mTOR: Mammalian target-of-rapamycin
MYCL1: L-myc-1 proto-oncogene
Mycn: N-myc proto-oncogene
Nek2: Never in mitosis related Kinase 2
NeuN: Neuronal nuclei antigen
NeuroD1: Neurogenic differentiation factor 1
Neurog1/2: Neurogenin-1/2
NICD: Notch intracellular domain
NMDA: N-Methyl-D-aspartic acid
NPC: Neural progenitor cell
NPHP: Nephronophthisis
NTZ: Nuclear transitory zone
Odf2: Outer dense fiber protein 2
oEGL: Outer external granular layer
Ofd1: Orofaciodigital Syndrome 1
Olig2: Oligodendrocyte transcription factor 2
Otx2: Orthodenticle homeobox 2
P: Post-natal day
PALB2: Partner and localizer of BRCA2
Par6a: Partitioning defective 6 homolog alpha
Pax2/5/6: Paired box 2/5/6
PC: Purkinje cell
PCL: Purkinje cell layer
Pcm1: Pericentriolar material 1
PDD: Processing determinant domain
PDGF: Platelet-derived growth factor
PDXs: Patient-derived xenograft
PI3K: Phosphatidylinositol 3-kinases
PIK3C2B/G: Phosphatidylinositol-4-phosphate 3-kinase catalytic subunit type 2 beta/gamma
PKA/C: Protein kinase A/C
Plk1/4: Polo-like kinase 1/4
PPM1D: Protein Phosphatase, Mg⁺⁺/Mn⁺⁺ dependent 1D,
PRC1: Polycomb repressive Complex 1
PRC2: Polycomb repressive complex 2

PRDM6: PR/SET domain 6
Ptch1/2: Patched homolog 1/2
PTEN: Phosphatase and TENsin homolog
Ptf1a: Pancreas associated transcription factor 1a
PTM: Post-translational modification
r1 - r8: Rhombomere 1 - Rhombomere 8
Rb1: Retinoblastoma 1
Rbpj: Recombination signal binding protein for immunoglobulin kappa J region
RL: Rhombic lip
RLS: Rostral rhombic lip migratory stream
RND: Resistance-nodulation-division
Robo1/2: Roundabout guidance receptor 1/2
RT: Radiotherapy
SC: Supporting cell
SCF: Skip-Cullin-F-box
SDF-1 α : Stromal cell-derived factor 1 alpha
SEM: Standard error of the mean
SHH: Sonic hedgehog
siRNA: small interfering RNA
Slit1/2: Slit Guidance Ligand 1
Smad4: Small mothers against decapentaplegic
SMARCA4: SWI/SNF related, matrix associated, actin dependent regulator of chromatin, subfamily A, member 4
Smo: Smoothened
SNCAIP: Synuclein alpha interacting protein
Spop: Speckle-type POZ protein
SSX2IP: SSX family member 2 interacting protein
TERT: Telomerase reverse transcriptase
TGF- β : Transforming growth factor-beta
Tieg1: TGFbeta inducible early gene-1
TP53: Tumor protein 53
Tuj1: Neuron-specific class III beta-tubulin
UBC: Unipolar brush cell
Unc5c: Uncoordinated-5C
uRL: Upper rhombic lip
USP9X: Ubiquitin specific peptidase 9 X-linked
UV: Ultraviolet
VZ: Venticular zone
WHO: World Health Organization
Wnt1/3: Wingless-type MMTV integration site family member 1/3
YAP1: Yes associated protein 1

Zic1: Zinc finger of the cerebellum family member 1
 β -TrCP: Beta-transducin repeats-containing protein
 γ -TURC: Gamma-tubulin ring complexes

Table of Figures

Figure I. Anatomy of the cerebellum.

Figure II. Functional classification of cerebellar regions.

Figure III. Cortical cerebellar neurons and main neuronal circuitries.

Figure IV. Early embryonic patterning of the vertebrate brain.

Figure V. Germinal zones in the early cerebellar anlage.

Figure VI. Sequential phases of embryonic and post-natal cerebellar development.

Figure VII. Developmental phases of GNPs in post-natal times.

Figure VIII. Pro-proliferative pathways active in GNPs in the EGL.

Figure IX. Anti-proliferative pathways triggering terminal differentiation of GNPs.

Figure X. Molecular subgroups of MB.

Figure XI. Heterogeneity in SHH-MB.

Figure XII. Structure of a cilium.

Figure XIII. Mechanisms of protein trafficking through the cilium.

Figure XIV. Cilium-centrosome behaviour during the cell cycle.

Figure XV. Synthesis steps of the active HH protein (HH-N) from the precursor.

Figure XVI. Relevant domains and sites in mouse Gli2 and Gli3 proteins.

Figure XVII. HH signaling in vertebrates.

Figure XVIII. Centriolar satellites.

Figure XIX. Mechanisms controlled by CS during ciliogenesis in normal conditions.

Figure XX. Major networks regulating Atoh1 expression in GNPs across embryonic and post-natal developmental stages.

Figure XXI. Expression of SHH target genes upon Atoh1 manipulation in GNPs.

Figure XXII. Positive feedback loop between Atoh1 and SHH in GNPs or SHH-MB cells.

Introduction

I.1 The Cerebellum

By housing more than half of the neurons of the whole brain, the cerebellum (Latin for "little brain") is one of the most architecturally complex region of the vertebrate central nervous system (CNS). Since the end of the XIX century, for over 80 years, the cerebellum has been considered the area of the CNS exclusively dedicated to motor control and coordination. However, this view has progressively expanded during the last three decades, as numerous studies based on novel functional imaging, neural tracing and clinical data analysis have highlighted new and unexpected roles in higher cognitive activities such as learning, attention, language and emotions.

In this first introductory chapter, the anatomy and functional compartmentalization of the cerebellum will be initially illustrated, before delving into the description of the histological architecture of the cerebellar cortex.

I.1.1 ANATOMY OF THE CEREBELLUM

Residing within the posterior fossa of the skull, the cerebellum represents the anteriormost region of the hindbrain, locating beneath the cerebral hemispheres and posterior to the brain stem¹ and the IVth ventricle.

At a first glance, the cerebellum can be clearly divided in three major parts consisting in two large lateral hemispheres separated by a narrow midline region called *vermis* (Latin for "worm"). In addition, the surface of the cerebellum is crossed by two deep transversal (medio-lateral) grooves called primary and posterolateral fissures, which delineate three major cerebellar lobes, namely the anterior, posterior and flocculonodular lobes (Roostaei et al., 2014) (**Figure I**). The anterior and the posterior lobes are further shaped by shallow transversal fissures which overall subdivide the entire cerebellum in a total of ten lobules, indicated with Roman numbers. In particular, the anterior lobe contains the first five lobules (I-V), the posterior lobe the following four (from VI to IX, with the lobule VII split in VIIA and VIIB),

¹ The brain stem includes the midbrain, the pons and the medulla.

while the flocculonodular lobe coincides with the lobule X (Roostaei et al., 2014) (**Figure I**). Next, the surface of each lobules is also shaped by a series of tiny parallel transversal gyrus, referred as *folia*, which adding up to the lobular organization, further increases the total surface of the cerebellum, eventually enabling the packaging of a large area of neural tissue in a relatively small volume (Roostaei et al., 2014).

The internal macro-organization of the cerebellum is relatively simple. It consists into an external cortex of grey matter, mainly composed by cell bodies, surrounding a large body of white matter, made primarily by myelinated neuronal fibers. Embedded within the white matter lie three pairs of "deep cerebellar nuclei" (DCN), composed of grey matter (Stilling, 1864). From medial to lateral, these nuclei are respectively called fastigial, interposed (which is further divided into globose and emboliform nuclei) and dentate (**Figure I**). With only few exceptions, the majority of the cerebellar outputs are projected from the DCN.

Morphologically, the cerebellum is connected to the brainstem via three pair of peduncles which, according to their relative position are named superior, middle and inferior. The totality of the afferent and efferent neuronal fibers directed toward and leaving the cerebellum pass through these peduncles, which therefore represent also the sole functional connection of the cerebellum with the other regions of the CNS (Roostaei et al., 2014).

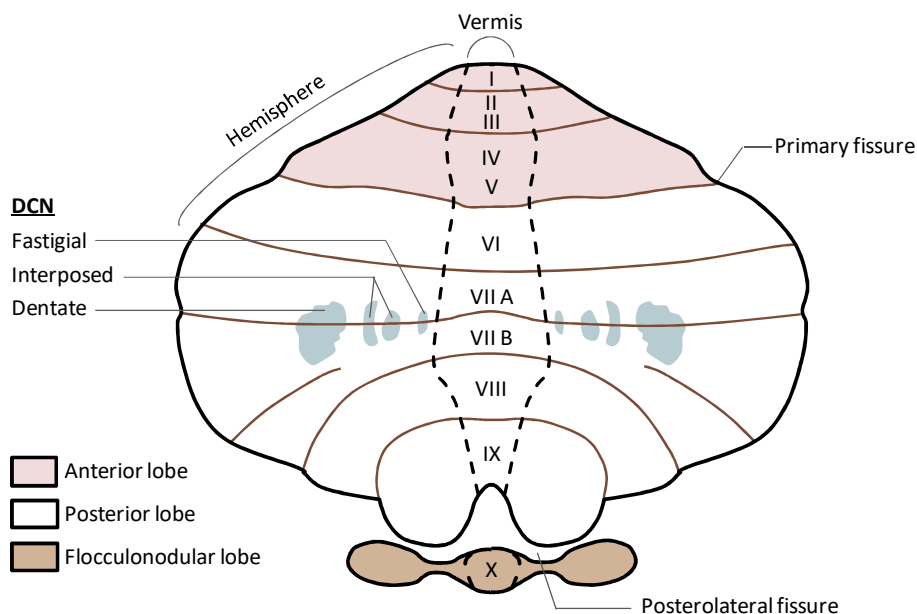


Figure I. Anatomy of the cerebellum. Schematic dorsal view of an unfolded human cerebellar cortex. The *vermis* in medial in the cerebellum and delimited from the lateral hemispheres by black gapped lines. The major fissures, including those dividing the three lobes (indicated with different colours) are represented by transversal brown lines. The position and name of the lobules is indicated with Roman numbers at the level of the vermis. The position of the deep cerebellar nuclei (DCN) inside the cerebellum is projected in the drawing by light blue areas.

I.1.2 MAIN FUNCTIONS OF THE CEREBELLUM

The major role of the cerebellum consists in controlling, coordinating and if needed correcting the body voluntary movements. Such complex activities occur in relation to memorized motor schemes and environmental or internal stimuli.

The cerebellum is believed to receive two major types of input information (Ito, 2013; Ohyama et al., 2003; Ramnani, 2012). The first information is motor type: it principally comes from the motor cortex, which contains the pre-motor and primary motor areas dedicated to the planning and execution of movement. This way the cerebellum is informed about the type of movement that is intended to perform. The second information is sensory type: it reports details about the actual status of the body and the surrounding environment at the onset of movement. Once received, these information are integrated and processed within the cerebellar circuitries which are supposed to store memories of "correct" motor schemes learnt by trials and errors during the individual's life. By basing on these schemes and by evaluating motor and sensory inputs, the cerebellum produces an output which is eventually directed to the motor cortex via a relay through the thalamus. Such output may correct the activity of cortical motor neurons, thus tuning their output to accomplish the best execution of the movement (Ito, 2013; Ohyama et al., 2003; Ramnani, 2012). Nevertheless, if the movement is not precisely or correctly executed, then an error signal is generated, conceivably at the level of the inferior olive of the medulla, and delivered to the cerebellum. Such error input is believed to re-wire the cerebellar circuitries in order to modify the stored motor memory and allow the cerebellum to correct such error in the future if similar conditions will be met again (Ito, 2013; Ohyama et al., 2003; Ramnani, 2012).

I.1.2.1 Functional compartmentalization of the cerebellum

Depending on the nature of the afferencies received, the efferencies projected and thus on the type of body activities controlled, the cerebellum can be divided into three main parts, namely vestibulocerebellum, spinocerebellum and cerebrocerebellum (**Figure II**). The vestibulocerebellum, is the posteriormost region of the cerebellum, it corresponds to the flocculonodular lobe and it is the most evolutionary ancient part of this organ. By receiving inputs from the vestibular nuclei on the brainstem and from the visual cortex, the vestibulocerebellum is dedicated to the regulation of the equilibrium, the posture and the coordination of eyes positioning upon head movements.

The spinocerebellum locates in the cerebellum midline and consists into the *vermis* and the medial part of the cerebellar hemispheres (also known as *paravermis*), the fastigial and interposed nuclei. It receives auditory, visual and somatosensory information from all the body thanks to its connections with the spinal cord and various brainstem nuclei (Roostaei et al., 2014). The somatosensory inputs coming from different parts of the body are processed in dedicated areas of the spinocerebellum, so that a somatotopic map of the body is created on its cortex (Manni and Petrosini, 2004). Also the spinocerebellum participates in the regulation of posture and equilibrium, but it is also involved in the coordination of regular movements of the limbs, like those required for walking.

Finally, the cerebrocerebellum corresponds to the lateral part of the cerebellar hemispheres and includes the dentate nuclei. It represents the most evolutionary recent functional part of the cerebellum and it has tremendously expanded with the appearance of the primates lineage (Herculano-Houzel, 2010). In humans it accounts for around 90% of the volume of the whole cerebellum. The cerebrocerebellum is primarily responsible for the functions described in the previous paragraph given its high connectivity with the cerebral cortex. Hence, the cerebrocerebellar is ultimately required for the planning and the proper timing of complex movements, as well as high cognitive activities, including language (Buckner, 2013).

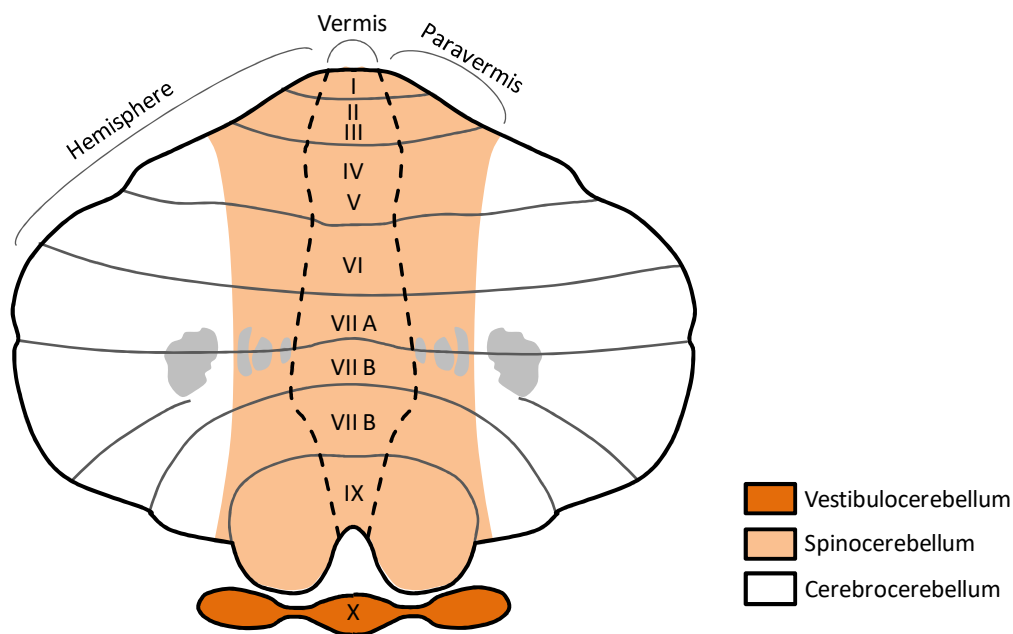


Figure II. Functional classification of cerebellar regions. The drawing depicts an equivalent representation of the cerebellum as shown in Figure I. The three functional regions of the cerebellum, namely the vestibulocerebellum, the spinocerebellum and the cerebrocerebellum are indicated with different colors.

I.1.3 MICROANATOMY OF THE CEREBELLAR CORTEX

I.1.3.1 Cells of the cerebellar cortex

Despite the functional compartmentalization described above, the cytoarchitecture of the cerebellar cortex seems to be essentially identical and repeated along its whole extension (Ito, 2006; Roostaei et al., 2014; Voogd and Glickstein, 1998) (**Figure III**).

Depending on the cell type composition, the cerebellar cortex can be subdivided into three layers. The deepest layer is also the thickest and it is called granular layer or internal granular layer (IGL), to distinguish it from its "external" counterpart that transiently appears during cerebellar development (as it will be described later). The IGL gets its name after the granule neurons (GNs), small, glutamatergic (excitatory) neurons that tightly packed reside in this layer. Interestingly, GNs account for the most abundant neuronal population of the whole adult brain. In addition to the GNs, the IGL hosts also some less abundant populations of interneurons as the GABAergic (inhibitory) Golgi and Lugaro cells and the glutamatergic unipolar brush cells (UBCs), the latter found only in the vestibulocerebellum.

Above the IGL there is the Purkinje cell layer (PCL), which consists of one single layer of cell bodies (or somata) of the Purkinje cells (PCs), a GABAergic neuron type responsible for transmitting the output of the cerebellar cortex (as described shortly). Alongside to the somata of PCs, the PCL also contains small interneurons called candelabrum cells, and the Bergmann glia cells, a particular type of astrocyte with roles in modulating PCs activity (Lainé and Axelrad, 1994).

The uppermost layer of the cortex is called molecular layer (ML) and it is composed mostly by the large and expanded dendritic tree of the PCs and by the axons of the GNs. Indeed, each GN in the IGL extends its axon toward the ML, where it bifurcates generating two characteristic T-shaped branches that extend parallel to the cerebellar surface, up to 4-6mm in humans (Ito, 2006). These specialized axons of the GNs are called parallel fibers and they transmit excitatory signal to the Purkinje cells by forming synapses with their dendritic trees. It is estimated that each GN can synapse with thousands of Purkinje cells. In addition to parallel fibers and PCs dendritic trees, the molecular layer also houses a set of inhibitory interneurons like the basket cells and the stellate cells.

I.1.3.2 Major cerebellar circuits

Similarly to its neuronal composition, the neuronal circuitries of the cerebellar cortex seem highly repeated and stereotyped (Ito, 2006; Roostaei et al., 2014; Voogd and Glickstein, 1998) (**Figure III**). Indeed, such neuronal networks can be ultimately reduced to a single functional module that is reproduced multiple times across the cerebellar cortex, with only few regional little diversifications.

Fundamentally, the cerebellum receives two major types of excitatory inputs relayed by two distinct afferent pathways, namely the mossy fibers (MFs) and the climbing fibers (CFs). The MFs are projections generated by a multitude of sources, including pre-cerebellar brainstem nuclei (as some pontine nuclei relaying the cerebral cortex inputs) and the spinal cord. They basically transport the motor and sensory type information required by the cerebellum for generating its output. The CFs instead originate from a unique source, the inferior olive, and are believed to relay the error inputs to the cerebellum.

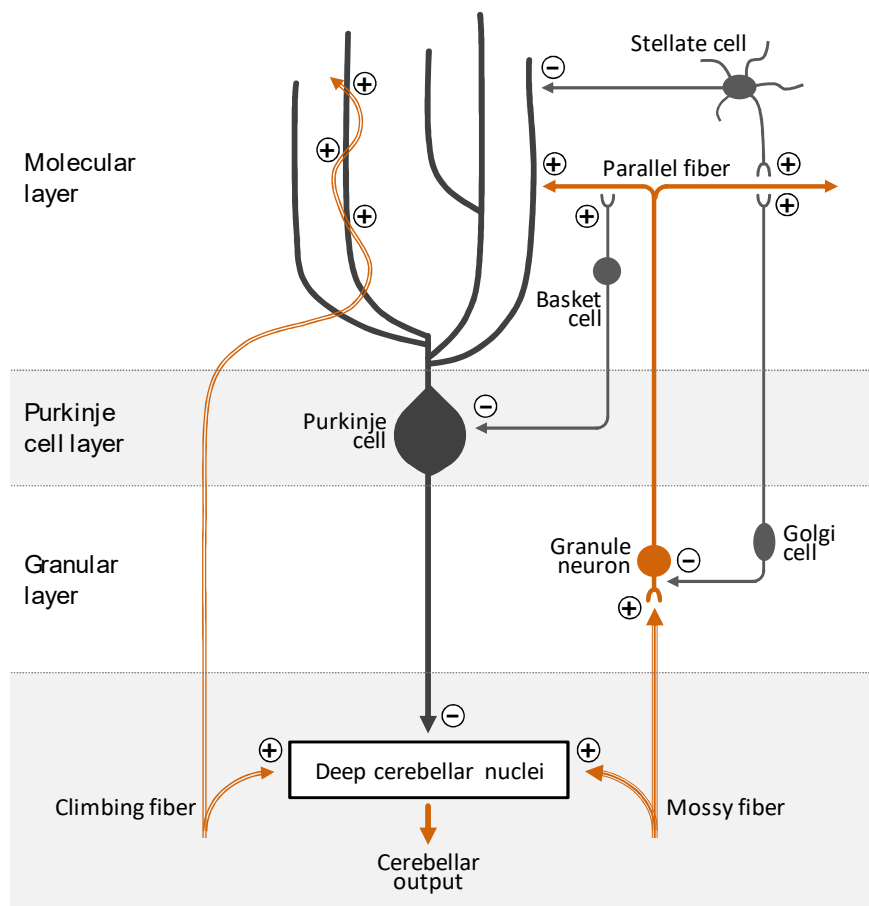


Figure III. Cortical cerebellar neurons and main neuronal circuitries. Major synaptic interaction between neurons of the cerebellar cortex. The (+) and (-) symbols at the synapses indicate excitatory and inhibitory synapses respectively. The neurotransmitter phenotype of neurons is color-coded: glutamatergic neurons are in orange and GABAergic in grey.

Once entered the cerebellum through the cerebellar peduncles, collaterals of both MFs and CFs are sent toward the cerebellar cortex and the DCN. In this way, the same excitatory input is received by the two neuronal substrates of the cerebellum.

At the level of the cortex, CFs are directed to the molecular layer where they literally "climb" the branches of the dendritic trees of PCs forming multiple synaptic connection with them. The number of synapses here generated is so high that a single action potential travelling along a CF is generally sufficient to activate a PC.

On the contrary, MFs are directed to the IGL where they extensively branch and contact the dendrites of GNs forming specialized synapses called "cerebellar glomeruli". Cerebellar glomeruli are morphologically unique synapses in the brain, displaying a typical globular shape where a MF terminal enlarges to engage up to fifty GN dendrites (Jakab and Hámori, 1988). In addition, cerebellar glomeruli contain the axon terminal of various Golgi cells, which by releasing GABA modulate the activation of GNs.

As GNs downstream signal to PCs through their parallel fibers, the cortical circuits are organized in such a way that either directly or indirectly, the excitatory signals of CFs and MFs are eventually received by PCs. Upon activation of PCs, their inhibitory output is sent toward the DCN via their long axons, which extends through the cerebellar white matter.

In the DCN, integration of the excitatory inputs from CFs and MFs and inhibitory inputs from PCs occurs, and, if generated, excitatory signals are sent out the cerebellum to various downstream targets (e.g. to the cerebral cortex via a thalamic relay from the dentate nuclei).

Besides the above described neuronal network, other elements add up to these circuitries to further refine and modulate the information processing. Cortical interneurons indeed participate in the signal propagation by regulating the activation of both GNs and PCs via local feedback and feedforward circuitries. As anticipated, Golgi cells in the IGL counteract the activation of GNs by the MFs at the level of the cerebellar glomeruli. As Golgi cells are themselves upstream activated by parallel fibers, this represents an example of a feedback inhibition on GNs (**Figure III**). Stellate and basket cells in the ML instead receive synaptic inputs from parallel fibers and form downstream inhibitory synapses with PCs. Therefore, these interneurons mediate a feedforward inhibition on PCs in the context of the GNs-PCs pathway (**Figure III**).

1.2 Development of Granule Neurons

Cerebellar GNs represent the most abundant neuronal pool of the whole adult brain. Their neurogenesis requires precise temporally regulated steps of specification, migration, proliferation and maturation happening during both embryonic development and early post-natal times in both human and mouse.

This second introductory chapter describes how the cerebellum is formed during embryogenesis and how histogenesis of GNs is achieved, highlighting the molecular modules implicated in such developmental process.

1.2.1 EARLY SPECIFICATION AND PATTERNING OF THE CEREBELLUM

1.2.1.1 Regionalization of the neural tube

The entire vertebrate CNS originates from the ectoderm, one of the three germ layers of the early embryo, which also contributes to the epidermis. During gastrulation, signals from the primitive node regionalize the ectoderm specifying the prospective CNS in the so-called "neural plate", a relatively uniform sheet of cells located at the dorsal midline of the embryo. Subsequently, a combination of migratory events, changes in cell shape, and mechanical pressure due to the expanding lateral epidermis will cause the borders of the neural plate to thick-up, bend over the midline and eventually fuse dorsally giving rise to the neural tube. The process that starts with formation of the neural plate and terminates with closure of the neural tube is denominated neurulation (Darnell and Gilbert, 2017; Stiles and Jernigan, 2010).

During neurulation, inductive signals from the anterior endoderm and the notochord initiate the spatial patterning of the neural plate both along the antero-posterior and the dorso-ventral axis. Even much before the complete closure of the neural tube, such regionalization becomes visible by the appearance of three swellings in the anterior neural tube, denominated neuromeres or brain vesicles. The neuromeres will give rise to the various brain structures and they are named, from anterior to posterior, forebrain (or prosencephalon), midbrain (or mesencephalon) and hindbrain (or rhombencephalon) (**Figure IV**). Conversely, the remaining posterior part of the

neural tube maintains its cylindrical shape and will become the spinal cord (Darnell and Gilbert, 2017)

Later on, the regionalized expression of *Hox* genes further transiently patterns the hindbrain into eight segmental units, called rhombomeres (r1 to r8) leading to initial neuronal identity diversification (Keynes and Krumlauf, 1994) (Figure IV).

Sometimes, the anatomical boundary between the midbrain and the hindbrain (midbrain-hindbrain boundary, MHB), also called isthmus or isthmic constriction (as the neural tube is here "squeezed" between these two neuromeres), is referred as the rhombomere 0.

Early fate mapping studies utilizing the quail-chick transplants system led to the nowadays accepted knowledge that all the cerebellar neurons arise from the dorsal (alar) r1. By embryonic day (E) 7.5 in mouse, the r1 territory is specified in the anteriormost part of the hindbrain, just posterior to the MHB, thanks to the regionalized expression of a group of homeobox transcription factors (Figure IV).

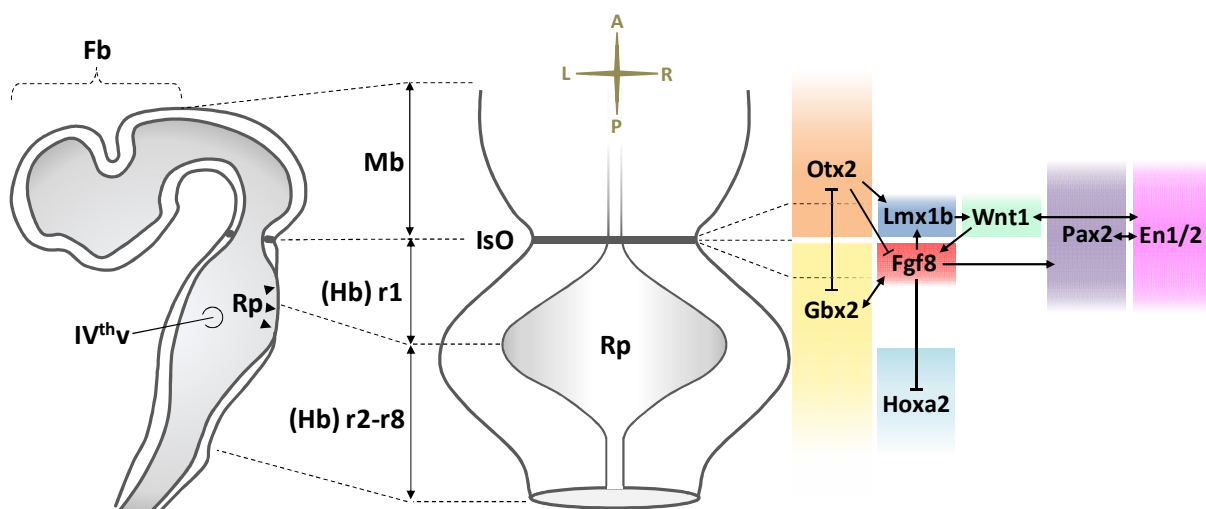


Figure IV. Early embryonic patterning of the vertebrate brain. (Left drawing) Schematic view of a sagittal section of the embryonic mouse brain at around E9. The anteriormost brain vesicle is the forebrain (Fb) followed by the midbrain (Mb) and by the hindbrain (Hb), the latter further divided into segmental units, the rhombomeres (r1 to r8). At the dorsal midline of the hindbrain, the roofplate (Rp) appears as a thin layer covering the IVth ventricle (IVth v). (Middle drawing) Schematic dorsal view of the boundary between midbrain and hindbrain at the same developmental stage. The isthmus organizer (IsO) localizes at the boundary between midbrain and hindbrain. The medio-lateral expansion of the roofplate at the level of the anterior hindbrain can be appreciated from this view. (Right scheme) Expression domains of the major genes implicated in anterior hindbrain patterning in relation to the middle drawing. In addition, the fundamental regulatory networks between these genes are shown, based on the reviews of Martinez *et al.* (2013), Wurst and Bally-Cuif, (2001b) and Sillitoe and Joyner (2007). Such networks establish, reinforce and maintain the represented gene expression pattern. The r1 is specified in a region devoid of *Otx2* and *Hoxa2* expression. *Lmx1b* may initiate the IsO gene expression program. *Fgf8* and *Wnt1* are expressed at the IsO, but into two distinct posterior and anterior domains respectively. *Pax2* and *En1/2* are expressed into broader territories encompassing the IsO and the r1.

In particular, the MHB coincides with the boundary between the expression domain of *Orthodenticle homeobox 2* (*Otx2*, expressed in the midbrain and in the forebrain) and *Gastrulation brain homeobox 2* (*Gbx2*, expressed from r1 to r3) (Simeone et al., 1992; Wassarman et al., 1997). Importantly, the expression of *Otx2* and *Gbx2* is mutually exclusive as both can cross-repress each other's expression. Notably, such regulation is functional at maintaining a neat separation between the midbrain and the hindbrain territories (Inoue et al., 2012). The posterior edge of the r1 is instead defined by the anteriormost outreach of *Homeobox A2* (*Hoxa2*) expression, which extends in the r2 and r3.

Therefore, the cerebellum ultimately originates in a territory of the hindbrain marked by the expression of *Gbx2*, and by the absence of *Otx2* and *Hoxa2* (**Figure IV**). This conclusion is supported by a number of genetic studies demonstrating that perturbing the expression of these genes results into either loss or ectopic specification of prospective cerebellar territories (Eddison et al., 2004; Gavalas et al., 1997; Wassarman et al., 1997).

1.2.1.2 Specification of cerebellar territories in rhombomere 1

Once it is formed, the r1 undergoes spatial patterning in order to regionally specify the identity of its derivatives, including the cerebellar neurons and glia. During embryogenesis, tissue patterning is generally controlled by signaling centers, also known as organizers, which by releasing morphogens or other signaling molecules play instructive roles on the fate of adjacent tissues. Patterning of the anterior hindbrain is principally orchestrated by a transversal ring of cells localizing at the MHB, which altogether constitute the so called isthmus organizer (IsO) (Marin and Puelles, 1994; Martinez et al., 1991; Martínez et al., 1995) (**Figure IV**). The IsO is established around E8.5 and its onset is marked by the expression of morphogens like Fibroblast growth factor 8 (*Fgf8*) and Wingless-type MMTV integration site family member 1 (*Wnt1*), whose secretion and diffusion mediate the instructive functions of the IsO in the surrounding territories (Crossley and Martin, 1995; Martinez et al., 2013; McMahon and Bradley, 1990).

Although seemingly dispensable for IsO formation, *Otx2* and *Gbx2* are instrumental for determining its positioning at the MHB. Indeed, genetic manipulations causing anterior or posterior shift of *Otx2* and *Gbx2* expression domains eventually reposition the IsO at the new *Otx2-Gbx2* interface (Simeone, 2000; Wurst and Bally-Cuif, 2001a).

Conversely, converging evidence from studies in mouse and chicken embryos, pinpointed the LIM homeobox transcription factor *Lmx1b* as the main responsible for IsO induction (Adams et al., 2000; Guo et al., 2007). *Lmx1b* is expressed in the posteriormost midbrain, where it

activates the expression of *Wnt1* at the MHB. Here, *Wnt1* signaling downstream activates *Fgf8* expression, thereby establishing the IsO (Guo et al., 2007; Matsunaga et al., 2002). In addition, also the Paired box 2 (*Pax2*) transcription factor is a known regulator of *Fgf8* expression, thus it may contribute to IsO formation as well (Ye et al., 2001).

Among the two principal IsO morphogens, *Fgf8* seems to be the main mediator of IsO patterning activity, while *Wnt1* may just have a limited role consisting into a mitogenic stimulus for neuroepithelial cells (Chi et al., 2003; Liu et al., 1999; Martinez et al., 1999). Hence, regionalization of the r1, which also includes specification and maintenance of the cerebellar identity in the alar r1, mainly requires the morphogenetic activity of *Fgf8*. However, by E9, also the transcription factors *Lmx1b* and *Pax2*, *Engrailed 1* (*En1*), *Engrailed 2* (*En2*) and *Paired box 5* (*Pax5*) add up to *Fgf8* signaling to regulate r1 patterning (Asano and Gruss, 1992; Davis and Joyner, 1988; Rowitch and McMahon, 1995; Sillitoe and Joyner, 2007; Wurst and Bally-Cuif, 2001a). Some of the known genetic interactions required for anterior hindbrain specification and patterning are represented in **Figure IV**.

1.2.2 EARLY HISTOGENESIS IN THE CEREBELLAR ANLAGE

Once the presumptive cerebellar territory is specified, cerebellar cells histogenesis initiates. As mentioned above, it is nowadays accepted that all the cerebellar neurons derive from the alar plate of r1. At E9.5 in mice, two molecularly and spatially distinct germinal regions can be there identified: the upper rhombic lip (uRL) and the ventricular zone (VZ) (Hatten and Heintz, 1995) (**Figure V**). The rhombic lip (RL) localizes at dorsal margin of the hindbrain neuroepithelium, lining adjacent to the roofplate of the IVth ventricle. The anterior segment of the RL, which is contained in the r1, is called "upper" RL (uRL), in contrast to the "lower" RL (IRL) which extends posteriorly in the remaining rhombomeres (**Figure V**). Importantly, the uRL is the source of all the cerebellar glutamatergic neurons, including the GNs, the UBCs and the large excitatory neurons of the DCN (Alder et al., 1996; Machold and Fishell, 2005; Wang et al., 2005; Wingate and Hatten, 1999) (**Figure VI and VI**). In addition, the uRL also contributes to some pre-cerebellar pontine nuclei part of the vestibular, auditory and proprioceptive sensory systems (Wang et al., 2005). Conversely, the IRL mainly gives rise to neurons populating different sets of precerebellar pontine and medullary nuclei (Rodriguez and Dymecki, 2000; Wang et al., 2005; Wingate, 2001).

The VZ is instead placed along the lining of the dorsal aspect of the IVth ventricle and produces all the cerebellar GABAergic neurons, including PCs, Golgi, basket, stellate cells and the small inhibitory neurons of the DCN (Hoshino et al., 2005; Leto et al., 2006; Maricich and Herrup, 1999; Sudarov et al., 2011) (**Figure V** and **VI**). In addition, VZ progenitors also contribute to great part of the cerebellar glial population (Sudarov et al., 2011).

Two genes encoding for class II-basic helix-loop-helix (bHLH) transcription factors, namely *Atonal homolog 1* (*Atoh1*) and *Pancreas transcription factor 1a* (*Ptf1a*), are required for the fate commitment of RL and VZ progenitors respectively and they are also used as *bona fide* markers for these two germinal zones (Akazawa et al., 1995; Ben-Arie et al., 1997; Hoshino et al., 2005; Machold and Fishell, 2005; Wang et al., 2005; Yamada et al., 2014) (**Figure V**). Interestingly, once the expression of *Atoh1* and *Ptf1a* is induced in the cerebellar anlage (around E9.5), these two transcription factors are able to repress each other's expression, hence robustly separating uRL and VZ (Yamada et al., 2014).

Therefore, similarly to what happens for forebrain cortical neurogenesis, generation of glutamatergic and GABAergic neurons is spatially compartmentalized in the cerebellum (Schuurmans et al., 2004) (**Figure V**).

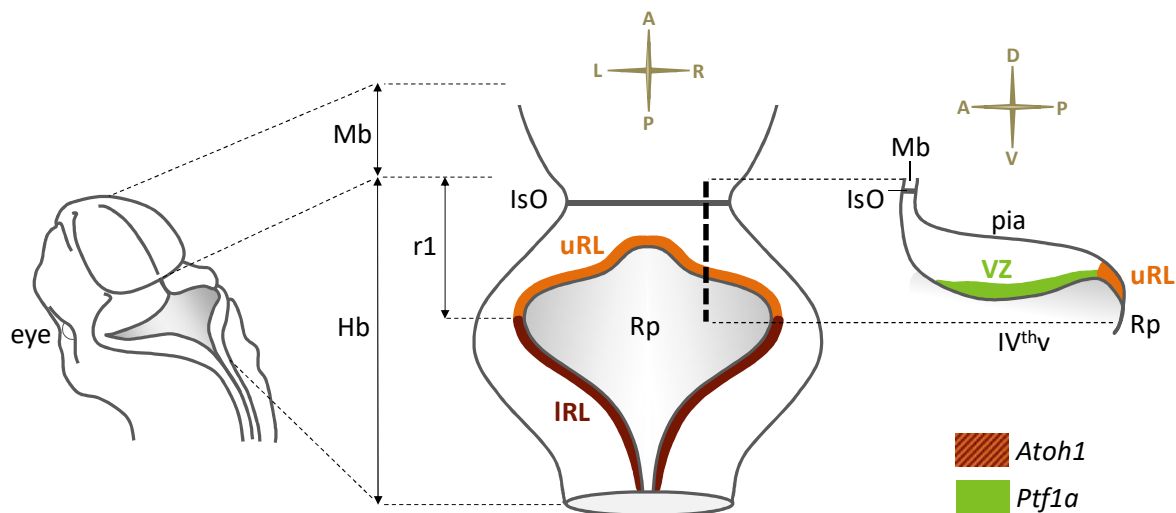


Figure V. Germinal zones in the early cerebellar anlage. (*Left drawing*) Dorso-lateral view of a mouse embryo's head at E9.5. (*Middle drawing*) Dorsal view of the hindbrain (Hb) at the same stage. The rhombic lip (RL, orange/brown) appears at the dorsal margins of the Hb, adjacent to the roofplate (Rp). The upper RL (uRL, orange) is specified anteriorly, within the rhombomere 1 (r1). In contrast the lower RL (IRL, brown) borders the remaining posterior part of the Hb. (*Top-right drawing*) Sagittal section view of the dorsal (alar) r1, which will give rise to the cerebellum. The uRL is visible posteriorly, next to the Rp, while the ventricular zone (VZ, green) is more anteriorly located and lines above the IVth ventricle (IV^{thv}). The dorsal surface or the alar r1 is covered by the meninges (pia). *Atoh1* is expressed in both the uRL and the IRL, while *Ptf1a* expression is observed only in the VZ. The uRL generates cerebellar glutamatergic neurons, while the VZ generates GABAergic neurons and glia.

I.2.2.1 Temporal origin of uRL derivatives

As stated above, starting from E9.5 the uRL (but also the IRL) territory is marked by the expression of *Atoh1*. Microscopy studies have shown that at later stages, the uRL becomes progressively spatially compartmentalized (Yeung et al., 2014). Indeed, by E13, *Atoh1* expression becomes slightly reduced at the interior face of the uRL, where neuron progenitors initiate to express the multipass transmembrane protein Wntless. The exterior face of the uRL instead continues to produce high levels of *Atoh1* and its transcriptional target Paired box 6 (*Pax6*). By E15, the separation between these two faces of the uRL becomes even more defined, when a thin layer of *Lmx1a*-expressing cells appears between them. However, the functional role of this regionalization is still poorly known, although it is likely that different uRL zones may give rise to different populations of uRL derivatives (Chizhikov et al., 2010; Yeung et al., 2014, 2016).

Conversely, much better characterized is the temporal pattern of neuronal subtype specification in the uRL from E9.5 onwards (**Figure VI**). Here, the use of various mouse models, including those expressing the inducible *CreER* recombinase under the control of *Atoh1* regulative regions, were useful for transiently or permanently tracing the fate of all *Atoh1*⁺ uRL precursors (Machold and Fishell, 2005; Wang et al., 2005). From these studies, it was found that the first subset of cerebellar glutamatergic neurons generated in the uRL are those eventually populating the DCN (together with the previously mentioned neurons of the pre-cerebellar pontine nuclei). Upon specification, these neuron precursors rapidly downregulate *Atoh1* and leave the uRL moving anteriorly and laterally along the cerebellar surface producing the so-called rostral RL migratory stream (RLS). Around E12.5, most of these migrating neurons cluster in a region at the anterior margin of the cerebellum named nuclear transitory zone (NTZ), which represents a primordium of the DCN (**Figure VI**).

Only subsequently, from E12.5 to E17, a second, distinct wave of fate-specification generates GN-committed cells. The GN progenitors (GNPs) here specified also take part to the RLS (sometimes referred as a "late" RLS), but differently from the "early" RLS precursors they maintain *Atoh1* expression and transitorily crowd on the cerebellar surface forming a mitotically active region denominated external granular layer (EGL). Here, GNPs first massively expand clonally and only after birth they gradually exit the cell cycle and migrate radially toward the IGL, where they complete their differentiation to GNs (**Figure VI**).

The last glutamatergic neuronal type generated within the uRL are the UBCs progenitors, which appear in the uRL concomitantly with GNPs, between E15.5 and E17.5 (Englund et al., 2006;

Sekerková et al., 2004). By birth, differentiating UBCs delaminate from the uRL, migrate through the immature cerebellar white matter and reach their final localization in the developing IGL of the prospective posteriormost cerebellar lobes.

Therefore, at least two, main, temporally distinct phases of neurogenesis take place in the uRL, with E12.5 roughly representing the temporal border between them.

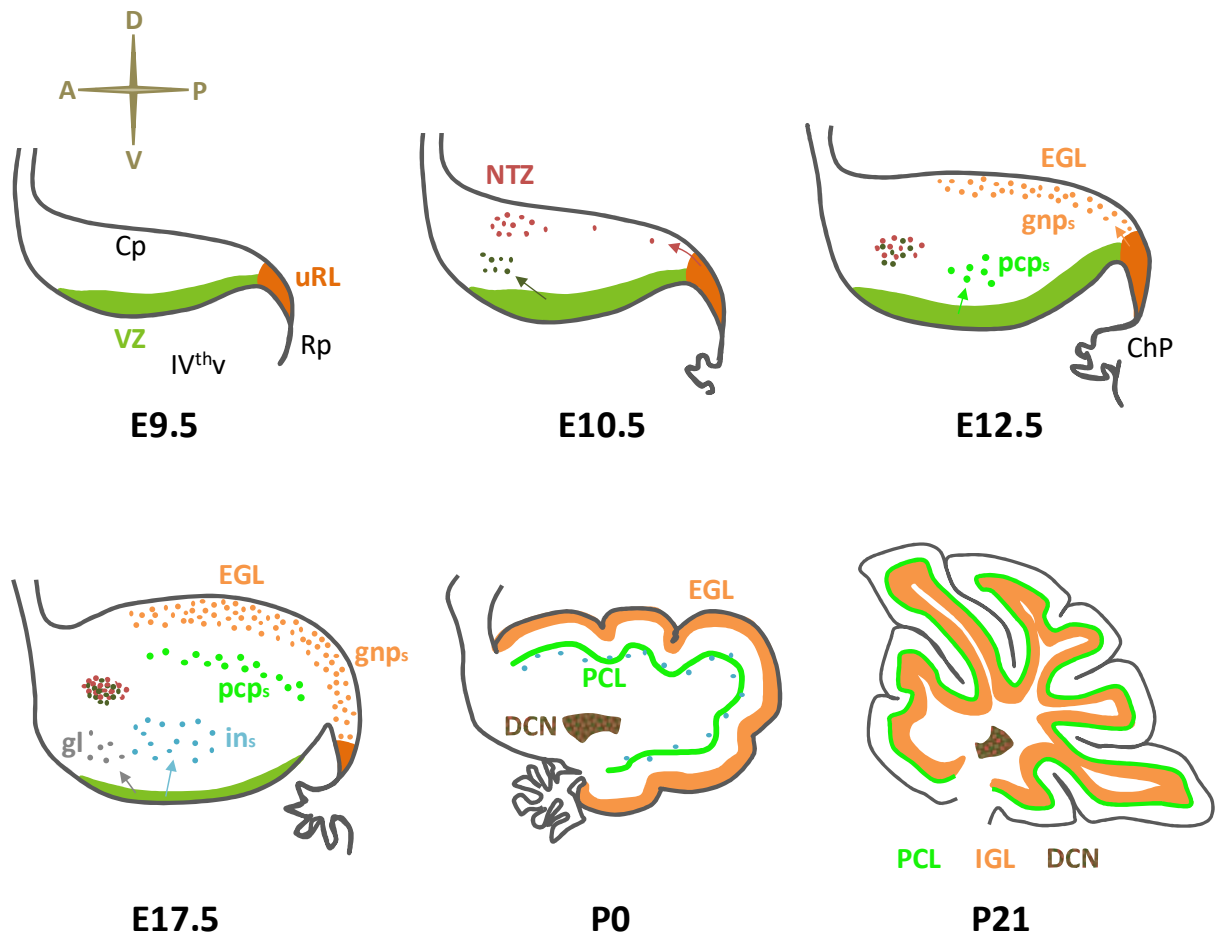


Figure VI. Sequential phases of embryonic and post-natal cerebellar development. Sagittal section of the dorsal r1 at progressive time-points during mouse development. By E9.5, the prospective cerebellum (Cp) is specified and the two germinal zones, namely the uRL and the VZ, appear. By E10.5, the uRL generates precursors of the glutamatergic DCN that crowd anteriorly in the cerebellum in the NTZ (red cells); simultaneously, the VZ produces the small GABAergic interneurons of the DCN (dark green cells). At E12.5, the uRL ceases to generate DCN neurons, and switches to GNPs (gnp_s in the picture) that initiate to populate the EGL; the VZ is instead actively forming PC precursors (pcp_s) since already 24 hours; the roofplate (Rp) is differentiating into the choroid plexus (ChP). At E17.5, the PC precursors initiate to arrange in the PCL, while the VZ produces cortical interneurons (ins) and glial cells (gl); the GNPs initiate to massively proliferate in the EGL. By birth (P0), the PCL is formed and the NTZ has differentiated to DCN. The GNPs in the EGL are actively expanding and as a result the cerebellar lobes begin to be shaped; in the following days GNPs will progressively terminally differentiate and migrate inward to populate the IGL. By three weeks after birth (P21), the cerebellar development is completed; all GNPs have differentiated to GNs and have reached the IGL below the PCL. (IVthv: IVth ventricle).

Interestingly, lineage tracing studies performed by Machold and Fishell (2005) demonstrated that all the *Atoh1*⁺ precursors present in the uRL at E10.5 had completely left this compartment via the RLS by E12.5. Nevertheless, *Atoh1*⁺ cells are still observed in the uRL at E12.5. This fact suggests that *Atoh1* expression is continuously *de novo* induced in the naïve neuron progenitors appearing or arriving in the uRL after departure of the earlier specified precursors. Interestingly, this hypothesis is consistent with the evidence that diffusible signals as Bone Morphogenetic Protein 7 (BMP7), secreted by the roof plate and its derivative, the choroid plexus, seem required for continuous *Atoh1* induction in the uRL (Alder et al., 1999; Chizhikov et al., 2006; Fernandes et al., 2012; Machold et al., 2007; Qin et al., 2006; Tong and Kwan, 2013).

Finally, how intrinsic and extrinsic cues temporally orchestrate lineage commitment of the uRL precursors remains puzzling. A potential role may be played by the BMP signaling itself, as variable temporal gradients of BMPs ligands could differentially instruct uRL cells about their fate (Tong et al., 2015). In this context, a fine modulation of such developmental program may be offered by the Notch1 signaling, which has been shown to contrast the activation of some BMPs responsive genes in the cerebellar anlage (Machold et al., 2007).

1.2.3 GNPs: TANGENTIAL MIGRATION FROM THE URL TO THE EGL

After specification, GNPs leave the uRL via the late RLS by moving tangentially and anteriorly over the dorsal surface of the cerebellar anlage, below the meninges, to form a new, transient germinal region, the EGL (Hatten and Heintz, 1995; Wingate and Hatten, 1999). At this stage GNPs are marked by expression of transcription factors as *Atoh1*, *Pax6*, the zinc finger protein *Zic1* and BarH-like 1 homeobox protein (*Barhl1*) (Rahimi-Balaei et al., 2018). Pioneer studies using chick embryos clearly showed that the anterior migratory route followed by GNPs is absent of any significant shift or deviation along the medio-lateral axis. Because of that, the medio-lateral position occupied by GNPs in the EGL corresponds to their original medio-lateral location in the uRL (Ryder and Cepko, 1994). In addition, also the timing of formation affects GNPs terminal position in the EGL: early specified GNPs move more rostrally compared to late ones, hence prospectively populating the anteriormost cerebellar lobules (Ryder and Cepko, 1994).

As it is typical of migrating neuron progenitors, also GNPs adopt a unipolar shape during their migration, extending a short cytoplasmic protrusion, called the leading process, toward the direction of movement. The leading process is believed to explore the territory, responding to attractive or repellent signals in the environment. Interestingly, while migration of neurons in the developing CNS is normally guided by glial fibers or neuron axons, the rostral migration of GNPs away from the uRL seems to be independent of these substrates. Rather, GNPs seem to form homotypic interactions between them resulting in the appearance of chain-like trails when leaving the uRL (Rieger et al., 2009). Another peculiarity of GNPs rostral migration is its saltatory pattern, which is characterized by relatively long pauses alternated to rapid forward twitches (Gilthorpe et al., 2002).

A number of extracellular signals and cell autonomous mechanisms regulate the tangential migration of GNPs at this stage.

Among them, the cell adhesion transmembrane protein N-Cadherin is required for polarizing GNPs during their path toward the EGL and for enabling the formation of their homotypic interactions (Rieger et al., 2009).

The secreted proteins Slit Guidance Ligand 1 and 2 (Slit1/2) produced in the uRL instead work as repellent cues for GNPs, inducing their departure from the uRL via binding to the Roundabout guidance receptors 1 and 2 (Robo1/2) (Gilthorpe et al., 2002; Marillat et al., 2002; Yuan et al., 1999).

On the contrary, the chemokine Stromal cell-derived factor 1 α (SDF-1 α) secreted by the dorsal meninges represents the major attractive signal for GNPs to the EGL (Zhu et al., 2002).

Finally, Netrin-1 is a secreted ligand generally implicated in migration and axon guidance, acting either as an attractive or a repellent signal depending on the surface receptor expressed by the responding cells (Lai Wing Sun et al., 2011). While Netrin-1 secreted by the hindbrain's floorplate is known to ventrally attract the prospective pontine and medullar neurons leaving the IRL (Gilthorpe et al., 2002; Serafini et al., 1996; Yung et al., 2018), its role in GNPs is less clear. Mutant mice for the Netrin-1 receptor *Unc5c*, which mediates a repellent activity of Netrin-1, display expanded migration of GNPs over the cerebellar surface with invasion of midbrain territories (Przyborski et al., 1998). This led to the initial hypothesis that Netrin-1 could exclude GNPs from migrating to undesired territories, as those outside the EGL. Nevertheless, no major cerebellar defects are observed in *Netrin-1* knockout (KO) mice by birth and direct administration of Netrin-1 does not influence the migration direction of uRL GNPs *in vitro* or *in vivo* (Alcantara et al., 2000; Bloch-Gallego et al., 1999; Gilthorpe et al., 2002).

Conversely, Netrin-1 expression is upregulated in the post-natal EGL and according to *in vitro* studies at this stage it would stimulate GNP's final radial migration to the IGL (Alcantara et al., 2000). Therefore, the influence of Netrin-1 on GNP's migration appears to be age dependent.

1.2.4 GNPs: FROM PROLIFERATION TO TERMINAL DIFFERENTIATION

1.2.4.1 Brief overview of the whole process

Once reached the EGL, GNPs undergo a phase of massive proliferation which accounts for the enormous number of mature GNs in the adult cerebellum. In mice, this clonal expansion initiates as soon as the first GNPs get to the EGL (around E13) and peaks around post-natal day (P) 7, the time at which the EGL thickens the most (Pons et al., 2001). However, after birth this exponential growth becomes increasingly counteracted by a progressive wave of cell cycle exit that will eventually convert all the dividing GNPs into post-mitotic cells by the end of the third post-natal week (Hanaway, 1967; Miale and Sidman, 1961). Once post-mitotic, GNPs slide below the still dividing progenitors, hence splitting the EGL into two sub-layers: the outer EGL (oEGL) containing the still mitotically active GNPs and the inner EGL (iEGL) constituted by their differentiating derivatives. Within the iEGL, post-mitotic GNPs undergo tangential migration that results in the extension of two long processes at the opposite poles of their somata. These processes will later mature into their axons, the parallel fibers in the ML. Finally, the somata of differentiating GNs leaves the iEGL descending radially through the immature ML and the PCL to reach their final localization, the IGL. While descending, GNs produce a new leading process oriented inward in the cerebellum. This new process extends perpendicular to the two previously generated, therefore forming the characteristic "T-shaped" parallel fiber. Once located in the IGL, GNs complete their maturation forming the synaptic connections with MFs terminals. The whole process is illustrated in **Figure VII**.

1.2.3.2 Proliferation and differentiation of GNPs at the histological level

During the last 25 years several lineage tracing experiments helped to dissect the fate of GNPs in the EGL.

One of the first fundamental and not obvious observation was that GNPs seem to be unipotent progenitors, hence irreversibly committed to become GNs (Zhang and Goldman, 1996a, 1996b).

Although this observation has always been confirmed *in vivo*, it was shown that treatment of primary GNPs with BMP2 *in vitro* can twist their fate toward the astrocyte lineage (Okano-Uchida et al., 2004). Whether this property is the result of artifacts of the culturing system or it is biologically relevant also *in vivo* under certain circumstances, remains unknown.

Another important property of GNPs is that they only undergo symmetrical divisions in the EGL. In other words, a single GNP undergoing mitosis generates two identical cells which will either both re-enter the cell cycle, or both differentiate (Espinosa and Luo, 2008; Nakashima et al., 2015). Thanks to this peculiarity, GNPs pool expansion follows an exponential curve, with each single GNP generating a progeny with a median of 250 cells from E17.5 to P21 (Espinosa and Luo, 2008).

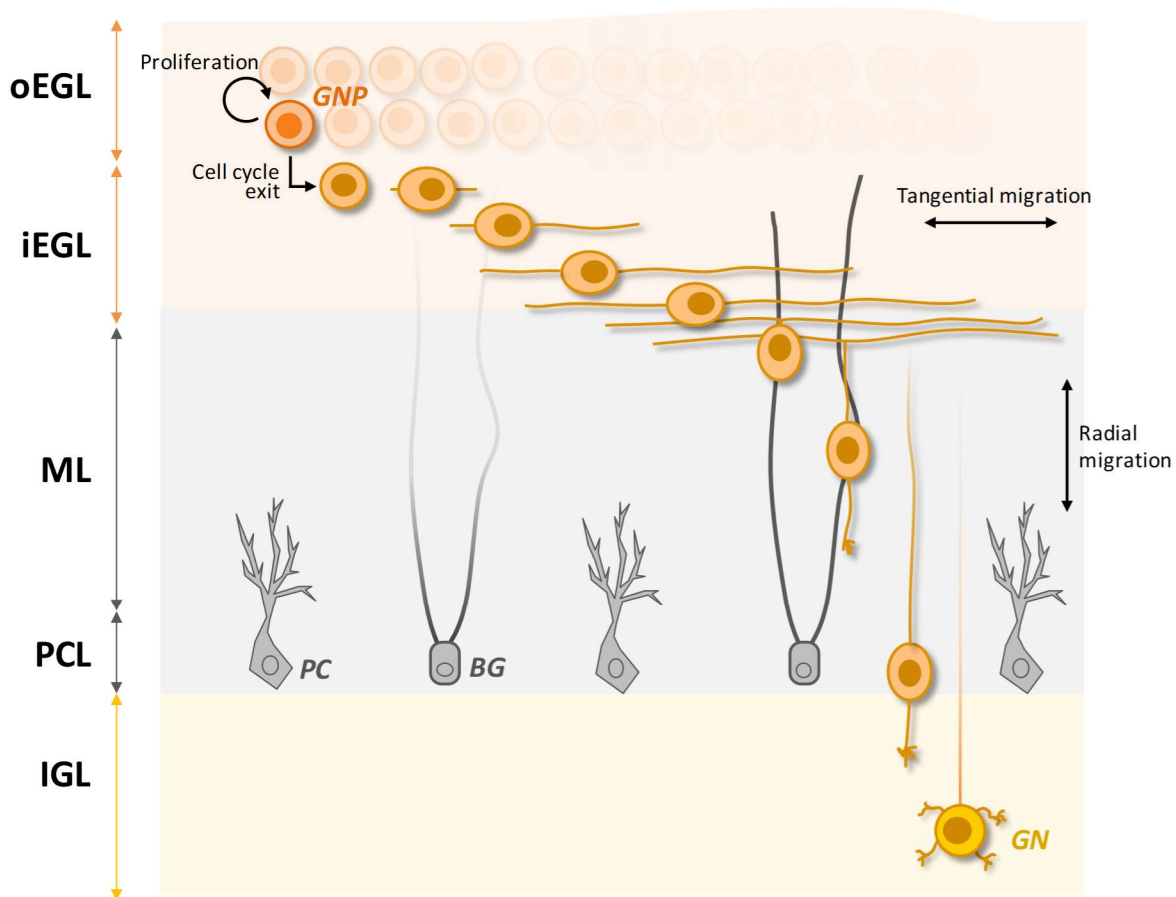


Figure VII. Developmental phases of GNPs in post-natal times. After the last division in the oEGL, GNPs exit the cell cycle and slide below forming the iEGL. Within the iEGL, GNPs migrate tangentially extending a leading and a trailing process that ultimately differentiate into the parallel fibers composing the ML (at this stage still immature). Subsequently, a third, perpendicular process is elongated inward in the cerebellum and the somata initiate to move along it. The fibers of the Bergmann Glia cells (BG) are utilized as substrate along which the radial migration proceeds. Migrating GNs reach the PCL, which hosts the PCs and BG cell bodies. From here, they will move to the IGL where they will terminate their differentiation to mature GNs. oEGL: outer external granule layer, iEGL: inner external granule layer, ML: molecular layer, PCL: Purkinje cells layer, IGL: internal granule layer, PC: Purkinje cell.

Interestingly, clonal pools of GNPs tend to exit the cell cycle synchronously and will also project their parallel fibers within the same sub-layer of the ML (Espinosa and Luo, 2008; Zong et al., 2005). In addition, while early born GNPs generally send their parallel fibers in deeper sub-layers of the ML, late born ones do it in upper sub-layers (Espinosa and Luo, 2008). This uneven spatio-temporal pattern of GN neurogenesis is likely to reflect precise requirements for proper wiring of cerebellar circuitries at later developmental stages. However, the actual nature of these requirements is still puzzling.

1.2.4.3 Discovery of SHH as the main mitogen for GNPs

During CNS development, various cell autonomous and non-cell autonomous mechanisms temporally and spatially control the expansion of neuron progenitors.

Aimed at dissecting these actors for GNPs proliferation in the EGL, the earliest works focused on a series of growth factors that were previously shown to mitotically activate other neuron progenitors in the developing brain. Thanks to these initial studies, it was shown that GNPs proliferation was elicited by Epidermal growth factor (Egf), Fibroblast growth factors (Fgf) and Insulin-like growth factors (Igf), all molecules produced in the developing cerebellum (Gao et al., 1991; Lin and Bulleit, 1997; Tao et al., 1996; Ye et al., 1996).

However, only from the end of the '90s it became clear that the most powerful signal driving GNPs divisions is Sonic Hedgehog (SHH), a secreted ligand produced by the PCs, which are arranging in the PCL at the time of EGL formation.

The first evidence of this regulation came from the fact that mutations in SHH pathway components were systematically found in certain types of medulloblastomas (MBs) malignant pediatric tumors arising from the developing cerebellum² (Goodrich et al., 1997; Pietsch et al., 1997; Raffel et al., 1997; Vorechovský et al., 1997). This suggested that SHH could act as a mitogen for some population of cerebellar neurons. Second, *in situ* hybridization revealed that a source of SHH in the cerebellum are the PCs (Wechsler-Reya and Scott, 1999). Very interestingly, it was previously shown that the selective ablation of PCs lineage, dramatically impaired GNPs pool expansion in the EGL, indicating that somehow PCs were required for GNPs proliferation (Smeyne et al., 1995). Therefore, the effects of the putative mitogen SHH were tested in primary GNPs cultures and, strikingly, it was found that it was capable of potently stimulating GNPs divisions (Dahmane and Ruiz-i-Altaba, 1999; Lewis et al., 2004; Wechsler-

² Nowadays, these types of MBs are referred as SHH-MBs, and GNPs are known to be their cell of origin. MB will be described in Chapter 1.3.

Reya and Scott, 1999). Finally, when all these observations were integrated with the confirmation that GNPs in the EGL express various transcriptional targets of SHH and that the blockade of SHH activity by anti-SHH antibodies impaired GNPs proliferation in cerebellar slices, it became clear that SHH functions as the main mitogen for GNPs (Dahmane and Ruiz-i-Altaba, 1999; Wallace, 1999; Wechsler-Reya and Scott, 1999).

Interestingly, SHH is expressed by PCs with a precise spatio-temporal pattern (Lewis et al., 2004). It is only after E17.5 that *Shh* is significantly up-regulated by PCs, and this is associated with concomitant activation of SHH targets in the overlying GNPs. In addition, SHH seems to be higher expressed by PCs occupying the anterior lobes compare to those in the posterior ones. A direct consequence is the uneven intensity of SHH signaling experienced by GNPs in the EGL along the anteroposterior axis. Such effect may be important for regulating the complexity of cortical foliation, which is in large part dependent on the extent of GNPs expansion (Corrales et al., 2004, 2006).

1.2.4.4 SHH boosts GNPs expansion by acting on the cell cycle machinery

The SHH signaling will be thoroughly described in Chapter **1.4**, while here only a brief overview will be presented.

The SHH pathway in GNPs is activated when SHH binds and inactivates the plasma membrane receptor Patched homolog 1 (Ptch1), thereby relieving its inhibition on the G-protein coupled receptor (GPCR) Smoothed (Smo). This event initiates a signaling cascade which primarily culminates with the activation of the zinc-finger protein Glioma-associated oncogene 2 (Gli2), the main transcriptional effector of SHH in GNPs. Activation of Gli2 is counteracted by a Gli2-binding partner, called Suppressor of Fused (SuFu). In addition, Gli2 activates the expression of its paralog Gli1, which further amplifies the SHH transcriptional response in GNPs (Corrales et al., 2004) (**Figure VIII**).

The SHH-driven proliferation of GNPs is achieved through various mechanisms, among which the regulation of the cell cycle G1/S checkpoint is crucial. Indeed, activation of SHH signaling in GNPs potently induces the upregulation of N-myc proto-oncogene (Mycn) protein which in turn activates the transcription of Cyclin D1 and Cyclin D2 (Ciemerych et al., 2002; Huard et al., 1999; Kenney and Rowitch, 2000; Kenney et al., 2003; Knoepfler et al., 2002; Ma et al., 2015). Accumulation of D-type Cyclins in the G1 phase is critical for cells to cross the G1/S restriction point. Indeed, D-type Cyclins bind and activate Cyclin dependent kinases as CDK4/6 which initiate the phosphorylation-dependent inhibition of Retinoblastoma-associated protein 1

(Rb1). This event liberates the E2F1 transcription factor from Rb1 inhibition, enabling it to activate the DNA replication genes required during the S phase.

In addition, SHH indirectly controls also the G2/M transition of the cell cycle. GNP treated with SHH show upregulation of the transcription factor Forkhead box protein M1 (FoxM1), although this regulation seems not to be direct. FoxM1 regulates mitotic entry and correct chromosome segregation and these functions are at least in part achieved via the transcriptional regulation of Cyclin B1 and the M-phase inducer phosphatase Cdc25b (Schüller et al., 2007). Another key mediator of the SHH-induced proliferation of GNPs is Bmi1, a fundamental component of the Polycomb Repressive Complex 1 (PRC1). PRC1 maintains the repression of large panels of genes via epigenetic regulation. Pieces of evidence reported that *Bmi1* is a SHH target and Bmi1 in GNPs negatively regulates the expression of various cell cycle inhibitors, including p21^{Cip1} (Leung et al., 2004; Subkhankulova et al., 2010). Therefore, SHH acts through Bmi1 in the PRC1 complex to repress genes that would otherwise promote GNPs cell cycle withdrawal.

Finally, although the topic will be deeply presented in chapter **I.6** and it is also dissected in the **Results** session of this Thesis, it is here important to mention that SHH signaling also promotes stabilization of Atoh1 protein in GNPs (Forget et al., 2014). This regulation is crucial because at this stage of development Atoh1 is somehow able to maintain GNPs into a SHH-responsive state (Ayrault et al., 2010; Flora et al., 2009; Forget et al., 2014). This interplay between SHH and Atoh1 generates a key positive feedback loop that contributes to the expansion of GNPs in the post-natal cerebellum.

I.2.4.4 Synergy and interplay with SHH during GNPs expansion

Being SHH the central mitogen of GNPs, it is not surprising that a number of other extracellular or intracellular cues synergize with it to further regulate the proliferation of GNPs in the oEGL. Some of them are here below described and illustrated in **Figure VIII**.

I.2.4.4.1 *SDF-1 α*

Besides working as chemoattractant to the EGL for GNPs, SDF-1 α was also shown to collaborate with SHH for GNPs proliferation. Indeed, while SDF-1 α alone does not stimulate GNPs proliferation, when it is added in combination to SHH, GNPs proliferation is synergistically enhanced. Mechanistically, it was proposed that by binding to the GPCR C-X-C chemokine receptor type 4 (Crx4), SDF-1 α causes a reduction of cAMP production that

eventually inactivates Protein Kinase A (PKA), a potent antagonist of SHH signaling (Klein et al. 2001) (**Figure VIII**).

1.2.4.4.2 *Igf-II*

In the developing cerebellum, *Igf2* transcripts can be detected in the meninges, in the choroid plexus and blood vessels (Corcoran et al., 2008; Hartmann et al., 2005). Interestingly, although Igf-II exerts a small, standalone positive effect on GNPs proliferation, its activity is synergistically enhanced in presence of SHH. It was proposed that this response may be mediated through activation of Phosphatidylinositol 3-Kinases (PI3K), which, as described shortly, supports SHH response (Dudek et al., 1997; Hartmann et al., 2005) (**Figure VIII**).

Interestingly this apparent role of Igf-II during normal GNs development, seems to be conserved in SHH-MB, as the KO of *Igf2* abolishes progression of SHH-MB in genetic mouse models (Corcoran et al., 2008; Hahn et al., 2000).

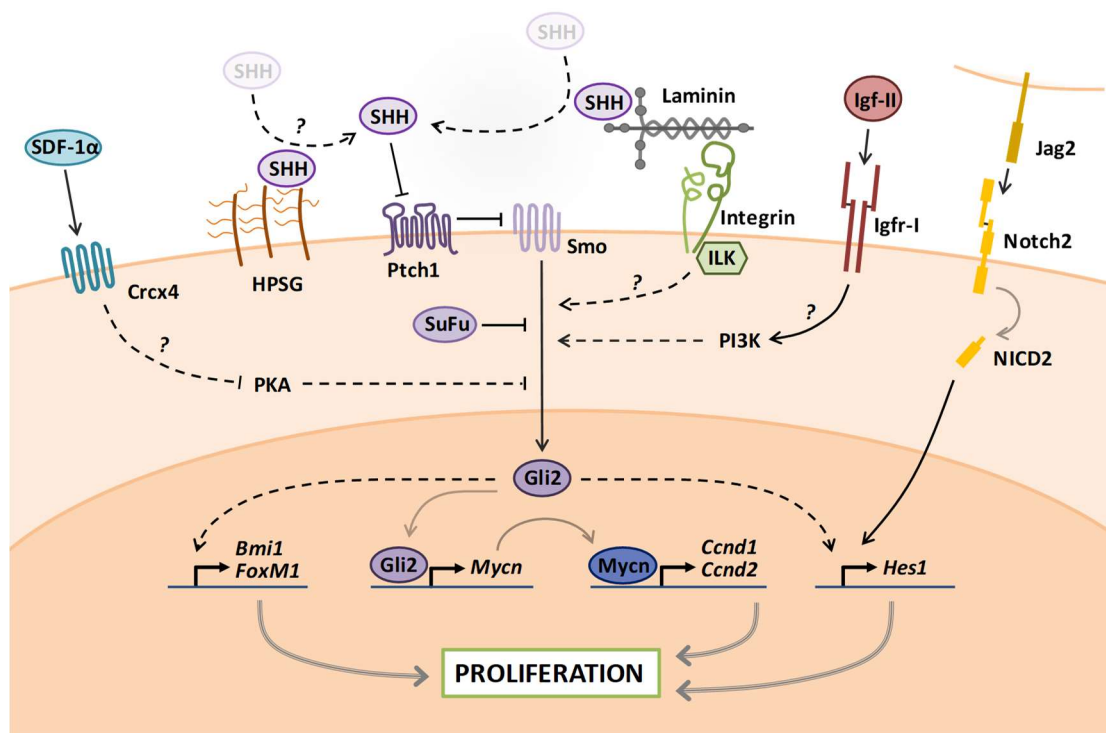


Figure VIII. Pro-proliferative pathways active in GNPs in the EGL. Gapped arrows indicate (supposed) indirect mechanisms, in contrast to continuous arrows which mark direct mechanisms. Question marks next to the arrows highlight uncertainty of the pathway. The SHH signaling, relayed through inhibition of Ptch1 by SHH and consequent activation of Smo and Gli2 is the major driver of GNPs proliferation. SuFu mainly acts as a negative regulator of Gli2 activation. Gli2 target genes include *Bmi1*, *FoxM1*, *Hes1* and *Mycn*, the latter controlling Cyclin D encoding genes (*Ccnd1/2*). SHH binding to Ptch1 may be helped by interaction with HPSGs and laminin. Laminin may also activate integrin receptors and promote SHH signaling via ILK activation. SDF1- α binds to Crcx4 and sustains SHH signaling perhaps via inhibition of PKA. Igf-II binds to the receptor Igfr-I and may lead to activation of PI3K, which promotes SHH signaling. Notch2 activation by Jag2 on adjacent GNPs, leads to transcription of *Hes1* in collaboration with SHH.

I.2.4.4.3 Heparan sulfate proteoglycans

Heparan sulfate proteoglycans (HSPGs) are a class of membrane-associated or secreted glycoproteins characterized by one or multiple covalently linked chains of heparan sulfate. During CNS development, HSPGs are involved in a number of cellular processes including proliferation, differentiation, migration and synapses formation. In post-natal GNP, expression of various types of HSPGs, including the members of syndecan and glypican families fluctuates during the first post-natal week (Araujo et al., 2010).

It was shown that HSPGs can interact with SHH, enhancing its pro-proliferative activity in GNP (Chan et al., 2009; Pons et al., 2001; Rubin et al., 2002) (**Figure VIII**). In addition, it was proposed that expression of specific HSPGs in the EGL defines a "GNP proliferative niche" where SHH concentrates and spatio-temporally confines its activity (Chan et al., 2009). However, the specific identity of these HSPGs and the exact molecular mechanism through which they promote SHH-mitogenic activity in GNP remain unknown.

I.2.4.4.4 Laminin-integrin signaling

Extracellular matrix (ECM) proteins participate to developmental processes including proliferation, differentiation and survival, through direct signaling to cells or by modulating the availability of morphogens and growth factors. Therefore, the different composition of the ECM in various territories of a developing organ is key for spatially restricting specific cell behaviors. *In vitro* assays demonstrated that GNP grown on laminin-coated plastic supports display enhanced proliferative response to SHH (Pons et al., 2001).

Immunostaining experiments revealed that laminins are broadly expressed in the developing cerebellum, but accumulate in the oEGL beneath the meninges. Consistently, proliferative GNP express the main laminin receptors, namely the $\alpha_6\beta_1$ and $\alpha_7\beta_1$ integrin heterodimers, which were shown to be required for GNP expansion *in vivo* (Blaess et al., 2004; Pons et al., 2001). How does the laminin-integrin interaction promote GNP proliferation in response to SHH? Importantly, some laminin are capable of binding SHH. Therefore it was suggested that the mere recruitment of laminin-SHH complexes to the cell surface by integrins may facilitate SHH binding to Ptch1 (Blaess et al., 2004). In addition, Mills and colleagues (2006) discovered that the interaction of β_1 integrin subunit with the cytoplasmic Integrin linked kinase (ILK) mediates its proliferative role in GNP. Hence, the laminin-integrin complex may also signal through ILK to modulate SHH response in GNP (**Figure VIII**).

I.2.4.4.5 *Notch2-Hes1* signaling

One histological feature of the early post-natal cerebellum is the tight crowding of GNPs in the EGL. GNPs are in strict contact to each other and can form homotypic interactions which were shown to cell autonomously stimulate their proliferation *in vitro* (Gao et al., 1991). A key signaling pathway whose activation relies on cell-to-cell vicinity is the Notch signaling, whose role in neurogenesis, especially in maintenance of stem-like or progenitor-like phenotypes in neural cells, is well documented.

Briefly, upon cell-to-cell apposition, the Notch receptors (Notch1 up to 4 in vertebrates) at the plasma membrane interact with their ligands Delta-like or Jagged localized at the surface of adjacent cells. Binding of Notch with its ligand triggers the proteolytic cleavage of the intracellular portion of Notch receptor (NICD, Notch intracellular domain). Once free in the cytoplasm, cleaved NICD leaves the plasma membrane to enter the nucleus. Here, in combination with the transcriptional co-activator Rbpj, NICD activates the expression of a panel of genes, among which the bHLH transcriptional repressor Hairy and Enhancer of split-1 and -5 (*Hes1/5*) (**Figure VIII**).

Notch2 is expressed in proliferative GNPs of the EGL, while it is downregulated upon differentiation concomitantly with the upregulation of *Notch1* (Solecki et al., 2001). Therefore, Notch proteins are differentially expressed during post-natal GN development. While little is known about the role of Notch1 signaling in GNPs, more details have emerged for Notch2. Specifically, activation of Notch2 pathway, either through overexpression of NICD2 (NICD of the Notch2 receptor), binding of its ligand Jagged-2 (*Jag-2*) or overexpression of its major target *Hes1* is sufficient to maintain GNPs in a proliferative state, blocking their differentiation (Solecki et al., 2001). In addition, Notch2 expression is typically found elevated in SHH-MB pinpointing a role in regulating the proliferation of tumor cells (Fan et al., 2004; Hallahan et al., 2004).

Nevertheless, Julian and colleagues (2010) strikingly reported that *Rbpj* deletion in the cerebellum does not significantly affect post-natal GNs development. This observation seems to contrast the results described above and opens to the possibility that Notch2 could signal through *Rbpj*-independent, non-canonical pathways in GNPs, as previously shown in other neuronal lineages (Mizutani et al., 2007). Alternatively, it is known that SHH can upregulate *Hes1* expression; therefore the SHH signaling could partially compensate for an impaired, *Rbpj*-deficient Notch2 signaling cascade (Julian et al., 2010; Solecki et al., 2001).

I.2.4.5 Mechanisms controlling cell cycle exit and differentiation of GNPs

All the pathways described above are essential for achieving the enormous number of GNPs that populate the adult cerebellum. Besides, tight regulation of cell cycle exit is equally important, as disruption of the ability of GNPs to terminally differentiate may lead to tumorigenesis (e.g. SHH-MB).

Cell cycle exit of GNPs is typically marked by downregulation of SHH target transcripts and *Atoh1* as well as by upregulation of cell cycle inhibitors as *p27^{Kip1}*, differentiation factors as Neurogenic differentiation factor 1 (*NeuroD1*) and neuronal maturation markers as the Neuronal nuclei antigen (*NeuN*) (Aruga et al., 1994; Ben-Arie et al., 1997; Corrales et al., 2004; Miyazawa et al., 2000; Pan et al., 2009; Weyer and Schilling, 2003).

Several pathways are at play to promote GNPs cell cycle exit and not surprisingly many of them provide a negative regulation of the SHH pathway or its pro-proliferative targets. Some of them are described in the next paragraphs and depicted in **Figure IX**.

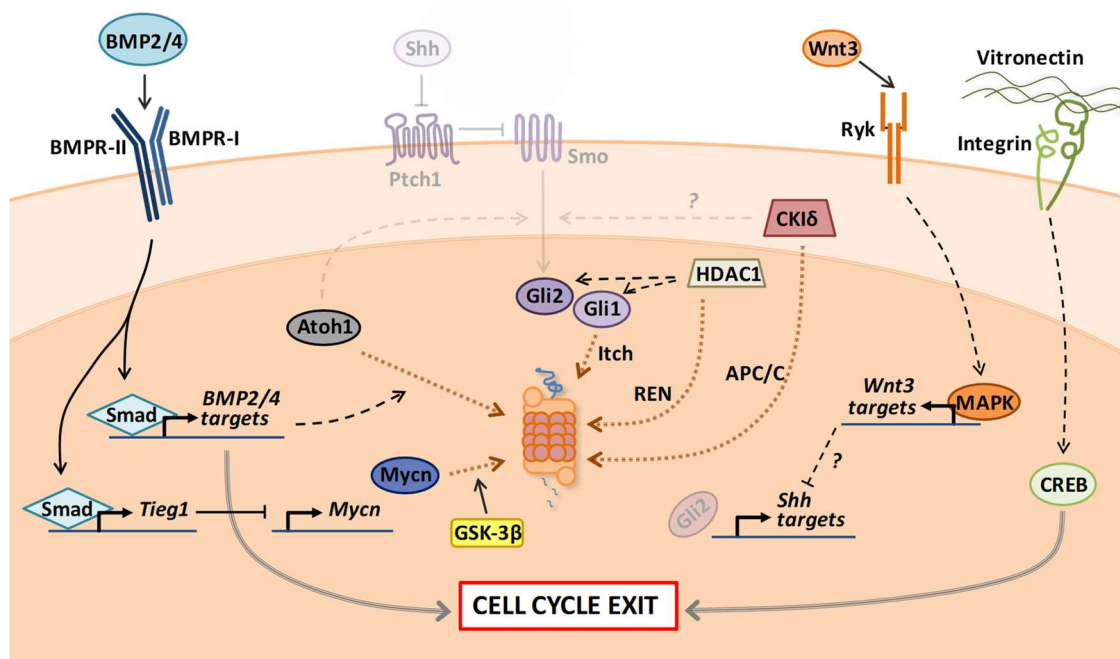


Figure IX. Anti-proliferative pathways triggering terminal differentiation of GNPs. Gapped arrows indicate indirect or supposed indirect mechanisms, in contrast to continuous arrows which mark direct mechanisms. Question marks next to the arrows highlight uncertainty of the pathway. When arrows or proteins are shadowed it means that the pathway is switching off in differentiating GNPs. BMP2/4 signal through its receptors to activate Smad proteins. BMP/Smad transcriptional targets may activate a general differentiation program in GNPs (grey arrow to CELL CYCLE EXIT) which also includes (i) repression of *Mycn* transcription via *Tieg1* and (ii) degradation of *Atoh1*. *Mycn* is also targeted to proteasomal degradation after GSK-3 β -dependent phosphorylation. In addition, *Gli1* is degraded after polyubiquitination by *Itch*, while *CKI δ* which may regulate multiple aspects of GNPs proliferation (perhaps the SHH signaling) is degraded through APC/C^{Cdh1} activity. Also HDAC1, which increases *Gli2* transcriptional activity is sent to the proteasome by REN^{KCTD11}-mediated polyubiquitination. Wnt3 stimulates a non-canonical signaling via binding to Ryk receptors and activation of MAPKs which culminates in repression of SHH pro-proliferative targets. Integrins bind vitronectin in the ECM of the iEGL and lead to CREB activation, which promotes GNPs cell cycle exit and differentiation.

I.2.4.5.1 *Non canonical Wnt3 signaling*

By acting through a non-canonical, β -catenin-independent pathway, Wnt3 was shown to directly downregulate the expression of a subset of key SHH target genes as well as *Atoh1* in GNP. Such Wnt3-mediated anti-proliferative activity relies on the activation of a Mitogen-activated protein kinase (MAPK) cascade triggered by the binding of Wnt3 to Tyrosine protein kinase receptors Ryk (Anne et al., 2013). The cerebellar source of Wnt3 was however not explored by the authors.

I.2.4.5.2 *BMP2 and BMP4 signaling*

The strong interplay between SHH and BMP proteins is widely appreciated in a large number of developmental instances. Consistently, GNP development is no exception as early works demonstrated that the BMP family members BMP4 and BMP2, which are expressed by the GNP themselves before and after cell cycle exit respectively, are potent inhibitors of SHH-dependent proliferation and inducers of differentiation in GNP (Anglely et al., 2003; Rios et al., 2004).

BMP proteins are secreted ligands that by engaging specific Serine-Threonine kinase membrane receptors lead to the phosphorylation of the transcriptional effectors Smad1/5/8. Phosphorylated Smad1/5/8 form complexes with their common partner, Smad4 and became able to enter the nucleus to regulate target gene expression. Although it was suggested that BMP2/4 signaling *per se* activates a defined gene expression program which contributes to GNP differentiation, some particular BMP2/4-triggered events prevent GNP to aberrantly over-proliferate in response to SHH (Álvarez-Rodríguez et al., 2007). Among them, BMP2/4 signaling was shown to destabilize *Atoh1* via the proteasome, hence strongly reducing GNP sensitivity to SHH (Zhao et al., 2008). In addition, BMP2 signaling leads to the expression of the transcription repressor *Tieg1*, which downregulates *Mycn* (Álvarez-Rodríguez et al., 2007). Interestingly, it was recently shown that the competence of GNP to BMP2/4 signaling seems to be provided by a key transcription factor, *Meis1*. Indeed, *Meis1* activates the expression of Smad1/5, and by doing that, it promotes cell cycle exit by making GNP capable of rapidly downregulating *Atoh1* and *Mycn* in response to BMP2/4 (Owa et al., 2018).

I.2.4.5.3 *Mycn protein degradation at mitosis*

Mycn is the principal mediator of SHH pro-proliferative effects in GNP, hence not surprisingly several pathways converge to its downregulation to induce cell cycle exit. One of them is the

above mentioned BMP2-Tieg1-Mycn axis. However, Mycn expression is also highly controlled at the post-translational level via the ubiquitin-proteasome system. By the end of each mitosis in GNPs, Mycn is phosphorylated on threonine-50 by the Glycogen synthase kinase-3 β (GSK-3 β) and consequently degraded in the proteasome (Kenney et al., 2004; Sjostrom et al., 2005). This mechanism is functional to eliminate all Mycn proteins at the end of every cell cycle in order to prevent an aberrant, SHH-independent cell cycle re-entry. It was also proven that GSK-3 β activity is inhibited by active PI3K signaling, which by consequence promotes Mycn stabilization (Kenney et al., 2004). Therefore, virtually all the pathways converging on PI3K activation, including integrin signaling (which can be also activated by cell-cell contact), SDF1- α or Igf-II may also ultimately lead to Mycn stabilization (Dudek et al., 1997).

I.2.4.5.4 Ubiquitin ligases

Proteins are targeted to degradation in the proteasome via covalent link of polyubiquitin chains by E3 ubiquitin-ligase enzymes (or E3s). Therefore, the expression or the activation of E3 enzymes represents an effective mechanism for depleting cells of specific proteins and consequently rapidly changing their behavior. As shown above for Mycn, also GNPs employ these strategies to transit from a proliferative to a differentiation state, as many pro-proliferative proteins are subjected to this type of regulation.

For example, Gli1 turnover is mediated (among the others) by the E3-ligase Itch, whose catalytic activity is enhanced by the adaptor protein Numb (Di Marcotullio et al., 2006a, 2011). In the post-natal cerebellum, Numb expression is restricted to differentiating GNPs of the iEGL, and its KO aberrantly maintains GNPs in proliferation (Klein et al., 2004). These results strongly prompt for a model in which onset of Numb expression triggers the rapid Itch-mediated Gli1 degradation and consequent reduction of the SHH-dependent pro-proliferative program. In addition, Gli1 and Gli2 proteins are subjected to numerous post-translational modifications (PTMs), including lysine acetylation which is known to reduce their transcriptional activity. Therefore, removal of acetyl groups from Gli1 and Gli2 by the Histone deacetylase 1 (HDAC1) supports the activation of SHH transcriptional program in GNPs. In the context of this regulation, the SCF-like E3 ubiquitin ligase complex constituted by Cullin3 and the BTB-containing adaptor protein REN^{KCTD11} targets HDAC1 to proteasomal destruction (Canettieri et al., 2010). Hence, REN^{KCTD11} expression in GNPs indirectly sustains Gli1 and Gli2 acetylation, consequently dampening proliferation (Canettieri et al., 2010; Gallo et al., 2002). Coherently,

the *REN* locus is found deleted in human SHH-MB where it acts as a tumor suppressor (Di Marcotullio et al., 2004).

Finally, the E3-ubiquitin ligase Anaphase Promoting Complex/Cyclosome bound to the activator Cdh1 (APC/C^{Cdh1}) is particularly active in post-mitotic neurons, where it prevents aberrant cell cycle re-entry by triggering the degradation of a number of proteins implicated in G1/S transition, including cyclins. Interestingly, besides these activities, APC/C^{Cdh1} was shown to recognize, bind and target to destruction the Casein kinase I δ (CKI δ) in GNPs (Penas et al., 2015). Although the mechanistic roles of CKI δ in GNPs development is unclear, CKI δ activity promotes GNPs proliferation in the EGL, while its inhibition leads to differentiation (Penas et al., 2015). Therefore, CKI δ appears to be a key substrate of APC/C^{Cdh1} for the onset and maintenance of GNs post-mitotic state.

I.2.4.5.5 Vitronectin

The hemopexin family member vitronectin is a secreted glycoprotein that was shown to decorate the extracellular matrix of the iEGL, the underneath immature ML and the IGL, all territories hosting differentiating or differentiated GNs (Pons et al., 2001). *In vitro* GNPs plated on vitronectin-coated supports show reduced proliferative response to SHH and enhanced differentiation rate, strongly suggesting that vitronectin distribution in the cerebellum may be functional at regulating GNs neurogenesis (Pons et al., 2001). Mechanistically, vitronectin was shown to enhance phosphorylation and consequent activation of the Cyclic AMP-responsive element-binding protein (CREB), whose transcriptional activity alone promotes differentiation of GNPs through a still unclear mechanism (Pons et al., 2001). Although it was not directly tested by Pons and colleagues, vitronectin may signal to CREB via binding to its main receptor, the integrin complex $\alpha_V\beta_3$, which is indeed expressed only by differentiating GNPs.

Therefore, changes in the environmental substrates on which GNs reside also exerts a role in their development.

I.2.4.6 Tangential migration and onset of parallel fibers formation

Once terminally exited the cell cycle, post-mitotic GNs initiate their journey toward the IGL, their final localization in the adult cerebellum (**Figure VII**). Time-lapse confocal imaging studies on mouse cerebellar slices unveiled incredible details of the behavior of migrating GNs (Komuro and Rakic, 1995, 1998; Komuro et al., 2001). Initially, early post-mitotic GNs slide in the iEGL, beneath the still cycling GNPs, where they will remain for 1 to 2 days. During this

time, major changes in their morphology occur. First, when GNs are still located in the upper part of the iEGL, their shape will transit from round (typical of a cycling progenitor) to a “spindle-like”, horizontal one. Concomitantly, GNs also adopt a unipolar morphology, by extruding a first, large and long process, usually referred as the leading process, characterized by a swollen lamellipodia at its tip. Subsequently, a second, shorter and thinner process (named trailing process), will arise at the other pole of the somata. The difference in size of the two extensions is likely to reflect their different function. Indeed, at this stage, GNs do not simply station in the iEGL, but they undergo tangential migration under the pial surface, along the medio-lateral axis. During this migration, the cell is highly polarized, and the movement direction corresponds to the one indicated by the leading process, which is supposed to explore the environment with its large lamellipodia, seeking for migratory cues. The rate of tangential migration slows down as the leading and the trailing processes lengthen and GNs are progressively displaced to the bottom of the iEGL. Here, sometimes, the migration direction of GNs may overturn, and this is preceded by a complete reorganization of the cell polarity (Komuro et al., 2001). Importantly, the leading and trailing process will eventually differentiate into the medio-lateral branches of GNs’ parallel fibers. These extensions indeed will eventually form synaptic connections with the dendritic trees of the PCs.

Although still much remains to be elucidated, molecular pathways regulating parallel fibers formation have emerged and some rely on the activity of the APC/C^{Cdh1} complex. APC/C^{Cdh1} regulates parallel fibers outgrowth by targeting to the proteasome a series of substrates. Among them, the transcriptional repressor proteins Id2 and SnoN are both important for promoting axon extension in GNs and their destruction via APC/C^{Cdh1} is required for restraining excessive axon overgrowth (Lasorella et al., 2006; Stegmüller et al., 2006, 2008).

1.2.4.7 Terminal radial migration toward the IGL

Once extended both horizontal branches of the parallel fibers, GNs localizing at the interface between the iEGL and the ML initiate to grow a third orthogonal process, oriented inward, toward the IGL (Komuro et al., 2001). This new extension becomes the new leading process for the GN radial migration to the IGL. Radial migration initiates when the whole GN cell somata translocates inside the leading process leaving behind a thin trailing process, orthogonally connected with the horizontal parallel fibers, which remain in the iEGL. The new leading and trailing processes will indeed eventually mature into the ascending branch of the parallel fibers (**Figure VII**).

The descent of GNs across the ML is guided by the fibers of the Bergmann glia cells, which at this stage act as migration substrate for the GNs (Rakic, 1971) (**Figure VII**). During this migratory phase, the somata of GNs modifies its shape and adopts a more vertically elongated outline. This shape changes again when GNs reach the PCL, where they pause for a couple of hours to detach from the Bergmann glia fibers and round up their cell body (Komuro and Rakic, 1998).

The following step of radial migration below the PCL is the conclusive one and will place GNs in their final position in the IGL. The whole journey of a post-mitotic GN from the EGL to the IGL takes in average 2 days in mice (Jiang et al., 2008).

Once again, many mechanisms direct the migration of GNs to the IGL. For instance, precise, timely-regulated patterns of calcium (Ca^{++}) influx in post-mitotic GNPs through the N-type Ca^{++} channels and NMDA-type glutamate receptors is key for initiation and progression of the GNs radial migration (Komuro and Rakic, 1992, 1993, 1996; Kumada and Komuro, 2004). Such Ca^{++} signaling may indeed promote actin cytoskeleton remodeling via activation of Protein kinase C (PKC) (Kumada et al., 2007).

Also the neurotrophin Brain-Derived Neurotrophic Factor (BDNF) seems to participate in the regulation of GNs migration. Various works demonstrated that there exists a gradient of BDNF in the developing cerebellar cortex, with higher levels in the IGL and lower concentration in the EGL (Rocamora et al., 1993; Zhou et al., 2007). Importantly, *Bdnf*KO mice show increased apoptosis of GNs and impaired radial migration, indicating that BDNF acts as a survival factor and, importantly, as an attractive signal for GNs to the IGL (Borghesani et al., 2002; Segal et al., 1992; Zhou et al., 2007)

Finally, mechanisms triggering GNs departure from the EGL also involve inhibition of signals that maintain them in this layer, as the chemoattractant SDF-1 α . This is the case of the reverse signaling activated by binding of Ephrin-B1 and B2 to their Eph receptor. Ephrin-B family ligands are surface proteins which normally signal via binding to their transmembrane Eph receptors upon cell-to-cell contact. However, ligand-to-receptor binding can trigger a reverse signal transduction also in the cells that express the Ephrin ligand. By P3, GNPs in the EGL express ephrin-B2 and its receptor EphB2. It was shown that the reverse signaling mediated by ephrin-B2 potently antagonizes SDF-1 α signal transduction (Lu et al., 2001). Consequently, ephrin-B2 stimulates GNs radial migration via blockade of SDF-1 α , the main EGL attractive cue (Lu et al., 2001).

Instructed by all these signals, GNs reach the IGL, where their development terminates with the formation of synapses with the MFs. All GNs localize in the IGL by the end of the third post-natal week in mice and by the second year of life in humans (Marzban et al., 2015).

1.3 Medulloblastoma

In the '20s, Drs. Harvey Cushing and Percival Bailey formally described for the first time a class of highly aggressive, fast-growing cerebellar tumors with characteristic histology consisting of small round, chromatin-rich nuclei surrounded by little cytoplasm. They named such tumors "medulloblastomas" after their assumption they had originated from "medulloblasts", one of the neural progenitor types believed to populate the developing brain at that time.

Since then, much progress has been made in the understanding of medulloblastoma. Today, the consensus view classifies medulloblastoma as a heterogeneous disease, comprising of at least four different major subgroups with distinct molecular features, incidence and clinicopathological outcomes. The first two subgroups are the better characterized and are named WNT and SHH medulloblastomas after the developmental signaling pathways whose deregulation is a key hallmark of these tumors. The other two are less understood in their biology and are generically named Group3 and Group4 medulloblastomas.

In this chapter the clinicopathological, biological and molecular characteristics of medulloblastoma are described, with higher emphasis put on the SHH-subgroup which originates from aberrant development of GNPs.

1.3.1 EPIDEMIOLOGY OF MEDULLOBLASTOMA

Medulloblastoma (MB) is an embryonic CNS malignant tumor arising within the posterior cranial fossa and representing the most common brain cancer of childhood. The incidence of MB indeed decreases with age and in the United States it is set to ~1 annual case per 250,000 individuals in children and adolescents (<19 years old), with the 1-4 and 5-9 years age-groups being the most exposed. Conversely, adults are only rarely diagnosed with MB, with ~1 annual case per 2 million individuals (Farwell and Flannery, 1987; Giordana et al., 1999; Ostrom et al., 2018). Consistently, between 70-80% of all MB cases are observed in children younger than 16 years old (Thomas and Noël, 2019). MB incidence is not uniform across genders, as males display between 1.5 and 2 times increased incidence compared to females, although variability

exists across MB subgroups (Johnston et al., 2014; Khanna et al., 2017; Northcott et al., 2019). No clear and evident differences of MB prevalence or incidence were reported across geographical or ethnical groups, even though inter-population-based epidemiological studies on MB are still scarce (Northcott et al., 2019).

The 5-years overall survival for MB patients who received current, risk-adapted therapy is ~70%, although marked differences are reported depending on MB clinicopathological risk class or molecular subgroups, as described later (Gajjar et al., 2006; Northcott et al., 2019). Hence, the outcome associated to MB is overall favorable; however, survivors frequently experience important life-long sequelae due to the aggressiveness and toxicity of current therapies, which essentially consist in the surgical resection of the tumor followed by combination of radiotherapy and chemotherapy.

1.3.1.1 Risk factors associated to medulloblastoma

MB arises upon disruption of cerebellar development and in most of the cases MBs are presented as sporadic tumors. However, several heritable genetic factors are known to increase the risk of developing MB. They consist of germline mutations of genes implicated in signaling pathways relevant for cerebellar (or hindbrain) development (e.g. SHH or WNT pathways) or other cellular modules regulating various aspects of tumor suppression activity (e.g. apoptosis and DNA repair). Hence, patients carrying loss-of-functions mutations in negative regulators of SHH signaling as *PTCH1* and *SUFU* are diagnosed with Gorlin syndrome and have significantly higher risk of developing MB (Goodrich et al., 1997; Hahn et al., 1996; Northcott et al., 2019; Smith et al., 2014; Taylor et al., 2002; Waszak et al., 2018). Similarly, MB tumorigenesis incidence is much higher in patients with Familial adenomatous polyposis syndrome which harbor mutations in the WNT signaling related *APC* gene. Also, patients with Li-Fraumeni syndrome with by *TP53* alterations or patients suffering of Fanconi anemia when *PALB2* and *BRCA2* genes are mutated, have higher probability to develop MB (de Chadarévian et al., 1985; Cohen, 1982; Kool et al., 2014; Northcott et al., 2019; Waszak et al., 2018). According to a retrospective study on a 1000 MB patients cohort, germline mutations in such genes account for ~6% of all MB cases, with higher prevalence in the SHH-subgroup where the totality of *PTCH1*, *SUFU* and *TP53* mutations are found (Waszak et al., 2018). Finally, other germline genetic alterations were shown to partially predispose to MB, although with much inferior penetrance compared to the those reported above (Northcott et al., 2019).

I.3.2 CLINICOPATHOLOGICAL FEATURES OF MEDULLOBLASTOMA

The WHO classifies MB as a Grade IV tumor, thus fast growing and highly aggressive with great propensity to metastasize. Although generally described as a posterior cranial fossa tumor, MB frequently arises in the cerebellum, where it can occupy different locations including the cerebellar hemispheres, the *vermis* or the cerebellar peduncles and invade surrounding regions as the IVth ventricle or the dorsal brainstem (Perreault et al., 2014; Teo et al., 2013).

Although type and gravity of symptoms may vary depending on the location of the tumor and presence of metastases in the CNS, MB patients typically display recurrent signs as issues at walking, coordinating movements and balance. Sometimes the tumor mass impedes the normal circulation of the cerebrospinal fluid (CSF), resulting into hydrocephalus. In these cases, patients may manifest headache, vomiting, vision defects, seizures and faint.

I.3.2.1 Histological characteristics

Before the advent of the "molecular era" which distinguished the four consensus MB subgroups, MBs were principally classified according to histological features identified through classic hematoxylin and eosin staining of fixed paraffin-embedded samples. Using these criteria, in 2007 the WHO classified MBs into five clinicopathologically relevant variants, namely MBs with "classic", "desmoplastic/nodular" (D/N), "extensive nodularity" (MBEN), "anaplastic" and "large cell" histology (Ellison, 2010). Briefly, classic MB are characterized by relatively regular sheets of small cells with the typical properties originally described by Cushing and Bailey, that is large and non-pleomorphic nuclei, and extremely reduced cytoplasm. D/N and MBEN MBs instead display different extents of nodules of non-proliferating differentiated neuronal cells embedded in internodular regions enriched of collagen and undifferentiated cells. Anaplastic MBs present highly mitotic cells, pleomorphic nuclei and abundant apoptotic cells. Finally MBs with large cell histology resemble anaplastic MBs, but are further characterized by the atypical presence of cells with abundant cytoplasm (Borowska and Józwiak, 2016; Ellison, 2010). As stated above, this histological classification is of clinical utility, as MB featuring classic, anaplastic and large cell organization are associated to more dismal outcome compared to the D/N and MBEN phenotypes (Borowska and Józwiak, 2016; Ellison, 2010).

I.3.2.2 Metastases and recurrence of medulloblastoma

Large part of the morbidity and mortality associated to MB is rarely due to the primary tumor, of which patients unfrequently succumb, but is rather due to the metastatic dissemination and recurrence of the disease.

Generally, upon primary MB diagnosis, which is assessed after detection of the tumor through MRI of the brain, MRI scans are also applied to the spine in order to hopefully rule out the presence of any metastatic lesion. Indeed, around ~40% of all MB patients show metastatic dissemination in the CNS at the time of presentation, although prevalence and burden are molecular subgroup-dependent. Anatomically, MB metastases are typically found in the leptomeningeal space that surrounds the entire CNS. The modality, and the actual route used by primary MB cells to disseminate in this compartment are still puzzling. For long it has been thought that the mere "shedding" of MB cells from an invasive primary tumor into the CSF, which is in communication with the leptomeninges, was the sole pathway for metastatic spread. Nevertheless, recent observations and convincing pieces of evidence showed that MB cells are also found in patients' peripheral blood and the hematogenous route seems an active modality utilized by MB cells to reach the leptomeninges (Garzia et al., 2018). In addition, very rare and sporadic cases of non-CNS MB metastases have been reported, hence supporting the view that MB cells could also disseminate via the circulatory system (Eberhart et al., 2003).

Genome, methylome, and gene expression analyses revealed that although metastatic lesions maintain identical molecular subgroup affiliation to the matched primary tumor, they are extremely divergent from it (Wang et al., 2015; Wu et al., 2012). This view well fits with the hypothesis that metastatic potential is an exclusive characteristic of a subclone existing within the primary tumor bulk. Such clone, would carry unique genetic and epigenetic alterations that eventually dominate in the metastatic compartment (Wu et al., 2012).

After standard treatments, regression of the tumor is generally observed. However, sometimes MB undergoes relapse, generating secondary tumors located at the original site and/or in form of multiple metastatic lesions (Ramaswamy et al., 2013). Unfortunately, recurrent MB almost universally results into death of the patient (Pizer et al., 2011; Ramaswamy et al., 2013).

Similar to what observed for metastases, genetic characterization of matched primary and recurrent MBs in both animal models and patient samples revealed that there exists substantial difference between the two compartments. Although maintaining identical subgroup affiliation, only ~10% of genetic events are shared by primary and relapsed matched tumors, with the latter typically displaying also higher mutational burden and convergent deregulation of specific

pathways (as TP53) (Hill et al., 2015; Morrissy et al., 2016; Ramaswamy et al., 2013). From these studies it emerges that clonal selection occurs during and after the therapy regimen, with some sub-represented clones existing at diagnosis that are spared by the treatment and eventually underpin MB relapse (Morrissy et al., 2016).

All these observations converge on the description of MB as a highly spatially (and temporally) heterogeneous disease, composed by genetically different clones, some of them able to disseminate and/or to survive to the therapy and sustain tumor regrowth. Normally, such clones are underrepresented in the primary tumor, hence their characterization is hindered when bulk primary MB samples are analyzed. To cope with this technical limitation, recent years' research has focused on the in-depth characterization of MB spatial heterogeneity, lately reaching also the single cell-resolution (Hovestadt et al., 2019; Vladoiu et al., 2019; Zhang et al., 2019).

1.3.3 MOLECULAR CLASSIFICATION OF MEDULLOBLASTOMA

In the last ten years, many research groups undertook extensive molecular characterization of large cohorts of human MB samples. Results of these analyses not only helped to gain deeper insights on MB biology and pathology, but also demonstrated that the molecular classification of MB works as a powerful predictor of clinical behavior and outcome.

The first use of large molecular analyses of MB, are dated back to 2002 when Pomeroy and colleagues leveraged microarray-based gene expression analysis concluding that MBs are molecularly (and clinically) separate entities from other embryonic CNS tumors (Pomeroy et al., 2002).

From that study on, several authors realized that MB is a heterogeneous disease and that several molecular subgroups could be readily identified through combined gene expression, DNA copy-number and single nucleotide variants profiling (Cho et al., 2011; Kool et al., 2008; Northcott et al., 2010; Thompson et al., 2006). However, the numbers and the identity and such subgroups was variable from one study to the other, therefore in 2010 the pediatric neuro-oncology community organized a meeting in Boston to reach a consensus view on this issue (Taylor et al., 2012). There, it was agreed the existence of four distinct MB subgroups, namely WNT, SHH, Group3 and Group4, featuring not only divergent molecular properties, but also different incidence, clinical progress and outcome (**Figure X**). Considering the importance of such MB subgrouping for prospectively better tailoring therapies to patients, in 2016 the WHO

integrated this information in a revised classification of brain tumors. Indeed, further taking into account the importance of *TP53* gene status as a prognostic value, today the WHO recognizes four classes of MB, namely "WNT", "SHH-TP53 wild type", "SHH-TP53 mutant" and "non-WNT/non-SHH MBs", with the latter class consisting of Group3 and Group4 MBs, which are sometimes difficult to unequivocally distinguish (Louis et al., 2016).





	WNT	SHH	Group3	Group4
Incidence	10%	30%	25%	35%
Metastases at diagnosis	<5%	20%	40%-50%	35%-40%
Age group				
Gender ratio	♂:♀	♂:♀	♂♂:♀	♂♂:♀
Outcome	Very good	Intermediate	Poor	Intermediate
Somatic gene-level mutations	<i>CTNNB1</i> (90%) <i>SMARCA4</i> (25%) <i>DDX3X</i> (50%) <i>TP53</i> (12%)	<i>PTCH1</i> (25%) <i>SUFU</i> (10%, infants) <i>SMO</i> (15%, adults) <i>TERT</i> (20%, adults) <i>IDH1</i> (5%, adults) <i>MLL2</i> (12%) <i>TP53</i> (15%)	<i>SMARCA</i> (10%) <i>CTDNEP1</i> (5%) <i>MLL2</i> (4%)	<i>KDM6A</i> (10%) <i>MLL3</i> (5%)
Germline gene-level mutations	<i>APC</i> (<5%)	<i>PTCH1</i> (25% infants, 10% older) <i>SUFU</i> (20%, infants) <i>TP53</i> (8%, infants)		
Focal copy number alterations		<i>MYCN</i> (8%) <i>GLI2</i> (5%)	<i>MYC</i> (15%) <i>OTX2</i> (7%) <i>GFI1/1B</i> activation (25%)	<i>SNCAIP</i> (10%) <i>MYCN</i> (6%) <i>CDK6</i> (5%) <i>GFI1/1B</i> activation (5%)
Large copy number alterations	Monosomy 6 (85%)	9q (35%) 10q (20%) 17p (18%)	i17q (22%) 8 (29%) 10 (45%) 11 (30%) 16 (48%) 1q (23%) 7 (25%) 18 (20%)	i17q (70%) 8p (50%) 11p (28%) X (80% of females) 7q (40%) 18q (20%)
High risk		<i>TP53</i> mutation <i>MYCN</i> amplification	Infants Metastases <i>MYC</i> amplification	Metastases
Cell-of-origin	IRL progenitors	GNPs	<i>Nestin</i> ⁺ VZ progenitors?	UBCs progenitors?

Figure X. Molecular subgroups of MB. Frequency of the indicated mutation or copy number alteration is reported between brackets. Copy number alterations are colour-coded: red are amplifications, blue are deletions. Chromosomes are indicated with their numbers. i17q: isochromosome 17q; IRL: lower rhombic lip; UBC: unipolar brush cell. Inspired by Ramaswamy and Taylor (2017).

After the consensus conference in Boston, more in-depth and new molecular analyses (including DNA methylation and whole genome sequencing) were performed on increasing number of MB samples. The enhanced statistical power of such analyses uniformly remarked the robustness of the four-group classification, but at the same time also identified novel clinically relevant molecular subtypes within MB subgroups (Cavalli et al., 2017; Northcott et al., 2017; Schwalbe et al., 2017). Some inconsistencies between these studies exist, especially for Group3- and Group4-subtypes. However, they are perhaps mainly attributable to the mathematical model utilized to cluster or differentiate subtypes. To cope with this problem, a recent consensus study equally leveraged either mathematical models in combination with opportune classification confidence measures on a 1500 Group3- and Group4-MBs cohort to derive an objective subtype classification (Sharma et al., 2019). As a result eight subtypes (I-VIII) were defined among Group3 and Group4 MBs, with subtypes I, V and VII interestingly (and yet inexplicably) showing mixed contribution from both subgroups (Sharma et al., 2019). It is nowadays accepted that the intrinsic molecular differences among the four main MB subgroups, mirror their divergent embryonic origin. In other words, MB subgroups are supposed to arise from different cells-of-origin populating the developing cerebellum; the identity of such cells is believed to ultimately determine the subgroup affiliation. Hence, some key molecular signatures reflecting the fate-commitment state of the cell-of-origin are supposed to remain conserved later on in the tumor cells, although they might have been re-shaped and "camouflaged" by the potent oncogenic pathways aberrantly activated in the tumor.

In the next paragraphs the major molecular and clinicopathological characteristics of the four MB subgroups are described, with more details dedicated to SHH-MB, which will be described at last.

I.3.3.1 WNT-medulloblastoma

WNT-MB is the less frequent among MBs, accounting only for around 10% of cases and it is typically observed in children and adolescents. The hallmark of this subgroup is an highly activated WNT signaling, which in most cases (~90%) is driven by somatic gain of function mutations on the gene encoding for β -catenin, *CTNNB1*, a key transcriptional co-activator of the pathway (Ellison et al., 2005; Kool et al., 2008; Thompson et al., 2006). Other less frequent, but still recurrent mutations are found in *SMARCA4*, *DDX3X* and *TP53*, although the latter does not represent a prognostic value (in sharp contrast to SHH-MB) (Jones et al., 2012; Northcott et al., 2019; Pugh et al., 2012; Robinson et al., 2012; Zhukova et al., 2013). As stated above,

also germline mutations on *APC* may predispose for WNT-MB. Typically observed is the loss of the entire chromosome 6 (Clifford et al., 2006; Thompson et al., 2006). WNT-MB have been proposed to originate from extracerebellar progenitors residing in the IRL in which WNT signaling was aberrantly activated (Gibson et al., 2010). WNT-MBs have the most favorable outcome among the other subgroups, with more than 90% 5-years overall survival of patients younger than 16 years, thanks to current treatment protocols (Clifford et al., 2006; Taylor et al., 2012). WNT-MBs indeed rarely relapse or metastasize and given the associated good prognosis, de-escalation of therapy load has been proposed as new therapeutic rationale and it is currently tested in clinical trials (Ramaswamy and Taylor, 2017).

I.3.3.2 Group3-medulloblastoma

Group3-MBs represent around 25% of MB cases and it affects only young children and infants (Taylor et al., 2012). Differently from WNT- and SHH-MB, no clear and unique active oncogenic signaling pathway has been identified so far, except for a GABAergic neuron signature and an intriguing activation of a photoreceptor genetic program (Cho et al., 2011; Garancher et al., 2018; Kool et al., 2008). Nevertheless, many Group3-MBs display elevated expression of the oncogene *MYC*. *MYC* can be found overexpressed also in WNT-MB, however, *MYC*-activated Group3 tumors are the only MBs harboring amplification of *MYC* locus (15 to 20% of all Group3 cases) which likely results after complex chromothripsis events (Northcott et al., 2010, 2012). Another gene recurrently amplified in Group3-MBs is *OTX2*, (~7% of cases), which is involved into maintenance of stemness/progenitor state of tumor cells, besides being also in part responsible for the activation of the photoreceptor program (Bai et al., 2012; Bunt et al., 2012; Garancher et al., 2018; Northcott et al., 2019). Moreover, amplifications of *ACVR2A* and *ACVR2B*, both encoding for type II activin receptors are also observed in some cases (Northcott et al., 2012). Finally, local genomic structural rearrangements observed in some Group3-MBs (but also Group4) cause the repositioning the *Growth factor independent 1* family of proto-oncogenes members *GFI1* and *GFI1B* in proximity of active superenhancers. This event, denominated "enhancer hijacking", results into high expression of *GFI1* family genes (Northcott et al., 2014). Mutation load at gene-level is generally low in Group3-MB. Conversely, large-scale chromosomal aberrations are recurrently found, consisting in various aneuploidy and, importantly, isochromosome 7q, which affects 20-30% of Group3 cases (note that the lost 7p arm contains *TP53* gene) (Northcott et al., 2012).

The Group3-MB cell-of-origin is nowadays still uncertain. Several pieces of evidence showed that various mouse cerebellar cells, including lineage restricted GNPs, GABAergic progenitors as well as early multipotent cerebellar stem cells can give rise to Group3-like cells when transformed by Myc overexpression and loss of Tp53 functions (Kawauchi et al., 2012, 2017; Pei et al., 2012). In addition, Vladoiu and colleagues (2019) recently confirmed through single-cell RNA-seq that human Group3-MB highly resembles *Nestin*⁺ cerebellar stem cells. Hence, whether Group3-MB derives from a transformed early multipotent stem cell or originates from lineage restricted progenitors reprogrammed to a stem-like state by oncogenic alterations remains obscure.

From the clinical point of view, Group3-MBs have the worst prognosis among the subgroups. Patients commonly show metastases at first diagnosis and tumor relapse is frequent and typically manifested in form of widespread disseminated lesions (Ramaswamy et al., 2013). Presence of metastases, *MYC* overexpression and especially amplification confer the poorest outcome to Group3 patients (Cavalli et al., 2017; Cho et al., 2011; Northcott et al., 2017; Ramaswamy et al., 2013, 2016; Schwalbe et al., 2017).

I.3.3.3 Group4-medulloblastoma

The most frequent subgroup of MB is Group4, accounting for around 35% of cases and affecting patients of all ages, but particularly children and adolescents (Ramaswamy and Taylor, 2017). Similar to Group3, the pathogenesis and the biology of Group4-MB is poorly known, mainly because of lack of reliable genetic animal models and the difficulty to grow human Group4 patient-derived xenografts (PDXs) (Ramaswamy and Taylor, 2017). Molecular analyses have so far identified few potential driver events, including an aberrant activation of ERBB4-SRC signaling recently detected through whole proteomic and phospho-proteomic analyses (Forget et al., 2018). Gene-level loss-of-function mutations are scarce also in this subgroup and limited to few genes encoding for histone-modifier proteins, as *KDM6A*, *KMT2C* or *KBTBD4* (Northcott et al., 2017; Pugh et al., 2012). Copy number variations leading to gene amplifications are more common, but never universally found in patients. Affected genes are *SNCAIP* (encoding for Synphilin-1), *CDK6*, *OTX2* and *MYCN* (Cho et al., 2011; Northcott et al., 2012, 2019). Enhancer hijacking occurs not only for *GFI* family genes, but also for the chromatin-modifier gene *PRDM6* (Northcott et al., 2014, 2017). The significant number of genetic events occurring on chromatin-modifier genes led to the hypothesis that a somewhat deregulated chromatin landscape may be a driving hallmark of Group4-MB. Large

chromosomal rearrangements are often observed and, like Group3-MB, isochromosome 7q is frequent (Northcott et al., 2012).

Group4-MB cell-of-origin is unknown, although UBCs progenitors were shown to strikingly resemble Group4-MB cells by two recent single-cell RNA-seq studies (Hovestadt et al., 2019; Vladoiu et al., 2019).

Overall, Group4 patients show intermediate prognosis, but reliable risk-categories based on clinical, genetic and cytogenetic features are hard to define. Nevertheless, metastases-free tumors, absence of i7q and presence of *MYCN* amplification seem associated to more fortunate outcomes (Schwalbe et al., 2017).

I.3.3.4 SHH-medulloblastoma

Accounting for around 30% of all cases, the SHH subgroup is perhaps the most understood in its biology and pathology compared to the other MB subgroups, mainly thanks the existence of reliable genetic mouse models and the well-established knowledge of its cell-of-origin, the GNPs. SHH-MB affects all age groups of MB patients, however it shows a typical bimodal age-distribution being more frequent in infants (<4 years old) and adults (>16 years old) than in children (Kool et al., 2012; Northcott et al., 2011). The incidence of the disease is basically identical in the two genders, with a slight predominance of males only in the adulthood (Kool et al., 2012). Prognosis for patients is intermediate, although wide differences exist depending on the age of diagnosis, presence of metastases and *TP53* status.

From the histological point-of-view, SHH-MB tumors encompass almost the totality of D/N and MBEN cases, although such histological features are found only in half of SHH cases (Kool et al., 2012). From the molecular perspective instead, the main hallmark of these tumors is a clear ligand-independent, hyperactivation of the SHH pathway, which boosts cell growth and proliferation and is caused by germline or somatic mutations in SHH pathway components (Berman et al., 2002; Taylor et al., 2012; Thompson et al., 2006). Germline mutations predisposing to SHH-MB affect the previously cited *PTCH1*, *SUFU* and *TP53* genes, all acting as tumor suppressors in SHH-MB. Somatic mutations include again deletions or loss-of-function mutations on *PTCH1* and *SUFU*, but also activating mutation on *SMO* or amplification of *GLI2*, *MYCN*, *CCND2* and very rarely of *GLI1* and *MYCL1* (another *MYC* family member) (Kool et al., 2014; Northcott et al., 2011, 2012, 2017). Somatic mutations are also frequently observed in *TP53*. However, regardless if somatic or inherited, *TP53* mutations are not SHH pathway-activating *per se*, hence they are always accompanied by other alterations, often *GLI2*

or *MYCN* amplification (Ramaswamy and Taylor, 2017). As anticipated, mutations in *TP53* are associated to very dismal outcomes in SHH-MB. In particular, loss of TP53 activity brings to cell cycle deregulation, DNA repair dysfunction and escape from apoptosis, all key cancer hallmarks. Indeed, these defects were proposed to contribute to chromothripsis events which indeed have been associated to *TP53* deficiency in SHH-MB and may heavily contribute to tumorigenesis (Rausch et al., 2012). Interestingly, other genetic alterations result into dysfunctional TP53 pathway in SHH-MB, including amplification of *MDM4* and *Protein Phosphatase 1D (PPM1D)*, both negative regulators of TP53, or inactivation of *CDKN2A*, which encodes for p16^{Ink4a}, a CDK inhibitor that tightly interplays with TP53 pathway (Northcott et al., 2012).

Besides the SHH pathway, SHH-MBs frequently harbor additional genetic mutations which cause deregulation of other pathways involved in tumor growth and survival. Among them, noteworthy are the PI3K signaling (amplification of *PIK3C2G* and *PIK3C2B*, and deletion of *PTEN*), the IGF signaling (amplification of *IGF1R*) and amplification of *Yes Associated Protein 1 (YAP1)* a critical HIPPO pathway component, whose role in SHH-MB is well documented (Fernandez-L et al., 2009; Northcott et al., 2012). Other somatic mutations are found on *TERT* promoter (which is involved in telomere maintenance) and in the *Isocitrate Dehydrogenase 1 (IDH1)* gene (Cavalli et al., 2017; Northcott et al., 2017; Remke et al., 2013). Recurrent cytogenetic rearrangements found in SHH-MB are mainly those leading to loss of heterozygosity (LOH) of *PTCH1* and *SUFU*, namely chromosomes 9q and 10q deletions (Northcott et al., 2019).

I.3.3.4.1 SHH-medulloblastoma intertumoral heterogeneity

Deeper and integrated genomic, epigenetic and transcriptomic analysis on an increasing number of samples enabled a better dissection of the heterogeneity within all SHH-MB cases. Cavalli and colleagues (2017) for instance subdivided SHH-MBs into four clinicopathologically and cytomolecularly distinct subtypes named α , β , γ and δ (**Figure XI**). This distinction strongly reflects the age of diagnosis at the first place, with β and γ corresponding to infants, α to children and δ to adults. SHH α typically shows genetic alterations as *GLI2* or *MYCN* amplifications and are frequently associated to *TP53* mutations, which is a marker of unfavorable prognosis in this subtype (Cavalli et al., 2017). SHH β and γ instead affect the same age group, however SHH β is characterized by higher rate of metastases, mutational burden and overall worse prognosis compared to SHH γ (Cavalli et al., 2017).

A similar age-dependent subtyping of SHH-MBs was also depicted by the analyses of Schwalbe and colleagues (2017). Here it was also found that *SUFU* mutations are highly enriched in infant cases, while *PTCH1* mutations are more equally represented across age groups (Figure XI). Adult cases of SHH are almost never germline mutated and are typically driven by somatic *PTCH1* or *SMO* mutations (Kool et al., 2014). The mutational burden is higher in adults and a significant overrepresentation of alterations on chromatin modifier genes is found compared to children and infant cases (Kool et al., 2014; Northcott et al., 2019). Moreover, these tumors typically display *TERT* promoter mutations, an event that is linked with poor prognosis (Cavalli et al., 2017; Remke et al., 2013) (Figure XI). Also, adult SHH-MBs interestingly show high expression of a panel of *HOX* genes, although the biological significance of this feature is unknown, but may reflect a precise developmental origin within the GN lineage (Northcott et al., 2011). Indeed, recent single-cell transcriptome analyses concluded that adult SHH-MB much more reflect the gene expression profile of early uRL GNPs/UBC progenitors, while infant SHH-tumors better correlate with late differentiating GNPs (Hovestadt et al., 2019). Finally, the divergent biology between infant and adult SHH-MBs is remarked also at the whole proteome level (Archer et al., 2018).

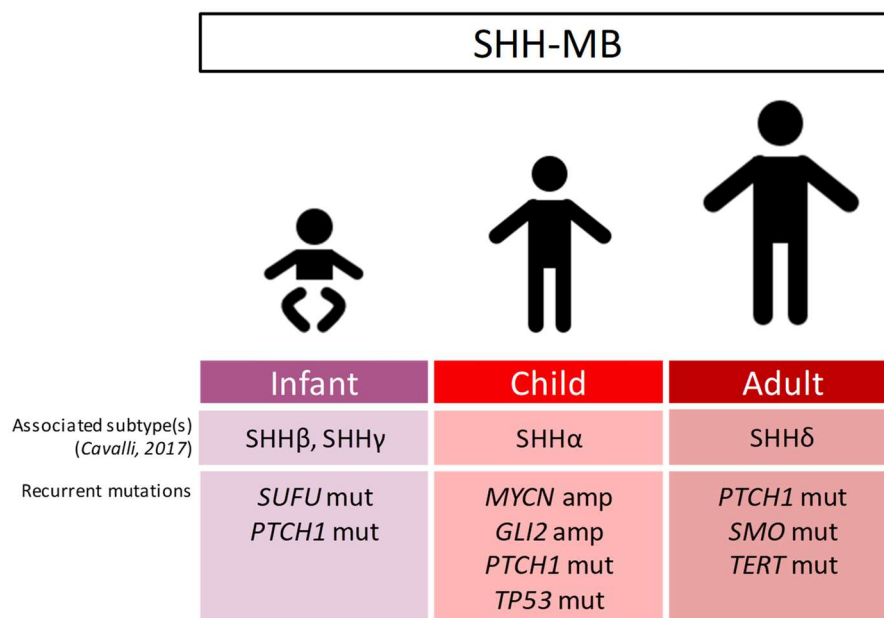


Figure XI. Heterogeneity in SHH-MB. Age group-associated subtypes (according to Cavalli and colleagues' (2017)) and recurrent mutations in SHH-MB.

I.3.3.4.2 Mouse models of SHH-medulloblastoma

The more advanced understanding of SHH-MB compared to Group3 and Group4, the other two deadliest subgroups, partially comes from the existence of reliable genetic mouse models. Such mouse lines not only enable to study how putative oncogenes and tumor suppressors contribute to SHH-MB tumorigenesis, but also serve as key models for pre-clinical tests.

The first SHH-MB murine model developed is perhaps also the most utilized and consists into a transgenic line carrying germline inactivation of one of the two *Ptch1* alleles (*Ptch1*^{+/*LacZa*} or simply *Ptch1*^{+/-}) (Goodrich et al., 1997). The *Ptch1*^{+/-} line was originally conceived to reflect the genetics of Gorlin syndrome patients and to explore its related developmental abnormalities and cancer predisposition. Seemingly in line with human cases, *Ptch1*^{-/-} mice do not complete embryogenesis, while *Ptch1*^{+/-} survive until adulthood with a spectrum of developmental defects compatible with Gorlin syndrome (Goodrich et al., 1997). Importantly, 15-20% of *Ptch1*^{+/-} mice develop posterior cranial fossa tumors during adulthood which overall highly resemble human SHH-MBs from the morphological, histological and, importantly, molecular point of view (Goodrich et al., 1997; Oliver et al., 2005; Pazzaglia et al., 2006). Reminiscent of the human counterpart, mouse *Ptch1*^{+/-}-derived MBs almost universally show LOH for *Ptch1*, typically occurring through genetic deletion or rarely through epigenetic silencing (i.e. gene methylation) of the remaining wild type allele (Berman et al., 2002; Oliver et al., 2005; Pazzaglia et al., 2006; Tamayo-Orrego et al., 2016). Importantly, recent pieces of evidence indicated that *Ptch1* LOH is the first key genetic event underpinning the development of a full-blown tumor in the *Ptch1*^{+/-} background (Tamayo-Orrego et al., 2016). Indeed, *Ptch1* LOH can be detected as early as the first MB preneoplastic lesions appear in the cerebellum of young *Ptch1*^{+/-} mice.

Given the low tumor incidence observed in *Ptch1*^{+/-} mice, many research groups hypothesized that additional mutations could cooperate with *Ptch1* loss-of-function in MB formation. Indeed, already at that time, mutations on genes as *TP53* had been characterized in both hereditary and sporadic human MBs. Under these assumptions, Wetmore and colleagues reported practically total penetrance of MB development in the *Ptch1*^{+/-}; *Tp53*^{-/-} mouse (Wetmore et al., 2001). Similarly, disruption of cell cycle regulation (e.g. *Ptch1*^{+/-}; *Cdkn1b*^{+/-} and *Ptch1*^{+/-}; *Cdkn2c*^{+/-} mice) or inactivation of the tumor suppressor *Hypermethylated in cancer 1* (*Ptch1*^{+/-}; *Hic1*^{-/-} mouse) that is frequently deleted in human MB, increases the incidence and accelerates tumor formation in the *Ptch1*^{+/-} background (Ayrault et al., 2009; Briggs et al., 2008; Uziel et al., 2005).

Furthermore, to bypass the need of a spontaneous second “hit” on the wild type *Ptch1* allele, and to spatiotemporally control the *Ptch1* deletion, the *Cre-LoxP* system was employed to generate *Ptch1* conditional biallelic KO mice (*Ptch1^{Flox/Flox}*).

In addition, incidence of SHH-MB can be augmented in the *Ptch1^{+/-}* model by increasing genomic instability either by subjecting neonatal mice to X-rays irradiation, or by insertional mutagenesis through the inducible Sleeping Beauty transposon system (Genovesi et al., 2013; Pazzaglia et al., 2002; Wu et al., 2012).

In human SHH-MBs, *Ptch1* loss-of-function is not the only SHH-activating driver mutations. Similarly, murine SHH-MBs can be obtained upon germline expression of constitutively active forms of Smo, which carry the same mutation normally found in human *SMO*-driven tumors (called *SmoM2*) or the equivalent one in the mouse gene (called *SmoA1*) (Hallahan et al., 2004; Mao et al., 2006). Alternatively, SHH-MBs bearing activation of the SHH pathway downstream *Ptch1* and Smo can be obtained from *SuFu^{+/-}; Tp53^{-/-}* mice, which develop tumors upon *SuFu* LOH (Lee et al., 2007).

Finally, murine SHH-MBs can also be obtained via orthotropic transplantation of opportunely modified primary GNPs. In these cases, GNPs are extracted from mice of various genotypes and transduced *in vitro* with retroviral vectors encoding for SHH-MB oncogenes (Ayrault et al., 2010; Kawauchi et al., 2012; Zindy et al., 2007).

To which extent the SHH-MB genetic mouse models above mentioned effectively recapitulate the genetics of the human counterparts? Comparative gene expression analysis indicated that *Ptch1*- and *Smo*-driven mouse MBs are more similar to human tumors than the *SuFu*-driven ones (Pöschl et al., 2014). In addition, both *Smo* and *Ptch1* mutated murine tumors strikingly resemble more to human adult SHH-MBs than to infant cases. Importantly this resemblance seems totally independent of the driving mutation in human tumors, hence irrespective of whether it is in *PTCH1*, *SMO* or other genes. Nevertheless, if gene expression profile well correlates mouse and human tumors, the mutational spectrum does not, as basically none of the most common mutations found in human SHH-MB are found in mouse (Pöschl et al., 2014).

I.3.3.4.3 Discovery of GNPs as the cell-of-origin of SHH-MB

For many years, a large number of observations have supported the hypothesis that the proliferative GNPs of the developing cerebellum could be at the origin of at least a subset of MBs, namely those showing an activation of the SHH pathway. Among them are the close morphological resemblance between GNPs and MB cells, the expression of same lineage-

specific marker genes (e.g. *Atoh1* or *Zic1*), the identical requirement of SHH signaling for proliferation and the description of preneoplastic lesions in the *Ptch1*^{+/-} model as remnants of the EGL in adult mice (Oliver et al., 2005; Salsano et al., 2004; Wechsler-Reya and Scott, 1999; Yokota et al., 1996). However, definitive experimental evidence was provided by two works in 2008 through the use of various MB transgenic mouse models. The conditional introduction of SHH-MB driving alterations as *Ptch1* deletion or *SmoM2* transgene expression into *Gfap*⁺ or *Olig2*⁺ cerebellar stem cells only gave rise to mouse SHH-MB *in vivo*, indicating that multilineage competent cerebellar cells may act as SHH-MB source (Schüller et al., 2008; Yang et al., 2008). However, virtually identical tumors were obtained when the driving mutations were restricted only to the unipotent GNPs, hence for example, when *Ptch1* deletion was conditionally introduced into *Atoh1*⁺ cells after E14.5 (using *Atoh1-Cre*^{ER}; *Ptch1*^{Flox/Flox} embryos tamoxifen-treated at E14.5) (Yang et al., 2008). These results indicated that the initial driving mutation may also appear into early multipotent cerebellar stem cells, but its true oncogenic effect arises only when such cells are fate-restricted to the GN lineage, thus perhaps in collaboration with lineage-related intrinsic and extrinsic cues (e.g. elevated competence to SHH response). Nevertheless, several independent observations seem to converge on the hypothesis that SHH-MBs may originate from cells located into temporally distinct phases of GNs development, resulting into the age-related heterogeneity underlying SHH-MBs (Hovestadt et al., 2019; Vladoiu et al., 2019). In such scenario, the SHH signaling hyperactivating mutation, despite being age-group related, may play only a limited role in shaping the tumor molecular landscape (Pöschl et al., 2014). Rather, intrinsic (e.g. epigenetic) or extrinsic (e.g. local environmental) factors associated to the developmental stage of the cell-of-origin may be primarily responsible of the way the tumor evolves.

1.3.4 STANDARD OF CARE, LIMITATIONS AND FUTURE DIRECTIONS

The current therapeutic pipeline employed for MB patients has been concluded from a prospective trial performed by Gajjar and collaborators (2006) and it essentially tailored on a two-groups patient risk-stratification system, namely “standard risk” and “high risk” patients. Affiliation into one or the other group depends on various criteria, whose prognostic value has been established by numerous precedent studies. Briefly, patients older than 3 years old, with no metastases or CSF circulating MB cells, less than 1.5cm³ residual tumor volume after

surgery and non-anaplastic/large cell histology are classified “standard risk”. If one of these criteria is not met, then the patient is considered “high risk”.

The standard of care for MB patients is multimodal and always begins with maximal safe surgical resection of the tumor. This first step is then followed by fractionated radiotherapy (RT) which is initiated within the first month after surgery (Gajjar et al., 2006; Merchant et al., 2008). At this stage, after sampling of tumor histology, the patient can be definitely allocated either into the standard or the high risk case. Hence, the dose of RT in terms of fractions and intensity is adjusted depending on this stratification. Specifically, standard-risk patients typically receive craniospinal irradiation (CSI) of 23.4Gy distributed into 13 fractions, while high-risk patients are subjected to 36-39.6Gy in 20 fractions³ (Merchant et al., 2008). In addition, in both cases a further ~55Gy boost is applied on the tumor bed, and only in high risk patients, if appropriate, a similar boost is focused on local CNS metastases (Gajjar et al., 2006). Normally, infants younger than 3 years old are spared from RT given the almost universal devastating effects of such treatment in a still developing CNS (Thomas and Noël, 2019).

After RT, patients initiate four cycles of chemotherapy (CT) which is also accompanied by bone marrow stem and progenitor cells reinfusion (Gajjar et al., 2006). The cycles of chemotherapy are typically composed by the sequential administration of drugs like cisplatin, vincristine and cyclophosphamide (Gajjar et al., 2006).

Such treatment regimen grants a 5-years overall survival of 85% for standard-risk patients and 70% for high-risk patients (Gajjar et al., 2006). However, this apparently bright scenario is obfuscated by the large spectrum of highly detrimental short- and long-term side effects often developed by patients. All the three sequential steps of the multimodal therapy may be causative of iatrogenic morbidities. Surgery, which is operated near to critical regions as the brainstem, may cause cerebellar mutism which often ends up into life-long speech defects (Robertson et al., 2006). CSI is proportionally less tolerated by young patients and typically results into short-term hematopoiesis defects (the vertebrae bone marrow in children contributes to hematopoiesis) and into serious long-term sequelae as cognitive decline, development of other CNS malignancies, growth defects and various dysfunctions at the endocrine, gynecological, vascular and hearing level (Bansal et al., 2015; Martin et al., 2014; Moxon-Emre et al., 2014; Packer et al., 2013; Thomas and Noël, 2019). Furthermore, the drug employed during cyclic CT have recognized side effects, including development of peripheral neuropathies and

³ The Gray (Gy) is a unit of measure recognised by the International System used to measure the dose of ionizing radiations. One Gray corresponds to one Joule of radiation energy absorbed by one kilogram of matter.

metabolic syndromes (vincristine), or ototoxicity and myelosuppression (cisplatin) (Kortmann et al., 2000; Martin et al., 2014; Thomas and Noël, 2019).

Hence, the current challenge in the field is not only to guarantee increased survival of patients, but also to significantly reduce the burden of therapy-associated side effects. As a consequence, better tailoring therapies to novel molecular data-based patient risk-stratification systems, as well as development of targeted approaches with the goal to spare healthy tissues from morbidity are the major objectives for the coming years (Ramaswamy et al., 2016; Thomas and Noël, 2019).

I.3.4.1 Targeted therapies in SHH-Medulloblastoma

Many *in vitro* and pre-clinical studies reported that SHH signaling is required for proliferation and survival of SHH-MB cells (Berman et al., 2002; MacDonald et al., 2014; Taipale et al., 2000). Hence, virtually all the treatments aimed at blocking the SHH pathway may be considered potential candidates for the development of a SHH-MB-targeted therapy (MacDonald et al., 2014). The small molecule drug Vismodegib (GDC-0449) binds SMO and impairs its activation, hence leading to blockade of SHH transcriptional response. A phase II clinical trials designed to test Vismodegib efficacy in recurrent MB cases showed an overall beneficial effect in those patients diagnosed with SHH-MB, while (expectedly) no response was reported for patients with non-SHH-MBs (Robinson et al., 2015). However, efficacy of Vismodegib or other similar SMO-inhibitors are today known to be dependent on the driving SHH-hyperactivating event. Indeed, patients with upstream alterations of the pathway, notably *PTCH1* loss-of-function or SMO activating mutations, were reported to well respond to the treatment, while those carrying downstream activation, as *SUFU* mutations or *GLI2* or *MYCN* amplification are insensitive to SMO inhibition (Kool et al., 2014; Robinson et al., 2015). To further complicate the picture, in some cases the administration of Vismodegib resulted in selection of resistant tumor sub-clones displaying specific SMO mutations that made the receptor refractory to the inhibition (Dijkgraaf et al., 2011; Rudin et al., 2009; Yauch et al., 2009). Also, similar observations were reported in preclinical mouse models, where resistance to Vismodegib was acquired not only through novel *Smo* mutations but also through emergence of downstream pathway activation events, as *Gli2* or *Ccnd1* amplification (Buonamici et al., 2010; Dijkgraaf et al., 2011).

Nowadays, a number of clinical trials are currently ongoing with the goal to test the efficacy of different classes of SMO-inhibitors provided either as monotherapy or in combination with

other drugs (MacDonald et al., 2014; Thomas and Noël, 2019). Nevertheless, the established non-universal efficacy of SMO-inhibitors in SHH-MB cases and the appearance of sporadic resistance mechanisms pinpoint to the need for development of novel targeted approaches.

For instance, small molecule inhibition of PI3K pathway was reported to be effective in restricting growth of preclinical models of SHH-MB harboring acquired resistance to SMO-inhibitors (Buonamici et al., 2010; Dijkgraaf et al., 2011). Moreover, drugs inhibiting the activity of GLI factors, as GANT-61 or arsenic trioxide, could represent interesting candidates for a pan-effective therapy for SHH-MB patients (Kim et al., 2013; Lin et al., 2016). Alternatively, downstream blockade of the SHH pathway can be achieved also through inhibition of Bromodomain and Extra-Terminal motif (BET) proteins. BET proteins regulate transcription of target genes by binding to acetylated chromatin. Specifically, the BET protein BRD4 was shown to positively regulate *GLI1* and *GLI2* transcription in SHH-MB. Interestingly, inhibition of BRD4 with anti-BET compounds (as JQ1), showed promising effects in reducing SHH-MB cells growth in preclinical models (Long et al., 2014; Tang et al., 2014).

In conclusion, research and clinical testing of novel effective targeted therapies for SHH-MB is still an ongoing process in the field.

I.4 The Primary Cilium

Although ciliary structures on cells were first observed around 350 years ago by Antonie van Leeuwenhoek, for long their functions remained overall unappreciated. Lack of evidence of clear roles for these cell surface antenna-like protrusions, alimented the concept that cilia were mere vestigial organelles. It was only during the few last decades that a number of studies contributed to uncover the large diversity underlying structure and functions of cilia. Incidentally, most of this research was boosted by the discovery that a wide panel of human genetic diseases, nowadays denominated ciliopathies, were caused by mutations in ciliary proteins. It was in this context that primary cilia emerged as essential requirements for proper SHH signaling in vertebrates.

This chapter illustrates what a primary cilium is, focusing on its structure and mechanisms of assembly and disassembly. Next, its functions in mediating the SHH signaling will be densely described. Finally, the state-of-art role and importance of the primary cilium in GNs development and SHH-MB will be reported.

I.4.1 DIFFERENT TYPES OF CILIA EXIST IN NATURE

Ciliary structures are observed in organisms belonging to virtually all eukaryotic clades (including protozoa, green algae, and some fungi, besides animals). In vertebrates there essentially exist two principal types of cilia, characterized by major structural and functional differences: motile cilia and primary (non-motile) cilia.

Motile cilia, are typically found in single or multiple copies on the surface of highly specialized cells. As suggested by their name, by using energy from ATP hydrolysis, they are capable of generating rhythmic strokes or rotational movements of their shaft. By doing that, motile cilia produce forces that can either move surrounding fluids, hence for instance displacing or clearing molecules and particles dissolved or immersed in them, or propel whole cells for movements. Examples of motile cilia are those found in single copy on cells of the organ of laterality, those found in multiple copies on the apical surface of airways and ependymal epithelia and the flagellum of sperm cells.

Primary cilia are instead immotile as they are not equipped with motility components. They are generally shorter than motile cilia (1-5 μ m), and typically solitary, hence present in single copy on the cell. Primary cilia are involved in sensory functions. Indeed, thanks to receptors and signal transducing molecules localizing in their shaft, they sense and relay numerous types of external stimuli, including mechanical, chemical, and luminous ones. Importantly, among the chemical stimuli, there are those of various (developmental) signaling molecules, as SHH, Wnt, growth factors and others (described later). Hence, stem cells or progenitor cells of various tissues sometimes possess primary cilia. Besides that, primary cilia are also found in kidney tubules epithelial cells where they are required for sensing and transducing fluid mechanical forces. In addition, primary cilia also protrude from the sensory neurons of the olfactory epithelium where they carry odorant receptors. Finally, highly specialized types of primary cilia are observed in the hair cells of the inner ear (the kinocilium) and in the photoreceptors of the retina (the connecting cilium of the outer segment) (Choksi et al., 2014).

Importantly, the distinction between motile and primary cilia is not strict, as nowadays it is known that some motile cilia may also display sensory function (Mirvis et al., 2018).

1.4.2 STRUCTURE OF CILIA

As anticipated, some essential structural differences exist between motile and primary cilia, however both of them are ultimately characterized by the same common basic architecture (**Figure XII**).

1.4.2.1 The ciliary shaft

In all cilia, the ciliary shaft protrudes in the extracellular environment and its core is constituted by a columnar microtubules-based structure, termed axoneme. The axoneme is then surrounded by the ciliary membrane which despite being in continuity with the plasma membrane, has different protein and lipid composition, making it a real biophysically and functionally distinct plasma membrane domain.

Structurally, the axoneme is composed by nine, circumferentially arranged, parallel microtubule doublets, whose plus-end is oriented toward the ciliary tip. Each doublet is composed by an "A" and a "B" microtubule, with the "A" microtubule being complete and the "B" microtubule incomplete and facing the gapped lateral surface toward the "A" microtubule (**Figure XII**).

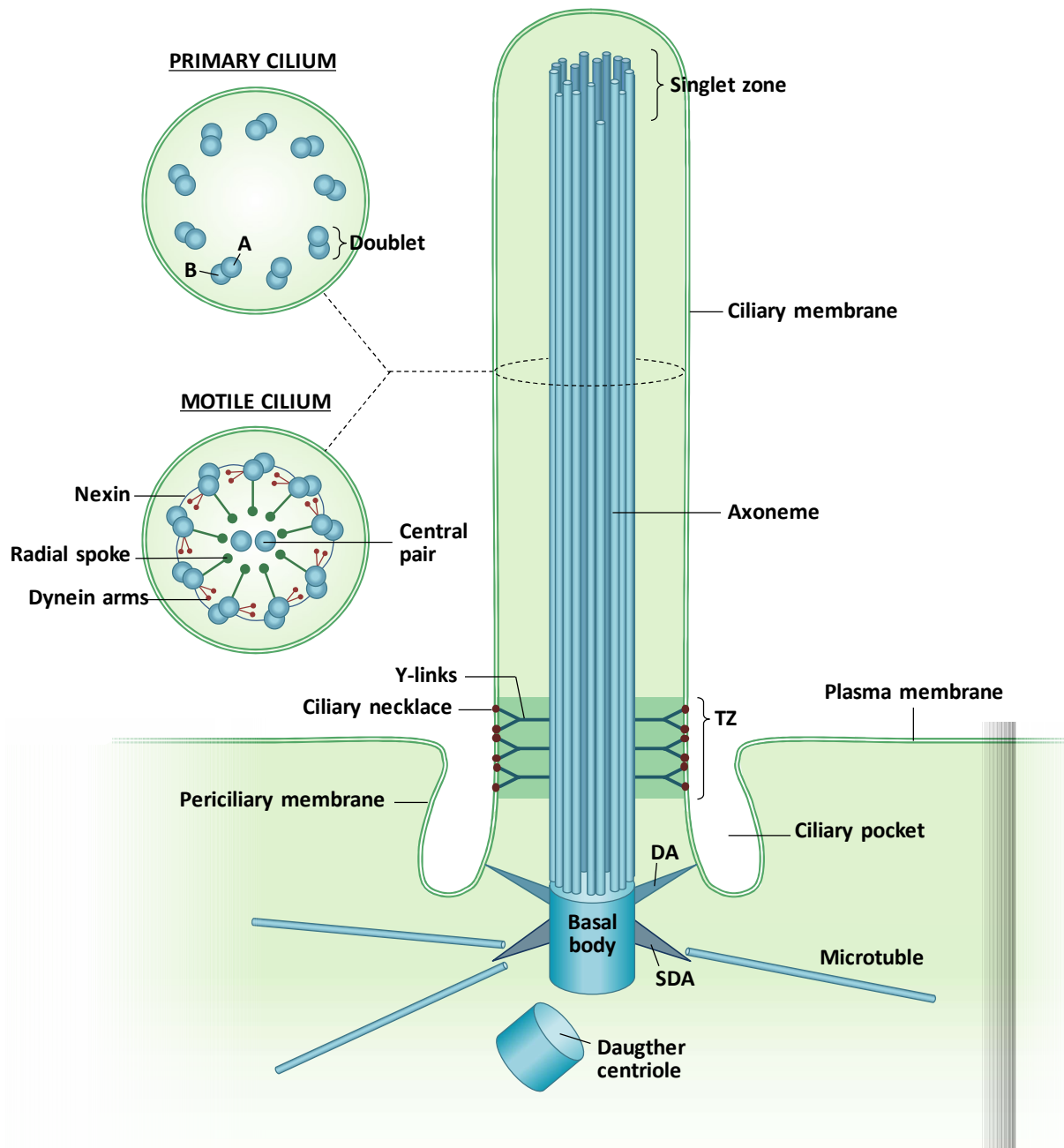


Figure XII. Structure of a cilium. The cilium is surrounded by the ciliary membrane which is in continuity with the plasma membrane. Between the two, the periciliary membrane invaginates inward in the cytoplasm forming the ciliary pocket. The axoneme is the microtubules-based backbone of the cilium and it is nucleated from a basal body which corresponds to the mother centriole of the centrosome. The basal body morphologically differs from its counterpart, the daughter centriole, by the presence of the distal (DA) and sub-distal (SDA) appendages. Above the basal body extends the transition zone (TZ), which includes the Y-links and the ciliary neck. The axoneme is composed of nine microtubule doublets, each formed by an “A” complete and a “B” incomplete microtubule. The axoneme tip may be partially composed by singlets of microtubule, and takes the name of singlet zone. Transversal sections of the axoneme reveals the sub-architecture of primary (non-motile) or motile cilia: the latter also includes a central pair of microtubules and sets of nexin links, radial spokes and dynein arms. Image inspired by Anvarian and colleagues (2019).

At the distal tip of the axoneme, the doublets can sometimes become singlets, as normally the "A" microtubule is longer than the "B" one. For this reason, the distal part of the axoneme is sometimes referred as the "singlet zone" (Fisch and Dupuis-Williams, 2011).

On the top of this fundamental structure, the axoneme of motile cilia also contains a pair of central complete microtubules elongating inside its lumen. This microtubules pair is connected radially to the surrounding doublets by electron-dense structures called radial spokes. Each doublet is then connected to the adjacent ones by proteinous elastic linkers called nexin links (**Figure XII**). In addition, motile cilia axonemes contain regularly spaced dynein arms which are fixed on an "A" microtubule and use ATP to "walk" on the "B" microtubule of the adjacent doublet. The coordinated activation of the dyneins motor domains provides the motor force responsible for bending the axoneme and thus moving the cilium (Gibbons and Rowe, 1965). The activity of the dynein arms is regulated by an associated complex of proteins called dynein regulatory complex (DRG) which includes numerous calcium binding proteins (Fisch and Dupuis-Williams, 2011; Lindemann and Lesich, 2010). Given the presence of the nine outer doublets and the central pair of microtubules, the axoneme of motile cilia is referred as 9+2 architecture in opposition to the 9+0 of the primary cilia one, which lacks the central two microtubules.

I.4.2.2 The basal body

Regardless of the 9+2 or 9+0 structure, all ciliary axonemes nucleate from a basal body, a plasma membrane-anchored modified form of a centriole. While in the case of multiciliated cells, the numerous basal bodies at the bottom of cilia are typically *de novo* generated, in monociliated cells the unique basal body derives from the mother centriole⁴ of the centrosome (Brooks and Wallingford, 2014) (**Figure XII**).

In cells, the centrosome is indeed composed by a pair of orthogonally oriented centrioles surrounded by a dense pericentriolar matrix. Centrioles, are 500nm-long barrel-shaped structures, whose walls are composed by nine triplets of highly stable microtubules, while the pericentriolar matrix contains the γ -TURC complexes from which the cytoplasmic network of microtubules nucleates. The centrosome is indeed referred as the principal microtubule organizing

⁴ The centrosome is replicated during the cell cycle in order to generate the two poles of the mitotic spindle. After mitosis each copy of the centrosome will be inherited by the two daughter cells. Because of the modality of centrosome replication, after mitosis, the inherited centrosome is composed by a *daughter* centriole, new, generated during the previous cell cycle, and by a *mother* centriole, older that functioned as template for the daughter one.

center (MTOC) of metazoan cells and it is required for nucleating and assembling the microtubule network in interphase cells and the mitotic spindle during chromosome segregation in mitosis. In addition to that, when cells display a single cilium (like a primary cilium), the mother centriole of the centrosome behaves as a basal body and supports the formation of the axoneme. From an architectural point of view, the "A" and the "B" microtubules of the axoneme doublets are nucleated by the corresponding "A" and "B" microtubules of the basal body triplets, while the third, or "C", microtubule of the basal body triplets is not or only partly utilized for nucleation. As anticipated, the basal body is physically anchored to the plasma membrane, and such interaction is granted by at least two series of radial, electron-dense proteinous fibers protruding from the distal and the medial portions of the basal body walls (**Figure XII**). The medial protrusions are called subdistal appendages and are composed by proteins as Outer dense fiber protein 2 (Odf2, a *bona fide* marker and essential constituent), Ninein and Centrosomal protein 110 (Cep110) (Huang et al., 2017; Ishikawa et al., 2005; Ou et al., 2002). Many functions have been associated to subdistal appendages, including interphase microtubules anchoring, trafficking of vesicles toward the ciliary membrane, axoneme elongation and, although indirectly, anchoring to the plasma membrane (Ibi et al., 2011; Ishikawa et al., 2005; Ou et al., 2002; Veleri et al., 2014). In contrast, the distal protrusions are called distal appendages (or transition fibers) and are composed by proteins as Cep83 (the main core component), and Cep164 (Graser et al., 2007; Tanos et al., 2013). Distal appendages are essential for the physical docking of basal body to the plasma membrane, but also take part in axoneme elongation and regulation of transport of proteins within the cilium (as described later) (Graser et al., 2007; Tanos et al., 2013).

I.4.2.3 The transition zone

As stated above, the ciliary compartment has a different composition compared to the cytosol or the plasma membrane, albeit being in communication with both of them. This implies that a selective barrier, often termed "ciliary gate", should exist at the base of the cilium in order to regulate the selective import or export of proteins.

This activity is mainly achieved by the transition zone, a functionally and architecturally specialized region of the cilium located at its base, just above the basal body. The major morphological feature is the presence of a series of electron-dense, champagne glass-shaped fibers, named Y-links, connecting the axoneme to the surrounding ciliary membrane. This connection is permitted by a set of transmembrane proteins in the ciliary membrane that

altogether constitute the so-called ciliary necklace (Fisch and Dupuis-Williams, 2011; Garcia-Gonzalo and Reiter, 2012; Gilula and Satir, 1972) (**Figure XII**).

Many proteins localize at the transition zone, either being part of the Y-links or the ciliary necklace or having a role in their assembly (Chih et al., 2011; Garcia-Gonzalo and Reiter, 2012; Garcia-Gonzalo et al., 2011; Sang et al., 2011). Interestingly mutations in their corresponding genes are often associated to ciliopathies like Meckel syndrome (MKS), Jubert syndromes (JBTS) and Nephronophthisis (NPHP), whose patients suffer of common symptoms and malformations as polycystic kidney, neural tube and cerebellar defects and retinal degeneration.

I.4.2.4 The ciliary pocket and the periciliary membrane

As described, the basal body is physically anchored to the cell plasma membrane by the distal appendages. In many cases, the distal appendages appear to pull the plasma membrane inside the cell generating a typical tubular-shaped invagination called ciliary pocket (Benmerah, 2013; Rohatgi and Snell, 2010) (**Figure XII**). The depth of the ciliary pocket can vary from one cell type to another, ranging from cases in which it is basically absent (as in kidney tubules epithelial cells) to cases in which almost the entire ciliary shaft is contained in it (as in pancreas β -cells). There is still uncertainty about the precise functional roles of the ciliary pocket and its corresponding plasma membrane domain, the periciliary membrane (**Figure XII**). The fact that electron microscopy studies revealed the presence of numerous clathrin-coated vesicles emerging from it raised the possibility that the periciliary membrane could represent an active substrate for endocytosis events (Ghossoub et al., 2011; Kaplan et al., 2012; Molla-Herman et al., 2010) (**Figure XIII**). This could serve as a mean for recycling ciliary membrane components or for clearance of cilium-mistargeted proteins. At the same time, the periciliary membrane seems also to represent a fusion site for secretory vesicles containing ciliary membrane proteins destined to the cilium (Geerts et al., 2011; Ghossoub et al., 2011).

I.4.3 TRAFFICKING OF CILIARY PROTEINS

Protein synthesis does not occur within cilia, hence the totality of ciliary proteins must be actively transported within the primary cilium from the cytoplasm, their site of production. In the next paragraphs it will be described first how ciliary proteins reach and move within the cilium, to accomplish key processes as ciliary biogenesis and functions (**Figure XIII**).

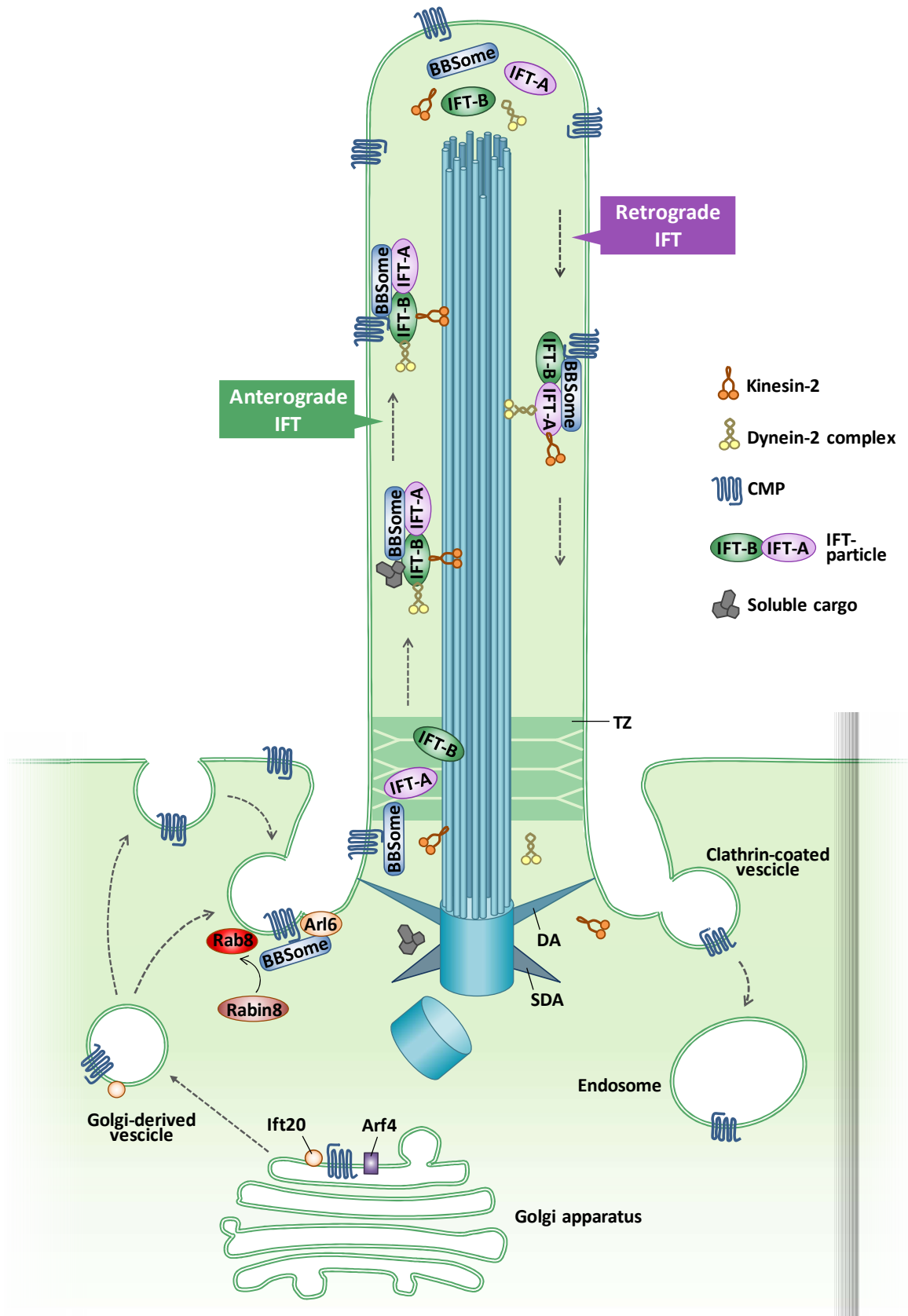


Figure XIII. Mechanisms of protein trafficking through the cilium. Ciliary membrane proteins (CMPs), as signaling receptors, are sorted into vesicles at the level of the trans-Golgi network through the activity of Arf4 and/or Ift20. Golgi-derived vesicles are then directed either to the plasma membrane or to the ciliary membrane, where they eventually fuse with these compartments bringing in both cases CMPs at the base of the cilium. Here, Arl6 permits the recruitment of the BBSome which is required for sorting the CMPs to the cilium and loading them into the anterograde IFT-trains. *(legend continued on next page)*

(legend continued from previous page) The BBSome also interacts with Rabin8 which in turn activates Rab8, the latter responsible for vesicle sorting and fusion. Hence the BBSome seems to help coupling vesicle trafficking and CMPs ciliary transport. IFT trains are likely to be assembled just above the distal appendages (DA). They are composed by IFT particles (made by IFT-A and IFT-B complexes), IFT motors (kinesin-2 and cytoplasmic dynein-2 complex), the BBSome (if CMPs are transported) and by transported cargoes, which can be soluble proteins (as a $\alpha\beta$ -tubulin dimer) or CMPs. Kinesin-2 and especially IFT-B are required for the anterograde transport, while dynein-2 and IFT-A for the retrograde transport. Remodelling of IFT-trains occurs at the ciliary tip, where the transported cargo is also released. CMPs leaving the cilium may be internalized in the cell via endocytosis with clathrin-coated vesicles ultimately directed to endosomes. Image inspired by Anvarian and colleagues (2019).

I.4.3.1 The intraflagellar transport

Biogenesis of the primary cilium requires the elongation of the axoneme, which primarily occurs by serial addition of $\alpha\beta$ -tubulin dimers at the distal end of the microtubule doublets. In addition, many structural molecules, including tubulin binding proteins, as well as signaling proteins, like transmembrane receptors, must enter and move along the cilium to reach their proper localization. At the same time, ciliary proteins must also be able to leave the cilium due to turnover needs, activation of signaling cascades or during ciliary disassembly.

Hence, to cope with cilia biogenesis, maintenance, retraction and functions, ciliary proteins must be transported bi-directionally along the ciliary shaft. This activity is traditionally referred as intraflagellar transport (IFT) and it is carried out by the so-called "IFT-trains". The first evidence of an IFT in cilia structures came from differential interference contrast microscopy studies in the flagella of the unicellular green alga *Chlamydomonas*. Here, "trains" of granular-like particles were observed to bidirectionally move in the space between the axoneme and the ciliary membrane (Kozminski et al., 1993). Nowadays it is known that similar "IFT trains" exist also in cilia of vertebrates and that their movement is powered by motor proteins as kinesin-2 and cytoplasmic dynein-2 complex (Pedersen and Rosenbaum, 2008). In addition to the motor components, also called IFT motors, IFT trains are composed by other constituents, namely the IFT particles, the BBSome complex and the IFT cargoes, the latter representing the actual ciliary proteins transported (**Figure XIII**).

I.4.3.1.1 IFT motors

The anterograde movement of IFT trains (that is from the base to the tip of cilia), is mediated by two members of the kinesin-2 family, namely the heterotrimer Kif3 and the homodimer Kif17, both moving along the "B" microtubules of the doublets (Stepanek and Pigino, 2016).

Kif3 is composed by the motor subunits Kif3a and either Kif3b or Kif3c and by the accessory subunit Kap3 whose function is uncertain, but it may work as a cargo-adaptor subunit or help

the assembly of Kif3 complex (Mueller et al., 2004). Kif3 activity is essential for building up and maintaining cilia, as genetic deletion or silencing of *Kif3a* gene is sufficient to impair ciliogenesis in virtually all ciliated cells (Kozminski et al., 1995; Nonaka et al., 1998; Takeda et al., 1999). Indeed, depletion of Kif3a is by far the most utilized strategy to specifically ablate primary cilia from cells in experimental settings.

By contrast, Kif17 does not seem to be as essential as Kif3 for ciliogenesis. Albeit localizing to cilia as well, it appears to be majorly implicated in the ciliary transport of peculiar proteins in some specialized cell types, as photoreceptors or olfactory sensory neurons (Insinna et al., 2008, 2009; Jenkins et al., 2006; Prevo et al., 2015).

The retrograde movement of IFT trains (that is from the tip to the base of cilia), is instead carried out by the cytoplasmic dynein-2 complex (Ishikawa and Marshall, 2017; Pazour et al., 1998, 1999). The precise composition and the stoichiometry of this motor complex is still hardly defined in vertebrates, as almost each subunit has paralogs with specific tissue-restricted expression. Nevertheless, the proposed structure consists in an homodimer of heavy chains containing the motor domain, assembled together with two subunits of intermediate chains, two subunits of light-intermediate chains and a variable number of light chains (Asante et al., 2014). Cytoplasmic dynein-2 complexes move cargoes along the "A" microtubules, thus collision with the anterograde IFT trains is prevented. Importantly, they are required for ciliogenesis but seem dispensable for ciliary maintenance (Engel et al., 2012; Pazour et al., 1999; Stepanek and Pigino, 2016).

I.4.3.1.2 IFT particles

Besides the IFT motors, IFT trains are composed by a series of IFT particles. Each IFT particle is made by two multiprotein subcomplexes, called IFT complex A (IFT-A) and B (IFT-B) (**Figure XIII**). IFT-A is composed by at least six polypeptides, while IFT-B by at least sixteen and they loosely associate to form the IFT particle. A number of genetic and biochemical studies showed that IFT-A and B have different roles during IFT-mediated transport of cargoes.

Specifically, IFT-B is required for the anterograde transport of cargoes, as it directly associates to kinesin-2 and mutations in its components cause impairment of ciliogenesis, mimicking the effects of kinesin-2 loss-of-function (Brazelton et al., 2001; Jonassen et al., 2008; Pazour et al., 2000). For example, hypomorphic mutations on *Intraflagellar transport protein 88 (Ift88)*, which encodes a central component of IFT-B, aborts the formation of primary cilia due to altered anterograde transport (Pazour et al., 2000).

IFT-A instead seems required for the retrograde transport of turnover products or signaling molecules. It is overall dispensable for ciliogenesis, however IFT-A mutants show impaired retrograde transport, as it is typically displayed by the accumulation of IFT-B at the tip of the cilium (Brown et al., 2015; Tsao and Gorovsky, 2008). This suggests that beside participating to protein cargos export from cilia, IFT-A functions are also required for returning IFT-B at the base of the cilium, where it can reassemble into a new anterograde IFT train (Lechtreck, 2015). However, according to some works, this classic repartition of roles between IFT-B and IFT-A might not be so strict. Indeed, some proteins seem to rely on specific IFT-A subunits for proper ciliary anterograde transport, while others require IFT-B also for their export (Liem et al., 2012; Liew et al., 2014).

I.4.3.1.3 *The BBSome*

Another key component of the IFT trains is a multimeric complex termed BBSome. The BBSome is composed by seven subunits, namely BBS1/2/4/5/7/8/9 and by a BBSome interacting protein, namely BBIP10 (Loktev et al., 2008). The BBS proteins are named after the Bardet-Biedl syndrome, a rare, multi-organ, autosomal recessive disorder associated with mutations in BBSome subunit encoding genes (Suspitsin and Imyanitov, 2016).

The BBSome mainly localizes both at the base of the cilium and along its shaft, where it interacts with the IFT-particles and it is transported by them (Blacque et al., 2004; Mykytyn and Sheffield, 2004) (**Figure XIII**). Although dispensable for proper formation of cilia in most tissues and ciliated organisms, the BBSome seems important for the correct trafficking and sorting of some ciliary membrane proteins at the base of the cilium. It would be also required for the loading and stabilization of such membrane proteins on the IFT-particles, which eventually transport them along the cilium as cargoes (Blacque et al., 2004; Jin et al., 2010; Malicki and Avidor-Reiss, 2014) (**Figure XIII**). In addition, the BBSome seems to play a role in organizing the turnaround of the IFT-trains at the ciliary tip (described in the next paragraph). Finally, it is also implicated in the IFT-mediated export of specific ciliary components, as result of signaling activation or recycling (Lechtreck et al., 2009, 2013).

I.4.3.2 Ciliary import, transport and export of IFT cargoes

Anterograde IFT-trains assemble at the base of the primary cilium, presumably at the level of distal appendages, which seem to work as docking sites (Deane et al., 2001; Wei et al., 2013) (**Figure XIII**). Here the IFT-A and B are coupled together and bound to active kinesin-2 and inactive cytoplasmic dynein-2 (Brown et al., 2015; Liang et al., 2014). At the same time, cargo proteins including both soluble and transmembrane⁵ ciliary proteins and the BBSome are loaded on IFT-particles. Such interactions are supposed to be granted by the numerous protein binding domains found in the IFT-A and B subunits, including tetratricopeptide, WD and coiled-coils domains. In addition, as stated above, the BBSome may help to stabilize and organize the cargo-IFT-particle interactions.

Once assembled, IFT-trains must pass through the transition zone, which, as described before, is part of the ciliary gate, thus it acts as a filter that excludes non-ciliary proteins from entering the cilium. However, how mechanistically this filter works is still puzzling. Some pieces of evidence indicate that the transition zone offers size-exclusion filtering properties, impairing the free diffusion of large molecules within the ciliary compartment (Kee et al., 2012). Therefore, large molecules (estimated to be >7.9nm in diameter, but it may vary depending on the cilium type) would require an active mechanism of transport (Lin et al., 2013; Malicki and Avidor-Reiss, 2014). One of such mechanisms is based on gradients of the small GTPase Ran and importin- β proteins (Dishinger et al., 2010), a mechanism that strikingly parallels the one observed at the nuclear pore complex during regulation of selective import and export of nuclear proteins. Similarly to what happens for the nuclear transport, the Ran-importin- β axis, relies on recognition of particular, short cilium-localization signals (CLSs) present in ciliary proteins (Berbari et al., 2008; Dishinger et al., 2010; Malicki and Avidor-Reiss, 2014; Tam et al., 2000). Various CLSs were identified in a number of ciliary proteins, especially in GPCRs where it consists on a simple VxP motif.

Importantly, importin- β is not the only molecule able to recognize and bind CLSs. Indeed, two small ciliary GTPases, namely ADP-ribosylation factor 4 (Arf4) and ADP-ribosylation factor-like protein 13b (Arl13b) and also the BBSome were shown to mediate the active ciliary trafficking of Opsins, GPCRs and other proteins by recognising specific and divergent CLSs along their sequence (Malicki and Avidor-Reiss, 2014).

⁵ Some transmembrane proteins seem not to require the IFT transport to enter and move along the ciliary membrane. In these cases, their movement along the axoneme seems driven by mere diffusion or by transient binding to IFT-trains (Ye et al., 2013).

Nevertheless, it appears that not all the ciliary proteins are equipped with a CLS, therefore they may utilize other strategies to enter the cilium. Maybe, the mere capability to strongly associate to IFT-particles could be a sufficient condition for freely passing through the ciliary gate.

Once crossed the transition zone, the kinesin-2 IFT-motor boosts the movement of the IFT-train toward the tip of the cilium, where the cargo is released. Release of the cargo is accompanied by a large remodeling of the anterograde IFT-train: kinesin-2 becomes inactivated, cytoplasmic dynein-2 takes its place and turnover products or signaling molecules are loaded. The result is the formation of a retrograde IFT-train which is appointed to export proteins from the cilium. The remodeling of the IFT train, or train turnaround, is a complicated event regulated by ciliary tip protein kinases, some IFT-particles subunits and the BBsome (Chaya et al., 2014; Liang et al., 2014; Pedersen et al., 2005; Tsao and Gorovsky, 2008; Wei et al., 2012).

I.4.3.2.1 *Transport of ciliary membrane proteins*

While soluble ciliary proteins, after synthesis in the cytoplasm, reach the base of the cilium via diffusion or through transport along the microtubule network, ciliary membrane proteins (CMPs) follow a different path. As the ciliary membrane is part of the plasma membrane, CMPs are first synthesized in the endoplasmic reticulum and then transported to the Golgi apparatus via the secretory pathway. At the trans-Golgi network, CMPs are included in budding vesicles and are transported at the base of the cilium (**Figure XIII**).

It is not fully elucidated how CMPs at the trans-Golgi network become targeted to cilia. However, the activity of at least two proteins seems important for this process, namely the previously cited Arf4 and the IFT protein Intraflagellar transport protein 20 (Ift20). Both Arf4 and Ift20 localize at the trans-Golgi membranes and are believed to mediate the sorting and packaging of CMPs into nascent vesicles (Blacque et al., 2017; Follit et al., 2006; Mazelova et al., 2009; Nachury et al., 2007). Although they seem to act through two different pathways and may not even share common CMPs as targets, the combined Arf4 and Ift20 activity ultimately converge on the activation of a key small GTPase, namely Rab8 (**Figure XIII**).

Rab8 works as the main regulator for vesicle accumulation and fusion at the base of the cilium. Upon activation by its guanine nucleotide exchange factor (GEF) Rabin8, active Rab8 mediates the docking of CMPs-containing vesicles to the basal body subdistal appendages, and eventually promotes their fusion likely in the periciliary membrane (Blacque et al., 2017; Malicki and Avidor-Reiss, 2014; Yoshimura et al., 2007).

Once in the periciliary membrane, at least a subset of CMPs, including many GPRCs, are sorted to cilia through the BBSome. This mechanism requires the activity of another small GTPase, ADP-ribosylation factor 6 (Arl6), which can recruit multiple copies of the BBSome at the membrane. Here, the BBSomes polymerize into a planar coat just beneath the phospholipids bilayer (Jin et al., 2010; Mourão et al., 2014). This mantle of BBSomes binds some CMPs (perhaps via recognition of specific CTSs, as reported before), and mediates their load on IFT-trains (Jin et al., 2010) (**Figure XIII**). Interestingly the BBSome interacts also with Rabin8, hence potentially coupling vesicle trafficking and fusion to ciliary membrane sorting of CMPs (Nachury et al., 2007).

I.4.4 CILIOGENESIS IS ENTANGLED TO CELL CYCLE PROGRESSION

In vertebrates, primary cilia are typically observed on the surface of post-mitotic, differentiated cells. Indeed, upon terminal entry in the G₀ phase, the centrosome, that during the last mitosis was organizing the mitotic spindle, approaches the plasma membrane and nucleates the ciliary axoneme through the mother centriole. Importantly, when involved in the nucleation of a primary cilium, the centrosome is “sequestered” and it cannot participate in the generation of the mitotic spindle (Nigg and Stearns, 2011). Therefore, the genesis of a primary cilium is generally seen as a mean to prevent a potential, undesired cell cycle re-entry.

There are however exceptions to this general rule. In some cases, primary cilia are grown also by actively proliferating cells, for instance when they are required for transducing mitogenic stimuli. In these cases, primary cilia are assembled after mitosis, during the early G₁/G₀ phase. Once generated, primary cilia sense and transduce proliferative signals that push the cell toward the G₁/S restriction point, committing it to a new cell cycle. Upon cell cycle re-entry, cells need to disassemble primary cilia in order to release the centrosome enabling it to nucleate the mitotic spindle. Therefore, in some cycling populations primary cilia are present, but they are actively assembled and disassembled in synchrony with the progression of the cell cycle (Plotnikova et al., 2009) (**Figure XIV**).

I.4.4.1 Biogenesis of primary cilia

Once completed the mitosis and disassembled the mitotic spindle, the distal extremity of the mother centriole becomes surrounded by a series of small vesicles deriving from the Golgi apparatus (Sorokin, 1962).

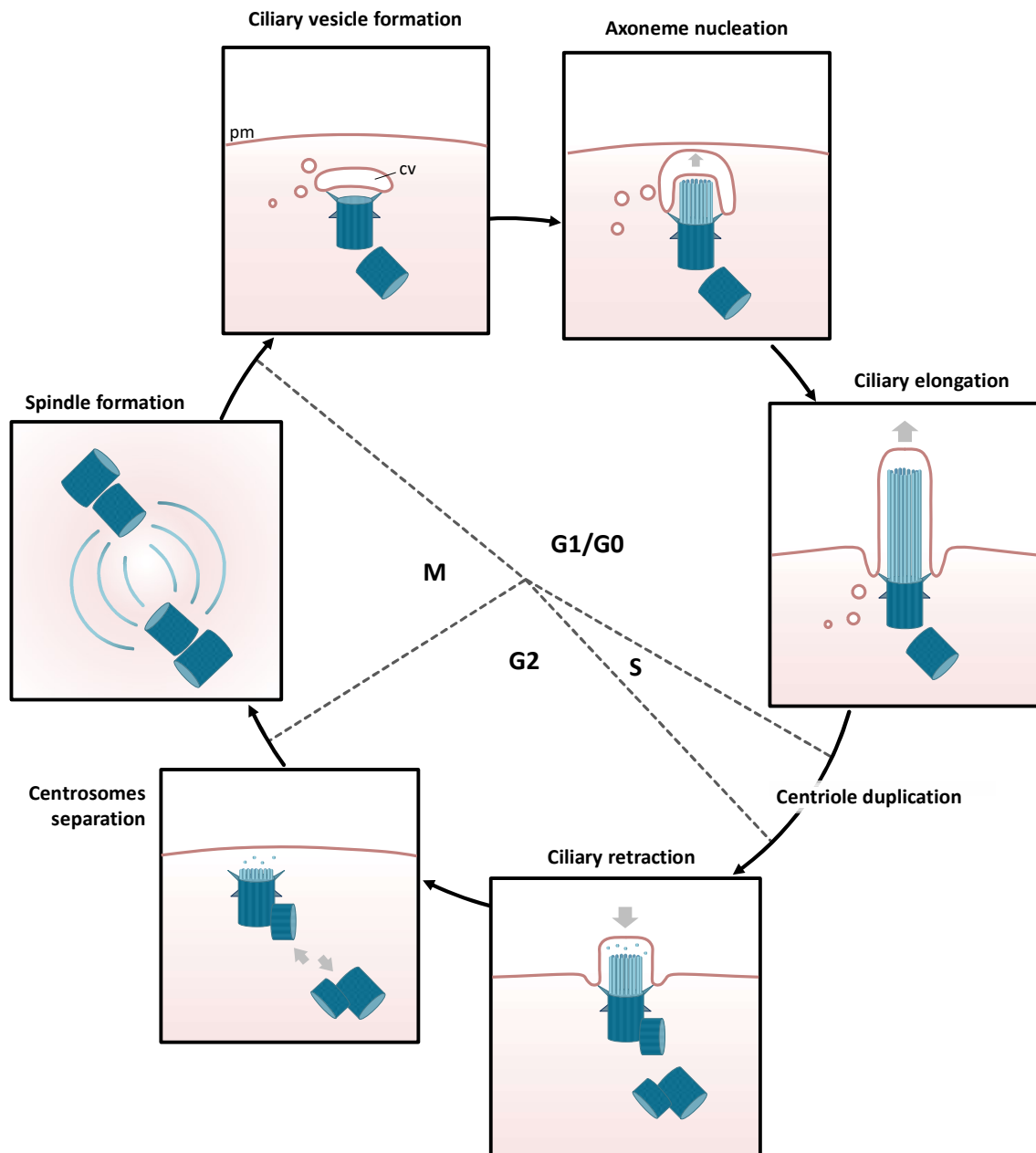


Figure XIV. Cilium-centrosome behaviour during the cell cycle. At early G1/G0 phase, Golgi derived vesicles fuse on the top of the mother centriole to generate the ciliary vesicle (cv). Next, the axoneme initiates its growth and the ciliary vesicle elongates surrounding it like a cap. Eventually the ciliary vesicle fuses with the plasma membrane (pm) making the cilium to protrude from the cell. If the cell is triggered to re-enter the cell cycle (sometimes thanks to cilium-dependent transduction of growth signaling pathways), then the cilium is committed to disassembly. During S phase, centrioles are duplicated and cilia may initiate their shortening. Complete retraction of the cilium is achieved during G2 phase. During late G2, the two pairs of centrioles separate to initiate the mitotic spindle nucleation. During mitosis (M phase) the spindle is fully formed and is used to segregate chromosomes (not shown). Once divided, the cell re-enters the G1/G0 phase starting a new cycle.

The formation and trafficking of these small vesicles depends once again by Rab8 which is recruited along with Rabin8, to the centriolar distal appendages by Cep164 (Tanos et al., 2013). Later, these vesicles fuse into a unique larger ciliary vesicle which represents a primordium of the ciliary membrane (**Figure XIV**).

Concomitantly, the distal extremity of the mother centriole acquires the ability to nucleate the ciliary axoneme, which starts to elongate. This is achieved through either displacement or inactivation of negative regulators of axoneme growth. For instance, Centriolar coiled-coil protein of 110 kDa (CP110) and Cep97 are centrosomal proteins that keep axoneme formation prevented apparently by physically capping the distal tip of the mother centriole. However, upon entry in G1/G0 phase, CP110 and Cep97 are removed, likely by degradation, thus enabling the growth of the axoneme (Spektor et al., 2007).

The elongation of the axoneme below the ciliary vesicle curves its membrane, making it to acquire a typical "hat" shape that covers the axoneme (**Figure XIV**). Moving along the actin cytoskeleton, the whole centrosome migrates toward the plasma membrane. During this route, the axoneme continues to grow (thanks to the IFT) and the ciliary vesicle elongates through the fusion with newly coming vesicles (Mirvis et al., 2018). Once approached to the plasma membrane, the distal surface of the ciliary vesicle fuses with it, generating the invagination of the plasma membrane that will become the ciliary pocket (**Figure XIV**). The proximal surface of the ex-ciliary vesicle now surrounds the axoneme and it is exposed to the extracellular environment protruding from the cell. This new plasma membrane domain becomes the ciliary membrane. Simultaneously the distal appendages stabilize the docking of the mother centriole/basal body to the plasma membrane.

1.4.4.2 Disassembly of primary cilia

While many details about the molecular mechanisms controlling ciliogenesis have been unraveled, cilium disassembly is less understood. In this context, the use of ciliated cell lines, as human retinal pigmented epithelial cells (RPE-1 cells) or mouse 3T3 fibroblasts, has been instrumental to gain insight on the bases of ciliary resorption. Upon cell cycle exit induced by serum withdrawal, these cells grow a primary cilium. However, upon serum re-addition, they synchronously re-enter the cell cycle and concomitantly retract the cilium. Using these models, it was found that a synchronized cell population tends to disassemble primary cilia into two separate temporal waves, that are just after the G1/S transition and just before the mitotic entry (Pugacheva et al., 2007; Wang et al., 2013) (**Figure XIV**). However, both the physiological

relevance and the actual occurrence in *in vivo* systems of such bimodal ciliary resorption are unknown.

Nevertheless, some cilia disassembly pathways have emerged, and interestingly most of them are orchestrated by mitotic protein kinases, highlighting the tight coupling between cilia retraction and cell cycle progression.

Among them, perhaps the most relevant is led by Aurora A (Aurka), a protein kinase involved in mitotic entry. Indeed, besides its well documented role during mitosis, Aurka was shown to be recruited at the basal body just prior the time of ciliary disassembly. Here, Aurka phosphorylates and activates Histone deacetylase 6 (HDAC6), which removes acetyl groups from α -tubulin promoting the depolymerization of the axonemal microtubules (Pugacheva et al., 2007). In addition, during mitosis Aurka phosphorylates and activates another protein kinase, namely Polo-like kinase 1 (Plk1), to regulate various aspects of cell division (Macûrek et al., 2008). Importantly, activated Plk1 was shown to collaborate with Aurka in promoting ciliary disassembly. Indeed, also Plk1 phosphorylates HDAC6, stimulating its enzymatic activity (Wang et al., 2013).

Another ciliary retraction pathway relies on the mitotic protein kinase Nek2. At the S/G2 transition, Nek2 is active at the basal body and phosphorylates Kif24, a kinesin-13 family member. Kif24 normally localizes at the mother centriole/basal body where it is implicated in the depolymerization of axonemal microtubules (Kobayashi et al., 2011). Nek2-dependent phosphorylation enhances Kif24 functions, thus promoting ciliary disassembly in a pathway that is independent of HDAC6 activity (Kim et al., 2015b).

1.4.5 PRIMARY CILIA ARE SIGNALING CENTERS IN VERTEBRATES

Dysfunctions of both motile or primary cilia, due to hereditary genetic mutations, cause a broad spectrum of human disorders collectively named ciliopathies.

Nowadays almost 200 genes have been associated to ciliopathies (Reiter and Leroux, 2017). Manifestation of such disorders include arrays of pathological phenotypes like obesity, polycystic kidneys, mental retardation, retinal degeneration and abnormal skeletal development. Therefore, as presumable, motile and primary cilia are involved into pleiotropic functions in the organism. In the case of primary cilia, these functions consist mainly in mediating a number of signaling pathways.

The first indications of such activity came from a study of Huangfu and colleagues (2003) where mouse ciliary mutants for IFT proteins (namely Ift172 and Ift88) displayed embryonic patterning abnormalities resembling those caused by defective SHH signaling. In the same work, the IFT in the primary cilium was shown to be required for the proper activation of the SHH signaling cascade.

Following studies further demonstrated that the primary cilia membrane is enriched in signaling receptors and many of their downstream transducers transit or localize at the cilium. Today we know that besides SHH, also WNT, Notch, Transforming Growth Factor- β (TGF- β), Platelet-derived growth factor (PDGF), Hippo, mammalian Target-of-Rapamycin (mTOR), many GPCRs and intracellular Ca^{++} influx-mediated signaling pathways completely or in part depend on primary cilia (Pala et al., 2017; Wheway et al., 2018).

Still puzzling is why such evolutionary ancient structures as cilia were reutilized by vertebrates for signaling. Perhaps concentrating receptors and downstream signaling proteins in the restricted ciliary compartment may favor their reciprocal interaction and promote efficient signaling. In addition, the exploitation of an already existing and specialized transport as the IFT might have been beneficial for moving signaling proteins in and out the cilium and thus enabling fast and effective pathway activation or repression.

I.4.5.1 Overview of the Hedgehog signaling

Among the signaling pathways flowing within primary cilia, the (Sonic) Hedgehog (HH) signaling is by far the best characterized. Initially discovered in *Drosophila melanogaster*, the HH signaling is conserved also in vertebrates where it is implicated a large variety of developmental, homeostatic and pathological processes. By acting as long range diffusing morphogen, HH proteins are responsible for the patterning of developing tissues and organs, as the brain, the neural tube, the limb buds and the teeth in vertebrates or the wing imaginal discs of *Drosophila* larvae (Dassule et al., 2000; Jessell, 2000; Riddle et al., 1993; Takahashi and Liu, 2006; Torroja et al., 2005). In addition, HH also works as axon guidance cue for spinal cord dorsal commissural neurons (Charron et al., 2003).

Besides its wide roles during development, the HH signaling is required for the maintenance of various adult stem cells pools, as those of the hair follicle, hippocampus and hematopoietic system, therefore contributing to tissue homeostasis and regeneration (Beachy et al., 2004). Finally, human germinal or somatic mutations can reduce or aberrantly activate the HH signaling leading to emergence of hereditary diseases, as the previously cited Gorlin syndrome

or the Pallister-Hall syndrome or cancers as certainly SHH-MB, but also basal cell carcinoma (BCC) (Hill et al., 2007; Teglund and Toftgård, 2010).

I.4.5.2 Major components of the Hedgehog signaling

Divergence has accumulated during evolution between the modality of HH signal transduction in vertebrates and in invertebrates. In vertebrates, large part of the active HH signaling cascade occurs within the primary cilium, which is also required for the suppression of the pathway in absence of HH. In invertebrates as *Drosophila* where primary cilia are absent, the HH cascade occurs in a cilium independent modality. Nevertheless, there exist a good degree of conservation between the key HH pathway proteins, which is also reflected by similar, although sometimes not identical, mechanisms of activity regulation

I.4.5.2.1 Hedgehog proteins

Drosophila genome harbors only one gene encoding for the ligand of the pathway, namely *hedgehog* (*hh*). The name “Hedgehog” was given after the typical bristles appearing at the surface of *hh* mutant larvae originally identified via genetic screenings by Nüsslein-Volhard and Wieschaus (1980). Years later, three orthologous genes were identified in vertebrates, namely *Indian Hedgehog* (*IHH*), *Desert Hedgehog* (*DHH*) and *SHH* (Echelard et al., 1993). While the activity of *IHH* and *DHH* is limited to specific tissues or niches in organs, *SHH* shows the broadest expression and involvement in multiple processes in the organism.

All the HH proteins are basically subjected to the same types of post-translational processing, modality of secretion and extracellular diffusion (**Figure XV**). HH polypeptides are initially translocated in the endoplasmic reticulum upon during their synthesis. After the canonical removal of the N-terminal signal peptide, HH polypeptides undergo an autoproteolytic cleavage which generates two polypeptides corresponding to the N- and C-terminal domains of the original protein. The C-terminal domain, which was required for catalyzing the autocleavage, is degraded, while the N-terminal domain (hereafter called HH-N or simply referred as HH) represents the biologically active HH protein (Lee et al., 1994; Porter et al., 1995). Simultaneously to the autocleavage a cholesterol group is covalently linked via ester bond to the novel C-terminus of the N-HH protein (Porter et al., 1996). In addition, also a palmitate group is added at the N-terminus in a following step (Pepinsky et al., 1998) (**Figure XV**).

These lipidations of HH-N notably increase its hydrophobicity, thereby promoting its retention on the plasma membrane of producing or neighboring cells, once secreted. Because of that, the

activity of a transmembrane protein, namely Dispatched, is required for helping the release of HH-N from the plasma membrane (Burke et al., 1999). Intriguingly, if on one side lipidations are generally important for limiting the diffusion of HH proteins, thus contributing to generate a sharp morphogen gradient, on the other, loss of HH lipidations was also shown to reduce its long-range diffusion (Buglino and Resh, 2012; Gallet et al., 2006; Lewis et al., 2001; Li et al., 2006). This apparent paradox can be explained by the fact that HH-N proteins do not only exist as monomers in the extracellular environment, but can also self-associate forming soluble multimers. In these multimers, the lipid moieties would be sequestered in the internal part of the complex, leaving the more hydrophilic HH-N polypeptides externally exposed. Once released from the membrane, such soluble multimers would be capable of diffusing and travel long distances (Chen et al., 2004).

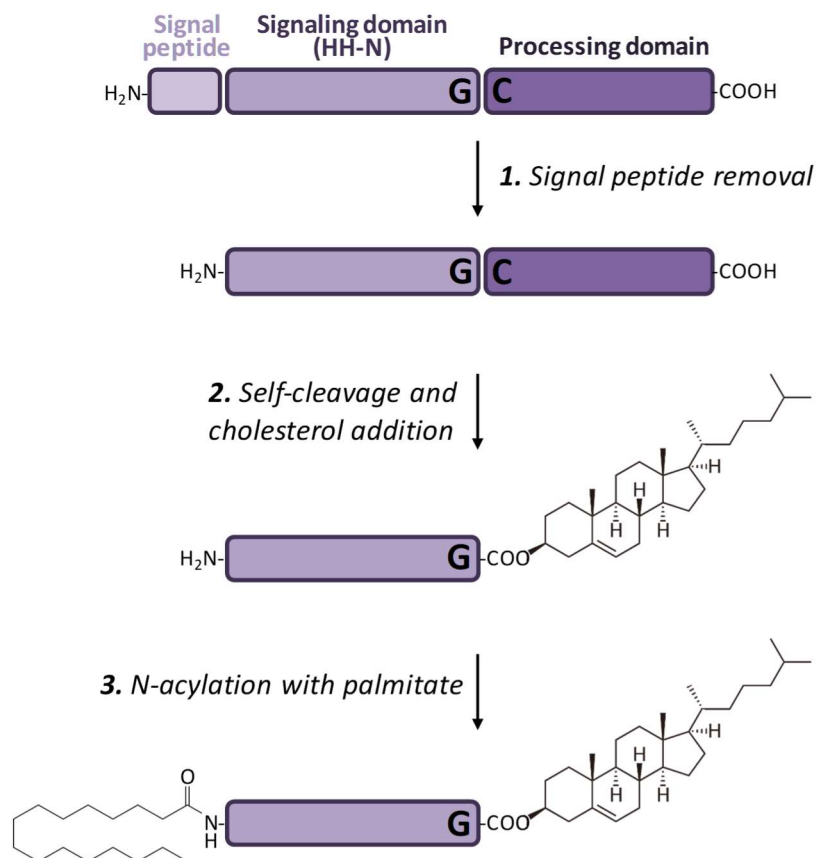


Figure XV. Synthesis steps of the active HH protein (HH-N) from the precursor. The full length HH polypeptide is synthesized while translocating in the endoplasmic reticulum, where the N-terminal signal peptide is cleaved. Soon after, the polypeptide itself catalyses a cleavage between two conserved residues of glycine (G) and cysteine (C), generating the N-terminal signaling competent domain (HH-N) and a C-terminal domain, which is eventually degraded. During the reaction, a cholesterol moiety is covalently linked to the glycine residue in the HH-N. Subsequently, the N-terminus of HH-N is acylated with a palmitate residue. The double-lipidated HH-N represents the mature, signaling functional HH protein.

I.4.5.2.2 *Patched is the HH receptor*

The HH receptor is a 12-span transmembrane protein named Patched (Ptc), discovered once again via genetic screening in *Drosophila* larvae mutants of segmental patterning (Nüsslein-Volhard and Wieschaus, 1980). Mammals have two highly conserved genes encoding for *Drosophila's ptc* homologs, namely *Ptch1* and *Ptch2*, (hereafter called *Ptch*) whose protein products are both capable to bind vertebrate HH ligands (Zhulyn et al., 2015). *Ptch* binds HH ligands via two large extracellular loops and requires the intracellular C-terminal tail for downstream signal transduction (Briscoe et al., 2001; Johnson et al., 2000; Marigo et al., 1996). Interestingly, sequence analysis of *Ptch* proteins revealed high homology to a class of prokaryotic membrane transporters, namely the resistance-nodulation-division (RND) family, implicated in the proton driven flux of hopanoids, molecules related to sterols. Whether a similar function of *Ptch* is conserved also in animals is not clear, although mutations of the critical conserved aminoacid residues potentially implicated in transport activity were shown to disrupt *Ptch* signaling ability (Strutt et al., 2001; Taipale et al., 2002).

Indeed, *Ptch* is believed to accomplish at least two major functions in the context of HH signaling. First, binding of HH triggers internalization of *Ptch* into endosomes. This event does not seem to have any particular readout in the HH signal transduction itself; however, as also HH is internalized, such event contributes at shaping the HH extracellular gradient within the tissue (Torroja et al., 2004). Second, more importantly, in the absence of HH binding, *Ptch* is required for maintaining the pathway repressed, by constantly inhibiting the activation of another transmembrane protein, Smoothened (*Smo*). Therefore, *Ptch* acts as a negative regulator of the HH pathway. Upon binding to HH, *Ptch* is inhibited and so the repression on *Smo* is relieved. The precise molecular mechanism employed by *Ptch* to maintain *Smo* inhibition is still matter of research and it is discussed in the next paragraph.

I.4.5.2.3 *Smoothened is repressed by Patched*

Both *Drosophila* and mammalian genomes encode for one *Smo* protein. This positive regulator of the HH signaling is a seven-span transmembrane protein belonging to the Frizzled class of GPCRs superfamily. In a classic and perhaps simplistic view, GPCRs can exist into at least two distinct conformations, corresponding to active and inactive states. Active forms are stabilized by binding to ligands, either proteins or small molecules, and are capable of signaling through activation of intracellular heterotrimeric G proteins. When the ligand is a protein, GPCRs are

equipped with large N-terminal extracellular domains required for ligand binding (Kobilka, 2007)

Also Smo can be found in at least two major conformational states: active, capable of downstream signaling, and inactive. However, despite the presence of a large N-terminal extracellular cysteine-rich domain (CRD), no protein ligand has ever been shown to bind and activate Smo. Rather, Smo activation seems more likely to be regulated by small molecules, notably sterols. This model is strongly suggested by a large panel of sterol-like natural or synthetic agonists and antagonists capable of modulating Smo by binding the CRD or the integral heptahelical transmembrane domain⁶. More importantly, some endogenous sterols, namely oxysterols, were shown to stimulate SHH pathway activation at the level of Smo by binding to the CRD domain (Byrne et al., 2016; Cooper et al., 2003; Corcoran and Scott, 2006; Dwyer et al., 2007; Huang et al., 2018b). In addition, very recent findings based on the characterization of Smo crystal structure when stabilized into a *bona fide*, fully active conformation, demonstrated that an uncharacterized sterol molecule lays in a hydrophobic pocket within the heptahelical transmembrane domain (Deshpande et al., 2019). In conclusion, it is nowadays clear that Smo contains at least two binding sites for sterols or sterol-derivatives: the CRD and the transmembrane domain. However, how and whether these binding events allosterically collaborate or independently influence the stabilization of Smo into its active form remains unclear.

Importantly, the discovery that Smo activity is modulated by sterols provides an interesting mechanistic link with its Ptch-mediated inhibition (Taipale et al., 2002). According to this model, Ptch would actually function as a sterol transporter, perhaps able to catalyze the "flip" of these molecules from one leaflet to the other of the plasma membrane. By doing that, Ptch would modify the availability of membrane sterols for Smo binding and activation, eventually maintaining Smo into an inactive state. Binding of HH to Ptch, would block this activity, thus enabling sterols to redistribute in the membrane leaflets and activate Smo.

Importantly, the activation of Smo determines a conformational switch at the level of its C-terminal cytoplasmic tail, which becomes heavily phosphorylated (Zhao et al., 2007). Several protein kinases are responsible for these phosphorylations, including GPCR kinase 2 (Gprk2), CKI α and PKA, the latter only in *Drosophila* (Chen et al., 2010, 2011; Jia et al., 2004).

⁶ Examples of antagonists, hence molecules inhibiting Smo activation in the presence of HH, are cyclopamine, SANT1, LY2940680 and the previously cited Vismodegib (GDC-0449). Agonists instead activate Smo in absence of HH and include SAG and purmorphamine (Chen et al., 2002a, 2002b; Frank-Kamenetsky et al., 2002; Robarge et al., 2009).

However, while Gprk2 activity is indispensable for pathway activation, whether this role is carried out only through Smo phosphorylation is not clear (Zhao et al., 2016).

Once fully activated, Smo becomes capable of downstream signaling to Gli transcription factors, leading to their activation. Importantly, this activity is performed at the level of the primary cilium where active Smo accumulates, as it will be discussed later.

I.4.5.2.4 The Gli transcription factors

Vertebrates possess three transcriptional mediators of the HH signaling, namely Gli1, Gli2 and Gli3, all homologous to *Drosophila*'s Cubitus interruptus (Ci) protein. They all belong to the Gli-Kruppel transcription factor family, and they are characterized by a common DNA-binding domain localizing at the center of the protein, composed by five tandem zinc finger motifs (Kinzler et al., 1988; Niewiadomski et al., 2019) (Figure XVI). The DNA-binding domain of Gli factors recognizes a nonameric consensus sequence, 5' GACCACCCA 3' localizing in the proximity of target genes (Kinzler and Vogelstein, 1990). Structurally, all Gli factors contain a C-terminal transactivation domain, which mediates the transcriptional activation of target genes via recruitment of cofactors required for transcription initiation. In addition, Gli2 and Gli3, but not Gli1, also possess a N-terminal repressor domain (Niewiadomski et al., 2019). Therefore, Gli2 and Gli3 can function both as transcriptional activator or repressor of target genes, while Gli1 acts only as an activator (McCleary-Wheeler, 2014).

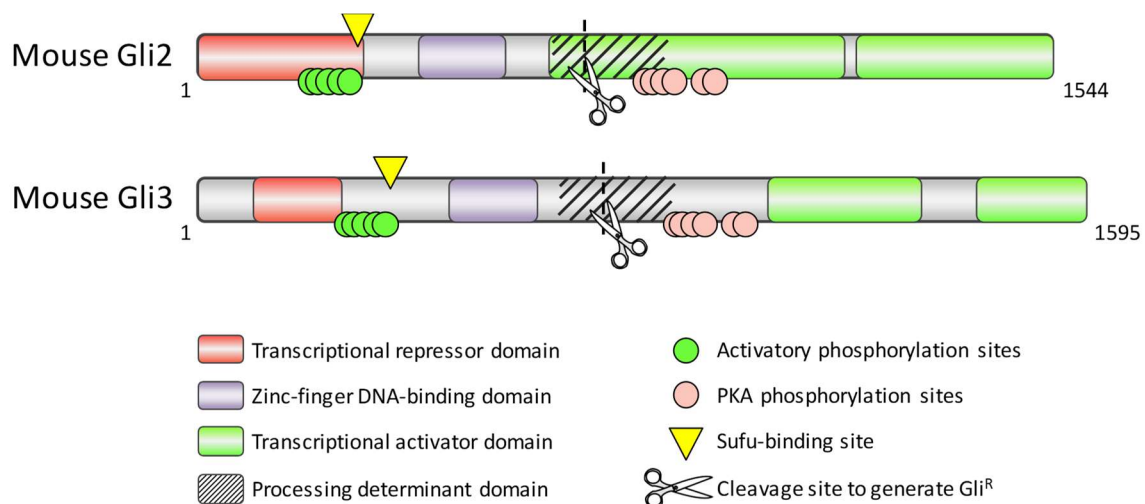


Figure XVI. Relevant domains and sites in mouse Gli2 and Gli3 proteins. Inspired by Kong and colleagues (2019).

In the case of Gli2 and Gli3, whether one or the other activity is favored is determined by the level of activation of the HH signaling. Indeed, the general output of the HH signaling consists in regulating of the balance between the activator and repressor functions of Gli. In general, the more the HH pathway is active, the more this balance is pushed toward the activator function of Gli. How is this regulation achieved?

In order to behave as transcriptional repressor, Gli2 and Gli3 must undergo a partial proteolytic cleavage mediated by the ubiquitin-proteasome system. This partial degradation removes the C-terminal activation domain, leaving the DNA binding and the N-terminal repressor domains intact. The so generated truncated Gli2 and Gli3 (hereafter named Gli^R, for Repressor, in contrast to Gli^{FL} for Full Length, non-processed forms) are thus only able to repress gene expression (Niewiadomski et al., 2019) (**Figure XVI**). This processing normally occurs when HH is not present, thus when Ptch exerts its inhibition on Smo.

In this "pathway OFF" condition, Gli^{FL} are initially phosphorylated by PKA, which primes these proteins for subsequent phosphorylations catalyzed by GSK-3 β and CKI. These phosphorylations concern a cluster of aminoacids localizing in a region, called processing determinant domain (PDD), situated centrally in the proteins (Niewiadomski et al., 2019) (**Figure XVI**). Phosphorylation of the PDD, creates a docking site for a F-box protein called β -Transducin repeats-containing protein (β -TrCP), which is part of a SCF E3-ubiquitin ligase complex (Jia et al., 2005). This interaction causes poly-ubiquitination of Gli^{FL} and consequent proteasomal targeting to generate the repressor forms.

Importantly, the processing of Gli3^{FL} to Gli3^R is typically much favored compared to Gli2^{FL}, which conversely is mainly fully degraded (Bhatia et al., 2006; Pan et al., 2006; Wang et al., 2000). Hence, Gli3 is considered the main mediator of Gli global repressor functions, while Gli2 the major transcriptional activator.

Importantly, the production of Gli^R is repressed when the pathway is activated by binding of HH to Ptch. The consequent activation of Smo triggers a still unclear mechanism culminating with Gli^{FL} escaping from the phosphorylations on their PDDs and thereby from the partial degradation. Importantly, not only the active HH signaling blocks Gli^R generation, but also it is believed to decorate Gli^{FL} with some PTMs, that potentiate their activity as transcriptional activators (indicated as Gli^A, for Activator). The nature of this activatory PTMs is still controversial, but some suggested that a series of phosphorylations occurring in the N-terminal region of Gli2 and Gli3 may be good candidates (Humke et al., 2010; Niewiadomski et al.,

2014) (**Figure XVI**). Once activated, Gli^A enters the nucleus to promote transcription of target genes, including Gli1 which amplifies the HH response.

I.4.5.3 Mechanisms of vertebrate HH signaling through the primary cilium

Whereas the HH signaling in *Drosophila* is relayed between the plasma membrane and the cytoplasm where it depends on an intact microtubule network, in vertebrates, large part of the signaling cascade requires the primary cilium (**Figure XVII**).

I.4.5.3.1 HH pathway OFF

In the absence of HH ligands, Ptch localizes in the proximal part of the ciliary membrane, in virtue of a ciliary localization signal (CLS) in its C-terminal cytoplasmic tail (Kim et al., 2015a). Conversely, Smo is mainly observed in intracellular vesicles and it is kept in its inactive state by the activity of Ptch in the cilium (Kim et al., 2015a). As described above, it is believed that Ptch regulates the behavior of Smo by mediating fluxes of regulatory sterols, hence modifying their availability and preventing Smo to be activated.

Locked in its inactive conformation, Smo is known to transit dynamically in and out the ciliary shaft, in a process that requires the ciliary IFT (Keady et al., 2012; Kim et al., 2009). However, the significance of this continuous trafficking remains unclear. Also in the case of Smo, a CLS localizes in its C-terminal tail and mediates its import in the cilium (Kim et al., 2015a).

Simultaneously, Gli2^{FL} and Gli3^{FL} are synthesized in the cytoplasm. Here, another key HH pathway component, namely SuFu, restrains them in the cytoplasm, by binding and sequestering them into complexes containing the kinesin Kif7 (Huang et al., 2018a). This regulation is supposed to prevent Gli2^{FL} and Gli3^{FL}, which may possess basal activator functions, to activate HH target genes in the absence of HH (Huang et al., 2018a; Humke et al., 2010). In the cytoplasm, Gli2^{FL} and Gli3^{FL} seem to utilize the microtubule network to reach the ciliary base, and subsequently enter in the ciliary compartment (Kim et al., 2009). Here, they dynamically transit through its shaft, in a route that once again is dependent on IFT (Kim et al., 2009; Wen et al., 2010).

The movement of Gli2^{FL} and Gli3^{FL} in the cilium is required for their conversion into repressor forms, which importantly makes the cilium essential also for HH pathway repression (Humke et al., 2010; Liu et al., 2005; Wen et al., 2010). At the exit of primary cilium, Gli2^{FL} and Gli3^{FL} are phosphorylated by PKA, CKI and GSK-3 β which localize at the base of the primary cilium.

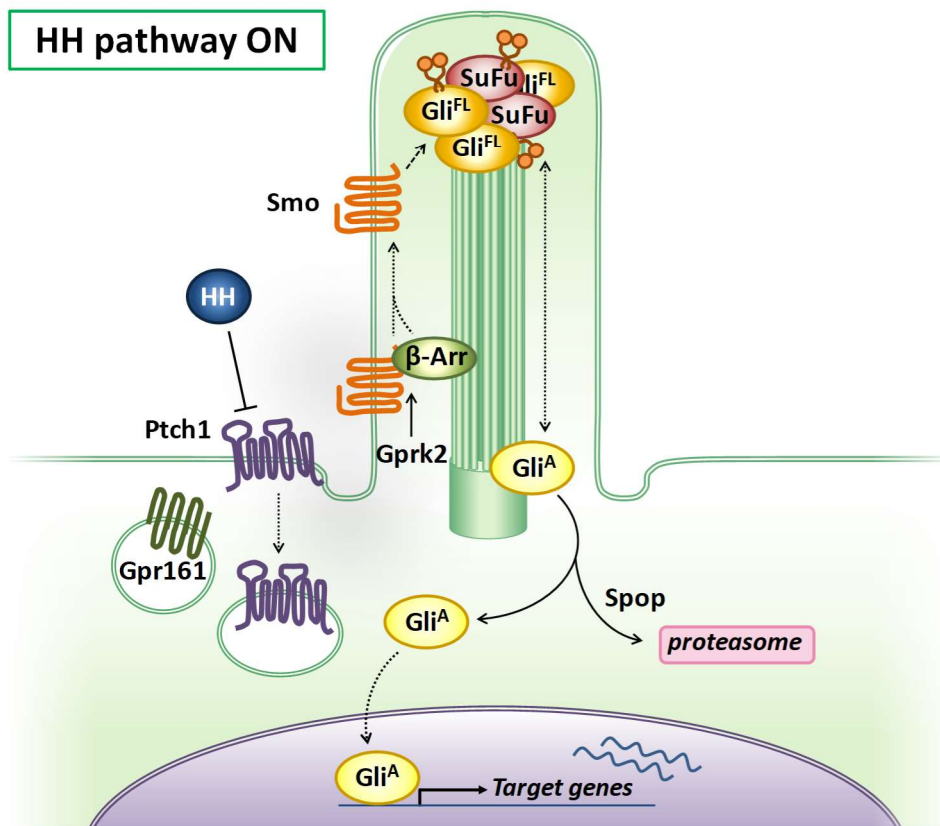
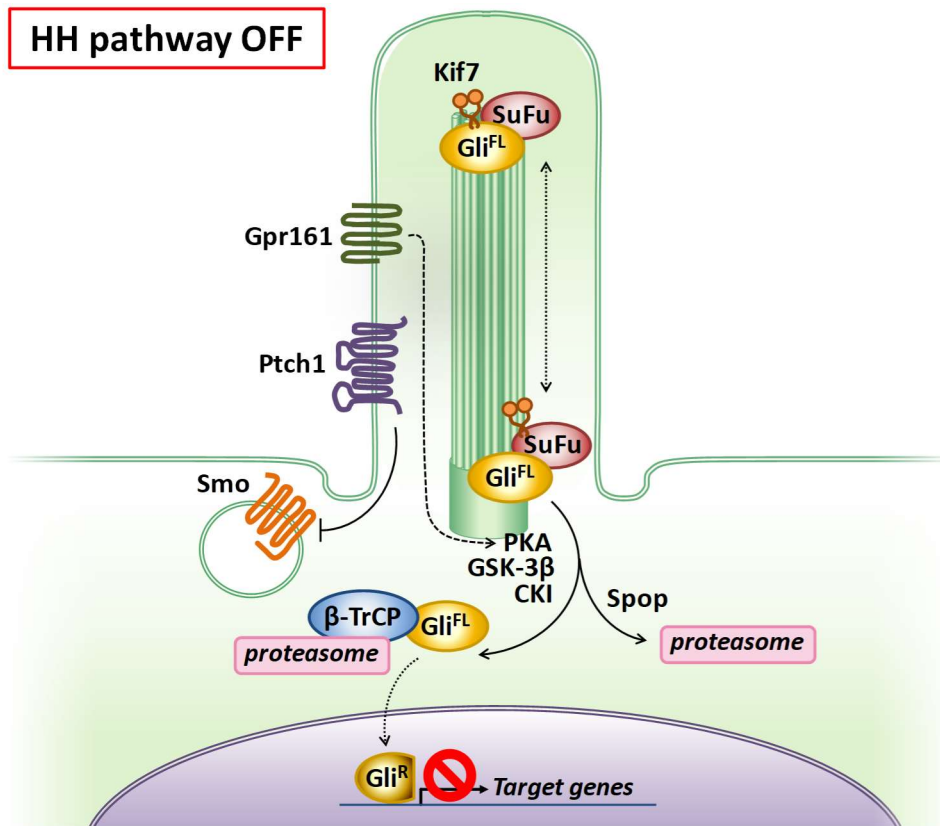


Figure XVII. HH signaling in vertebrates. (Upper drawing) In the absence of HH, the pathway is kept in a repressed state (OFF). Ptch1 localizes in the initial segment of the ciliary membrane and it represses Smo, which is mainly maintained into endosomes, although it also transits through the cilium. (legend continued on next page)

(legend continued from previous page) The full-length form of Gli2 and Gli3 (Gli^{FL}) dynamically move along the ciliary axoneme in combination with SuFu and Kif7. Gli^{FL} are targeted to degradation by Spop, but this interaction is reduced by SuFu. At the ciliary base, multiple phosphorylations operated by PKA, GSK-3 β and CK1 target Gli^{FL} to polyubiquitination by β -TrCP and consequent partial degradation in the proteasome. High PKA activity is maintained by the orphan GPCR Gpr161 in the cilium. The proteasomal-processed Gli^R is a truncated form of Gli which works as a transcriptional repressor. Once in the nucleus, Gli^R keeps HH target genes repressed.

(Lower drawing) In the presence of HH, Ptch1 is inhibited and internalized in the cell. The repression on Smo is thus relieved, and it becomes fully activated by Gprk2 phosphorylations. Active Smo accumulates in the cilium, induces Gpr161 internalization, and leads to accumulation of Gli^{FL}-SuFu-Kif7 complex at the ciliary tip. Here Gli^{FL} is converted to a potent transcriptional activator, Gli^A, which exits the cilium bypassing the proteolytic cleavage and enters in the nucleus where it activates the transcription of target genes. Gli^A levels are controlled by Spop.

Importantly, the generation of Gli2^R and especially Gli3^R is promoted by the association of SuFu to the full-length forms. SuFu binding to Gli^{FL} indeed protects them from degradation, thus providing the initial substrate for Gli^R production and, additionally, may also help the recruitment of GSK-3 β (Humke et al., 2010; Infante et al., 2018; Kise et al., 2009; Wang et al., 2010). Simultaneously, interaction with SuFu also restricts Gli^{FL} conversion to Gli^A (Humke et al., 2010). Hence, SuFu acts at multiple levels to overall restrain HH pathway activation. Once proteolytically processed, Gli2^R and the more abundant Gli3^R enter in the nucleus to repress HH target genes transcription.

Finally, similarly to Ptch, the orphan G-protein coupled receptor 161 (Gpr161) was recently shown to localize in the ciliary membrane in the absence of HH and to work as a potent HH signaling repressor. Ciliary Gpr161 activates activatory α -subunits of trimeric G-proteins to downstream stimulate ciliary adenylate cyclases to synthesize cAMP. By maintaining elevated the cAMP concentration within the ciliary compartment, Gpr161 is supposed to indirectly sustain PKA activation, which in turn promotes Gli2^R and Gli3^R production (Mukhopadhyay et al., 2013).

1.4.5.3.2 HH pathway ON

At the surface of HH responsive cells, Ptch is not the sole protein bound by HH. Besides proteoglycans that were already discussed in paragraph 1.2.3.4.3, a series of co-receptors, namely Growth arrest specific1 (Gas1), Cell adhesion molecule-related/down-regulated by oncogenes (Cdo) and Brother of Cdo (Boc), facilitate the interaction between HH and Ptch. Conversely, the membrane protein Hedgehog-interacting protein 1 (Hhip1) has high affinity for HH, thereby it dampens signaling activation by reducing HH availability for Ptch.

Upon HH binding, Ptch is inhibited and exits the primary cilium, relieving its repression on Smo, that can now be activated. The ciliary exit of Ptch, seems however dispensable for Smo activation, whereas it is the HH binding the real triggering event (Kim et al., 2015a).

Activated Smo is subjected to phosphorylations on its C-terminal tail by CKI and Grk2 which promote its binding to β -arrestin and the anterograde IFT motor subunit Kif3a (Kovacs et al., 2008). Such process leads to entry and accumulation of active Smo in the ciliary membrane, where it forms a complex with the transmembrane proteins Evc and Evc2, whose mutations are linked to the Ellis van Creveld syndrome, a ciliopathy. Evc and Evc2, coupled to Smo were shown to mediate at least part of its downstream effects on Gli (Caparrós-Martín et al., 2013; Yang et al., 2012).

Another event simultaneously triggered by HH, is the ciliary exit of Gpr161, which causes consequent reduction of PKA activity at the ciliary base. Such process seems to be induced by Smo activation and ciliary accumulation, but the precise mechanism remains obscure (Mukhopadhyay et al., 2013; Pal et al., 2016). In addition, it has been proposed that active Smo itself could act like a canonical GPCR and relay through an inhibitory trimeric G-protein α -subunit to block adenylate cyclases-mediated cAMP production. Also this route is believed to eventually reduce ciliary PKA activity (Mukhopadhyay and Rohatgi, 2014; Ogden et al., 2008). Therefore, one first major output of the HH signaling is the reduction of ciliary PKA activity. Importantly, activated Smo in the cilium downstream leads to accumulation of Gli2^{FL} and Gli3^{FL} in complex with SuFu and Kif7 at the tip of the cilium, a process that requires Kif7 and the IFT (Endoh-Yamagami et al., 2009; Humke et al., 2010; Kim et al., 2009; Liem et al., 2009; Tukachinsky et al., 2010). Such event is key for Gli activation. At the ciliary tip, indeed the Gli^{FL}-SuFu interaction is broken, and Gli^{FL} are converted to Gli^A. Without SuFu, Gli^A bypasses the phosphorylations induced by the almost inactive PKA, thereby escaping from the partial proteasomal degradation (Humke et al., 2010; Tukachinsky et al., 2010). Still today, the precise order of the events and the mechanism underlying the Smo-Gli^A relay is poorly known. Nevertheless, the reduction of ciliary PKA activity and other findings like a Smo-Kif7 interaction or a proposed role for Evc2 in regulating the dissociation of Gli3^{FL}-SuFu complex, have begun to illuminate this process (Caparrós-Martín et al., 2013; Endoh-Yamagami et al., 2009; Yang et al., 2012).

The so generated Gli^A, translocate in the nucleus where especially Gli2^A activates the transcription of HH target genes. Among these genes, that vary depending on the cell type, some have key feedback regulatory effects on the pathway. As already mentioned, Gli1 is

among the HH targets and by working as an activator it is believed to amplify the Gli2^A-dependent response. Additionally, transcripts encoding for negative regulators as Ptc1, Ptc2 and Hhip are also produced, aimed at restricting any possible excessive activation of the pathway.

Interestingly, Gli^A displays markedly shorter half-life compared to Gli^{FL}. Gli turnover is mainly regulated by the E3 ubiquitin ligases Speckle-type POZ protein (Spop) and Itch, which by adding polyubiquitin chains target Gli^{FL}/Gli^A to complete proteasomal degradation (Di Marcotullio et al., 2006b; Wang et al., 2010). The higher turnover of Gli^A than Gli^{FL}, may be just a consequence of detachment from SuFu (Humke et al., 2010; Wang et al., 2010). Therefore, Spop- and Itch-mediated rapid degradation of Gli^A may reflect a mechanism that prevents prolonged activation of the pathway, once the HH stimulus has extinguished.

1.4.5.4 Roles of primary cilia in normal GNs development

As extensively reviewed above, SHH released from Purkinje cells drives the post-natal proliferation of GNP in the EGL. Being capable of responding to SHH, it is not surprising that GNP's surface is decorated by a primary cilium (Chizhikov et al., 2007; Del Cerro and Snider, 1972; Spassky et al., 2008). Perhaps, more unexpected is the observation that primary cilia become shorter or are completely reabsorbed upon differentiation of GNP (Di Pietro et al., 2017). This fact will be deeply tested and discussed in the **Results** session of this Thesis.

Several studies showed that impairment of ciliogenesis in the cerebellum, via conditional KO (cKO) of essential IFT-B genes as *Ift88* or *Kif3a*, strongly dampened the post-natal expansion of GNP, leaving however unaltered their ability to migrate and differentiate (Chizhikov et al., 2007; Spassky et al., 2008). This reduced GNP proliferation was linked to inability to transduce the mitogenic SHH signal for multiple reasons. First, GNP in the post-natal cerebellum of *Ift88* or *Kif3a* cKO mice show markedly reduced expression of SHH-targets, as *Gli1* and *Ccnd1* (Chizhikov et al., 2007; Spassky et al., 2008). Second, *Kif3a*-depleted GNP fail at proliferating *in vitro*, when recombinant SHH is exogenously provided (Spassky et al., 2008). Third, although primary cilia are already detected in GNP at E15.5, ablation of primary cilia at this stage does not affect their growth (Shimada et al., 2018; Spassky et al., 2008). The first signs of reduced proliferation are observed in EGL-located GNP by E18.5, which is the exact time at which GNP initiate to substantially respond to SHH.

Nevertheless, although dispensable for GNP development prior to E18.5, primary cilia in embryonic GNP are required for mediating the basal suppression of SHH operated by Gpr161

(Shimada et al., 2018). Indeed, while *Gpr161* deletion in early GNP causes premature, ligand-independent activation of SHH signaling, these effects are abolished when ciliogenesis is impaired by *Ifi88* KO (Shimada et al., 2018).

I.4.5.5 Roles of primary cilia in SHH-MB tumorigenesis

Primary cilia are required for mediating numerous signaling pathways, many of which may display oncogenic activity when hyperactivated or repressed. In addition, the presence of a primary cilium is tightly linked with cell cycle progression which is typically dysregulated in cancer cells. Hence, it is not surprising that primary cilia functions may impact tumorigenesis. Many studies have so far shown that primary cilia are typically less numerous or even completely lost in various cancers, when compared to the respective tissues-of-origin. This is the case of breast, pancreatic, ovarian, skin, kidney and cartilage cancers, where the reduced ciliogenesis is normally associated to deregulated activity of signaling pathways underlying their pathology (Liu et al., 2018). Importantly, downregulation of ciliogenesis seems an active oncogenic event in some tumors. For example, ovarian cancer cells might inhibit cilia formation by maintaining high level of Aurka, which as described above, promotes ciliary axoneme destabilization (Egeberg et al., 2012). Also, in melanoma, the high expression of EZH2, a Polycomb Repressive Complex 2 (PRC2) subunit, suppresses the activation of pro-ciliogenesis genes in cells, hence blocking formation of primary cilia (Zingg et al., 2018).

Conversely, in other tumors the competence to assemble primary cilia is an essential requirement, as signaling pathways driving proliferation, survival or resistance to therapy, may completely rely on intact primary cilia (Hoang-Minh et al., 2016; Jenks et al., 2018; Li et al., 2016; Wong et al., 2009).

The SHH signaling is found aberrantly activated in a number of cancers. As described its dependency on primary cilia has a dual nature, being the primary cilium mediating both the repression and the activation of the pathway. Therefore, the presence or absence of primary cilia in SHH-activated tumors, appear to depend on which of the two activities is majorly executed by the cilium in the specific tumor context (Liu et al., 2018).

In the case of SHH-MB, the requirement of primary cilia for tumorigenesis has been first explored by Han and colleagues (2009) by using opportune SHH-MB mouse models. In their work they showed that driving the expression of SmoM2 (the constitutively active form of Smo) in the mouse developing cerebellum causes formation of SHH-MB, which could be efficiently prevented by removal of primary cilia via *Kif3a* or *Ifi88* cKO. This result seems in accordance

with the requirement of integral ciliary structures to allow wild type Smo or SmoM2 to accumulate within for downstream signaling to Gli. However, unexpectedly, the transgenic expression of an activated form of Gli2 lacking the repressor domain, was not sufficient *per se* to drive SHH-MB formation, unless primary cilia were ablated from the same cells. Although seemingly paradoxical, this result was explained by hypothesizing that primary cilia would counteract the constitutively active Gli2 through sustained production of Gli3^R. Thus, loss of primary cilia would block Gli3 processing to Gli3^R, consequently unleashing Gli2 to drive tumor formation. These observations and others indicate that primary cilia can strikingly promote or suppress SHH-driven tumorigenesis, apparently depending on the nature of the driving mutation. According to the actual model, primary cilia would be indispensable for SHH-MB formations if the driving event occurs upstream the cilium, like *Ptch1* loss-of-function or *Smo* gain of function (Barakat et al., 2013; Bay et al., 2018; Han et al., 2009). Conversely, if the driving event affects a downstream component, as *Gli2*, then primary cilia would restrict tumorigenesis, by mediating their repressive functions on the pathway (Han et al., 2009). Whether this paradigm, extrapolated from genetic mouse models studies, is also true in human SHH-MB is not clear. Currently, it is only known that primary cilia are detected on human samples of SHH-MB and also in WNT-MB, highlighting the likely requirement of this organelle also for oncogenic WNT signaling (Han et al., 2009).

1.5 Centriolar Satellites

Pioneer electron microscopy studies in the '60s were beneficial for getting insights into the ultrastructure of the centrosome. It was thanks to these works that mysterious electron-dense bodies with a 70-100nm diameter were observed around the pericentrosomal matrix (Bernhard and de Harven, 1960). These granular structures were called centriolar satellites (CS) and for long time remained poorly studied. It was only in the '90s, after the identification of their major component, Pericentriolar material 1 (Pcm1), that CS began to be properly characterized. Nowadays CS are defined as large, non-membranous multiprotein complexes, that tethered to the microtubule network orbit around the centrosome of vertebrate cells. Although many information about their structure, regulation, dynamics and functions are still missing, CS are known essential contributors and regulators of a number of centrosome activities, ranging from the most classic MTOC functions, to duplication, stability and also ciliogenesis.

1.5.1 COMPOSITION OF CENTRIOLAR SATELLITES

1.5.1.1 Pericentriolar material 1 is the major component of CS

Initially identified through a screening of a cDNA expression library with a centrosome-reactive antiserum, Pcm1 is by far considered the principal component of CS (Balczon et al., 1994). Sequence analysis of this 230kDa protein, revealed the presence of numerous internal coiled-coil domains which were later shown to be required for Pcm1 self-oligomerization and interaction with other CS proteins (Balczon et al., 1994; Kubo and Tsukita, 2003; Lopes et al., 2011; Tollenaere et al., 2015). Importantly, genetic depletion of *Pcm1* from cells leads to massive disaggregation of CS, which is accompanied by disappearance or dispersion in the cytoplasm of the other CS proteins (Dammermann and Merdes, 2002).

Altogether these findings led to the accepted notion that Pcm1 works as a scaffold protein, that by self-oligomerizing generates a large platform on which all the other CS components can assemble (Kubo et al., 1999). As a corollary, the nowadays criteria used to assess whether or not a new protein is part of CS are (i) its interaction with Pcm1 and (ii) its cytoplasmic dispersal upon Pcm1 loss.

Interestingly, while most of CS proteins also localize in other cellular compartments, as the centrosome or the primary cilium, Pcm1 is exceptionally only observed on CS (Tollenaere et al., 2015). This fact can be exploited in immunofluorescence studies, where Pcm1 is indeed typically used as a *bona fide* marker for identifying CS structures (**Figure XVIII**).

1.5.1.2 CS are mainly composed by centrosomal proteins

The identification of Pcm1 as a reliable component of CS, paved the way for the discovery of the other constituents. Thanks to recent large-scale mass spectrometry-based approaches, nowadays hundreds of proteins are known to stably or transiently localize to CS (Conkar et al., 2017; Gheiratmand et al., 2019; Gupta et al., 2015; Quarantotti et al., 2019).

As anticipated, it was striking to realize that virtually all these proteins (with the important exception of Pcm1) did not exclusively localize to CS. Indeed, many CS proteins are also observed at the centrosome, where they are part of various centriolar structures (e.g. Ninein and Odf2 in the subdistal appendages; Talpid3, Cep290, Cep72, Cep131, Orofaciodigital Syndrome 1 (Ofd1) at the distal end of the mother centriole), or of the pericentriolar matrix (e.g. Pericentrin).

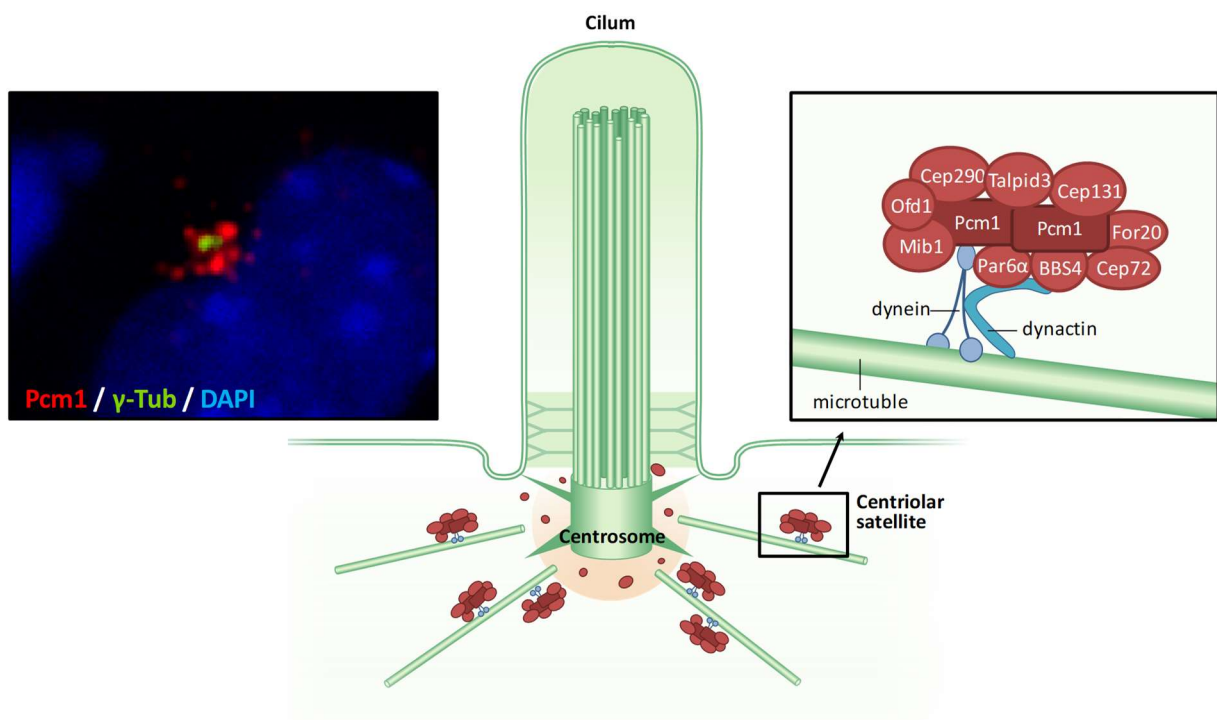


Figure XVIII. Centriolar satellites. Centriolar satellites (CS) are large multiprotein assemblies which orbit around the centrosome tethered to the microtubule network by the dynein-dynactin complex. The immunofluorescence picture on the top-left illustrates how these tiny structures appear in cells when immunostained with anti-Pcm1 (their major component) antibodies (red). The centrosome is marked in green with γ -Tubulin (γ -Tub) and the cell nucleus in blue with a DAPI staining. The image on the top-right is a schematic magnification of a CS with some of the major components represented. Note that Pcm1 can oligomerize generating a platform for assembling the whole complex.

In addition, in ciliated cells, some CS components are also observed along the ciliary shaft (e.g. BBS4) or at the level of the ciliary transition zone (e.g. Cep290, Cep131, Talpid3).

Therefore, the current consensus envisions CS as large agglomerates of centrosomal and ciliary proteins crowding around the centrosome itself (**Figure XVIII**). This led to the hypothesis, nowadays supported by a large pieces of evidence, that CS may work as shuttles involved in trafficking of centrosomal and ciliary proteins to their final localizations, that is indeed the centrosome-cilium compartment. By remaining in close proximity to the centrosome, but not in direct physical contact with it, CS can either facilitate or prevent specific components to join the various centrosomal or ciliary structures. In other words, they may work as temporary storage of centrosomal-ciliary proteins, capable of delivering or sequestering such proteins depending on the actual circumstances. Through this way, CS may finely tune the proteostasis of the centrosome-cilium compartment, representing a fast and efficient mean to modify its characteristics and behavior in response to various intracellular or extracellular cues (e.g. cell cycle progression, different types of stress, etc.).

1.5.2 CENTRIOLAR SATELLITES INTEGRITY AND LOCALIZATION

In both ciliated and non-ciliated cells, CS crowd around the centrosome. When immunostained for Pcm1, they appear as a characteristic granular cloud of puncta, whose density peaks in proximity to the centrosome and reduces while distancing to it (**Figure XVIII**). Sometimes some cell types also show sparse Pcm1-immunoreactive granules in the cytoplasm far from the centrosome. However, they account for a minority of Pcm1-immunofluorescent signals and probably represent assembling, immature CS.

A plethora of genetic, microscopy and functional studies indicated that this typical distribution pattern of CS is critically maintained by several mechanisms, that when disrupted result into a panel of effects ranging from CS disappearance, dispersal or accumulation around the centrosome (Hori and Toda, 2017).

Besides Pcm1, today more than 200 proteins have been implicated in CS integrity and pericentrosomal distribution, and their discovery has been accelerated by large scale microscopy screenings (Gupta et al., 2015). Nevertheless, only for few of these proteins, it is

known at which step of assembly, maintenance or transport of CS they are required for maintaining proper CS integrity and localization.

I.5.2.1 The trafficking of CS depends on microtubules

The characteristic pericentrosomal localization of CS is granted by their binding to the microtubule network (**Figure XVIII**). Indeed, disruption of the interphase microtubules results in CS scattering in the cytoplasm. In addition, live imaging tracking of CS (marked with GFP-tagged Pcm1) dynamics in cells demonstrated that CS move preferentially along the minus-end of the microtubules, hence explaining their pericentrosomal localization (Kubo et al., 1999). Such directed movement along microtubules is powered by cytoplasmic dyneins 1, and indeed impairment of dynein functions phenocopies the effects of microtubules disruption on CS (Dammermann and Merdes, 2002; Kim et al., 2004). Cytoplasmic dyneins 1 mediate cargoes transport via dynactin, an essential cofactor complex. In particular, the dynactin subunit p150^{Glued} interacts with two CS components, namely Partitioning defective 6 homolog α (Par6 α) and BBS4, the BBsome subunit. Such interaction is supposed to mediate the anchoring of CS to the dynein-dynactin complex (Kim et al., 2004; Kodani et al., 2010) (**Figure XVIII**). However more mechanistic details about the regulation of CS trafficking are missing. For instance, it is not clear if CS are also transported toward the plus-end of microtubules, as no interaction with kinesins has ever been reported. Probably, once reached the microtubule minus-end, CS detach from the dynein-dynactin complex and move away from the centrosome by simple diffusion before being reloaded on microtubules via a new dynein-dynactin interaction event. In conclusion, CS transport remains rather enigmatic.

I.5.2.2 CS integrity and localization depends on many integral components

Not only Pcm1 is required for the proper assembly of CS, but also other CS components share similar properties. For instance, knockdown of BBS4 disrupts CS organization, perhaps because of loss of anchorage to microtubules through the dynein-dynactin complex (Chamling et al., 2014; Kim et al., 2004; Lopes et al., 2011).

Another example, although much less characterized, is represented by Cep290. Unlike BBS4, Cep290 silencing causes aberrant aggregation of CS around the centrosome (Kim et al., 2008; Stowe et al., 2012). As in previous reports Cep290 was shown bind microtubules motors (both dyneins and kinesins), this phenotype was attributed to an excessive CS transport toward the

minus-end of microtubules, which eventually caused an impaired spatial turnover of CS at the pericentrosomal region (Kim et al., 2008; Stowe et al., 2012).

Interestingly, in other cases the mechanistic explanation could be much easier and more straightforward. Mapping of the domains required for reciprocal CS protein-protein interactions, revealed that these proteins are extremely entangled together when loaded on CS (Wang et al., 2016). As consequence, many CS proteins are mutually required for their respective CS localization, as it is the case for Pcm1, Cep290, BBS4, Cep72, Cep131, SSX2IP and many others (Klinger et al., 2014; Lopes et al., 2011; Stowe et al., 2012). That suggests that even lack of one single key CS component may simply impair the correct recruitment of a large number of other proteins, hence physically impairing the assembly of these structures.

However, sometimes the requirement of certain CS components for proper CS assembly seems to be controversial, as opposite results were obtained by different groups. This fact may reflect artifacts due to the different experimental approaches utilized. Alternatively, different cell types, under different conditions may change the composition of their CS, hence making specific proteins dispensable, or vice-versa indispensable for CS integrity depending on the situation. By using ultra-resolution microscopy, it was indeed recently discovered that pools of CS with different composition can intriguingly co-exist also within the same cell (Gheiratmand et al., 2019).

I.5.2.3 Post-translational modifications contribute at shaping CS

Not only the physical presence of proteins is required for maintaining CS integrity. Indeed, emerging pieces of evidence indicate that composition, structure and also functions of CS can be controlled by PTMs on their subunits.

Among the most common PTMs, there are phosphorylations. It was shown that Polo-like kinase 4 (Plk4), a central regulator of centrosome duplication, is also critical for maintaining the stability of CS, by phosphorylating Pcm1 and Cep131, on serine 372 and 78 respectively. Indeed, loss of Plk4 functions or abrogation of such phosphorylations on Pcm1 and Cep131 leads to CS scattering in the cytoplasm (Denu et al., 2019; Hori et al., 2016).

Other phosphorylations on Pcm1 are required for generating binding sites for other CS proteins. In paragraph [I.4.4.2](#), the role of Plk1 in ciliary disassembly was described. During this process, Plk1 must localize at the centrosome before mitotic entry and such event is achieved via CS recruitment. In particular, the threonine-703 of (human) PCM1 is phosphorylated by CDK1 in late G2, creating a docking site for Plk1 (Wang et al., 2013). Hence, a single phosphorylation

on Pcm1, which in this case is cell cycle controlled, enables the recruitment of new proteins at the CS, contributing at modifying the functions of these complexes.

Another PTM playing a role in CS biology is ubiquitination; indeed many E3 as well as deubiquitinating enzymes were reported to interact with CS (Čajánek et al., 2015; Quarantotti et al., 2019; Villumsen et al., 2013; Wang et al., 2016). For instance, the E3 enzyme Mindbomb1 (Mib1) recognizes Pcm1 and Cep131 as substrates and catalyzes both their mono- or polyubiquitination. While the monoubiquitination seems just required to regulate the reciprocal interaction of Pcm1 and Cep131, the polyubiquitination targets them to proteasomal degradation (Villumsen et al., 2013; Wang et al., 2016). Hence, Mib1 controls the composition of CS by regulating interaction and turnover of specific subunits.

The activity of Mib1 at CS is counteracted by the deubiquitinase USP9X, which by removing the polyubiquitin chains from Pcm1 and Cep131 promotes stabilization of the two proteins (Han et al., 2019; Li et al., 2017). Similarly, another deubiquitinase, namely Cyld, was recently shown to antagonize Mib1, ultimately sparing Pcm1 from degradation (Douanne et al., 2019). The net balance between ubiquitination and deubiquitination of target proteins, dictates their fate in CS, hence regulating CS composition and functions.

1.5.2.4 Cell cycle dependent regulation of CS localization and integrity

CS normally cluster around the centrosome under physiological conditions, but this is not always the case in cycling cells. Indeed, since their very first descriptions, it was shown that during mitosis CS lose their pericentrosomal localization becoming dispersed in the cytoplasm, for then reassembling around the centrosome upon G1/G0 entry (Balczon et al., 1994). The biological reason of this behavior it is still overall unclear as this area of research has remained poorly characterized. On the top of that, also the regulators implicated in this process are largely unknown, even though the celerity of such phenomenon and its reversibility strongly suggest that cell cycle-dependent PTMs might be involved. Indeed, as previously described, Pcm1 is phosphorylated by cell cycle kinases including Plk4, CDK1, but also Plk1 (Santamaria et al., 2011). It is thus tempting to speculate that (de)phosphorylations of specific sites on Pcm1 or other CS components upon mitotic entry may cause temporary disassembly of these complexes. The simple reversion of such PTMs may promote the regrouping of CS around the centrosome at the end of mitosis.

1.5.3 FUNCTIONS OF CENTRIOLAR SATELLITES

As described above, the great majority of CS proteins are also localizing at the centrosome or at the primary cilium. CS indeed are believed to work like guardians of the centrosome/cilium proteome, able to sort specific proteins to these organelles depending on the cellular status, as the cell cycle phase, stress conditions, etc. Supporting this general view, numerous pieces of evidence reported that disruption of CS integrity results into aberrant accumulation or depletion of CS proteins in the centrosome or in the cilium (Chamling et al., 2014; Dammermann and Merdes, 2002; Kim and Rhee, 2011; Stowe et al., 2012; Wang et al., 2016). On the other hand, it is thorough to report that most of the centrosomal proteins do not require CS for proper targeting to these organelles, but evidently they utilize different or alternative pathways (Hori and Toda, 2017).

Given these premises, it is not surprising that many functions and activities of the centrosome/cilium compartments are directly or indirectly controlled by CS (**Figure XIX**).

1.5.3.1 CS are required for numerous centrosome functions

One of the main functions of the centrosome is working as the MTOC of the cell. Early works showed that the anchoring of microtubules to the centrosome was disrupted by Pcm1 silencing, suggesting that some microtubule anchoring factor may require CS for their localization at the centrosome (Dammermann and Merdes, 2002). Such factor was proposed more than ten years later, when the CS protein SSX2IP was found to interact with the γ -tubulin complexes that nucleate microtubules from the centrosome (Hori et al., 2014). This work showed that SSX2IP centrosomal recruitment depends on CS.

CS are also involved in centrosome duplication, as many of the factors required for this process are transported and delivered to growing daughter centrioles. For example, Cep152 is necessary for reliable centriole duplication as it guarantees the hierarchical recruitment of a series of downstream proteins implicated in this process (Brown et al., 2013). To pursue these functions Cep152 must leave the CS and localize at the duplicating centrioles. The proper delivery of Cep152 is controlled by Cep131, whose absence impairs the centrosomal localization of Cep152 and causes defects in centrosome duplication (Kodani et al., 2015). Once correctly docked at the centrosome, Cep152 can downstream recruit Cep63, another centrosome duplication factor. Before that, also Cep63 is hosted into CS and its departure is finely controlled by two other CS proteins, namely the Coiled-Coil domain containing protein 14

(Ccdc14) and Moonraker, with the former promoting Cep63 retention to CS and the latter facilitating its dissociation (Firat-Karalar et al., 2014).

Overall, CS seem to offer a dual, antagonistic regulation of centriole duplication acting on centrosomal availability of critical duplication determinants.

1.5.3.2 CS are regulators of ciliogenesis

The first evidence linking ciliogenesis and CS came from the very early studies, when the CS of multiciliated nasal epithelial cells were shown to partially modify their subcellular distribution pattern upon cilia biogenesis (Kubo et al., 1999). Nowadays, thanks to genetic and functional studies, dozens of CS proteins have been associated to ciliogenesis.

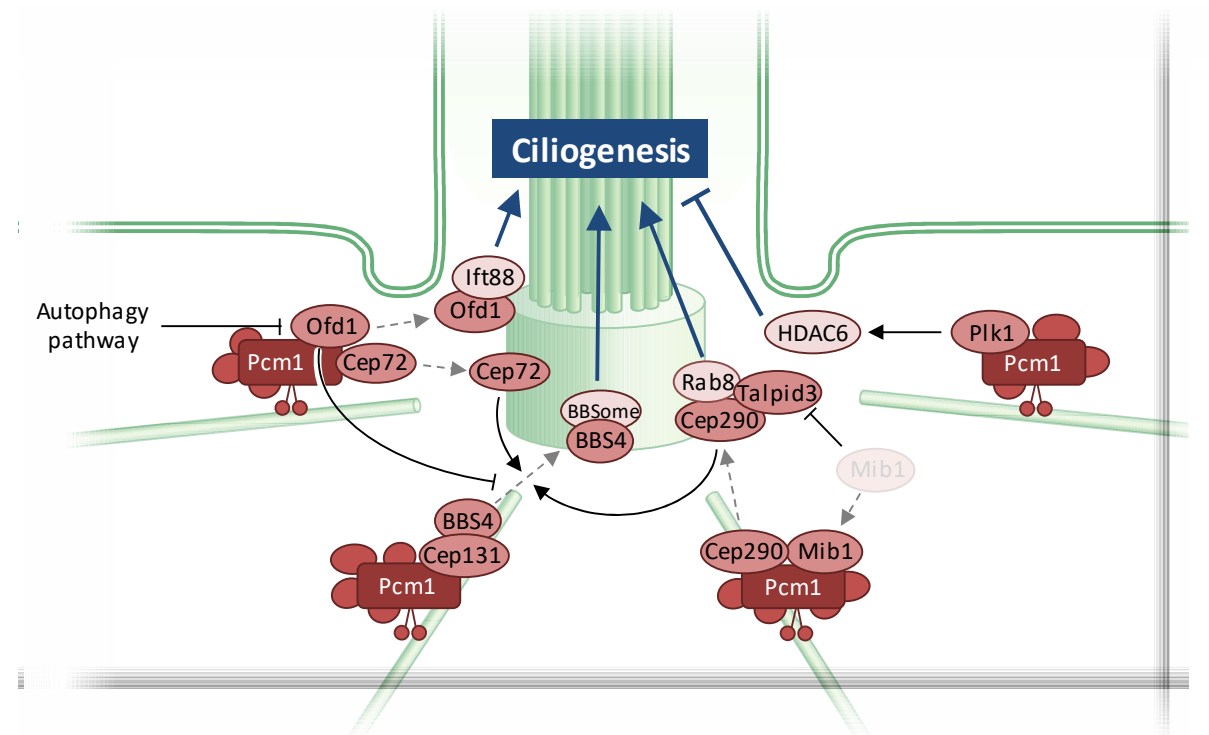


Figure XIX. Mechanisms controlled by CS during ciliogenesis in normal conditions. Many proteins, including Ofd1, Cep72, BBS4 and Cep290 are believed to shuttle between CS and the basal body (gapped arrows), where they are actively implicated in ciliogenesis. During the formation of a cilium, centrosomal Ofd1 recruits Ift88, hence helping the establishment of the IFT. Conversely, Ofd1 in CS is degraded via the autophagy pathway, seemingly to promote the release of BBS4 from CS. Indeed, BBS4 interacts with Cep131 at the CS, where Cep131 buffers its relocalization to the centrosome. At the centrosome, Cep72 and Cep290 collaborate for the recruitment of BBS4 which eventually assembles in the BBSome and contributes to ciliogenesis. Moreover, both Cep290 and Talpid3 permit the recruitment of Rab8, hence participating in the ciliary vesicles trafficking and fusion at the ciliary base, a key requirement for ciliogenesis. The E3 ligase Mib1 is sequestered by the CS, thus centrosomal Talpid3 is spared from proteasomal degradation and can execute its ciliogenic functions. Finally, CS recruit Plk1 in late G2 phase to promote activation of HDAC6 and consequent ciliary retraction upon mitotic entry.

Loss-of-function mutations or genetic depletion of these proteins may only negatively impact ciliogenesis (e.g. FOP and Cep131, the latter only in some cell types), but sometimes it could also affect CS integrity, therefore virtually abrogating multiple CS functions (e.g. Pcm1, Cep131, Cep290, Cep72, BBS4, Ofd1, For20, Cep131, Talpid3, SSX2IP) (Chamling et al., 2014; Gupta et al., 2015; Kim et al., 2008; Klinger et al., 2014; Kobayashi et al., 2014; Lee and Stearns, 2013; Lopes et al., 2011; Sedjâi et al., 2010; Stowe et al., 2012; Villumsen et al., 2013). Strikingly, despite the high number of studies linking CS to ciliogenesis, a clear picture of the underlying mechanisms is still overall missing, and only few CS-controlled ciliogenesis-pathways have been characterized (**Figure XIX**). Nevertheless, the majority of the results produced so far agree on one generally accepted paradigm: with only few exception (discussed later), integral and correctly placed CS are paramount conditions for proper ciliary assembly, maintenance and also disassembly. Loss of CS organization typically results into disrupted ciliogenesis (Tollenaere et al., 2015).

The first CS-controlled pathway for ciliogenesis described consists in the assembly and trafficking control of the BBSome at the base of the cilium. As described before, the BBSome is required for proper ciliary IFT and CMPs transport. In addition, by recruiting Rabin8, it orchestrates the activity of Rab8, which regulates vesicular trafficking (Nachury et al., 2007). The assembly of the BBS proteins into the BBSome occurs at the base of the cilium and it is highly hierarchically regulated, with BBS4 being the last protein to be added to the complex (Zhang et al., 2012a). Importantly, BBS4 stably localizes to CS, where it is sequestered primarily by the interaction with Cep131 (Chamling et al., 2014; Kim et al., 2004; Lopes et al., 2011; Nachury et al., 2007). Indeed, loss of Cep131 causes aberrant ciliary accumulation of BBS4 as well as the other BBSome components, leading to ciliogenesis defects (Chamling et al., 2014). Therefore, CS may control ciliogenesis by finely tuning the rate of BBSome formation through the controlled release of BBS4 (Chamling et al., 2014; Nachury et al., 2007) (**Figure XIX**).

Tightly intermingled with this pathway are also the CS proteins Cep290, Cep72, Talpid3 and Ofd1. All these proteins also localize at the distal tip of the mother centriole, where they are involved in the proper recruitment of BBS4 (Cep290 and Cep72), Rab8 (Cep290 and Talpid3), and the IFT-B protein Ift88 (Ofd1) (Ferrante et al., 2006; Kim et al., 2008; Kobayashi et al., 2014; Singla et al., 2010; Spektor et al., 2007; Stowe et al., 2012) (**Figure XIX**). Therefore, by balancing the localization of all these proteins at the centrosome, CS seem to regulate the overall

activity of the BBSome-Rabin8-Rab8 module and the assembly of IFT, both of which are crucial for cilia biogenesis and functions.

It remains however unclear which events regulate the CS-centrosome shuttling of all these proteins, although some mechanisms have emerged.

For instance, Talpid3 abundance at the centrosome is controlled by CS through sequestration of its E3 enzyme, namely Mib1. Indeed, experimental disruption of CS after Pcm1 knockdown, causes relocalization of Mib1 at the centrosome where it leads to polyubiquitination and degradation of Talpid3, thereby blocking ciliogenesis (Wang et al., 2016) (**Figure XIX**).

In addition, the CS pool of Ofd1 seems required for impairing BBS4 trafficking from CS to the basal body. However, upon onset of ciliogenesis, Ofd1 on CS is degraded via the autophagy pathway, hence freeing BBS4 to leave these organelles and relocalize to the basal body (Tang et al., 2013) (**Figure XIX**). Therefore, considering also what stated above, it is interesting to note that Ofd1 seems to exert dual and opposite roles on ciliogenesis depending on its localization: while the CS pool of Ofd1 inhibits ciliogenesis by restraining BBS4 trafficking, the centrosomal pool promotes ciliogenesis by recruiting Ift88.

Although integral and properly localized CS are considered essential prerequisite for ciliogenesis, exceptions have been observed. Villumsen and collaborators (2013) found that various types of stresses applied to cell lines, including UV radiations, genotoxic agents or heat shocks can induce ciliogenesis (and cell cycle exit) by causing an extraordinary remodeling of CS. Such remodeling consists in a fast displacement of Pcm1, Cep290 and Cep131 from the CS upon stress application. Interestingly, the authors reported that CS structures were not completely abrogated, as the pericentrosomal localization of other proteins, as Ofd1, was not affected by this complex reorganization. Nevertheless, the growth of a primary cilium after Pcm1, Cep290 and Cep131 dispersal seem in sharp contrast with the notion that genetic depletion the same proteins negatively impacts ciliogenesis also in the same cell lines used by Villumsen and colleagues. However, there could be an explanation to this apparent paradox. While abrupt depletion of proteins simulates a pathological condition in cells, application of stresses may be more physiologically tolerated, thanks to dedicated cellular programs that once activated enable cells to cope with environmental challenges. Therefore, under certain stress conditions, the activation of such programs may make cells exceptionally capable of undergoing ciliogenesis independently of the presence of integral CS around the centrosome. Interestingly, Villumsen and colleagues identified such program in the stress-induced activation of the p38 MAPK and in the inhibition of Mib1 activity at the CS.

As a concluding remark, CS are not only required for primary cilia formation, but also for ciliary disassembly. This is well exemplified by the recruitment of Plk1 by Pcm1 in order to activate HDAC6 and initiate the ciliary axoneme depolymerization (paragraph **I.4.4.2** and **Figure XIX**). Therefore, CS are nowadays considered essential global regulators of ciliogenesis, taking part to events necessary for the very beginning of ciliary assembly, ciliary maintenance and also disassembly.

I.6 Atoh1

Atoh1, also known as HATH1 in human or Math1 in mouse, is the homolog of the Drosophila proneural gene Atonal (Akazawa et al., 1995). Atoh1 gene localizes in chromosome 4 in humans and chromosome 6 in mice and it is composed by a single exon encoding for a 37 kDa protein belonging to the family of class II bHLH transcription factors.

This last introductory chapter is dedicated to Atoh1. First, the general functions of proneural bHLH transcription factors in the developing nervous system will be briefly reported. Next, the expression regulation and the functions of Atoh1 in GNs and SHH-MB, but also in other cell types, will be described.

I.6.1 ROLES OF bHLH TRANSCRIPTION FACTORS IN NEUROGENESIS

In order to generate the proper number and the large variety of neural and glial cells of the adult nervous system, the massive proliferation of neural progenitor cells (NPCs) must be followed by differentiation to the appropriate neuron or glia subtype. In the case of NPCs differentiating to neurons, such process is named neurogenesis and it includes both the acquisition of general neuronal characteristics as well as the specification of a precise neuronal subtype identity (Imayoshi and Kageyama, 2014). Interestingly, both these activities are carried out by a relatively small class of "proneural" transcription factors, all evolutionary related to the *Drosophila*'s Achaete-Scute, Atonal, and dTap/Neurogenin families (Baker and Brown, 2018). In particular, while all proneural factors are able to confer pan-neuronal features to NPCs, the expression of one member or another is instrumental for specifying a particular subtype identity, as the neurotransmitter phenotype (glutamatergic or GABAergic) (Bertrand et al., 2002; Imayoshi and Kageyama, 2014). For instance, in the developing vertebrate telencephalon, Neurogenin-1 and Neurogenin-2 (Neurog1 and Neurog2) are expressed in the dorsal pool of NPCs, while Achaete-Scute homolog 1 (Ascl1) is produced in the ventral pool. In both the two regions, Neurog1/2 and Ascl1 activities restrict NPCs to a neuronal fate, hence excluding them

from acquiring astrocytes or oligodendrocytes phenotypes. However, while Neurog1/2 activates a program for the neurogenesis of cortical pyramidal glutamatergic neurons, Ascl1 will convert the differentiating NPC into GABAergic interneurons (Imayoshi and Kageyama, 2014).

Among the downstream targets of proneural factors there are the so-called "neuronal differentiation factors", which orchestrate further subtype identity specification in concert with terminal differentiation. Examples of differentiation factors are members of the Neuronal differentiation (Neurod) and Nescient helix-loop-helix (Nhlh) families in vertebrates (Imayoshi and Kageyama, 2014).

Structurally, proneural factors (but also neuronal differentiation factors) are class II-bHLH transcription factors. They contain a basic domain important for DNA binding to the conserved 5' CANNTG 3' motif, also called E-box, and a HLH domain required for dimerization, interaction with other proteins and, in part, DNA binding (Bertrand et al., 2002; Massari and Murre, 2000; Murre et al., 1989). In order to regulate gene expression of their targets, proneural factors must form heterodimers with the broadly expressed E-proteins, that are class I-bHLH factors including members as E12, E47, HEB and E2-2 (Wang and Baker, 2015).

The expression and the activity of proneural proteins must be tightly regulated in order to maintain an appropriate balance between NPCs proliferation/self-renewal and differentiation. For instance, the Notch and the BMP signaling play pivotal roles in this, by specifically restraining proneural activity and thereby keeping NPCs into an undifferentiated state.

Mechanistically, high Notch signaling in NPCs leads to the expression of its targets Hes1 and Hes5. Hes1/5 are also bHLH factors, but differently from proneural factors they function as transcriptional repressors. Hes1/5 work by switching off the expression of proneural factors in NPCs. Moreover, they can also bind to residual proneural factors and block their activity when bound to E-boxes, thus keeping repressed neuronal differentiation genes (Imayoshi and Kageyama, 2014).

The BMP signaling in NPCs instead antagonizes proneural factors by driving the expression of Inhibitor of DNA-binding/differentiation (Id)-proteins, which belong to class V-HLH factors (Massari and Murre, 2000; Wang and Baker, 2015). Id-proteins lack the basic domain, hence they are unable to bind DNA. However, being equipped with a HLH domain, they can heterodimerize with E-proteins, thereby depriving proneural factors of their essential transcriptional partners.

Additionally, PTMs as phosphorylations added on proneural factors represent a further level of regulation of their activity. For example, Neurog2 is phosphorylated by protein kinases as CDKs or GSK-3 β on multiple sites and such phosphorylations were shown to influence its turnover, its DNA binding properties and the selective interaction with partners (Ali et al., 2011; Imayoshi and Kageyama, 2014; Ma et al., 2008; Quan et al., 2016; Vosper et al., 2007). Therefore, differential spatio-temporal phosphorylation pattern of proneural factors represents an important variable during neurogenesis.

Finally, although proneural factors commit NPCs to a neuronal fate, hence typically promoting cell cycle exit and differentiation, some exceptions exist to this paradigm. Some proneural factors in some tissues, as *Ascl1* in the telencephalon, *Asense* in *Drosophila* and, importantly, *Atoh1* in the post-natal cerebellum, were also shown to promote proliferation and self-renewal of NPCs (Ayrault et al., 2010; Castro et al., 2011; Flora et al., 2009; Urbán et al., 2016; Wallace et al., 2000). It is however still unclear how the same proneural factor could apparently both promote seemingly mutually exclusive activities as proliferation and differentiation.

1.6.2 STRUCTURE AND EXPRESSION OF ATOH1

1.6.2.1 Structure of Atonal/Atoh1 proteins

Mammalian *Atoh1* was initially identified through a screening from a mouse embryonic CNS-derived cDNA library while seeking for novel bHLH domain-encoding clones (Akazawa et al., 1995). *Atoh1* was recognized as the homolog of the fruitfly's *Atonal*, as the two proteins shared around 70% homology in the bHLH domain. Interestingly, the bHLH domain of *Atonal* localizes at the C-terminus of the protein, while in *Atoh1* it is found in the middle of the protein. However, this difference seems not big enough to significantly diversify the functions of these two proteins. Replacement of *Atoh1* locus with *Atonal* in transgenic mice results in normal embryonic development of virtually all the organs in which *Atoh1* is expressed, indicating high functional conservation between *Atoh1* and *Atonal* (Wang et al., 2002).

Comparison of *Atoh1* sequences from different vertebrate species, reveals that not only the bHLH domain results highly conserved, but also the C-terminal region. Such region of the protein is enriched in serine residues, many of which undergo phosphorylation events that are important for regulating *Atoh1* protein turnover in cells (Cheng et al., 2016; Forget et al., 2014). In addition, there is a certain degree of interspecies conservation also in the N-terminal region

of the protein, which has been shown to mediate the transcriptional activity of Atoh1 (Aragaki et al., 2008).

The bHLH domain of Atoh1 is required for binding to E-proteins and to the DNA. Chromatin-immunoprecipitation sequencing (ChIP-seq) studies in the developing cerebellum unraveled the preferred E-box-containing consensus site bound by Atoh1, consisting in a 10-nucleotide sequence renamed AtEAM (Atoh1 E-box associated motif: 5' G/A, C/A, CA, G/T, C/A, TG, G/T, C/T 3') (Klisch et al., 2011). AtEAMs can be found at the promoter of Atoh1-target genes as well as at a distance, localizing in 5' or 3' intergenic regions as well as within genes bodies, in both introns and exons (Klisch et al., 2011).

I.6.2.2 Atoh1 is expressed in many tissues, besides the cerebellum

In vertebrates, the proneural activity of Atoh1 directs the development of multiple cell lineages within the central and peripheral nervous system, but also in non-nervous tissues as the intestinal epithelium. During embryonic development the expression of Atoh1 is prevalently observed in the dorsal hindbrain, the dorsal neural tube, in the inner ear, in the Merkel cells of the skin and in the gut. During adulthood, Atoh1 expression becomes restricted only to the gut epithelium and to Merkel cells (Ben-Arie et al., 2000).

I.6.2.2.1 *Atoh1* in the hindbrain

In the hindbrain, Atoh1 starts to be detected around E9.5 in the RL, where its activity is required for the generation of a multitude of neuron types that will eventually leave the RL and populate different regions of the cerebellum and brainstem (Machold and Fishell, 2005; Rose et al., 2009a; Wang et al., 2005). In the uRL, Atoh1 is involved in the formation of cerebellar neurons as the GNs, the UBCs and those of the DCN, but also neurons of extracerebellar nuclei as the parabrachial, the vestibular and the lateral lemniscus' nuclei. In the IRL instead, Atoh1⁺ progenitors are committed to form other brainstem precerebellar nuclei as the cochlear, the reticulotegmental, the basal pontine gray, the lateral reticular and external cuneate nuclei. Other brainstem nuclei were then shown to derive from Atoh1⁺ progenitors, but it is not clear from which extent of the RL (Machold and Fishell, 2005; Rose et al., 2009a; Wang et al., 2005). Incidentally, among these nuclei, the parafacial respiratory group and retrotrapezoid nucleus are responsible for controlling respiratory rhythms. The failed generation of these nuclei in *Atoh1* double KO mice is the cause of perinatal mortality of these animals. Indeed, *Atoh1* double KO mice die just after birth due to breathing failure (Ben-Arie et al., 1997; Rose et al., 2009b).

I.6.2.2.2 *Atoh1* in the dorsal neural tube

In the dorsal neural tube, *Atoh1* is expressed from E9.5 in an heterogeneous population of cycling and early differentiating NPCs located just adjacent to the presumptive neural crests and the roofplate territories (Bermingham et al., 2001; Helms and Johnson, 1998). This *Atoh1*⁺ population corresponds to the developing D1⁷ pool of interneurons, which are destined to mature into dorsal commissural interneurons (DCIs) of the deep dorsal spinal horn (Helms and Johnson, 1998; Lee et al., 1998). When *Atoh1* is genetically deleted, D1 precursors mostly fail at differentiating into DCIs. Their proliferation, which precludes differentiation, seems not affected by *Atoh1* absence, but D1 precursors fate is in part switched to roofplate identity (Bermingham et al., 2001). Therefore, expression of *Atoh1* defines the D1 identity and is required for initiating the differentiation of D1 neuron progenitors.

I.6.2.2.3 *Atoh1* in the inner ear

Atoh1 is also required for the proper development of hair cells (HCs) in the sensory epithelia of the inner ear. Briefly, the inner ear is composed by the cochlea and the vestibular organs, which are responsible for hearing and balance, respectively. Both the cochlea and the vestibular organs contain a sensory epithelium composed by HCs and supporting cells (SCs), with the former representing the actual mechanosensory receptors. By E13, *Atoh1* is initially broadly expressed in the developing sensory epithelia of the inner ear, before becoming progressively restricted to the sole HCs, upon their appearance by E18.5 (Bermingham et al., 1999). Few days after birth in mice, *Atoh1* expression is permanently turned off in HCs.

HCs and SCs derive from a common multipotent progenitor whose fate-commitment toward the HC or the SC identity is regulated by the process of lateral inhibition mediated by the Notch signaling. *Atoh1* is a key player in this developmental program. *Atoh1* is initially transiently expressed in these multipotent progenitors, but its expression is only maintained in those cells fated to differentiate into HCs by low Notch activation. Conversely, *Atoh1* expression is lost in progenitors committed to the SC fate by high Notch signaling (Lanford et al., 1999; Woods et al., 2004; Zine et al., 2001). Importantly, it was reported that loss of *Atoh1* completely blocks the formation of both the HCs and the SCs in the inner ear sensory epithelia (Pan et al., 2011;

⁷ Dorso-ventral patterning of the developing neural tube subdivides it into different domains in which neuron progenitors are specified to different identities. All the spinal cord sensory interneurons are specified in the dorsal aspect of the neural tube, where at least four population of distinct precursor pools are identified. From dorsal to ventral, these populations are called D1, D2, D3 and D4 and are respectively marked by the expression of the LIM-containing homeobox transcription factors *Lh2A/B*, *Islet1*, *Lim1/2* and *Lmx1b* (Gowan et al., 2001).

Woods et al., 2004). However, only HCs, where *Atoh1* expression is maintained after fate-specification, do require *Atoh1* for differentiation (Woods et al., 2004). Therefore disruption of the SCs lineage upon *Atoh1* KO is a consequence of HCs loss and possibly of a defective Notch-mediated cell-fate selection program (Woods et al., 2004).

In addition, the persisting late-embryonic and early post-natal expression of *Atoh1* in HCs seems required for their survival (Chonko et al., 2013).

The ability of *Atoh1* to direct differentiation of HCs is also supported by data showing that *Atoh1* overexpression can reprogram various inner ear epithelial cells to acquire HCs identity (Zheng and Gao, 2000). Incidentally, all these discoveries boosted numerous studies aimed at employing gene therapy-mediated re-expression of *Atoh1* in the inner ear epithelia to regenerate HCs in patients suffering of hearing loss (Lee et al., 2017).

I.6.2.2.5 *Atoh1* in the intestine

Starting from E16.5, *Atoh1* is sparsely detected also in the intestinal epithelium, where its expression continues throughout adulthood. Here, *Atoh1* activity in multipotent epithelial progenitors (MEPs) of the intestinal crypts commits them to differentiate into secretory cells, including Paneth, enteroendocrine and goblet cells (Yang et al., 2001). Further allocation into one or another secretory type is then regulated by other transcription factors acting downstream *Atoh1* (Lo et al., 2016; Noah et al., 2010; Shroyer et al., 2005). Deletion of *Atoh1* completely prevents the formation of all the intestinal secretory cells and MEPs that would have contributed to this lineage fail at leaving the cell cycle and remain proliferative (Yang et al., 2001). Conversely, enforced *Atoh1* expression promotes ectopic production of secretory cells at the expense of absorptive enterocytes, indicating that *Atoh1* alone is sufficient for directing a full secretory lineage differentiation program in MEPs (VanDussen and Samuelson, 2010).

I.6.2.2.6 *Atoh1* in Merkel cells

In the skin, Merkel cells are specialized mechanoreceptor cells of the basal epidermis involved in the perception of mechanical stimuli. Fate mapping studies demonstrated that they originate from slowly cycling epidermal progenitors marked by the expression of *Atoh1* (Wright et al., 2015). These *Atoh1*⁺ progenitors generate and maintain the pool of Merkel cells starting from E14.5, throughout development and for the entire life of the individual (Ben-Arie et al., 2000; Van Keymeulen et al., 2009; Wright et al., 2015). Therefore differentiation of Merkel cells

during embryogenesis and adult skin homeostasis entirely depends on *Atoh1* (Kervarrec et al., 2019).

I.6.2.2.7 Concluding remarks

In conclusion, there emerge some interesting functional similarities between the cell types that require *Atoh1* for their development. For instance, Merkel cells and intestinal enteroendocrine cells are both types of endocrine cells found in epithelia. In addition, cochlear and vestibular HCs, Merkel cells, DCIs of the spinal cord, various *Atoh1*-derived pontine nuclei and the cerebellum all participate, although in different extent, to the proprioceptive and auditory sensory pathways, which relay body positional information to the CNS to regulate movements. Therefore, the various transcriptional programs orchestrated by *Atoh1* during development, although globally different from cell type to cell type, may share some key similitude that are eventually reflected into common functional properties.

I.6.2.3 *Atoh1* expression is highly regulated in the GN lineage

The expression of proneural bHLH transcription factors is typically transient in NPC and their post-mitotic derivatives. Such temporal pattern of expression seems important for proper neurogenesis, as its perturbation disrupts neuronal commitment and subsequent differentiation (Imayoshi and Kageyama, 2014). Therefore, the onset, the amplitude and the duration of proneural factors expression must be precisely orchestrated during neurogenesis. This is true also for *Atoh1* in the context of GNs development (**Figure XX**).

By E12.5 *Atoh1*-expressing uRL progenitors are committed to become GNs, therefore they become GNPs. *Atoh1* expression is then maintained during the whole rostral migration of GNPs over the cerebellum anlage and also during their massive expansion phase in the EGL (Akazawa et al., 1995; Wang et al., 2005). Progressively, *Atoh1* expression is turned off during the first 2 post-natal weeks upon GNPs cell cycle exit and inward migration toward the IGL (Helms and Johnson, 1998). Many mechanisms were shown to regulate *Atoh1* expression in the GN lineage and they act at both transcriptional and post-translational level.

I.6.2.3.1 Transcriptional control of *Atoh1* gene in the cerebellum

Early studies aimed at uncovering the modules implicated in *Atoh1* transcription identified two highly conserved regulative regions of around 500bp located 3' to *Atoh1* locus, named enhancer A and enhancer B (Helms et al., 2000).

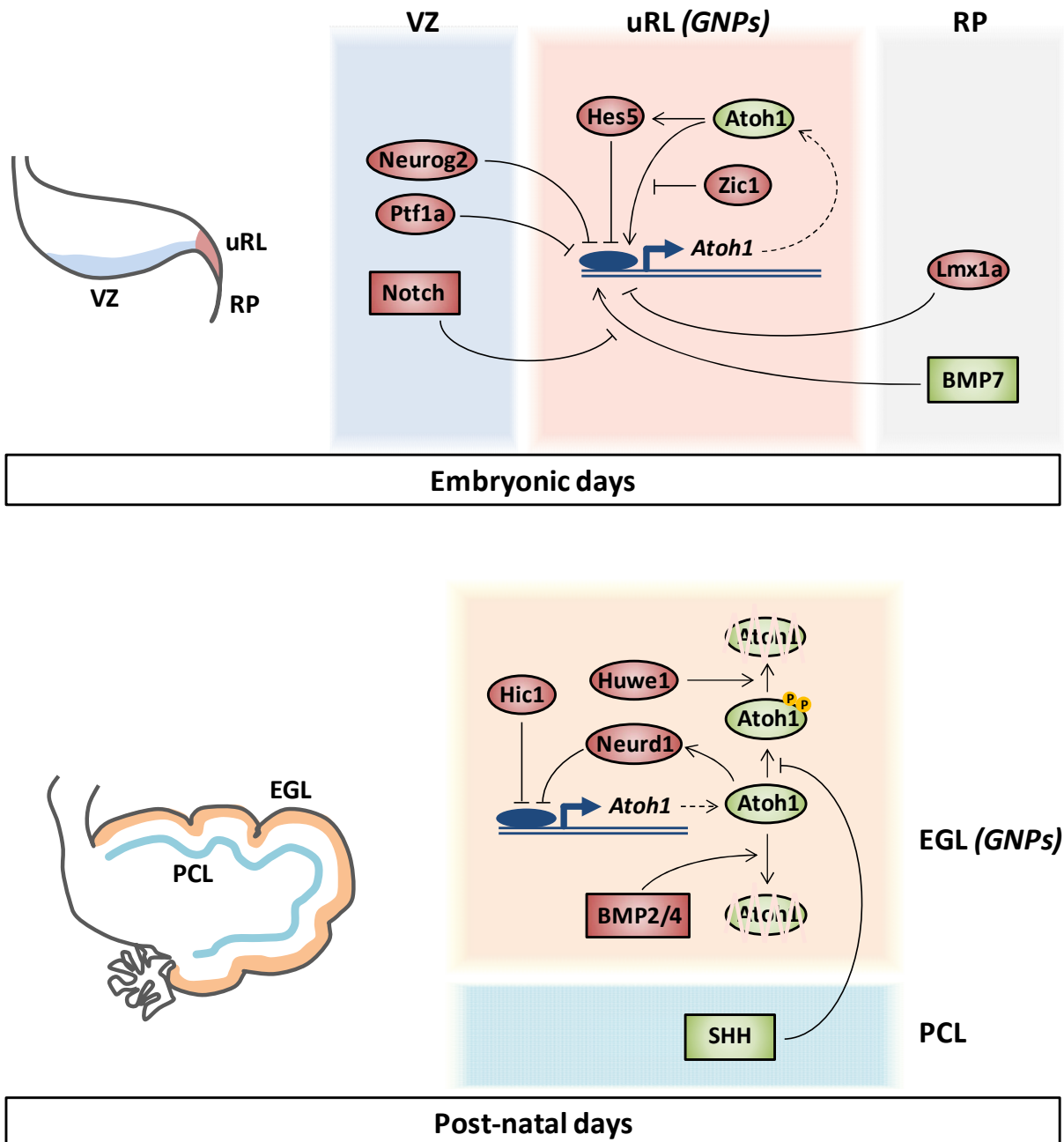


Figure XX. Major networks regulating *Atoh1* expression in GNP cells across embryonic and post-natal developmental stages. During embryonic development, *Atoh1* is expressed in GNP cells of the uRL. *BMP7* released from the roofplate (RP) is believed to initiate and perhaps maintain *Atoh1* expression in multipotent progenitors of the uRL. Transcription factors as *Lmx1a* expressed in RP cells and *Neurog2* and *Ptf1a* in the ventricular zone (VZ) progenitors block *Atoh1* expression in these territories. Similarly, Notch signaling inhibits *BMP7* pathway activation in VZ cells. In GNP cells several cell-autonomous mechanisms regulate *Atoh1* expression. *Atoh1* self-sustains its own expression through a positive feedback loop. At the same time, *Atoh1* regulates *Hes5* which is supposed to silence *Atoh1*, hence feeding a negative feedback loop. *Zic1* may partially interfere with *Atoh1* auto-regulatory loop. During post-natal days, GNP cells are in the EGL where *Atoh1* expression is maintained by the SHH signaling through inhibition of the phosphorylations targeting *Atoh1* to proteasomal destruction via *Huwe1* recognition. Also *BMP2/4* signaling promotes degradation of *Atoh1* through an alternative pathway. At the same time *Hic1* and *Neurod1*, with the latter being a transcriptional target of *Atoh1*, silence *Atoh1* expression promoting GNP cells cell cycle exit. It is not clear if the *Atoh1* auto-regulatory loop, the *Atoh1*-*Hes5* negative feedback loop and the repression provided by *Zic1* are still active events during post-natal times.

These enhancers were shown to be required and sufficient to drive *Atoh1* expression in practically all its known expression territories of the whole mouse embryo, including the cerebellum (Helms and Johnson, 1998; Helms et al., 2000). Therefore, transcription factors and modulators of *Atoh1* transcription are all virtually supposed to bind exclusively these enhancers when regulating *Atoh1* expression (**Figure XIX**).

Atoh1 induction in the RL is known to be triggered by secretion of morphogens as BMP7 by the dorsally juxtaposed roofplate, which at this stage is marked by the expression of its master regulator *Lmx1a* (Alder et al., 1999; Chizhikov et al., 2006; Duval et al., 2014). In the r1, the expression of *Atoh1* is then spatially confined to the sole uRL by various mechanisms. In the anterior cerebellar anlage, high level of Notch1 signaling in the VZ counteracts the activation of BMP-dependent transcriptional program, hence preventing *Atoh1* induction in this territory (Machold et al., 2007). In addition, bHLH transcription factors as *Ptf1a* and perhaps *Neurog2*, both expressed in the VZ, further contribute at limiting *Atoh1* expression to the sole uRL (Florio et al., 2012; Gowan et al., 2001; Yamada et al., 2014). Finally, also *Lmx1a* seems to negatively regulate *Atoh1* expression, thereby confining its transcription outside the roofplate region. Thoroughly, the relation between *Lmx1a* and *Atoh1* was characterized in the dorsal spinal cord, between D1 interneurons precursors and roofplate cells, but it could be active also in the r1 (Chizhikov and Millen, 2004).

Once activated, the expression of *Atoh1* is then tightly controlled by positive and negative mechanisms, that intermingled together sometimes create feedback loop regulations (**Figure XX**). Notably, these mechanisms are also temporally regulated, as the duration of *Atoh1* expression is different in the neuronal lineages specified in the uRL. Indeed, as described in paragraph **I.2.2.1**, while between E9.5 and E12.5 *Atoh1* is soon rapidly downregulated after specification of extracerebellar and DCN neurons, after E12.5 *Atoh1* expression is maintained in GNPs until post-natal days.

Interestingly, one of the positive regulators of *Atoh1* expression is *Atoh1* itself. By dimerizing with E12 and binding to a conserved E-box located in the enhancer B, *Atoh1* can self-sustain its own expression (Helms et al., 2000). Pieces of evidence indicate that such auto-regulatory loop is counteracted by *Zic1*, which is expressed in GNPs and in the dorsal neural tube. In the neural tube, *Zic1* represses the transcription of *Atoh1* by binding to enhancer B and interfering with *Atoh1* self-activation. Although such regulation was described in the neural tube, it could be active also in GNPs where *Zic1* may keep *Atoh1* levels in check by restraining any possible excessive overexpression (Ebert et al., 2003).

As expected from a proneural factor, *Atoh1* expression in GNPs seems to be repressed by the Notch signaling target *Hes5* (Gazit et al., 2004). Interestingly, *Hes5* expression itself is dependent of *Atoh1* in GNPs, revealing the existence of a negative feedback loop that would supposedly reduce *Atoh1* expression when sufficient *Atoh1* protein is produced. However, being these studies performed *in vitro*, hence spatio-temporally disengaged from the cerebellar context, it is not clear when (and whether) such regulation takes place during GNPs development. Nevertheless, *Atoh1* and the Notch signaling are known to be tightly interconnected to each other, as extensively shown in the developing sensory epithelium of the inner ear (Zine and de Ribaupierre, 2002; Zine et al., 2001).

In the post-natal EGL, it was suggested that the neuronal differentiation factor *Neurod1*, which is a direct downstream target of *Atoh1*, negatively regulates *Atoh1* expression, enabling GNPs to terminally differentiate (Jahan et al., 2010; Klisch et al., 2011; Pan et al., 2009).

Similarly, the transcriptional repressor *Hic1* directly switches off *Atoh1* transcription by binding to its 3' regulative region (Briggs et al., 2008).

I.6.2.3.2 *Post-translational control of Atoh1 protein expression in the cerebellum*

As it happens for many proneural factors, also the turnover of *Atoh1* is highly regulated by cell autonomous and non-cell autonomous mechanisms (**Figure XX**).

It was already reported in paragraph **I.2.4.5.2** that *Atoh1* protein is destabilized by BMP2/4 signaling in post-natal GNPs (Zhao et al., 2008). Therefore, it is interesting to notice that the a same signaling pathway, namely BMP, mediated by different ligands (*BMP7 vs BMP2/4*) and activated in GNPs at different spatio-temporal stages of development (embryonic/uRL *vs* post-natal/EGL) is required for both inducing and repressing *Atoh1* expression.

Conversely to BMP and through a totally independent pathway, the SHH signaling was shown to promote *Atoh1* protein expression in proliferating GNPs of the EGL, by protecting it from proteasomal degradation. In post-natal GNPs, *Atoh1* turnover is regulated by the E3 ligase *Huwe1*, which recognises *Atoh1* when the latter is phosphorylated at serine 328 and 339. The SHH signaling was shown to reduce the level of *Atoh1* phosphorylation on these two residues by activating the protein phosphatase *PP2A*. Through this way, SHH reduces the phosphorylation-dependent degradation of *Atoh1* mediated by *Huwe1*, hence promoting its expression in proliferating GNPs (Forget et al., 2014).

1.6.3 FUNCTIONS OF ATOH1 IN THE GRANULE NEURON LINEAGE

1.6.3.1 Functions of Atoh1 during normal GNs development

The first insights in the roles of Atoh1 in development of GNs came from the analysis of *Atoh1* deleted mice. While a single copy of *Atoh1* seems sufficient to drive normal cerebellar development, the homozygote KO show massive disruption of the embryonic cerebellum architecture (Ben-Arie et al., 1997). Atoh1 loss causes a reduction of size of the uRL, which contains fewer and less proliferative cells. In addition, after E14.5 GNPs fail to migrate to the EGL, hence completely abolishing the formation of GNs (Ben-Arie et al., 1997; Gazit et al., 2004). However, it appears that the Atoh1-deficient uRL progenitors can be anyway fate-committed to GNs, as revealed by the expression of the GNPs marker *Zic1* (Gazit et al., 2004). Therefore, the proneural activity of Atoh1 may not be absolutely required for GN identity specification, although it cannot be excluded that it might play an important role.

If on one side GNs specification is not completely compromised, neural differentiation is disrupted. *Atoh1* KO GNPs fail to form the typical neurites observed when they are cultured *in vitro* for multiple days, indicating failure of neuronal maturation (Gazit et al., 2004). Similar loss of differentiation competence was obtained also by knocking down *Atoh1* in the developing embryo by *in utero* electroporation of Atoh1-targeted siRNAs (Kawauchi and Saito, 2008). Conversely, when *Atoh1* is orthotopically overexpressed *in vivo*, then GNPs are formed and many of them make it to migrate and form an EGL (Grausam et al., 2017; Helms et al., 2001). Nevertheless, upon arrival in the EGL, the prolonged and enhanced *Atoh1* expression promotes premature induction of early differentiation markers (e.g. *Neurod1*, *Doublecortin* and *Tuj1*, the neuronal-specific β -tubulin III) and eventually perturbs the inward migration and complete maturation of GNs (Helms et al., 2001).

Taken together, these observations indicate that maintenance of adequate levels of Atoh1 followed by its terminal, post-natal downregulation are paramount for enabling proper GNs formation.

Importantly, besides regulating migration to the EGL and global differentiation to GNs, Atoh1 is also absolutely required for the post-natal expansion phase of GNPs in the EGL. Indeed, Atoh1 was shown to maintain GNPs competence to SHH over time, hence enabling them to respond to the mitogen. *In vivo* and *in vitro* deletion of *Atoh1* in post-natal GNPs blocks their SHH-driven proliferation, leading to their differentiation (Flora et al., 2009). On the contrary, Atoh1 overexpression *in vitro* potentiates the mitogenic response to SHH and enables a greater

percentage of GNPs to re-enter the cell cycle after transient deprivation of SHH from the culture medium (Ayrault et al., 2010). Similarly, overexpression of *Atoh1* in GNPs of cultured cerebellar slices delays their inward migration to the IGL maintaining them in the EGL (Forget et al., 2014). Although it is evident that *Atoh1* can sensitize GNPs to their major mitogen SHH, the underlying cellular and molecular bases are still poorly understood, even though some have attributed it to the capacity of *Atoh1* to activate the expression of *Gli2* (Flora et al., 2009).

All these studies demonstrate that *Atoh1* orchestrates GNs formation by controlling multiple, sometimes seemingly opposite aspects of their development. Coherently, such pleiotropic roles of *Atoh1* are reflected by the extremely wide range of functions associated to its direct transcriptional targets. Although some *Atoh1* target genes had already been found through “candidate gene approach”-driven studies (Flora et al., 2009; Gazit et al., 2004; Helms et al., 2001; Kawauchi and Saito, 2008), the publication of the *Atoh1* “targetome” by Klisch and colleagues (2011) was beneficial in providing a global, unbiased view of *Atoh1* functions in GNPs. By combining together *Atoh1*-ChIP-seq, transcriptomic and histone signature data such study identified more than 600 putative *Atoh1* target genes in GNPs *in vivo*. Biological and molecular function assignment revealed that most of these genes are implicated in signaling pathways related to GNPs development, such as SHH, Notch, TGF- β /BMP, but also directly involved in cell cycle (*Ccnd2*, *Cdc25b*, *E2f1*) or neuronal differentiation and migration (*Pax6*, *Neurod1*, *Nhlh1/2*, *Semaphorin 6a*) (Klisch et al., 2011). Whether *Atoh1* coordinates the expression of subsets of these genes in a precise spatio-temporal pattern to orchestrate sequential phases of the GNs developmental program remains overall unknown.

In conclusion, *Atoh1* works as an essential master regulator for GNs formation, actively governing both proliferation and differentiation phases within the GN developmental lineage.

I.6.3.2 Functions of *Atoh1* during SHH-MB formation and expansion

Atoh1 transcripts and protein are typically found highly expressed in both mouse and human SHH-MB, when compared to the cell-of-origin (mouse GNPs) or to other human MB subgroups (Ayrault et al., 2009; Lee et al., 2003; Zhao et al., 2008). This high expression of *Atoh1* is not odd, but functional as *Atoh1* plays a fundamental role also in SHH-MB formation and expansion.

Indeed, cKO of *Atoh1* in the cerebellum completely blocks SHH-MB formation in the *SmoM2* tumor-prone mouse model and treatment with BMP2/4 of primary mouse SHH-MB cells downregulates *Atoh1* protein and arrests proliferation (Flora et al., 2009; Zhao et al., 2008). In

addition, in tumor formation experiments it was shown that *Atoh1* cooperates with aberrantly activated SHH signaling to efficiently transform GNPs into SHH-MB initiating cells. Specifically, when *Atoh1* is overexpressed in GNPs carrying SHH-MB predisposing alterations like *Ptch1*^{+/+}; *Cdkn2c*^{-/-} status or *Gli1*-overexpression, it increases the tumorigenic potential of such cells when they are grafted into recipient mice (Ayrault et al., 2010). Although more penetrant and aggressive, *Atoh1*-overexpressing tumors did not exhibit enhanced expression of pro-proliferative genes compared to control tumors, but showed reduced expression of differentiation genes. Therefore, in accordance with the role of *Atoh1* during normal GNPs expansion in the EGL, it was suggested that also in SHH-MB *Atoh1* does not promote proliferation *per se*, but somehow contrasts neuronal differentiation prolonging the sensitivity of cells to the SHH signaling. Coherently, overexpression of *Atoh1* alone in wild-type GNPs does not drive tumor formation and neither increases their proliferation when cultured in absence of SHH (Ayrault et al., 2010).

All these results taken together indicate that *Atoh1* is essential for SHH-MB initiation and growth, but its overexpression alone does not act as a key oncogenic driver event unless other opportune SHH-hyperactivating alterations are present. For these reasons, *Atoh1* is typically considered a lineage-dependency transcription factor in SHH-MB.

Furthermore, it was also recently shown that *Atoh1* participates in the metastatic spread of SHH-MB cells in mouse models and that its transcriptional program (explored through ChIP-seq and gene expression analysis) is partially rewired the context of metastases.

Interestingly, although *ATOH1* is typically overexpressed in human SHH-MB, *ATOH1* locus is never found mutated or neither amplified, therefore other mechanisms should be at play to keep its levels elevated in tumor cells. Candidate mechanisms could be the typical downregulation of *HUWE1* observed in human (and mouse) SHH-MB, which in collaboration with aberrantly sustained SHH signaling may lead to *ATOH1* protein stabilization (Forget et al., 2014). In addition, high *ATOH1* amounts could promote further *ATOH1* transcription via the auto-regulatory positive feedback loop identified by Helms and colleagues (2000) in normal GNPs. Finally, genes encoding for negative regulators of *ATOH1*, as *NEUROD1* or *HIC1*, are typically found downregulated (or also deleted for *HIC1*) in human SHH-MB (Briggs et al., 2008; Pan et al., 2009; Waha et al., 2003).

It is interesting to note that while *Atoh1* is required for SHH-MB growth, in other tumors as in colorectal cancer (CRC) or Merkel cell carcinoma (MCC), *ATOH1* is normally deleted or downregulated and works as a tumor suppressor gene (Bossuyt et al., 2009; Leow et al., 2004;

Peignon et al., 2011). Apparently, part of this tumor suppressor activity of ATOH1 is accomplished via activation of a c-Jun N-terminal kinase (JNK)-mediated cell cycle arrest and apoptotic pathway (Bossuyt et al., 2009). Incidentally, this role of ATOH1 in CRC and MCC is in accordance with its function in the cells-of-origin of these tumors, where it directs lineage-restricted differentiation of intestinal and skin progenitor cells.

Therefore, Atoh1 contribution to tumorigenesis depends on the cell type-of-origin and reflects the functions of Atoh1 in the normal developmental or homeostatic context.

1.7 Objectives of the Study

By E12.5 in mice, neural progenitors of the uRL are committed to the GN lineage, hence they initiate to give birth to the GNPs. After specification, GNPs leave the uRL to settle on the subpial surface of the cerebellum forming the EGL (Alder et al., 1996; Wingate, 2001; Wingate and Hatten, 1999). Here, the mitogen SHH secreted by the PCs by E17.5 on, stimulates a massive wave of GNPs expansion that completely terminates only at the third post-natal week (Dahmane and Ruiz-i-Altaba, 1999; Lewis et al., 2004; Wechsler-Reya and Scott, 1999). Indeed, after birth, a series of intrinsic and extrinsic cues are thought to progressively restrict GNPs proliferation, eventually leading to their cell cycle exit and migration to the IGL where they complete their differentiation. Failure in restraining GNPs expansion may result in the development of malignancies as SHH-MB, a pediatric cancer originating from GNPs (Schüller et al., 2008; Yang et al., 2008). Unfortunately, a clear and comprehensive understanding of the molecular pathways regulating the balance between proliferation and differentiation in GNPs is still missing.

SHH is transduced by GNPs through the primary cilium, an organelle that seems to be irreversibly disassembled when these cells are committed to terminal differentiation (Chizhikov et al., 2007; Di Pietro et al., 2017; Spassky et al., 2008). Importantly, genetic studies showed that loss of primary cilia in GNPs prevents the activation of SHH pathway, blocking GNPs proliferation and potential transformation into SHH-MB cells (Barakat et al., 2013; Han et al., 2009; Spassky et al., 2008). Therefore, we reasoned that triggering the permanent retraction of primary cilia could represent a developmentally regulated mechanism for extinguishing the SHH signaling in GNPs and enabling their consequent differentiation. At the same time, maintaining the competence to generate a primary cilium may provide an essential determinant for sustaining the expansion of GNPs and SHH-MB cells, as it would equip these cells with the mean to transduce SHH signals. Hence, understanding how ciliogenesis is regulated in the developing GN lineage is a key interest.

We thought that a potential candidate regulator of ciliogenesis in GNPs could be *Atoh1*. *Atoh1* is essential for GNs neurogenesis and it was shown to maintain GNPs into a SHH-sensitive and

proliferate competent state during post-natal development in mouse (Ayrault et al., 2010; Ben-Arie et al., 1997; Flora et al., 2009). In addition, its occurrence during GNs development appears to follow a similar kinetics as the one of primary cilia, that is downregulation/disappearance upon terminal differentiation. Importantly, *Atoh1* is required for SHH-MB to originate and progress, suggesting that it may regulate similar pro-proliferative pathways in both tumor and normal developmental context (Ayrault et al., 2010; Flora et al., 2009).

In conclusion, the biological questions that we wish to answer with our work are the following:

- **Does *Atoh1* control ciliogenesis in GNPs?**
- **If yes, does *Atoh1* maintain GNPs responsiveness to SHH by regulating the presence of primary cilia on their surface?**
- **How does mechanistically *Atoh1* control ciliogenesis?**
- **Does *Atoh1* conserve such functions also in the context of SHH-MB?**

Our investigation is enforced by a collaboration with the laboratory of Dr. Jin-Wu Tsai in Taipei (Taiwan), which groups experts in neurodevelopment and imaging techniques.

Our work may reveal novel, important tiles in the mosaic of cellular and molecular pathways underpinning the development of the largest brain neuron population and the etiology of a deadly pediatric brain tumor.

Results

Article and Main Figures

Atoh1 Controls Primary Cilia Formation to Allow for SHH-Triggered Granule Neuron Progenitor Proliferation

Chia-Hsiang Chang^{1,2*}, Marco Zanini^{3,4*}, Hamasseh Shirvani^{3,4*}, Jia-Shing Cheng¹, Hua Yu^{3,4}, Chih-Hsin Feng¹, Audrey L. Mercier^{3,4}, Shiue-Yu Hung⁵, Antoine Forget^{3,4}, Chun-Hung Wang¹, Sara Maria Cigna^{3,4}, I-Ling Lu¹, Wei-Yi Chen⁶, Sophie Leboucher^{3,4}, Won-Jing Wang⁶, Martial Ruat⁷, Nathalie Spassky⁸, Jin-Wu Tsai^{1,9#} and Olivier Ayrault^{3,4,10#}

¹Institute of Brain Science, School of Medicine, National Yang-Ming University, Taipei 112, Taiwan.

²Taiwan International Graduate Program (TIGP) in Molecular Medicine, National Yang-Ming University and Academia Sinica, Taipei, Taiwan.

³Institut Curie, PSL Research University, CNRS UMR 3347, INSERM U1021, F-91405, Orsay, France.

⁴Université Paris Sud, Université Paris-Saclay, CNRS UMR 3347, INSERM U1021, F-91405, Orsay, France.

⁵Department of Medicine, School of Medicine, National Yang-Ming University, Taipei 112, Taiwan.

⁶Institute of Biochemistry and Molecular Biology, College of Life Sciences, National Yang-Ming University, Taipei 112, Taiwan.

⁷CNRS, UMR-9197, Neuroscience Paris-Saclay Institute, 1 Avenue de la Terrasse, F-91198, Gif-sur-Yvette, France.

⁸Ecole Normale Supérieure, Institut de Biologie de l'ENS, IBENS, F-75005 Paris, France; CNRS, UMR8197, F-75005 Paris, France; Inserm, U1024, F-75005 Paris, France.

⁹Brain Research Center (BRC), and Biophotonics and Molecular Imaging Research Center (BMIRC), National Yang-Ming University, Taipei 112, Taiwan.

¹⁰Lead contact

to whom requests should be addressed: olivier.ayrault@curie.fr, Phone: +33 (0)1 69 86 71 36; Fax: +33 (0)1 69 86 30 17; tsaijw@ym.edu.tw, Phone: +886-2-2826-7305 Fax: +886-2-2827-3123

Running title: Atoh1 governs cerebellar progenitor ciliogenesis

*These authors contributed equally to this work

SUMMARY

During cerebellar development, granule neuron progenitors (GNPs) proliferate by transducing Sonic Hedgehog (SHH) signaling via the primary cilium. Precise regulation of ciliogenesis, thus, ensures proper GNP pool expansion. Here, we report that Atoh1, a transcription factor required for GNPs formation, controls the presence of primary cilia, maintaining GNPs responsiveness to SHH. Loss of primary cilia abolishes the ability of Atoh1 to keep GNPs in a proliferative state. Mechanistically, Atoh1 promotes ciliogenesis by transcriptionally regulating Cep131, which facilitates centriolar satellite (CS) clustering to the basal body. Importantly, ectopic expression of Cep131 counteracts the effects of Atoh1 loss in GNPs by restoring proper localization of CS and ciliogenesis. This Atoh1-CS-primary cilium-SHH pro-proliferative pathway is also conserved in SHH-type medulloblastoma, a pediatric brain tumor arising from the GNPs. Together, our data reveal how Atoh1 modulates the primary cilium to regulate GNPs development.

Keywords: Cerebellar development, granule neuron progenitors, Sonic Hedgehog, primary cilium.

INTRODUCTION

The cerebellum ensures crucial functions in motor coordination as well as higher cognitive activities, such as learning, attention, and emotion (Buckner, 2013; Ito, 2008). Its development involves complex steps of neurogenesis, differentiation, and migration. At postnatal stages, cerebellar granule neuron progenitors (GNPs) massively proliferate in the external granule layer (EGL) in response to Sonic Hedgehog (SHH), the diffusible mitogen secreted by Purkinje cells (Dahmane and Ruiz i Altaba, 1999; Wallace, 1999; Wechsler-Reya and Scott, 1999). Subsequently, GNPs undergo cell cycle exit, differentiation and migration along the Bergman glial fibers through the molecular layer (ML) until they reach the internal granule layer (IGL), their final destination within the cerebellum.

SHH activates GNP proliferation through a cascade of signaling pathways within the primary cilium, an antenna-like protrusion on the cell surface. Its central core consists of an axoneme nucleating from a basal body, a specialized form of the mother centriole (Kobayashi and Dynlacht, 2011). The binding of SHH to its receptor Patched1 (Ptch1) leads to the accumulation of Smoothed (Smo) into the ciliary membrane, followed by the activation of Gli transcription factors at the tip of the primary cilium. Subsequently, Gli transcription factors translocate to the nucleus and activate pro-proliferative genes in GNPs (Kim et al., 2009). For these reasons, primary cilia are essential for cerebellar development as they allow expansion of the progenitor pool of granule neurons (Chizhikov et al., 2007; Spassky et al., 2008). Primary cilia are also crucial for the formation of SHH-type medulloblastoma (SHH MB), a malignant pediatric brain tumor originating from GNPs (Schuller et al., 2008; Yang et al., 2008). Removal of primary cilia by ablation of *Kif3a*, a kinesin-2 subunit essential for ciliogenesis, blocks SHH MB cells proliferation *in vitro* and prevents tumorigenesis in various SHH MB-prone mouse genetic models (Han et al., 2009; Barakat et al., 2013). Although primary cilia play a critical role in cerebellar development and SHH MB formation, how this organelle is regulated in GNPs remains to be elucidated.

A master regulator of cerebellar development and SHH MB formation is the basic helix-loop-helix (bHLH) transcription factor *Atoh1*. While *Atoh1* is required for the formation of GNPs (Ben-Arie et al., 1997), its expression is also essential for SHH MB formation (Flora et al., 2009). Interestingly, several pieces of evidence have shown a cooperation between *Atoh1* and SHH for proper cerebellar development and SHH MB formation (Flora et al., 2009; Ayrault

et al., 2010; Forget et al., 2014). Given the crucial crosstalk between Atoh1 and the SHH signaling, we investigated whether Atoh1 could play a role in ciliogenesis. Here, we first show that Atoh1 expands the neural progenitor pool *in vivo* by regulating and utilizing the primary cilium. Mechanistically, Atoh1 facilitates clustering of centriolar satellites (CS), tiny organelles essential for ciliogenesis (Kim et al., 2008; Tollenaere et al., 2015a) through the transcriptional regulation of Cep131 (the centrosomal protein of 131 kDa). Together, our work unravels the cellular and molecular mechanism whereby Atoh1 controls primary cilia maintenance and functions to orchestrate GNP's development.

RESULTS

Sustained Atoh1 expression delays neuronal differentiation during postnatal cerebellar development

To study the role of Atoh1 *in vivo*, we utilized electroporation of green fluorescent protein (GFP)-expressing constructs into GNPs in the developing cerebellum at postnatal day 6 (P6; [Figure S1A and S1B](#)) (Umeshima et al., 2007) and examined the GFP-labeled cells 1, 2, 3, and 4 days later ([Figure 1A](#)). Cells electroporated with the control vector pCIG2 were largely found within the external granule layer (EGL) 1 day after electroporation and then progressively redistributed to the internal granule layer (IGL). By day 4, almost all of the cells have reached the IGL, leaving behind visible parallel fibers external to the molecular layer (ML). However, in cerebella electroporated with pCIG2-Atoh1, the majority of Atoh1 overexpressing cells still located in the EGL at day 2, and about one third of them remained in the EGL by day 4 ([Figure 1A and S1C](#)). Thus, sustained Atoh1 expression in GNPs delayed cell redistribution to the IGL during postnatal cerebellar development *in vivo*.

In order to determine at which stage GNPs were affected by sustained Atoh1 expression, cerebellar sections were stained with markers for cell proliferation (Ki67) and neuronal differentiation (Tuj1) 3 days after electroporation, when the difference in cell distribution became evident ([Figure 1B and S1D](#)). At this time point, very few GFP-labeled control cells were Ki67+, indicating that the majority of cells have exited cell cycle. By contrast, many GNPs overexpressing Atoh1 were still Ki67+. Moreover, when stained with Tuj1, the vast majority of control cells were positive for this marker. However, among the GNPs electroporated with

Atoh1-overexpressing construct, Tuj1+ cells were significantly reduced, suggesting a delay in GNP differentiation. Therefore, sustained Atoh1 expression in the cerebellum maintains GNPs in cell cycle and delays their differentiation *in vivo*.

Primary cilia are essential for expansion of GNPs as they enable the SHH signal transduction in the cerebellum during its postnatal development (Chizhikov et al., 2007; Spassky et al., 2008). To examine the distribution of primary cilia, we immunostained P8 cerebella with the ciliary markers Arl13b (ADP-ribosylation factor-like protein 13B) and Ift88 (Intraflagellar transport protein 88), and found that primary cilia were mainly detectable in the EGL (Figure S1E). Similarly, ciliary-associated structures, such as the ciliary axoneme and ciliary pocket, were mostly found at centrioles in the EGL by electronic microscopy (Figure S1F). These results suggest that primary cilia are lost upon GNPs differentiation, consistent with previous reports (Di Pietro et al., 2017).

To test whether Atoh1 can regulate GNP proliferation through cilia functions, we first examined the relationship between Atoh1 and primary cilia in *Atoh1^{GFP}* mice, in which endogenous Atoh1 is fused to GFP (Rose et al., 2009). Staining of Arl13b in P6 cerebella revealed that Atoh1 and primary cilia coexist in GNPs in the outer EGL (oEGL) (Figure 1C), while primary cilia are often short or undetected in the inner EGL (iEGL) where Atoh1 is absent. Furthermore, in cultured P6 GNPs from *Atoh1^{GFP}* mice, we defined Atoh1's level based on the GFP intensity (GFP^{low} vs GFP^{high}) and found that the percentage of ciliated cells was higher in GFP^{high} cells compared to GFP^{low} expressers (Figure 1D). Altogether, these results show that the presence of primary cilia are highly correlated with Atoh1 expression in the proliferating GNPs.

Atoh1 controls the presence of the primary cilium in GNPs *in vitro* and *in vivo*

Since primary cilia are associated with Atoh1 expression, we next examined whether Atoh1 could affect the presence of primary cilia in GNPs during cerebellar development. To achieve this aim, we depleted *Atoh1* in cultured P6 GNPs by infection with lentiviruses encoding GFP and a short-hairpin RNA against *Atoh1* (sh-*Atoh1*; Figure S2A) or non-targeting shRNA as control (sh-Ctrl), and scored the presence of primary cilia after 3 days. Strikingly, *in vitro* *Atoh1* knockdown significantly decreased the percentage of ciliated GNPs (Figure 2A). Importantly, by this time, the cell cycle progression of GNPs, monitored through BrdU incorporation, was not yet affected by *Atoh1* silencing (Figure S2B), although the transcription

of the SHH target genes *Ptch1*, *Ccnd1*, *Gli1* and *Mycn* was reduced (Figure S2C). Conversely, when we enforced Atoh1 expression by infecting GNP with retroviruses encoding Atoh1 and GFP (MSCV-Atoh1-I-GFP), the percentage of ciliated cells was increased after 2 days compared to control cells (MSCV-I-GFP) (Figure S2D).

To investigate whether Atoh1 could also affect the presence of primary cilia in GNPs *in vivo*, we generated *Atoh1^{CreER};Atoh1^{F1/F1}* mice, in which *Atoh1* was deleted specifically in GNPs when mouse pups were injected with tamoxifen at P3. Immunostaining of cerebellar sections at P7 with markers labelling primary cilia (Arl13b), centrioles (γ -Tub) and proliferative status (Ki67) enabled us to score for the presence of primary cilia only in proliferating GNPs, excluding postmitotic cells (Figure 2B). Consistently with our *in vitro* studies, the conditional knockout (cKO) of Atoh1 in *Atoh1^{CreER};Atoh1^{F1/F1}* mice largely reduced the fraction of ciliated cycling GNPs in the EGL, compared to *Atoh1^{F1/F1}* control littermates.

Next, we applied *in vivo* cerebellar electroporation to manipulate Atoh1 expression with higher spatiotemporal precision. P6 cerebella were electroporated with si-*Atoh1* and GFP or si-Ctrl and GFP for two days, followed by labelling of primary cilia by Arl13b or Ift88 staining. Remarkably, *Atoh1*-knockdown GNPs were less likely to display a primary cilium compared to control GNPs electroporated with si-Ctrl, confirming the results obtained in *Atoh1^{CreER};Atoh1^{F1/F1}* mice (Figure 2C and S2E). On the other hand, overexpression of Atoh1 via electroporation of pCIG2-Atoh1 plasmids in the cerebellum enhanced the proportion of ciliated GNPs compared to control (pCIG2) *in vivo* (Figure S2F).

As Atoh1 is crucial for SHH MB formation, we further explored whether Atoh1 could also regulate the primary cilium in primary SHH MB cells obtained from the tumor-prone *Ptch1^{+/-}* mouse model (Goodrich et al., 1997). Upon *Atoh1* knockdown, we observed a decrease of ciliated cells (Figure 2D); conversely, Atoh1 overexpression significantly increased the number of ciliated cells in SHH MB cells (Figure S2G). Altogether, these results suggest that Atoh1 controls the presence of primary cilia in GNPs and in SHH MB cells.

Atoh1 controls GNP expansion by maintaining the primary cilium

So far, we have shown that Atoh1 maintains GNP proliferation and their primary cilia, which are lost after differentiation. We therefore postulated that Atoh1 could keep GNP proliferation through the maintenance of primary cilia. To test this hypothesis, pCIG2-Atoh1

was co-electroporated in cerebella along with shRNAs targeting *Kif3a* (sh-*Kif3a*; [Figure S3A](#)) to impair ciliogenesis in GNPs ([Figure S3B](#)) (Spassky et al., 2008). As expected, overexpression of *Atoh1* with sh-Ctrl at P6 for 36 hrs maintained a higher percentage of GNPs in a Ki67+ undifferentiated state ([Figure 3A and 3B](#)). Strikingly, the ablation of primary cilia by *Kif3a* knockdown completely abolished this effect induced by *Atoh1* overexpression, restoring the percentage of Ki67+ cells back to normal ([Figure 3B](#)). Importantly, knockdown of *Kif3a* alone caused only a minor decrease in the percentage of proliferating GNPs within the same period, suggesting that the rescue effect, which brought down the percentage of proliferating GNPs, was specific to *Atoh1* overexpression ([Figure 3B](#)).

To confirm this result, we used shRNA against *Ift88* (sh-*Ift88*; [Figure S3C](#)) as a second approach to ablate the primary cilium ([Figure S3B](#)). Again, co-electroporation of sh-*Ift88* with pCIG2-*Atoh1* prevented GNPs from being aberrantly maintained within the cell cycle, while *Ift88* knockdown alone did not significantly affect proliferation after 36 hours *in vivo* ([Figure S3D](#)). Collectively, these data demonstrate that *Atoh1* keeps GNPs in a proliferative state through the maintenance of primary cilia during cerebellar development.

Atoh1 shapes centriolar satellites in GNPs

The transport of cargos toward the primary cilium is tightly regulated during ciliogenesis and ciliary maintenance (Sung and Leroux, 2013). Centriolar satellites (CS), composed of multi-protein complexes surrounding centrioles, are essential for cargo trafficking. Hence, loss of some components on CS hinders ciliogenesis, leading to ciliopathies (Kim et al., 2008; Waters and Beales, 2011; Tollenaere et al., 2015a). Based on their importance during ciliogenesis, we thus explored the distribution of CS in the granule neuron lineage in the P6 *Atoh1^{GFP}* mouse cerebellum. By using *Pcm1* and *Cep131* as markers for CS, we found that both proteins were highly expressed in *Atoh1* expressing GNPs in the oEGL, suggesting a potential link between CS and *Atoh1* ([Figure 4A](#)). To examine the potential function of *Atoh1* on CS, we infected P6 GNPs *in vitro* with lentiviruses encoding sh-Ctrl or sh-*Atoh1* for 2 days, followed by immunostaining of *Pcm1*, *Cep131* and pericentrin (*Pcnt*), a centriolar marker. While CS displayed typical clusters around the centrioles in control GNPs, *Atoh1* depletion led to mostly dispersed and scattered patterns for these two proteins, indicating that loss of *Atoh1* disturbed the subcellular distribution of CS ([Figures 4B](#)).

Because Atoh1 functions as a transcription factor, we hypothesized that its depletion may reduce the expression of key proteins involved in the regulation of CS integrity or localization. To look for potential Atoh1 target genes implicated in these functions, we took advantage of several published datasets (Figure 4C). Based on an automated microscopy screening in human cells, we started from a list of 239 genes whose knockdown halts the pericentrosomal clustering of the CS proteins Pcm1 or Cep290 (Gupta et al., 2015). Next, by using RNA-seq data from *Atoh1*^{null} versus wild-type embryonic cerebella (Klisch et al., 2011), we selected genes whose expression was significantly changed by *Atoh1* KO ($p < 0.01$ and $-0.5 < \log_2FC < 0.5$), thereafter reducing the list to 17 genes. At last, according to the Atoh1 ChIP-seq profile in the postnatal cerebellum (Klisch et al., 2011), we discarded the genes that did not present an Atoh1-binding signal (ChIP “peak”) in their proximity, rendering a list with 7 putative Atoh1 targets (Figure 4C and Table S1).

By RT-qPCR, we compared the expression of these candidate genes in GNPs infected with MSCV-Atoh1-I-GFP to control GNPs (MSCV-I-GFP) for 2 days. Interestingly, only two of them, *Cep131* and *Mtap7dl*, were significantly up- and down-regulated respectively upon Atoh1 overexpression (Figure 4D). Given that Cep131 physically localizes in CS and its requirement for ciliogenesis is well documented (Graser et al., 2007; Wilkinson et al., 2009; Hall et al., 2013; Chamling et al., 2014), we decided to further investigate this candidate. Therefore, we further validated whether the expression of Cep131 is regulated by Atoh1 through RT-qPCR in GNPs infected with sh-Ctrl and sh-*Atoh1* lentiviruses for two days *in vitro*. As expected, Cep131 mRNA was notably reduced by *Atoh1* knockdown while the transcription of other well-known CS genes implicated in ciliogenesis, including *Pcm1*, *Cep290*, *Odf1*, *For20*, *Bbs4* and *Talpid3*, was not affected (Figure 4E).

Finally, immunoblotting on GNP lysates revealed a reduction of Cep131 protein when Atoh1 was silenced (Figure 4F); by contrast, Cep131 protein was elevated upon enforced Atoh1 expression (Figure 4G), confirming that Cep131 is regulated by Atoh1 in GNPs. Taken together, our data show that Atoh1 regulates both the subcellular localization of CS and the expression of the CS component Cep131 in GNPs.

Cep131 is a direct transcriptional target of Atoh1

Given that the protein and RNA level of Cep131 correlate with Atoh1 expression, we next aimed to decipher if Cep131 is a direct transcriptional target of Atoh1. According to the ChIP-seq data (Klisch et al., 2011), Atoh1 interacts with a region spanning the last exon of Cep131 where three consensus E-boxes (bHLH factors-binding sites) are identified (Figure 5A). Therefore, we transduced SHH MB cells derived from the *Ptch1*^{+/+} mouse (Figure S4A) with HA-tagged Atoh1 (MSCV-Atoh1-HA-I-GFP) and, by using ChIP followed by qPCR (ChIP-qPCR), we confirmed that Atoh1 interacts with this putative *Cep131* regulatory region, similarly to other previously characterized Atoh1-bound sites (i.e. *Atoh1* and *Gli2* enhancers) (Flora et al., 2009; Klisch et al., 2011) (Figure 5B). In addition, using luciferase reporter assay (Krizhanovsky et al., 2006), we showed that Atoh1 expression significantly increased luciferase expression from the *Cep131*-reporter construct (Figure 5C), which contains a 365-bp region covering these three consensus E-boxes (Figure 5A). Mutation of the bHLH domain (K194R) in Atoh1 (Figure S4B) impeded this increase in the luciferase activity (Figure 5C), indicating that Atoh1 requires direct DNA binding to activate gene expression from this *Cep131* regulatory region.

Altogether, our results demonstrate that Atoh1 directly regulates the expression of *Cep131* by binding a regulatory region localized at the 3' of *Cep131* gene.

Atoh1 modulates the centriolar satellites for ciliogenesis through Cep131

To test the effects of Cep131 depletion in neuron progenitors, we infected P6 GNPs with lentiviruses encoding *Cep131* targeting shRNAs (sh-*Cep131*, Figure S4C) or sh-Ctrl *in vitro* for two days. Similar to *Atoh1* knockdown, Cep131 depletion dispersed the CS in GNPs stained with Pcm1 and reduced the percentage of ciliated cells (Figure 6A). Likewise, electroporation of sh-*Cep131* in P6 cerebella remarkably reduced the percentage of ciliated cells in the EGL after two days *in vivo* (Figure S4D). Notably, electroporation of sh-*Pcm1* (Figure S4E) in cerebella, which is known to disaggregate CS, also led to a reduction of primary cilia, indicating that CS integrity is essential for GNPs' ciliogenesis (Figure S4D). In addition, the loss of primary cilia after *Cep131* or *Pcm1* knockdown was rescued by co-electroporation of the respective RNAi-resistant human versions of these two genes (pCIG2-CEP131 and pCIG2-PCM1) *in vivo*, demonstrating the specificity of the used shRNA constructs (Figure S4D).

Overall, these findings indicate that loss of Cep131 phenocopies the effects of *Atoh1* silencing on CS integrity and primary cilia both *in vivo* and *in vitro* in neuron progenitors.

To investigate whether *Atoh1* promotes ciliogenesis in GNPs through the regulation of Cep131 expression, we examined whether ectopic expression of Cep131 could overcome the effects of *Atoh1* knockdown. P6 GNPs or murine SHH MB cells were co-infected with lentiviruses encoding sh-*Atoh1* and dsRed-fused Cep131 (dsRed-Cep131) for 3 days *in vitro*. We found that enforced dsRed-Cep131 expression counteracted the dispersion of CS in *Atoh1*-silenced cells (Figure 6B), enabling GNPs and SHH MB cells to reform primary cilia (Figure 6C and S5A). Coherently, co-electroporation of sh-*Atoh1* and human pCIG2-CEP131 rescued the loss of primary cilia after 2 days *in vivo* (Figure S5B). These results suggest that Cep131-dependent CS integrity acts downstream of *Atoh1* to enable ciliogenesis. Furthermore, disruption of CS integrity by either *Cep131* or *Pcm1* silencing compromised the ability of *Atoh1* overexpression to enhance ciliogenesis 2 days after electroporation *in vivo* (Figure S4D), indicating that *Atoh1* requires integral CS to maintain primary cilia in GNPs. Therefore, this *Atoh1*-Cep131-CS integrity pathway is responsible for ciliogenesis in GNPs and SHH MB cells.

***Atoh1* maintains SHH signaling through the primary cilium**

After having elucidated the molecular details underlying the ability of *Atoh1* to regulate primary cilia existence in GNPs, we investigated the impact of *Atoh1* on primary cilia functions. As primary cilia are essential for SHH signal transduction, we tested the effect of *Atoh1* expression on SHH signaling in NIH-3T3 mouse fibroblasts, a commonly used cell line for studying the biology of primary cilia. Using a Gli-responsive luciferase construct, we found that *Atoh1* significantly enhanced the response of NIH-3T3 cells to SHH. Strikingly, this effect was abolished when primary cilia functions were impaired by *Kif3a* or *Ift88* knockdown, demonstrating that *Atoh1* regulates SHH activity through the primary cilium (Figure 7A). We next assessed the effect of *Atoh1* on SHH signaling in GNPs using *Ptch1*, a primary target of SHH signaling, as a readout of pathway activation (Goodrich et al., 1996). Importantly, we found that while *Ptch1* expression decreased through time in control cells *in vitro*, the overexpression of *Atoh1* maintained *Ptch1* elevated, demonstrating that *Atoh1* keeps GNPs in a SHH-responsive state (Figure 7B).

Subsequently, we studied the ciliary distributions of key players in the SHH pathway (Figure S6A). We first looked at the protein localization of GFP-tagged Smo, Ptc1 and Gli2 in NIH-3T3 cells (Taipale et al., 2000; Rohatgi et al., 2007; Murdoch and Copp, 2010; Tukachinsky et al., 2010). Upon SHH stimulation for 6 hrs, Smo was redistributed into the primary cilium as previously described (Chen et al., 2002). When Atoh1 was overexpressed, we detected an accumulation of Smo and Gli2 at the tip of each primary cilium (Figure S6A and S6B). In the absence of SHH, Smo signals were majorly concentrated at the base of primary cilium in both control and Atoh1-expressing cells although Atoh1 slightly promoted redistribution of Smo from the ciliary base to the ciliary shaft (Figure S6C).

To investigate Smo localization in neuron progenitors, endogenous Smo was immunostained in cultured GNPs infected with Atoh1-overexpressing (MSCV-Atoh1-I-GFP) or control (MSCV-I-GFP) retroviruses. Interestingly, we found an accumulation of Smo signal in the primary cilium of GNPs overexpressing Atoh1 (Figure 7C and S6D). Moreover, when mouse SHH MB cells were infected with sh-*Atoh1* lentiviruses, the ciliary Smo signal was significantly decreased (Figure 7D). Taken together, these data suggest that Atoh1 regulates SHH pathway activation in GNPs and SHH MB cells.

In conclusion, our results demonstrate that Atoh1 sustains ciliogenesis in neuron progenitors and SHH MB by controlling Cep131 expression, and maintains SHH signaling activation through the primary cilium.

DISCUSSION

Impact of primary cilia regulation on cerebellar development

Primary cilia are required for proper cerebellar development, as they allow the SHH-driven proliferation of GNPs (Spassky et al., 2008). Therefore, elucidation of mechanisms underlying primary cilia regulation during development represents an important question in the field. Recently, it has been reported that primary cilia become shorter and fewer during GNP maturation (Di Pietro et al., 2017; Bay et al, 2018). In this study, we show that primary cilia are under the control of Atoh1 (Figure 2), a master regulator expressed in the cycling GNPs but absent in mature granule neurons (Akazawa et al., 1995; Ben-Arie et al., 1997). Importantly, this regulation seems to be crucial for the spatiotemporal regulation of GNPs expansion. Indeed,

upon inward migration, differentiating GNPs may experience higher concentration of SHH as they approach the Purkinje cell layer. In addition, previous reports indicated that SHH ligand is also continuously produced in the adult cerebellum (Traiffort et al., 1998; Lewis et al., 2004). Although other factors have been already suggested to limit SHH activity to the sole EGL (Klein et al., 2001; Pons et al., 2001; Solecki et al., 2001; Rubin et al., 2002), the retraction of primary cilia, caused by *Atoh1* loss upon GNPs differentiation, may represent an effective mechanism for preventing granule neurons from being aberrantly activated by SHH outside the EGL or in later stages of development.

Interestingly, the primary cilium plays distinct roles between embryogenesis and postnatal cerebellar development. In contrast to the postnatal stage, deletion of the primary cilium has no impact during embryonic development of the cerebellum (Han et al., 2009). On the same line, Purkinje cells start to express the mitogen SHH at E18.5 within the cerebellum (Lewis et al., 2004), which clearly demonstrates that SHH signaling and the primary cilium could collaborate only during postnatal cerebellar development, as implicated in our study.

Atoh1 regulates the primary cilium to maintain GNPs

We previously reported that *Atoh1* sensitizes GNPs to SHH, enabling a greater fraction of GNPs to re-enter the cell cycle after transient SHH deprivation (Ayrault et al., 2010). Here, we report a cellular mechanism whereby *Atoh1* keeps GNPs in a SHH-sensitive state by maintaining the primary cilium on their surface (Figure 2), and therefore enabling the activation of the mitogenic SHH signal transduction. As a consequence, *Atoh1* overexpression delays GNPs differentiation (Figure 1); conversely, *Atoh1* silencing inhibits cell proliferation and promotes cell cycle exit (Flora et al., 2009; Ayrault et al., 2010) by inducing primary cilium retraction (Figure 2). Importantly, our study further characterizes the complex relationship between *Atoh1* and the SHH signaling in GNPs.

Indeed, not only *Atoh1* maintains activation of SHH signaling through the cilium as we show here (Figure 7), but the SHH signaling itself also stabilizes *Atoh1* protein in a phosphorylation-dependent manner (Forget et al., 2014). These two pathways form a positive feedback loop that drives GNPs expansion in the developing cerebellum before some intrinsic and extrinsic mechanisms initiate to deplete *Atoh1* from cells (Briggs et al., 2008; Zhao et al., 2008). Therefore, we propose that deregulation of this circuit by an accumulation of *Atoh1*

resulting from inactivation of the transcriptional repressor HIC1 (Briggs et al., 2008) or the E3 ubiquitin ligase Huwe1 (Forget et al., 2014) would then constitutively activate SHH signaling, thus enhancing the positive feedback loop and contributing to SHH MB formation.

Contribution of Atoh1 to ciliogenesis in GNPs

Ciliogenesis is a complex event that requires activation of "ad hoc" transcriptional networks during development (Choksi et al., 2014). Here we describe the specific and essential contribution of Atoh1 to these cascades in the context of the cerebellar granule neuron lineage. Interestingly, a ciliogenic role for Atoh1 was previously reported in *Drosophila*, in which its homolog Atonal controls the expression of the ciliogenesis transcription factors Rfx and Fd3F (related to mammalian Foxj1), as well as ciliary functional components, such as Dilatory (related to Cep131), during mechanosensory cilia formation in chordotonal neurons (Cachero et al., 2011; zur Lage et al., 2011). However, we found that Foxj1 is undetectable in the cerebellum and the expression of mammalian Rfx factors is not affected by Atoh1 overexpression in GNPs (Figure S7). Conceivably, Atoh1 may not need to utilize Rfx factors and Foxj1 in the biogenesis of primary cilia due to their major role in regulating the genes specific for motile mechanosensory cilia, such as radial spokes, dynein arms, and Nexin-Dynein Regulatory Complex (N-DRC) (Choksi et al., 2014). Apparently, only the regulation of Dilatory is conserved as Atoh1 directly controls Cep131 expression in GNPs (Figure 4 and 5). This pathway plays a key role in GNPs' ciliogenesis, as the expression of Cep131 mostly restores the CS integrity (Figure 6B) and rescues the loss of primary cilia provoked by *Atoh1* knockdown (Figure 6C and S5B). Moreover, neither CS structures nor Pcm1 homologous proteins were found in *Drosophila* (Hodges et al., 2010); thus the role of Atoh1 in controlling the recruitment of CS may have emerged later during evolution (Figure 4B and 6B). Therefore, our results highlight the functional diversity of Atoh1 in regulating cilia between flies and mammals.

Notably, the nature of Cep131's contribution to ciliogenesis is still contentious, as the consequence of Cep131 reduction varies between different tissues and organisms, ranging from no ciliary defects to complete ciliary loss (Graser et al., 2007; Wilkinson et al., 2009; Ma and Jarman, 2011; Hall et al., 2013; Chamling et al., 2014). In our study, we provide evidence that Cep131 is required for ciliogenesis in GNPs, as *Cep131* knockdown reduces the percentage of ciliated cells *in vitro* and *in vivo* during postnatal cerebellar development (Figure 6A and S4D).

Most importantly, we also show that the loss of primary cilia in Cep131-depleted GNP results from the disruption of CS integrity, as indicated by Pcm1 scattering from the pericentrosomal region (Figure 6A), pinpointing a precise action of Cep131 in the context of GNP's ciliogenesis. It is interesting to note that in other works, Cep131 reduction does not always result in Pcm1 dispersion, largely depending on the cell types and environmental stimuli (Tollenaere et al., 2015b; Hori and Toda, 2017). For example, Cep131 depletion does not affect CS integrity in HeLa cells (Staples et al., 2012), whereas its reduction was shown to alter Pcm1 intensity and distribution in an automated microscopic screening (Gupta et al., 2015).

Altogether, our findings indicate that Atoh1 utilizes Cep131 to regulate CS integrity in the developing cerebellum (Figure 6). In turn, CS, assembled on the scaffold protein Pcm1, will contribute to ciliogenesis by enabling the required protein trafficking between the cytoplasm and the basal body-ciliary compartment (Kim et al., 2008; Waters and Beales, 2011; Tollenaere et al., 2015a). Therefore, the Atoh1-Cep131-CS integrity axis would act as a gatekeeper during GNP's ciliogenesis, as it would provide cells an essential machinery (i.e. the CS) for building the primary cilia.

Primary cilia and cancer

In cancer, the absence of primary cilia is often associated with tumor formation (Hassounah et al., 2012). By contrast, the presence of the primary cilium is required for the initiation and expansion of SHH MB driven by upstream activation of the SHH pathway, as in the case of *Ptch1* or *Gpr161* deletion or Smo activating mutations (Han et al., 2009; Barakat et al., 2013; Bay et al., 2018; Shimada et al., 2018). Current treatments for MB include surgical section, radiotherapy, and chemotherapy. Targeted therapies through the inhibition of Smo have been validated for their efficacy in SHH MB *in vivo*; however, they are often associated with toxicity or drug resistance, such as the GDC-0449 compound (Yauch et al., 2009). Thus, new approaches for targeting specific mechanisms in SHH MB are desperately needed. Interestingly, it was shown that ablation of primary cilia in MB cells blocks SHH MB proliferation *in vitro* and *in vivo* (Barakat et al., 2013). Recently, inhibition of Plk4, implicated in CS integrity and centriole biogenesis (Tang, 2013; Hori et al., 2016), was also proposed to serve as a promising target in treating MB (Sredni et al., 2017).

In conclusion, we uncovered a molecular mechanism controlled by the transcription factor *Atoh1* through the primary cilium, both of which are required for the formation of cerebellar neuron progenitors. Our results suggest that the *Atoh1*-*Cep131*-CS integrity program, which modulates primary cilium functions and SHH signaling pathway, may serve as new routes for therapeutic interventions to treat SHH MBs and cerebellar developmental disorders.

ACKNOWLEDGEMENTS

We thank Drs. Frédéric Saudou, Martine F. Roussel, Judith Souphron, Celio Pouponnot, Béatrice Durand, Laure Bihannic, Tang K. Tang (Academia Sinica), and Jun-An Chen (Academia Sinica) for helpful discussions. We especially thank Christophe Alberti, Elodie Belloir, Adlin Thadal, and Isabelle Grandjean for mouse colony management, Fabrice Cordelières, Marie-Noëlle Soler, Claire Lovo, Pei-Jun Hsen, and Yung-Yu Lu for confocal imaging assistance, Charlene Lasgi for cell sorting. We thank Drs. Mineko Kengaku and Hiroki Umeshima (Kyoto U) for their technical support of cerebellar electroporation, and Dr. Wann-Neng Jane (Academia Sinica) for technical support in electron microscopy. We thank Drs. Franck Polleux (pCIG2-GFP), Didier Trono (pLVTHM), Martine F. Roussel (MSCV vectors), Philip Beachy (pEGFP-mSmo, pCEFLmGFP-Gli2), Matthew Scott (Ptch1-YFP), Jenn-Yah Yu (Gli-luciferase vectors) and Lei Shi (pLV-3xFlag-puro-dsRed-Cep131) for providing plasmids. We also thank Philip Beachy for the HEK293T cell line expressing a secreted form of SHH. The *Atoh1* monoclonal antibody developed by Jane Johnson was obtained from the Developmental Studies Hybridoma Bank developed under the auspices of the NICHD and maintained by the Department of Biology, University of Iowa. This work was funded by grants from PHC ORCHID 2014 (#31272ND), PHC ORCHID 2017 (#38428YM), l'Institut National du Cancer (AVENIR TEAM, INCa R10067LS), Ligue Nationale Contre le Cancer (H.S. postdoctoral fellowship, Comité de l'Essonne), the Ministère Français de l'Enseignement Supérieur et de la Recherche (A.L.M.), Cancéropôle Ile-de-France and Fondation ARC pour la recherche sur le cancer (S.M.C., A.L.M. and M.R.), Fondation de France (A.F. post-doctoral fellowship), Marie Curie Integration grant FP7-PEOPLE-2011-CIG 294010, CNRS/INSERM, and Institut Curie to O.A. and from Ministry of Sciences and Technology, Taiwan (MOST-101-2320-B-010-077-MY2, 103-2911-I-010-504, 104-2633-H-010-001, 105-2633-B-009-003,

106-2628-B-010-002-MY3, 106-2911-I-010-508, 107-2628-B-010-002-MY3, 107-2221-E-010-014, and 107-2321-B-075-001), National Health Research Institute, Taiwan (NHRI-EX103-10314NC), Academia Sinica, Taiwan (AS-104-TP-B09), NYMU School of Medicine (107F-M01-0502) and Ministry of Education (Featured Areas Research Center Program) to J.W.T.

AUTHOR CONTRIBUTIONS

Conceptualization, J.W.T and O.A.; Methodology, C.H.C., M.Z., and H.S.; Formal Analysis, C.H.C., M.Z., H.S., J.W.T., and O.A.; Investigation, C.H.C., M.Z., H.S., J.S.C., H.Y., C.H.F., A.L.M., S.Y.H., A.F., C.H.W., S.M.C., I.L.L., and S.L.; Resources, W.Y.C., W.J.W., M.R., and N.S.; Writing - Original Draft, C.H.C., M.Z., H.S., J.W.T., and O.A.; Writing - Review & Editing, C.H.C., M.Z., H.S., J.S.C., H.Y., C.H.F., A.L.M., S.Y.H., A.F., C.H.W., S.M.C., I.L.L.; S.L., W.J.W., M.R., N.S., J.W.T., and O.A.; Supervision, J.W.T., and O.A.; Project Administration, J.W.T., and O.A.; Funding Acquisition, J.W.T., and O.A.

DECLARATION OF INTERESTS

The authors declare no competing interests.

REFERENCES

- Akazawa, C., Ishibashi, M., Shimizu, C., Nakanishi, S., and Kageyama, R. (1995). A mammalian helix-loop-helix factor structurally related to the product of *Drosophila* proneural gene *atonal* is a positive transcriptional regulator expressed in the developing nervous system. *The Journal of biological chemistry* *270*, 8730-8738.
- Anne, S.L., Govek, E.E., Ayrault, O., Kim, J.H., Zhu, X., Murphy, D.A., Van Aelst, L., Roussel, M.F., and Hatten, M.E. (2013). WNT3 inhibits cerebellar granule neuron progenitor proliferation and medulloblastoma formation via MAPK activation. *PLoS One* *26*, e81769.
- Ayrault, O., Zhao, H., Zindy, F., Qu, C., Sherr, C.J., and Roussel, M.F. (2010). *Atoh1* inhibits neuronal differentiation and collaborates with *Gli1* to generate medulloblastoma-initiating cells. *Cancer research* *70*, 5618-5627.

Barakat, M.T., Humke, E.W., and Scott, M.P. (2013). Kif3a is necessary for initiation and maintenance of medulloblastoma. *Carcinogenesis* *34*, 1382-1392.

Bay, S.N., Long, A.B., Caspary, T. (2018). Disruption of the ciliary GTPase Arl13b suppresses Sonic hedgehog overactivation and inhibits medulloblastoma formation. *Proceedings of the National Academy of Sciences of the United States of America* *115*, 1570-1575.

Ben-Arie, N., Bellen, H.J., Armstrong, D.L., McCall, A.E., Gordadze, P.R., Guo, Q., Matzuk, M.M., and Zoghbi, H.Y. (1997). Math1 is essential for genesis of cerebellar granule neurons. *Nature* *390*, 169-172.

Briggs, K.J., Corcoran-Schwartz, I.M., Zhang, W., Harcke, T., Devereux, W.L., Baylin, S.B., Eberhart, C.G., and Watkins, D.N. (2008). Cooperation between the Hic1 and Ptch1 tumor suppressors in medulloblastoma. *Genes & development* *22*, 770-785.

Buckner, R.L. (2013). The cerebellum and cognitive function: 25 years of insight from anatomy and neuroimaging. *Neuron* *80*, 807-815.

Cachero, S., Simpson, T.I., Zur Lage, P.I., Ma, L., Newton, F.G., Holohan, E.E., Armstrong, J.D., and Jarman, A.P. (2011). The gene regulatory cascade linking proneural specification with differentiation in *Drosophila* sensory neurons. *PLoS biology* *9*, e1000568.

Chamling, X., Seo, S., Searby, C.C., Kim, G., Slusarski, D.C., and Sheffield, V.C. (2014). The centriolar satellite protein AZI1 interacts with BBS4 and regulates ciliary trafficking of the BBSome. *PLoS genetics* *10*, e1004083.

Chen, J.K., Taipale, J., Cooper, M.K., and Beachy, P.A. (2002). Inhibition of Hedgehog signaling by direct binding of cyclopamine to Smoothened. *Genes & development* *16*, 2743-2748.

Chizhikov, V.V., Davenport, J., Zhang, Q., Shih, E.K., Cabello, O.A., Fuchs, J.L., Yoder, B.K., and Millen, K.J. (2007). Cilia proteins control cerebellar morphogenesis by promoting expansion of the granule progenitor pool. *The Journal of neuroscience : the official journal of the Society for Neuroscience* *27*, 9780-9789.

Choksi, S.P., Lauter, G., Swoboda, P., and Roy, S. (2014). Switching on cilia: transcriptional networks regulating ciliogenesis. *Development (Cambridge, England)* *141*, 1427-1441.

Dahmane, N., and Ruiz i Altaba, A. (1999). Sonic hedgehog regulates the growth and patterning of the cerebellum. *Development (Cambridge, England)* *126*, 3089-3100.

Di Pietro, C., Marazziti, D., La Sala, G., Abbaszadeh, Z., Golini, E., Matteoni, R., and Tocchini-Valentini, G.P. (2017). Primary Cilia in the Murine Cerebellum and in Mutant Models of Medulloblastoma. *Cellular and molecular neurobiology* *37*, 145-154.

Flora, A., Klisch, T.J., Schuster, G., and Zoghbi, H.Y. (2009). Deletion of *Atoh1* disrupts Sonic Hedgehog signaling in the developing cerebellum and prevents medulloblastoma. *Science (New York, NY)* *326*, 1424-1427.

Forget, A., Bihannic, L., Cigna, S.M., Lefevre, C., Remke, M., Barnat, M., Dodier, S., Shirvani, H., Mercier, A., Mensah, A., *et al.* (2014). Shh signaling protects *Atoh1* from degradation mediated by the E3 ubiquitin ligase *Huwe1* in neural precursors. *Developmental cell* *29*, 649-661.

Goodrich, L.V., Johnson, R.L., Milenkovic, L., McMahon, J.A., and Scott, M.P. (1996). Conservation of the hedgehog/patched signaling pathway from flies to mice: induction of a mouse patched gene by Hedgehog. *Genes & development* *10*, 301-312.

Goodrich, L.V., Milenkovic, L., Higgins, K.M., and Scott, M.P. (1997). Altered neural cell fates and medulloblastoma in mouse patched mutants. *Science (New York, NY)* *277*, 1109-1113.

Graser, S., Stierhof, Y.D., Lavoie, S.B., Gassner, O.S., Lamla, S., Le Clech, M., and Nigg, E.A. (2007). *Cep164*, a novel centriole appendage protein required for primary cilium formation. *Journal of Cell Biology* *179*, 321-330.

Gray, E.G. (1961). The granule cells, mossy synapses and Purkinje spine synapses of the cerebellum: Light and electron microscope observations. *Journal of Anatomy* *95*, 345-356.347.

Gupta, G.D., Coyaud, E., Goncalves, J., Mojarad, B.A., Liu, Y., Wu, Q., Gheiratmand, L., Comartin, D., Tkach, J.M., Cheung, S.W., *et al.* (2015). A Dynamic Protein Interaction Landscape of the Human Centrosome-Cilium Interface. *Cell* *163*, 1484-1499.

Hall, E.A., Keighren, M., Ford, M.J., Davey, T., Jarman, A.P., Smith, L.B., Jackson, I.J., and Mill, P. (2013). Acute versus chronic loss of mammalian *Azi1/Cep131* results in distinct ciliary phenotypes. *PLoS genetics* *9*, e1003928.

Han, Y.G., Kim, H.J., Dlugosz, A.A., Ellison, D.W., Gilbertson, R.J., and Alvarez-Buylla, A. (2009). Dual and opposing roles of primary cilia in medulloblastoma development. *Nature medicine* *15*, 1062-1065.

Hand, R., Bortone, D., Mattar, P., Nguyen, L., Heng, J.I., Guerrier, S., Boutt, E., Peters, E., Barnes, A.P., Parras, C., *et al.* (2005). Phosphorylation of *Neurogenin2* specifies the migration properties and the dendritic morphology of pyramidal neurons in the neocortex. *Neuron* *48*, 45-62.

Hassounah, N.B., Bunch, T.A., and McDermott, K.M. (2012). Molecular pathways: the role of primary cilia in cancer progression and therapeutics with a focus on Hedgehog signaling.

Clinical cancer research : an official journal of the American Association for Cancer Research *18*, 2429-2435.

Hoch, L., Faure, H., Roudaut, H., Schoenfelder, A., Mann, A., Girard, N., Bihannic, L., Ayrault, O., Petricci, E., Taddei, M., *et al.* (2015). MRT-92 inhibits Hedgehog signaling by blocking overlapping binding sites in the transmembrane domain of the Smoothed receptor. *FASEB Journal* *29*, 1817-1829.

Hodges, M.E., Scheumann, N., Wickstead, B., Langdale, J.A., and Gull, K. (2010). Reconstructing the evolutionary history of the centriole from protein components. *Journal of cell science* *123*, 1407-1413.

Hori, A., Barnouin, K., Snijders, A.P., and Toda, T. (2016). A non-canonical function of Plk4 in centriolar satellite integrity and ciliogenesis through PCM1 phosphorylation. *EMBO reports* *17*, 326-337.

Hori, A., and Toda, T. (2017). Regulation of centriolar satellite integrity and its physiology. *Cellular and molecular life sciences : CMLS* *74*, 213-229.

Ito, M. (2008). Control of mental activities by internal models in the cerebellum. *Nature reviews Neuroscience* *9*, 304-313.

Jacquet, B.V., Salinas-Mondragon, R., Liang, H., Therit, B., Buie, J.D., Dykstra, M., Campbell, K., Ostrowski, L.E., Brody, S.L., and Ghashghaei, H.T. (2009). FoxJ1-dependent gene expression is required for differentiation of radial glia into ependymal cells and a subset of astrocytes in the postnatal brain. *Development* *136*, 4021-4031.

Kim, J., Kato, M., and Beachy, P.A. (2009). Gli2 trafficking links Hedgehog-dependent activation of Smoothed in the primary cilium to transcriptional activation in the nucleus. *Proceedings of the National Academy of Sciences of the United States of America* *106*, 21666-21671.

Kim, J., Krishnaswami, S.R., and Gleeson, J.G. (2008). CEP290 interacts with the centriolar satellite component PCM-1 and is required for Rab8 localization to the primary cilium. *Human molecular genetics* *17*, 3796-3805.

Klein, R.S., Rubin, J.B., Gibson, H.D., DeHaan, E.N., Alvarez-Hernandez, X., Segal, R.A., and Luster, A.D. (2001). SDF-1 alpha induces chemotaxis and enhances Sonic hedgehog-induced proliferation of cerebellar granule cells. *Development* *128*, 1971-1981.

Klisch, T.J., Xi, Y., Flora, A., Wang, L., Li, W., and Zoghbi, H.Y. (2011). In vivo Atoh1 targetome reveals how a proneural transcription factor regulates cerebellar development.

Proceedings of the National Academy of Sciences of the United States of America *108*, 3288-3293.

Kobayashi, T., and Dynlacht, B.D. (2011). Regulating the transition from centriole to basal body. *The Journal of cell biology* *193*, 435-444.

Krizhanovsky, V., Soreq, L., Kliminski, V., and Ben-Arie, N. (2006). Math1 target genes are enriched with evolutionarily conserved clustered E-box binding sites. *Journal of molecular neuroscience : MN* *28*, 211-229.

Kubo, A., Yuba-Kubo, A., Tsukita, S., Tsukita, S., and Amagai, M. (2008). Sentan: a novel specific component of the apical structure of vertebrate motile cilia. *Molecular Biology of the Cell* *19*, 5338-5346.

Lewis, P.M., Gritli-Linde, A., Smeyne, R., Kottmann, A., and McMahon, A.P. (2004). Sonic hedgehog signaling is required for expansion of granule neuron precursors and patterning of the mouse cerebellum. *Developmental biology* *270*, 393-410.

Li, X., Song, N., Liu, L., Liu, X., Ding, X., Song, X., Yang, S., Shan, L., Zhou, X., Su, D., *et al.* (2017). USP9X regulates centrosome duplication and promotes breast carcinogenesis. *Nature communications* *8*.

Lin, Y.T., Ding, J.Y., Li, M.Y., Yeh, T.S., Wang, T.W., and Yu, J.Y. (2012). YAP regulates neuronal differentiation through Sonic hedgehog signaling pathway. *Experimental cell research* *318*, 1877-1888.

Ma, L., and Jarman, A.P. (2011). Dilatory is a Drosophila protein related to AZI1 (CEP131) that is located at the ciliary base and required for cilium formation. *Journal of cell science* *124*, 2622-2630.

McCormick, M.B., Tamimi, R.M., Snider, L., Asakura, A., Bergstrom, D., and Tapscott, S.J. (1996). NeuroD2 and neuroD3: distinct expression patterns and transcriptional activation potentials within the neuroD gene family. *Molecular and cellular biology* *16*, 5792-5800.

Murdoch, J.N., and Copp, A.J. (2010). The relationship between sonic Hedgehog signaling, cilia, and neural tube defects. *Birth defects research Part A, Clinical and molecular teratology* *88*, 633-652.

Pons, S., Trejo, J.L., Martínez-Morales, J.R., and Martí, E. (2001). Vitronectin regulates Sonic hedgehog activity during cerebellum development through CREB phosphorylation. *Development* *128*, 1481-1492.

Rohatgi, R., Milenkovic, L., and Scott, M.P. (2007). Patched1 regulates hedgehog signaling at

the primary cilium. *Science (New York, NY)* *317*, 372-376.

Rose, M.F., Ren, J., Ahmad, K.A., Chao, H.T., Klisch, T.J., Flora, A., Greer, J.J., and Zoghbi, H.Y. (2009). Math1 is essential for the development of hindbrain neurons critical for perinatal breathing. *Neuron* *64*, 341-354.

Rubin, J.B., Choi, Y., and Segal, R.A. (2002). Cerebellar proteoglycans regulate sonic hedgehog responses during development. *Development* *129*, 2223-2232.

Sasaki, H., Nishizaki, Y., Hui, C., Nakafuku, M., and Kondoh, H. (1999). Regulation of Gli2 and Gli3 activities by an amino-terminal repression domain: implication of Gli2 and Gli3 as primary mediators of Shh signaling. *Development (Cambridge, England)* *126*, 3915-3924.

Schuller, U., Heine, V.M., Mao, J., Kho, A.T., Dillon, A.K., Han, Y.G., Huillard, E., Sun, T., Ligon, A.H., Qian, Y., *et al.* (2008). Acquisition of granule neuron precursor identity is a critical determinant of progenitor cell competence to form Shh-induced medulloblastoma. *Cancer cell* *14*, 123-134.

Shimada, I.S., Hwang, S.H., Somatilaka, B.N., Wang, X., Skowron, P., Kim, J., Kim, M., Shelton, J.M., Rajaram, V., Xuan, Z., *et al.* (2018). Basal Suppression of the Sonic Hedgehog Pathway by the G-Protein-Coupled Receptor Gpr161 Restricts Medulloblastoma Pathogenesis. *Cell reports* *22*, 1169-1184.

Solecki, D.J., Liu, X.L., Tomoda, T., Fang, Y., and Hatten, M.E. (2001). Activated Notch2 signaling inhibits differentiation of cerebellar granule neuron precursors by maintaining proliferation. *Neuron* *30*, 557-568.

Spassky, N., Han, Y.G., Aguilar, A., Strehl, L., Besse, L., Laclef, C., Ros, M.R., Garcia-Verdugo, J.M., and Alvarez-Buylla, A. (2008). Primary cilia are required for cerebellar development and Shh-dependent expansion of progenitor pool. *Developmental biology* *317*, 246-259.

Sredni, S.T., Bailey, A.W., Suri, A., Hashizume, R., He, X., Louis, N., Gokirmak, T., Piper, D.R., Watterson, D.M., and Tomita, T. (2017). Inhibition of polo-like kinase 4 (PLK4): a new therapeutic option for rhabdoid tumors and pediatric medulloblastoma. *Oncotarget* *8*, 111190-111212.

Staples, C.J., Myers, K.N., Beveridge, R.D., Patil, A.A., Lee, A.J., Swanton, C., Howell, M., Boulton, S.J., and Collis, S.J. (2012). The centriolar satellite protein Cep131 is important for genome stability. *Journal of cell science* *125*, 4770-4779.

Sung, C.H., and Leroux, M.R. (2013). The roles of evolutionarily conserved functional modules

in cilia-related trafficking. *Nature cell biology* *15*, 1387-1397.

Taipale, J., Chen, J.K., Cooper, M.K., Wang, B., Mann, R.K., Milenkovic, L., Scott, M.P., and Beachy, P.A. (2000). Effects of oncogenic mutations in Smoothed and Patched can be reversed by cyclopamine. *Nature* *406*, 1005-1009.

Tang, T.K. (2013). Centriole biogenesis in multiciliated cells. *Nature cell biology* *15*, 1400-1402.

Tollenaere, M.A., Mailand, N., and Bekker-Jensen, S. (2015a). Centriolar satellites: key mediators of centrosome functions. *Cellular and molecular life sciences : CMLS* *72*, 11-23.

Tollenaere, M.A., Villumsen, B.H., Blasius, M., Nielsen, J.C., Wagner, S.A., Bartek, J., Beli, P., Mailand, N., and Bekker-Jensen, S. (2015b). p38- and MK2-dependent signalling promotes stress-induced centriolar satellite remodelling via 14-3-3-dependent sequestration of CEP131/AZI1. *Nature communications* *6*, 10075.

Traiffort, E., Charytoniuk, D.A., Faure, H., and Ruat, M. (1998). Regional distribution of Sonic Hedgehog, patched, and smoothed mRNA in the adult rat brain. *Journal of neurochemistry* *70*, 1327-1330.

Tsai, J.W., Lian, W.N., Kemal, S., Kriegstein, A.R., and Vallee, R.B. (2010). Kinesin 3 and cytoplasmic dynein mediate interkinetic nuclear migration in neural stem cells. *Nature Neuroscience* *13*, 1463-1471.

Tukachinsky, H., Lopez, L.V., and Salic, A. (2010). A mechanism for vertebrate Hedgehog signaling: recruitment to cilia and dissociation of SuFu-Gli protein complexes. *The Journal of cell biology* *191*, 415-428.

Umeshima, H., Hirano, T., and Kengaku, M. (2007). Microtubule-based nuclear movement occurs independently of centrosome positioning in migrating neurons. *Proceedings of the National Academy of Sciences of the United States of America* *104*, 16182-16187.

Uziel, T., Zindy, F., Xie, S., Lee, Y., Forget, A., Magdaleno, S., Rehg, J.E., Calabrese, C., Solecki, D., Eberhart, C.G., *et al.* (2005). The tumor suppressors Ink4c and p53 collaborate independently with Patched to suppress medulloblastoma formation. *Genes & development* *19*, 2656-2667.

Wallace, V.A. (1999). Purkinje-cell-derived Sonic hedgehog regulates granule neuron precursor cell proliferation in the developing mouse cerebellum. *Current biology : CB* *9*, 445-448.

Waters, A.M., and Beales, P.L. (2011). Ciliopathies: an expanding disease spectrum. *Pediatric nephrology (Berlin, Germany)* *26*, 1039-1056.

Wechsler-Reya, R.J., and Scott, M.P. (1999). Control of neuronal precursor proliferation in the

cerebellum by Sonic Hedgehog. *Neuron* 22, 103-114.

Wilkinson, C.J., Carl, M., and Harris, W.A. (2009). Cep70 and Cep131 contribute to ciliogenesis in zebrafish embryos. *BMC cell biology* 10, 17.

Wiznerowicz, M., and Trono, D. (2003). Conditional suppression of cellular genes: lentivirus vector-mediated drug-inducible RNA interference. *Journal of Virology* 77, 8957-8961.

Yang, Z.J., Ellis, T., Markant, S.L., Read, T.A., Kessler, J.D., Bourboulas, M., Schuller, U., Machold, R., Fishell, G., Rowitch, D.H., *et al.* (2008). Medulloblastoma can be initiated by deletion of Patched in lineage-restricted progenitors or stem cells. *Cancer cell* 14, 135-145.

Yauch, R.L., Dijkgraaf, G.J., Alicke, B., Januario, T., Ahn, C.P., Holcomb, T., Pujara, K., Stinson, J., Callahan, C.A., Tang, T., *et al.* (2009). Smoothed mutation confers resistance to a Hedgehog pathway inhibitor in medulloblastoma. *Science (New York, NY)* 326, 572-574.

Zhao, H., Ayrault, O., Zindy, F., Kim, J.H., and Roussel, M.F. (2008). Post-transcriptional down-regulation of Atoh1/Math1 by bone morphogenic proteins suppresses medulloblastoma development. *Genes & development* 22, 722-727.

zur Lage, P.I., Simpson, T.I., and Jarman, A. (2011). Linking specification to differentiation: From proneural genes to the regulation of ciliogenesis. *Fly* 5, 322-326.

Chang et al, FIGURE 1

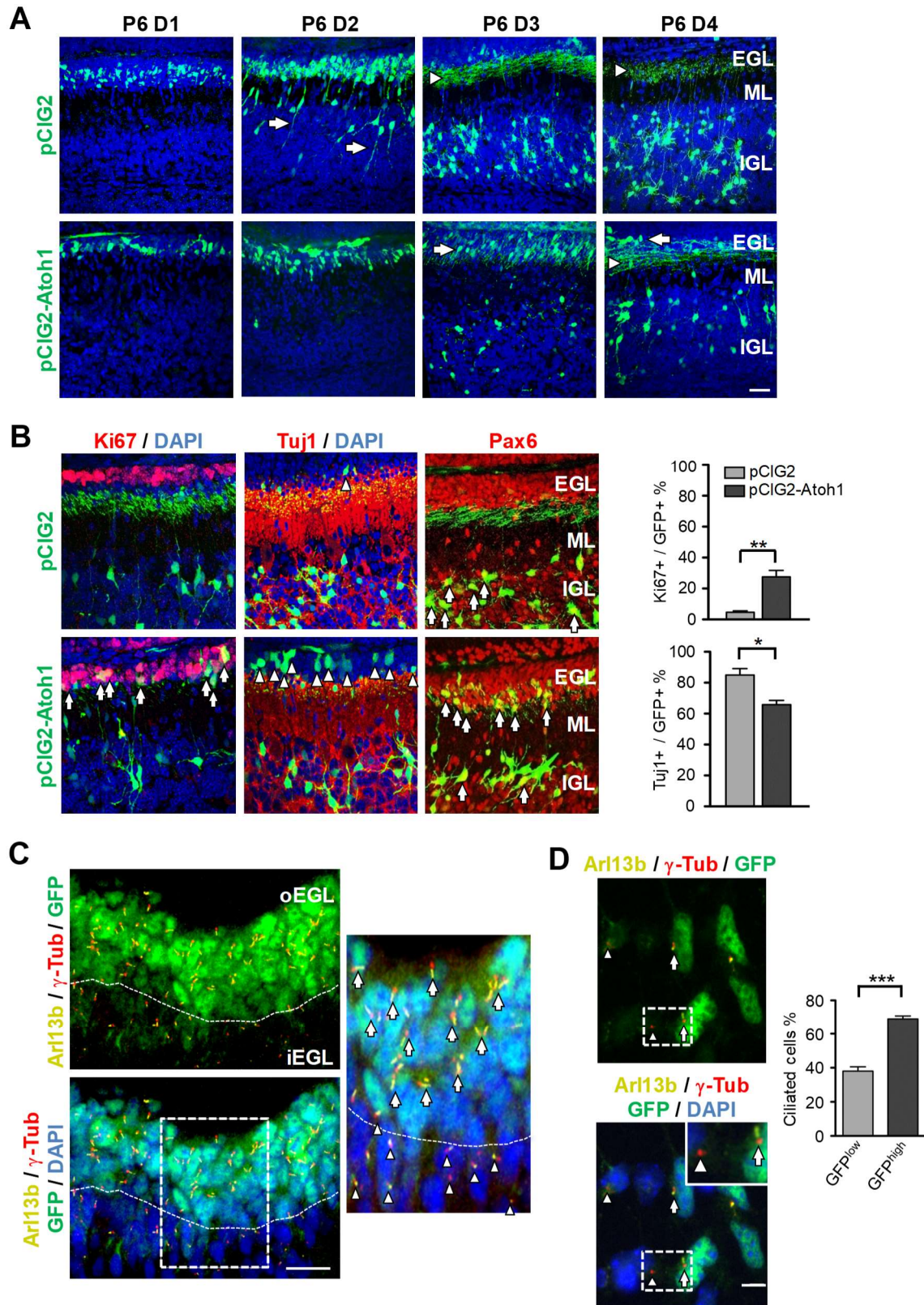


Figure 1. Sustained Atoh1 expression delays GNPs differentiation *in vivo* and correlates with primary cilia in the EGL

(A) Representative images showing the distributions of GNPs in the cerebella 1, 2, 3, 4 day(s) (D1, D2, D3, D4) after electroporation *in vivo* at P6 with pCIG2 (upper panels) or pCIG2-Atoh1 (lower panels). Arrows indicate migrating granule neurons from the ML (P6 D2) to the IGL and GNPs still located in the EGL (P6 D3 and P6 D4). Note that parallel fibers are prominent in the EGL (arrowheads). Scale bar: 20 μ m. [See also Figure S1C](#).

(B) Immunostaining for cell cycle (Ki67), neuronal differentiation (Tuj1) and granule cell lineage (Pax6) markers (red) in cerebellar slices at 3 days after electroporation with pCIG2 (upper panels) or pCIG2-Atoh1 (lower panels). Arrows indicate Ki67⁺ / GFP⁺ cells (left column) and Pax6 / GFP⁺ cells (right column), while arrowheads indicate GFP⁺ cells in the Tuj1⁻ layer (middle column). Green: GFP, blue: DAPI. Scale bar: 50 μ m. Bar graphs show the percentage of Ki67⁺ / GFP⁺ and Tuj1⁺ / GFP⁺ cells in each condition. Student's *t* test. *: $p < 0.05$, **: $p < 0.01$; $n = 4$ animals in which around 800 electroporated cells were counted. Data are represented as mean \pm SEM. [See also Figure S1D](#).

(C) Co-existence of primary cilia and Atoh1 expression in P6 cerebellar sections from *Atoh1*^{GFP} knockin mouse immunostained with Arl13b (yellow), γ -tubulin (red), GFP (green) and DAPI (blue). An enlarged view from the boxed region (right panel) shows that intact primary cilia (arrows) are detectable in Atoh1-expressing cells (GFP⁺), while most primary cilia in GFP⁻ cells are short or absent (arrowheads). Dashed lines separate the outer EGL (oEGL) from the inner EGL (iEGL), which is also the boundary of Atoh1 expression. Scale bar: 20 μ m.

(D) Purified P6 GNPs from *Atoh1*^{GFP} mice, cultured in presence of SHH, were immunostained for Arl13b (yellow), γ -tubulin (red), and DAPI (blue). Arrows indicate intact primary cilia, while arrowheads show basal bodies devoid of primary cilia. Scale bar: 5 μ m. Bar graph indicates the percentage of primary cilia according to the GFP intensity, which corresponds to Atoh1 expression. Student's *t* test. ***: $p < 0.001$; $n = 3$; 500 cells per experiment. Data are represented as mean \pm SEM.

Chang et al, FIGURE 2

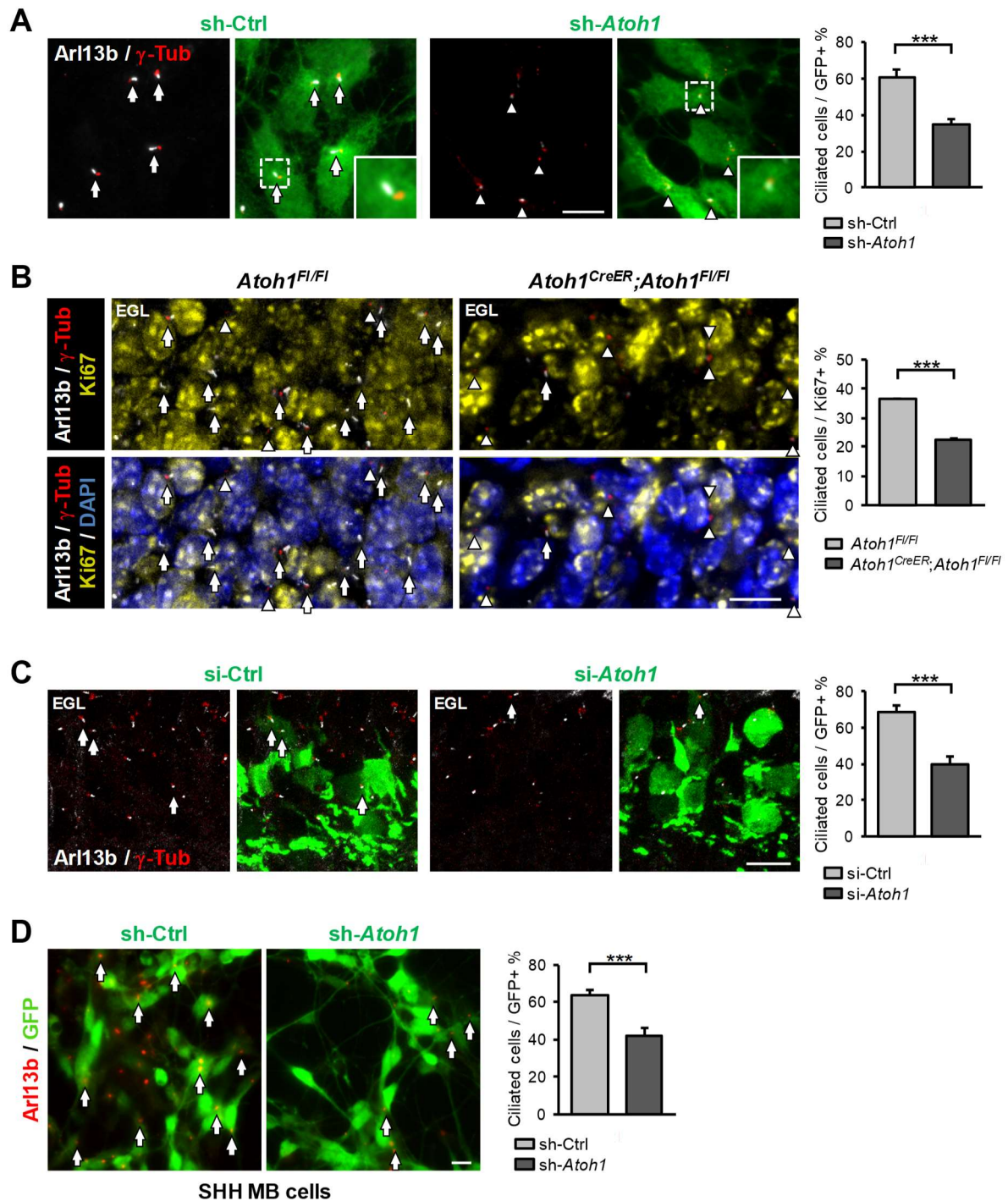


Figure 2. *Atoh1* governs the presence of primary cilia *in vitro* and *in vivo*

(A) Primary cilia in *Atoh1*-knockdown GNPs *in vitro*. Cultured P6 wild-type GNPs were infected with lentiviruses encoding sh-Ctrl (left two panels) or sh-*Atoh1* (right two panels) for 72 hrs. Arrowheads represent basal bodies without protruding of Arl13b+ signals, while arrows

indicate fully formed primary cilia. Green: GFP, white: Arl13b, red: γ -tubulin. Scale bar: 10 μ m. Bar graph reveals the percentage of ciliated cells after 72 hrs *in vitro* in each group. Student's *t* test. ***: $p < 0.001$; $n = 4$; 1500 cells per experiment. Data are represented as mean \pm SEM. See also Figure S2B and S2C.

(B) P7 cerebella sections from *Atoh1^{CreER};Atoh1^{F1/F1}* mice treated with tamoxifen at P3, were immunostained with Arl13b (white), γ -tubulin (red), Ki67 (yellow) and DAPI (blue). Arrows indicate intact primary cilia, while arrowheads point to basal bodies devoid of ciliary structures. Scale bar: 10 μ m. Bar graph represents the percentage of ciliated GNPs among cycling (Ki67+) GNPs. EGL: external granule layer. Student's *t*-test ***: $p < 0.001$; Animal number: $n = 3$ for each condition; Around 350 cells counted per animal. Data are represented as mean \pm SEM.

(C) Cerebella were electroporated with control RNAi (si-Ctrl, left two panels, $n = 4$ animals) or *Atoh1* RNAi (si-*Atoh1*, right two panels, $n = 6$ animals) for 36 hrs. Immunostaining by Arl13b (white) and γ -tubulin (red) represent the primary cilium (arrows) in each group. Scale bar: 10 μ m. Bar graph displays the percentage of ciliated GNPs in GFP+ cells. 450 electroporated cells were counted per experiment. Student's *t* test. ***: $p < 0.001$. Data are represented as mean \pm SEM.

(D) Immunostaining for primary cilia by Arl13b (red) in mouse SHH MB cells infected with lentiviruses encoding sh-Ctrl (left panel) or sh-*Atoh1* (right panel) for 72 hrs. Green: GFP. Arrows represent the primary cilium in GFP+ cells. Scale bar: 10 μ m. Bar graph indicates the percentage of ciliated SHH MB cells in each group. Student's *t* test. ***: $p < 0.001$; $n = 4$; 700 cells counted per experiments. Data are represented as mean \pm SEM. See also Figure S2.

Chang et al, FIGURE 3

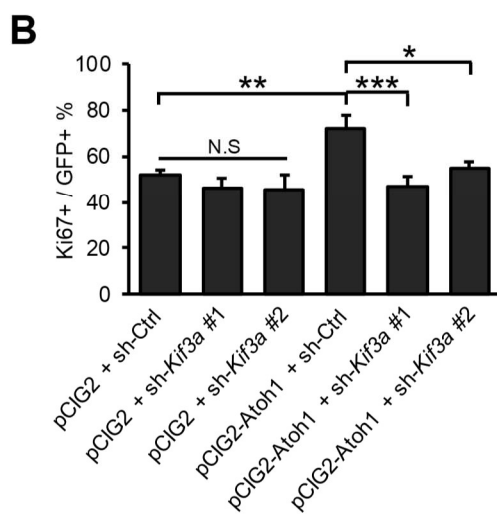
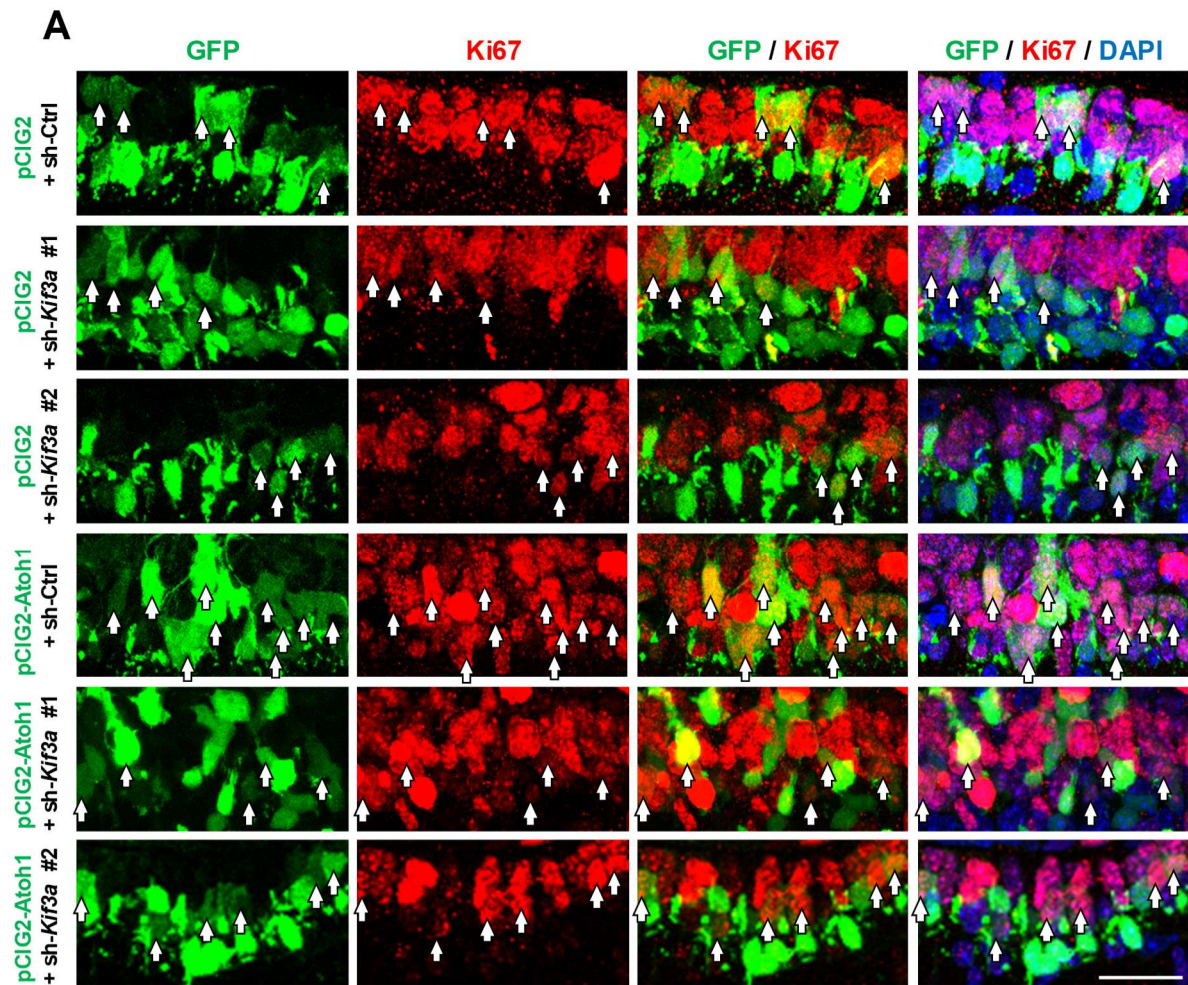


Figure 3. Primary cilia are required for Atoh1 to maintain GNP proliferation *in vivo*

(A) Proliferation status of GNPs overexpressing Atoh1 (pCIG2-Atoh1) or control (pCIG2) in combination with *Kif3a* shRNAs (sh-*Kif3a* #1 or #2) in cerebella 36 hrs after electroporation at P6. Arrows indicate the proliferating GNPs (Ki67+, red) in electroporated cells (GFP+). Blue: DAPI. Scale bar: 10 μ m. [See also Figure S3](#).

(B) Bar graph represents the quantification of (A), and indicates the percentage of Ki67+ / GFP+ cells in each group. Two-way ANOVA, $p=0.004$. Post-hoc: LSD test. *: $p<0.05$, **: $p<0.01$, ***: $p<0.001$. Animal number: $n = 4$ for pCIG2 + sh-Ctrl, pCIG2 + sh-*Kif3a* #1, pCIG2-Atoh1 + sh-Ctrl, and pCIG2-Atoh1 + sh-*Kif3a* #1, $n = 3$ for pCIG2 + sh-*Kif3a* #2 and pCIG2-Atoh1 + sh-*Kif3a* #2. Around 1000 electroporated cells were counted. Data are represented as mean \pm SEM.

Chang et al, FIGURE 4

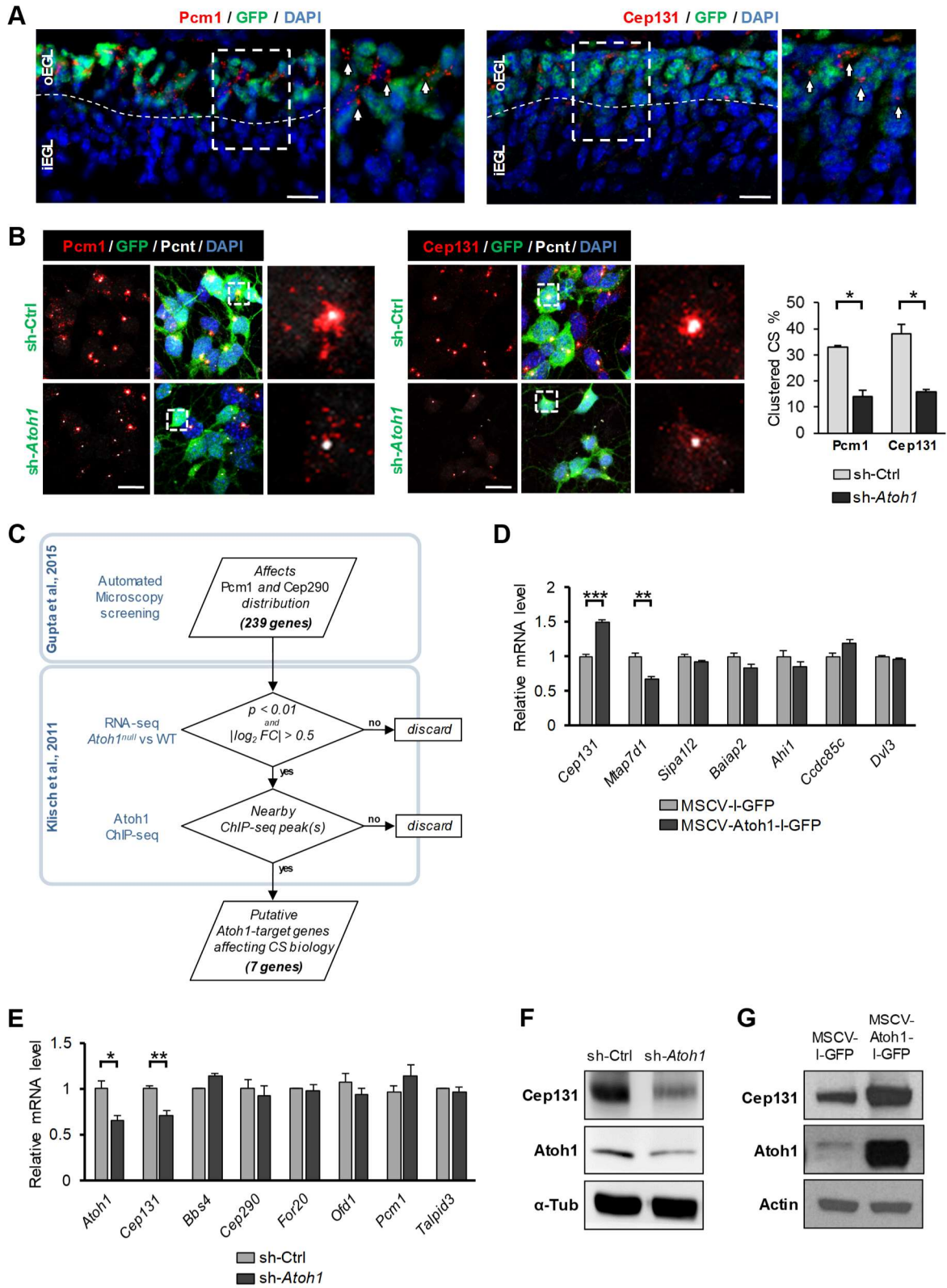


Figure 4. *Atoh1* shapes the centriolar satellites and correlates with *Cep131* expression

(A) Distribution of centriolar satellites (CS, arrows) in the cerebellar EGL at P6. Immunostaining of cerebellar sections from the *Atoh1^{GFP}* mouse revealed the localization of clustered CS (red, arrows), represented by *Pcm1* (left panel) and *Cep131* (right panel). Green: GFP, Blue: DAPI. Dashed lines mark the boundary between oEGL and iEGL. Boxed regions (dashed squares) are enlarged at the right of each panel. Scale bar: 20 μ m.

(B) Effects of *Atoh1* knockdown on CS localization. P6 GNPs were infected with lentiviruses encoding sh-Ctrl or sh-*Atoh1* (green) for 2 days *in vitro*. Immunostaining shows *Pcm1* (red, left panels), *Cep131* (red, right panel) and the centrioles (*Pcnt*, white). Boxed regions (dashed squares) are magnified at the right of each panel. Blue: DAPI. Scale bar: 10 μ m. Bar graph represents the quantification for the percentage of clustered CS in GFP+ infected cells. Student's *t* test. *: $p < 0.05$; around 1500 neurons from 3 independent experiments. Data are represented as mean \pm SEM.

(C) Workflow exhibits the applied dataset and exclusion criteria for searching candidate *Atoh1*-targeted genes involved in the regulation on CS integrity or distribution.

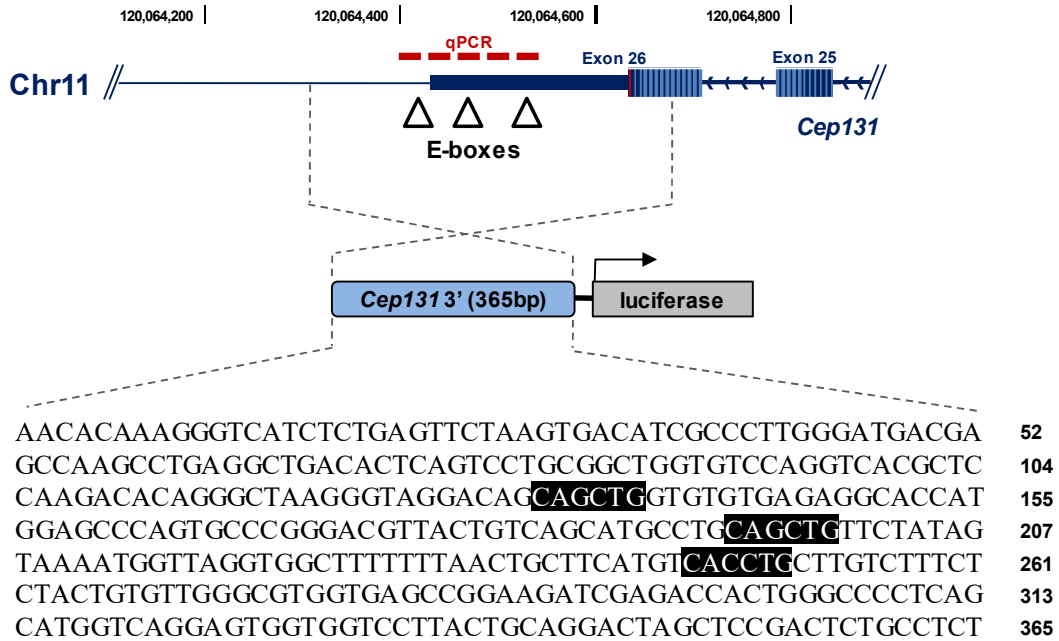
(D) Relative mRNA expression of the seven genes derived from (C) was measured by RT-qPCR in P6 GNPs infected with MSCV-*Atoh1*-I-GFP or MSCV-I-GFP retroviruses for 2 days. Student's *t* test. **: $p < 0.01$, ***: $p < 0.001$; $n = 3$. Data are represented as mean \pm SEM.

(E) Relative mRNA expression of *Cep131* and a panel of CS genes involved in ciliogenesis in P6 GNPs infected with sh-Ctrl or sh-*Atoh1* lentiviruses for 2 days. Student's *t* test. *: $p < 0.05$, **: $p < 0.01$; $n = 3$ for *Atoh1*, *Cep131*, *Bbs4*, *Cep290*, *For20* and *Talpid3*, $n = 4$ for *Ofd1* and *Pcm1*. Data are represented as mean \pm SEM.

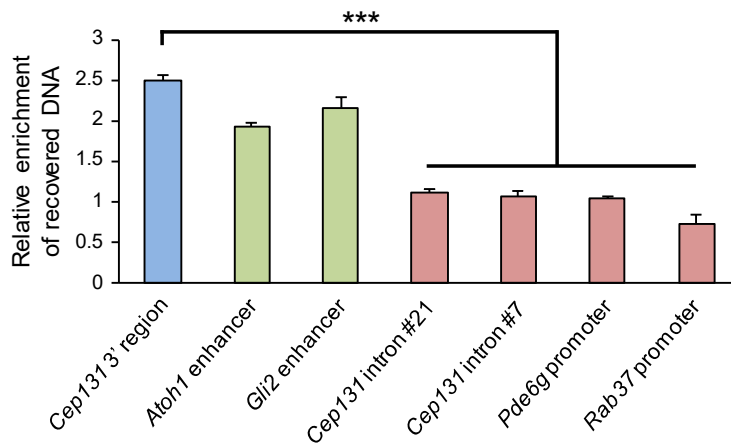
(F-G) Effects of *Atoh1* on *Cep131* protein expression in GNPs. Whole cell lysates of cultured P6 GNPs infected with lentiviruses encoding either sh-Ctrl / sh-*Atoh1* (F) or MSCV-I-GFP / MSCV-*Atoh1*-I-GFP (G) were immunoblotted by using antibodies against *Cep131* and *Atoh1*. Actin and α -Tub were used as loading control.

Chang et al, FIGURE 5

A



B



C

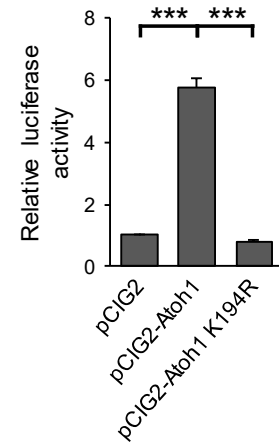


Figure 5. Atoh1 directly regulates *Cep131* transcription

(A) The 3' region of *Cep131* locus in mouse genome containing 3 E-boxes (arrowheads). Dashed red line spanning the 3 E-boxes corresponds to the DNA sequence amplified in the ChIP-qPCR for the *Cep131* 3' region (see also Figure 5B). Cloning strategy for the *Cep131*-reporter construct and the nucleotide sequence of the cloned region (see also Figure 5C) are shown at the bottom.

(B) Atoh1 ChIP-qPCR in murine SHH MB cells infected with MSCV-Atoh1-HA-GFP and sorted by FACS for GFP expression. Bar graph shows the relative amount of recovered DNA measured by qPCR after ChIP. The putative *Cep131* 3' regulatory region containing three E-boxes (dashed red line in (A)) is shown in blue. Known Atoh1-bound enhancers (i.e. *Atoh1* and *Gli2*), are shown as green bars and were used as positive controls (Flora et al., 2009; Klisch et al., 2011). E-box-containing sequences in promoters of *Cep131* proximal genes (*Pde6g* and *Rab37*) and *Cep131* introns were used as negative controls and are shown as red bars. One-way ANOVA, $p < 0.001$. Post-hoc: Dunnett's test. ***: $p < 0.001$; $n = 4$. Data are represented as mean \pm SEM. [See also Figure S4A.](#)

(C) Bar graph shows the normalized luciferase activity when the *Cep131*-reporter construct was co-transfected with plasmids encoding either empty vector (pCIG2), Atoh1 (pCIG2-Atoh1) or transcriptionally inactive Atoh1 (pCIG2-Atoh1 K194R) in N2a cells. One-way ANOVA, $p < 0.001$. Post-hoc: Bonferroni test. ***: $p < 0.001$; $n = 3$ from 3 independent experiments. Data are represented as mean \pm SEM. [See also Figure S4B.](#)

Chang et al, FIGURE 6

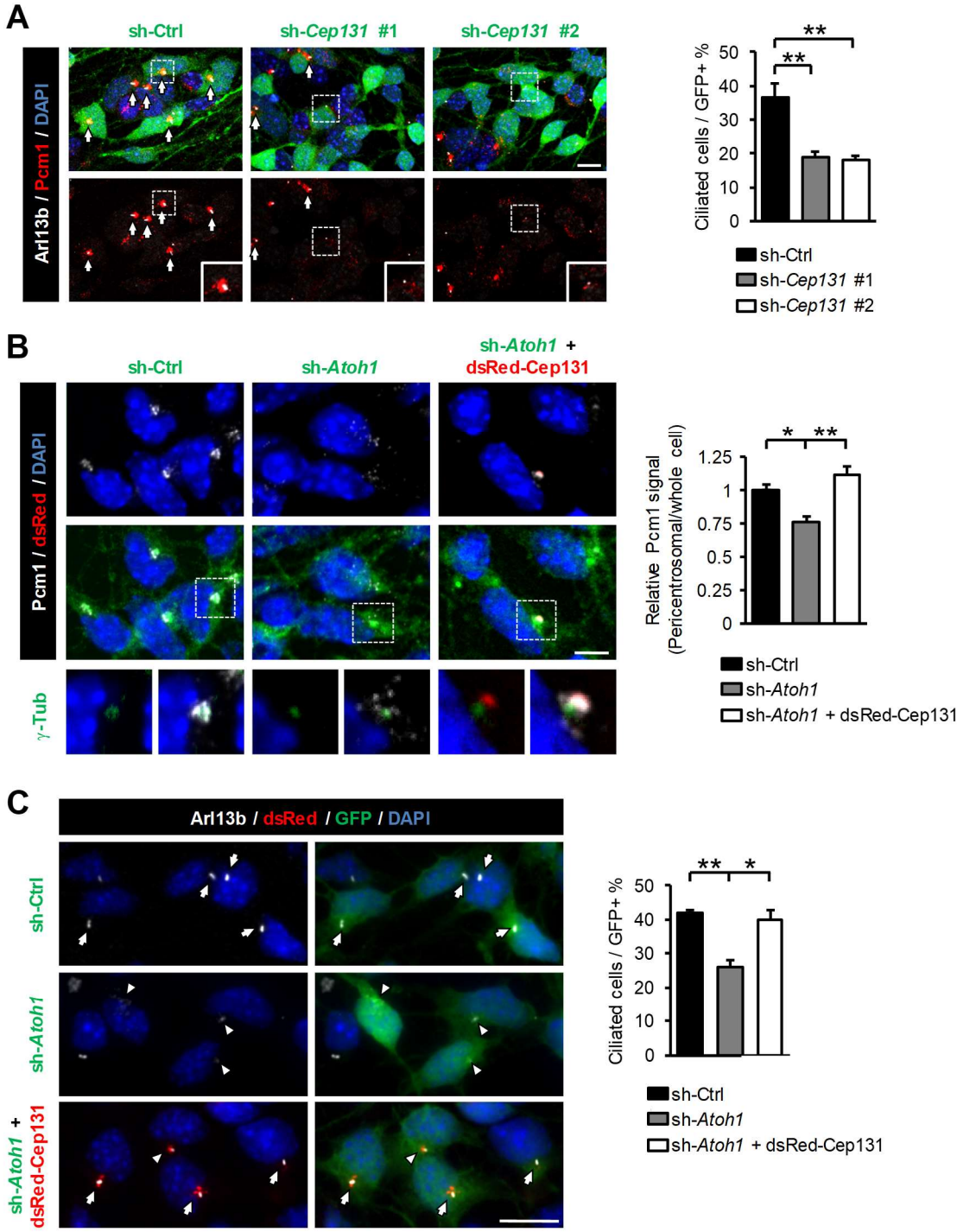


Figure 6. *Atoh1* modulates centriolar satellites for ciliogenesis through *Cep131* in GNP

(A) Effects of *Cep131* knockdown on the CS morphology (*Pcm1*, red) and primary cilia (*Arl13b*, white). Cultured P6 GNPs were infected with lentiviruses encoding for sh-RNAs (green) targeting *Cep131* (sh-*Cep131* #1 and #2) or sh-Ctrl for 2 days. Arrows indicate clustered CS with intact cilia. Insets show representative CS morphology of GFP+ GNPs in each group. Scale bar: 10 μ m. Bar graph represents the percentage of ciliated cells in GFP+ GNPs. One-way ANOVA, $p < 0.001$. Post-hoc: Bonferroni test. **: $p < 0.01$; Around 1400 neurons from 3 independent experiments. Data are represented as mean \pm SEM. See also Figure S4C.

(B) Rescue effect of *Cep131* on *Pcm1* localization in cultured P6 GNPs upon *Atoh1* knockdown. GNPs were infected *in vitro* with indicated combinations of lentiviruses encoding for sh-Ctrl, sh-*Atoh1* (green) and a dsRed-tagged *Cep131* (dsRed-*Cep131*) for 3 days. Immunostaining revealed *Pcm1*-containing CS (*Pcm1*, white), and centrioles (γ -tubulin, green). Boxed regions are enlarged at the bottom of each panel. Scale bar: 5 μ m. Bar graph represents the *Pcm1* intensity from pericentrosomal region normalized to the whole cell. One-way ANOVA, $p < 0.01$. Post-hoc: Bonferroni test. *: $p < 0.05$, **: $p < 0.01$; $n = 4$, around 300 cells counted per condition in each replicate. Data are represented as mean \pm SEM.

(C) Rescue effect of *Cep131* on primary cilia upon *Atoh1* knockdown in GNPs. GNPs were treated as in (B). Arrows indicate fully formed primary cilia in contrast to defective primary cilia (arrowheads). Green: GFP, red: dsRed-*Cep131*, white: *Arl13b*, blue: DAPI. Scale bar: 10 μ m. Bar graph represents the percentage of ciliated GNPs among GFP+ cells. One-way ANOVA, $p < 0.01$. Post-hoc: Bonferroni test. *: $p < 0.05$, **: $p < 0.01$; $n = 3$, around 500 cells counted per condition in each replicate. Data are represented as mean \pm SEM. See also Figure S5.

Chang et al, FIGURE 7

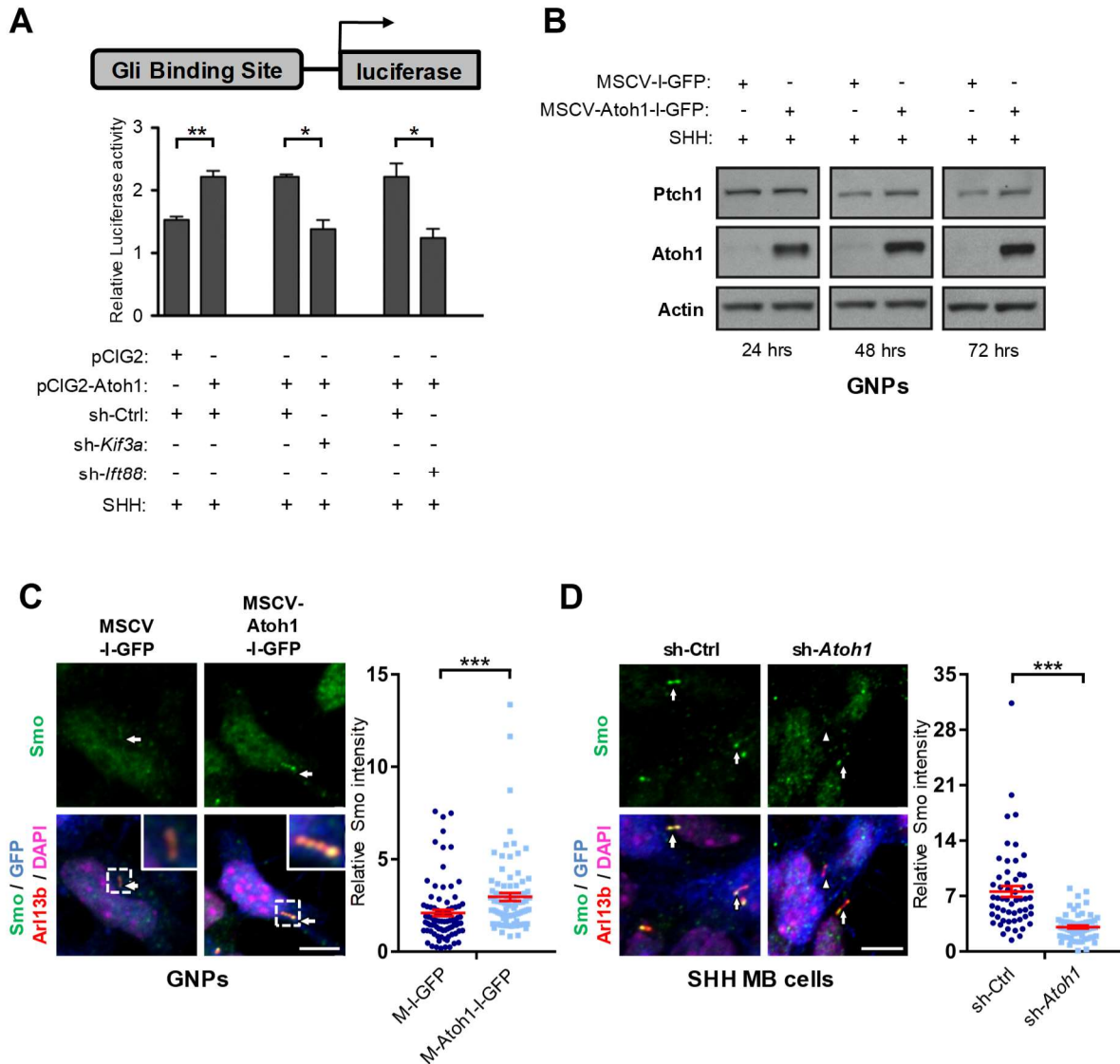


Figure 7. Atoh1 maintains SHH signaling through the primary cilium

(A) SHH signaling activity in NIH-3T3 cells overexpressing Atoh1 in combination with primary cilia ablation by *Kif3a* or *Ift88* silencing. SHH-treated NIH-3T3 cells were transfected with a plasmid encoding the firefly luciferase under the control of a promoter sequence with Gli binding sites in combination with indicated plasmids. The values of Gli-luciferase activities are normalized to the activity in cells without SHH activation. Student's *t* test. *: $p < 0.05$, **: $p < 0.01$; $n = 3$. Data are represented as mean \pm SEM.

(B) P6 wild-type GNP cells were infected with indicated retroviruses in presence of SHH. Lysates of GNP cells were analyzed at indicated times by immunoblotting using antibodies against Ptch1, Atoh1 and Actin.

(C) Endogenous Smo (green) staining in cultured P6 wild-type GNP cells infected with retroviruses carrying GFP (left two panels, MSCV-I-GFP) or Atoh1 and GFP (right two panels, MSCV-Atoh1-I-GFP) in the presence of SHH. Blue: GFP, green: Smo, red: Arl13b, magenta: DAPI. Scale bars: 5 μ m. Scatter plot shows the Smo intensity residing in the primary cilium (arrows in the images) relative to its intensity within the cytoplasm for individual cells. Red lines mark the mean and SEM for control GNP cells (dark blue, $n = 86$) and Atoh1-overexpressing GNP cells (light blue, $n = 87$). Mann-Whitney U test. ***: $p < 0.001$. See also Figure S6D.

(D) Smo (green) localization (arrows) in primary mouse SHH MB cells from the *Ptch1*^{+/-} model infected with lentiviruses encoding sh-Ctrl ($n = 56$ cells) or sh-*Atoh1* ($n = 67$ cells) for 72 hrs. Arrowheads indicate less accumulation of Smo signal inside the primary cilium, compared to arrows. Green: Smo, red: Arl13b, blue: GFP, magenta: DAPI. Scatter plot reports Smo intensity within the primary cilium relative to its intensity within the cytoplasm for individual cells. Red lines mark the mean and SEM for control and sh-*Atoh1* cells. Mann-Whitney U test. ***: $p < 0.001$. Scale bar: 5 μ m.

STAR*METHODS

Detailed methods are provided in the online version of this paper and include the following:

CONTACT FOR REAGENT AND RESOURCE SHARING

Further information and requests for resources and reagents should be directed to and will be fulfilled by the Lead Contact, Olivier Ayrault (olivier.ayrault@curie.fr).

EXPERIMENTAL MODEL AND SUBJECT DETAILS

Animal Husbandry

Pups at various Postnatal (P) ages were obtained from CD-1 (RjOrl:SWISS) mice for GNP culture or *in vivo* electroporation. Mouse SHH MB cells were generated from *Ptch1*^{+/-} mice (Jackson Laboratory, 003081) (Goodrich et al., 1997). *Atoh1*^{GFP} knockin (referred to as *Atoh1*^{tm4.1Hzo}), *Atoh1*^{CreER} (referred to as *Tg(Atoh1-cre/Esr1*)14Fsh*) and *Atoh1*^{Fl/Fl} (referred to as *Atoh1*^{tm3Hzo}) mice were obtained from Jackson Laboratory. To achieve the conditional knockout of *Atoh1* in GNPs, *Atoh1*^{CreER}; *Atoh1*^{Fl/Fl} mice were intraperitoneally injected with tamoxifen at P3. We followed the European and national regulations for the care and use of animals in order to protect vertebrate animals for experimental and other scientific purposes (Directive 86/609). The project “*Atoh1/Math1* regulation and function during cerebellar normal development and medulloblastoma” obtained the ethical approval (#2011-0012) from the reporting ethical committee IDF Paris-Comité 1. The animal use was also approved by the Institutional Animal Care and Use Committee (IACUC) of National Yang-Ming University (1030503, 1040625).

Cerebellar electroporation *in vivo*

In vivo cerebellar electroporation was modified from the protocol described previously (Umeshima et al., 2007). Briefly, mouse pups at P6 were anesthetized on ice for 2-5 minutes until unresponsiveness to pain stimuli. An incision was made to expose the underlying skull above the cerebellum. A needle was used to make a tiny hole in the skull and then a 33-gauge needle was inserted into the cerebellum to deliver DNA (0.7 µl) into the primary fissure of the cerebellum. Electroporation was achieved by a tweezer-type electrodes connected to a square

wave generator (ECM 830, Harvard Apparatus), providing a short current of 70 V, with 6 pulses over a 50 ms duration and 150 ms intervals over the head. The wound was then sutured and sterilized with 70 % alcohol.

Cell lines, GNPs and SHH-MB culture

NIH-3T3, Neuro-2a (N2a), and HEK293T cells were cultured in Dulbecco's Modified Eagle's Medium supplemented with 10% calf serum or fetal bovine serum as instructions from ATCC, 4 mM L-glutamine and 100 unit penicillin and streptomycin. SHH was purchased (SHH-N Terminus recombinant, R&D) or obtained from a conditioned medium (HEK293 cell line expressing a secreted form of SHH (ShhN-pIND), gift from Philip Beachy, (Johns Hopkins Medical School, Baltimore, MD). Cerebellar GNPs and SHH MB cells were purified and cultured as previously described (Zhao et al., 2008). GNPs were cultured with SHH-conditioned medium, SHH-N Terminus recombinant or the Smoothened ligand (SAG) 100 nM (Enzo Life Sciences). P6 GNPs from *Atoh1^{GFP}* pups were purified and cultured in presence of SHH and fixed 6 hrs after plating. *In vitro*, GNPs were incubated with 10 μ M BrdU (BD Biosciences) for 2 hrs and stained with anti-BrdU as previously described (Uziel et al., 2005).

METHOD DETAILS

Plasmids and siRNA

For *in vivo* cerebellar electroporation, pCIG2-Atoh1-HA was used to enforce Atoh1-HA expression while pCIG2 was used as a control (Forget et al., 2014). pC2 and pC2-Atoh1-HA were generated from pCIG2 and pCIG2-Atoh1-HA respectively, in which GFP cassette was removed. MSCV-IRES-GFP (MSCV-I-GFP), MSCV-Atoh1-IRES-GFP, MSCV-IRES-RFP and MSCV-Atoh1-IRES-RFP were previously described (Ayrault et al., 2010). The lentiviral pLV-3xFlag-puro-dsRed-Cep131 plasmid, kindly provided by Dr. Lei Shi (Li et al., 2017), was used to ectopically express Cep131 in cultured GNPs. Human version of CEP131 and PCM1 cDNA were generous gift from Dr. Tang K. Tang, and these cDNAs were sub-cloned into pCIG2 vector. pEGFP-mSmo (Addgene #25395) (Chen et al., 2002), pCEFLmGFP-Gli2

(Addgene#37672) (Kim et al., 2009), Ptch1-YFP (Addgene #58456) (Rohatgi et al., 2007) were obtained from Addgene.

For Gli-luciferase assay, the promoter region of the luciferase reporter contained eight copies of the wild-type Gli binding motif (GAACACCCA, GliBS), or mutant Gli binding motif (GAAGTGGGA, mGliBS) as previously described (Sasaki et al., 1999; Lin et al., 2012). US2-renilla luciferase construct was used as internal control. Details information for siRNA targeting sequences are listed in [Table S2](#).

Virus production and Lipofectamine transfection

Viruses were generated as previously described (Forget et al., 2014). NIH-3T3 cells and Neuro2a (N2a) were transfected with Lipofectamine 3000 (Invitrogen) in accordance to the manufacturer's protocol. For primary cilia studies, NIH-3T3 cells were serum deprived after transfection (5% serum, 24 hrs). Subsequently, SHH-N Terminus recombinant protein (R&D) was added (0.6 µg/ml) for 6 hrs (for immunoblotting) or 8 hrs (for luciferase assay). To visualize Ptch1, Gli2 and Smo within the primary cilium, transient transfection and sparse labeling was achieved by using 0.8 µg of each plasmid (Ptch1-YFP, pCEFLmGFP-Gli2, or pEGFP-mSmo), simultaneously transfected with 3.2 µg of pC2 or pC2-Atoh1-HA in 2×10^5 NIH-3T3 cells on a 3.5 cm diameter glass-bottom dish. Next, cells were serum starved for 24 hrs after transfection and SHH-N Terminus recombinant protein was added for an additional 6 hrs.

Immunofluorescence and imaging

The cerebella were harvested at indicated time. After terminally anaesthetized on ice, mice pups were transcardially perfused with 4% PFA in PBS and post-fixed in 4% PFA overnight. Sagittal sections (100 µm) were performed using Vibrotome (VT1000S, Leica) or cerebella were cryoprotected in 30% (w/v) sucrose in PBS before embedding in tissue-Teck. Serial sections (8 µm) were made on a cryostat. Primary antibodies used *in vivo* are listed in the [Key Resources Table](#). Secondary antibodies (Alexa Fluor, 1:500, Thermo Fisher Scientific) were applied for 2 hrs at room temperature. Finally, the slices were counterstained with 0.5 µg/ml DAPI (Invitrogen) for 1 hr. VECTASHIELD Mounting (Vector Laboratories) was added before sealing the slides. For NIH-3T3 and GNP staining, cells were fixed with 4% PFA for 15 minutes

and then permeabilized in PBST solution (0.3% Triton X-100 in PBS) for 30 min. Primary antibodies, listed in the [Key Resources Table](#), were applied for 2 hrs at room temperature, following by secondary antibodies and DAPI as described above.

Microscopy

Slices or cells were imaged under an inverted laser scanning confocal microscope by either (LSM-700, Zeiss) or (SP5, Leica) with a 63x objective (N.A 0.7, LEICA) at a resolution of 2048x2048 (pixel size 0.246 μ m) and a 100x objective (N.A 1.4 oil, Zeiss) respectively. Images acquisition for the GNPs was performed using a 3D microscope (Optigrid, Leica) with a 63x objective (N.A 1.40, LEICA) connected to a CCD camera (pixel size 6.5 μ m x 6.5 μ m). The excitation wavelengths were 405 nm for DAPI, 488 nm for EGFP, 555 nm for red fluorescence, and 635 nm for infrared. Zeiss LSM 7MP with 20X (N.A. 1.0) was used to observe the granule neurons with T-shape morphology. A femtosecond pulsed infrared laser (MaiTai HP, SpectraPhysics) tuned at 910 nm was used as the excitation light source.

Electron Microscopy

P6 mice pups were transcardially fixed with a buffer containing 2.5% glutaraldehyde, 4% PFA in 0.1M PBS. Next, cerebella were processed and sectioned at the Transmission Electron Microscope Facility in Academia Sinica as previously described (Gray, 1961). Cerebella sections were observed under JEOL JEM-1400 PLUS system.

Image analysis and fluorescent intensities quantification

For primary cilia counting *in vivo* and *in vitro*, all the cells in mitosis were excluded from our analysis, as primary cilia are retracted during this phase of the cell cycle.

For distinguishing the morphology of centriolar satellites (i.e., cluster or disperse), GNP images were analyzed using ITCN plugin in ImageJ software (NIH). Individual satellite was measured and defined as one dot according to the instructions from Academic Technology at Keene State College (https://www.youtube.com/watch?v=PqHFsmS1_JY). If there are more than 3 dots located around Pcnt-labeled centriole, this pattern will be classified as “clustered.”

For centriolar satellite localization rescue experiment upon dsRed-Cep131 expression in GNPs, the extent of Pcm1 clustering around the centrosome was determined as follow, using the ImageJ software (NIH). We first measured the signal intensity of Pcm1 (called PC_{signal}) within a circular area of $4.8 \mu\text{m}^2$ centered on the peak intensity of γ -tubulin in infected cells. The $4.8 \mu\text{m}^2$ value was estimated from the average surface of the Pcm1 pericentrosomal "cloud" in wild-type GNPs. Second, we measured the Pcm1 signal intensity in the whole cell cytoplasm (WC_{signal}) of infected cells. Finally, the reported "Pericentrosomal to whole cell Pcm1 signal ratio" was calculated as $PC_{signal} / WC_{signal}$. The relative values were obtained from the normalization to sh-Ctrl cells. Additionally, in order to highlight the γ -tubulin staining, the contrast relative to the green signal was enhanced in the magnified cropped images.

For NIH-3T3 cells transiently transfected with pEGFP-mSmo, GFP signals were measured in the individual primary cilium by the Zen software (Carl Zeiss, Germany). Upon SHH stimulation, the "tips to shaft width ratio" was calculated as $0.5 \times (A+B) / C$ in each labeled primary cilium where: A: width for the tip of primary cilium, B: width for the base of primary cilium, C: width for the shaft of primary cilium. For the Smoothened staining in GNPs or SHH MB cells, Smoothened signals were measured under Image J software (NIH). The "relative Smo intensity" was calculated by the normalization of the averaged smoothened signal from the entire primary cilium to the averaged smoothened signal within the cytoplasm in individual cells. Scatter plot was drawn under the Excel software (Microsoft).

Immunoblotting

Cell were lysed in RIPA buffer (50mM Tris-HCl, pH 8.0, 150mM NaCl, 1% Nonidet P-40, 0.5% sodium deoxycholate, 0.1% SDS) and mixed with protease inhibitor cocktail (Sigma Aldrich). Proteins were quantified by BCA protein assay (Pierce) and were resolved by SDS-Page. Primary antibodies are listed in the [Key Resources Table](#).

RNA extraction, cDNA synthesis and qPCR

Total RNA extraction from cultured GNPs was performed with TRIzol Reagent (Thermofisher Scientific) according to manufacturer's instructions. Removal of potential genomic DNA

contaminations was achieved by DNase I treatment (Sigma-Aldrich) and, subsequently, cDNA was synthesized using SuperScript III Reverse Transcriptase (Thermofisher Scientific) following provider's protocols. qPCR was performed with Power SYBR Green PCR Master Mix (Applied Biosystems). Primers for RT-qPCR are listed in [Table S3](#).

ChIP-qPCR

To test the physical binding of Atoh1 to the *Cep131* regulatory region, 10×10^6 murine SHH MB cells, previously transduced with MSCV-Atoh1-HA-IRES-GFP and FACS-sorted for GFP expression, were harvested, washed with cold PBS and incubated at room temperature with 1% formaldehyde (Thermofisher Scientific) for 10 minutes on a rotator. The crosslinking reaction was stopped by adding glycine 140 mM for 5 minutes at room temperature. After two washes in cold PBS, cells were lysed in 700 μ l of RIPA buffer with protease inhibitors for 1 hour on ice. The lysate was then sonicated at 4°C to shear the chromatin to an average size of 200-500 bp and centrifuged to remove cell debris. To perform the ChIP, 40 μ l of anti-HA antibodies-conjugated agarose beads (Sigma) were pre-blocked in 80 μ l of RIPA buffer containing 4 μ g of BSA and 3 μ g of herring sperm DNA (Thermofisher Scientific) for 3 hrs. 50 μ l of lysate was used as input and the remaining was incubated with the pre-blocked beads at 4°C on a rotator O/N. The beads were then washed with a buffer containing 250 mM LiCl, 1% NP-40, 1% sodium deoxycholate, 1 mM EDTA and 10 mM Tris-HCl in pH8. Antibodies-bound chromatin was finally eluted with SDS 1% and 100 mM NaHCO₃ in water. Precipitated and IP-input chromatin was de-crosslinked O/N at 65°C in presence of 300 ng/ μ l proteinase K (Thermofisher Scientific) and 200 mM NaCl. Subsequently, DNA was extracted using phenol:chloroform. Recovered DNA was finally used as template for qPCR using the primers listed in [Table S4](#). The relative quantification of recovered DNA for each tested genomic region was calculated as $2^{-(C_{t_{input}} - C_{t_{IP}})}$ where $C_{t_{input}}$ and $C_{t_{IP}}$ are the qPCR threshold cycles relative to the input and the IP-eluted chromatin respectively. Obtained values were then normalized to the mean of the negative controls.

Luciferase reporter assay

To test the transcriptional activity of Atoh1 K194R mutant, 0.2×10^6 HEK293T cells were plated in 6 wells plate and, co-transfected with 0.25 μ g of pCIG2-Atoh1-HA or pCIG2-Atoh1-K149R-

HA or pCIG2 as negative control as well as 0.12 µg of p4RTK-Luc (p4RTK-Luc) (McCormick et al., 1996) and 0.025 µg of renilla luciferase. The p4RLTK-Luc plasmid contains 5 multimerized E-boxes driving the expression of the firefly luciferase.

For *Cep131*-reporter assay, the E-boxes containing 3' regulatory region of *Cep131* (Figure 5A) was sub-cloned into the pGL3-basic vector. Next, 0.15×10^6 Neuro-2a (N2a) cells in 24-well plates were co-transfected with 0.025 µg US2-renilla luciferase and 0.4µg *Cep131*-reporter constructs. Meanwhile, 0.4 µg of either pCIG2, pCIG2-Atoh1-HA, or pCIG2-Atoh1-K194R-HA were transfected as different groups.

For Gli-reporter assay, 0.5×10^5 NIH-3T3 cells in 24-well plates were co-transfected with 0.025 µg US2-renilla luciferase and 0.35µg firefly luciferase with either wild-type or mutant Gli binding sites as the promoters. 0.05 µg pCIG2 or pCIG2-Atoh1-HA was transfected in NIH-3T3 cells under half serum for 24 hrs. Subsequently, recombinant SHH-N (R&D) was added to achieve final concentration at 0.6 µg/ml for additional 8 hrs.

In all above cases, cell lysis and luciferase assay were performed using the Dual Luciferase Assay kit (Promega), according to the manufacturer's protocol. For both two Atoh1 assays, the luciferase activity is determined as the normalized ratio between firefly luciferase and Renilla luciferase in the same cells. For the Gli reporter assay, the luciferase activity is calculated as the following formula: (GliBS firefly luciferase / Renilla luciferase in the same cells), followed by normalization with (mutant GliBS firefly luciferase / Renilla luciferase in the same cells), in accordance to previous study (Lin et al., 2012).

Statistical analysis

Statistical significance was determined with GraphPad Prism software (version 5.0), Excel software (Microsoft), and PASW Statistics 18 (IBM).

Supplemental Information

Atoh1 Controls Primary Cilia Formation to Allow for SHH-Triggered Granule Neuron Progenitor Proliferation

Chia-Hsiang Chang^{1,2*}, Marco Zanini^{3,4*}, Hamasseh Shirvani^{3,4*}, Jia-Shing Cheng¹, Hua Yu^{3,4}, Chih-Hsin Feng¹, Audrey L. Mercier^{3,4}, Shiue-Yu Hung⁵, Antoine Forget^{3,4}, Chun-Hung Wang¹, Sara Maria Cigna^{3,4}, I-Ling Lu¹, Wei-Yi Chen⁶, Sophie Leboucher^{3,4}, Won-Jing Wang⁶, Martial Ruat⁷, Nathalie Spassky⁸, Jin-Wu Tsai^{1,9#} and Olivier Ayrault^{3,4,10#}

Supplemental Figure 1

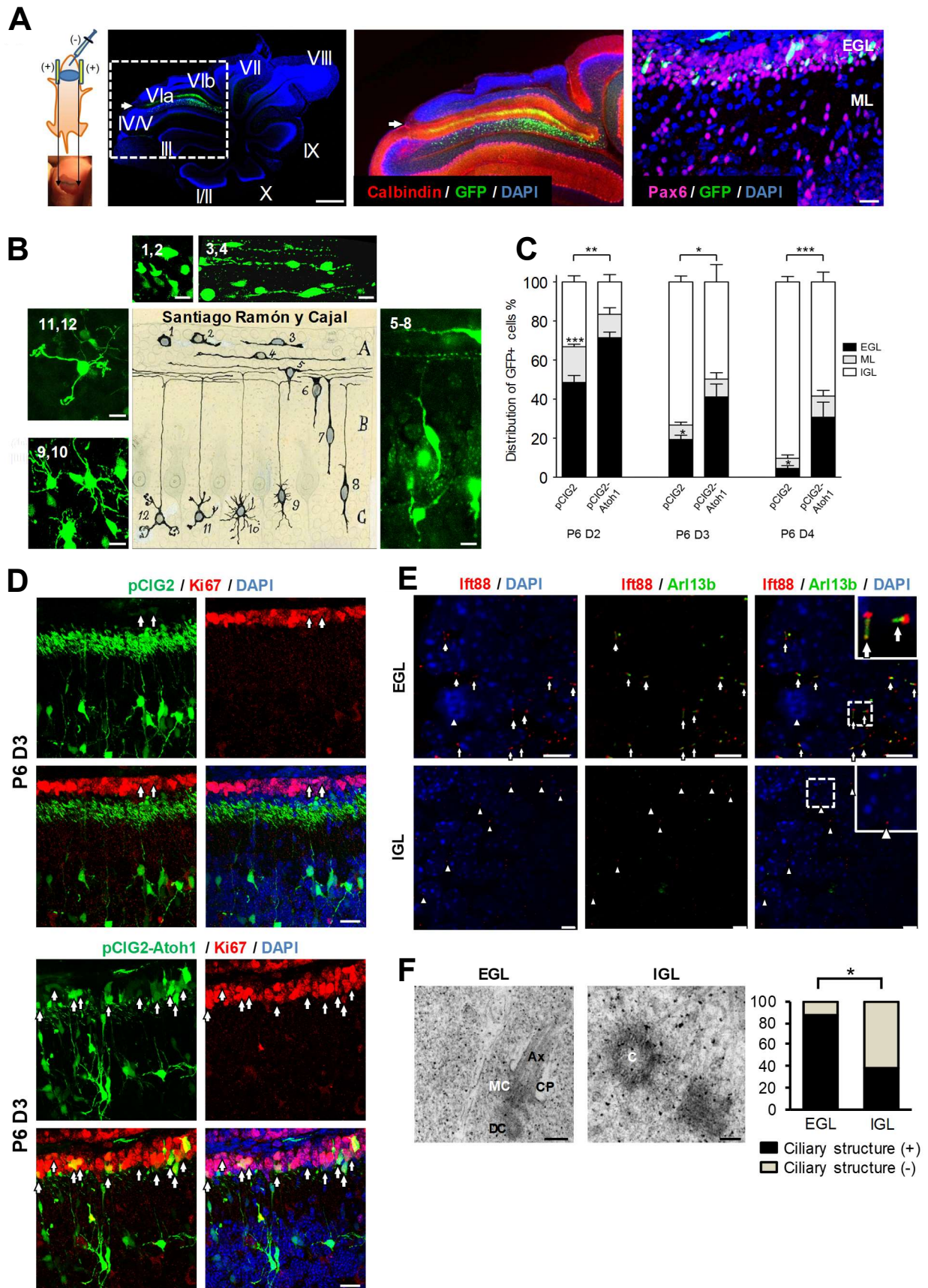


Figure S1. Scheme of *in vivo* cerebellar electroporation and the morphology of primary cilia in the developing cerebellum (Related to Figure 1)

(A) **Left Panel:** Scheme for the procedure of electroporation. The bottom panel shows the top view of a P6 pup head after DNA solution containing fast green was injected and diffused along the primary fissure. **Middle two panels:** A tissue section from P14 cerebellum electroporated with a vector encoding for GFP at P6. GFP signals (green) were specifically detected around the primary fissure between lobules IV/V and VIa (white arrow). Scale bar: 500 μ m. An enlarged view from the box shows layers of the cerebellum by Calbindin (red) and DAPI (blue) staining. GFP: electroporated cells. Scale bar: 500 μ m. **Right panel:** A tissue section from a cerebellum electroporated *in vivo* at P6 with a plasmid encoding for GFP, observed 30 hrs after electroporation. GFP cells (green) appeared specifically in the EGL. The cerebellum was stained with Pax6 (magenta) and DAPI (blue). EGL: external granular layer, ML: molecular layer. Scale bar: 20 μ m.

(B) *In vivo* cerebellar electroporation with GFP labeling at P6 to P9 can reveal the morphological transition from GNPs to granule neurons, the same as the depiction of Santiago Ramón y Cajal, more than 100 years ago. Numbers (from 1 to 12) in each panel represent the corresponding stages in Santiago Ramón y Cajal's manuscript. Scale bar: 10 μ m.

(C) Quantification of the distribution of GFP+ cell from Figure 1A. EGL: external granule layer, ML: molecular layer, IGL: internal granule layer. Student's *t*-test. *: $p < 0.05$, **: $p < 0.01$, ***: $p < 0.001$. Around 3200 electroporated cells were counted. Data are represented as mean \pm SEM.

(D) Separated channels for the Ki67+ cells (Red) from Figure 1B. Arrows indicates the Ki67+ / GFP+ cells. Scale bar: 50 μ m.

(E) Tissue sections of wild-type cerebella collected at P8 and immunostained with Ift88 (red), Arl13b (green), and DAPI (blue) in the EGL (upper three panels) and the IGL (lower three panels). White arrows show Ift88 signals in the EGL while arrowheads indicate a dot-like structure. Scale bar: 5 μ m.

(F) Representative electron micrographs of the centriolar structures in the cerebellum of P6 wild-type mice. Primary cilia were mostly found in the EGL (left panel) with daughter centriole (DC), mother centriole (MC), ciliary axoneme (Ax), and ciliary pocket (CP), whereas the centrioles (C) found in the IGL were not associated with ciliary structures (right panel). Scale bar: 200nm, left panel; 100nm, right panel. Bar graph displays the percentage of ciliary structures found in centrioles. Chi-square test, *: $p < 0.05$; $n = 8$ centrioles from about 100 cerebellar sections in each group.

Supplemental Figure 2

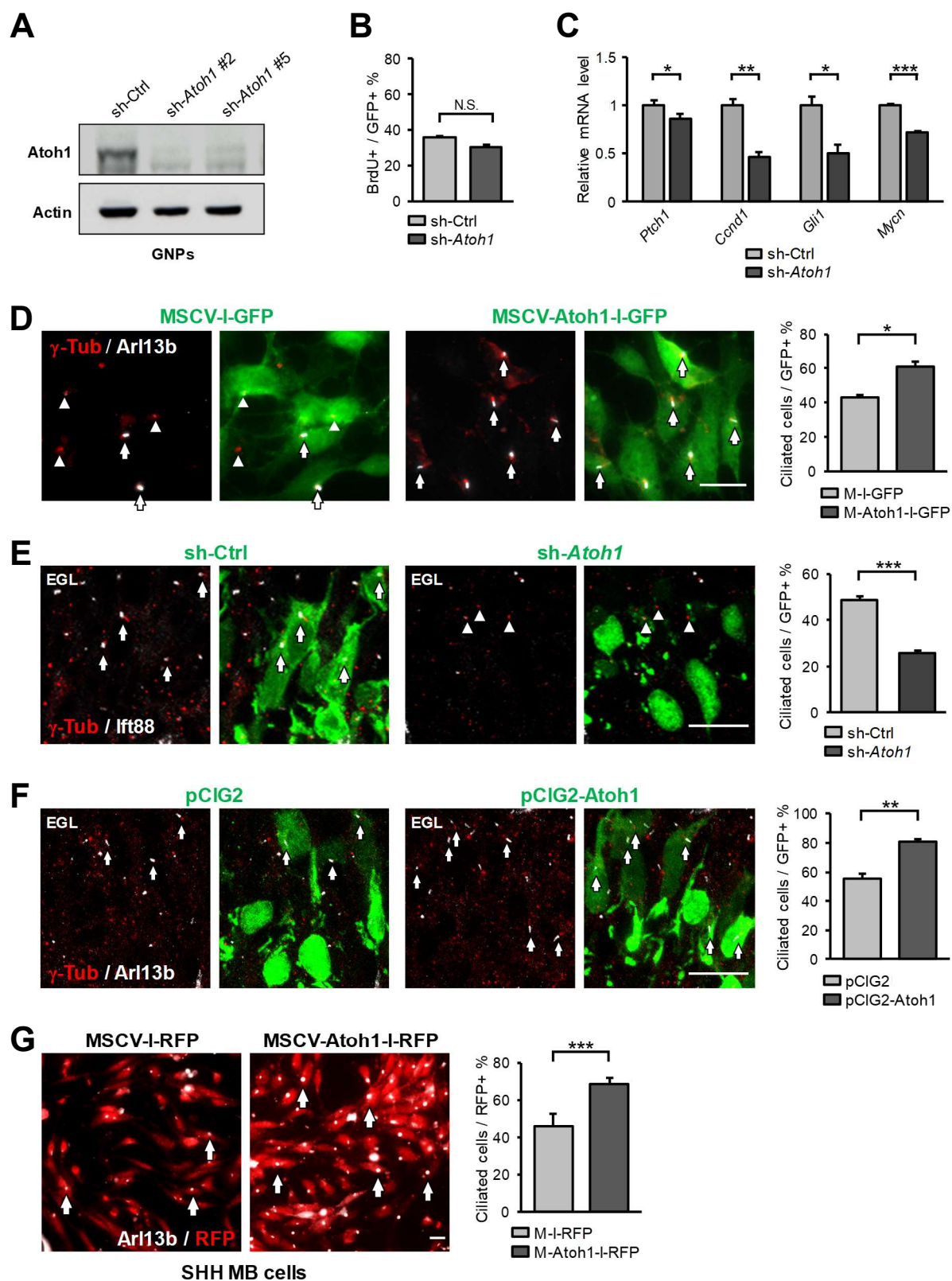


Figure S2. *Atoh1* governs the presence of primary cilia *in vitro* and *in vivo* (Related to Figure 2)

(A) Lysates from GNPs infected with lentiviruses encoding sh-Ctrl or sh-*Atoh1* (#2 and #5) for 2 days *in vitro* were analyzed by immunoblotting. Protein lysates were analyzed by anti-Atoh1 and anti-Actin antibodies.

(B) Bar graph (relative to Figure 2A) indicates the percentage of BrdU+ GNPs (after a 30 min BrdU pulse before fixation) among those infected with sh-Ctrl or sh-*Atoh1* lentiviruses for 3 days *in vitro*. Student's *t* test. Data are represented as mean \pm SEM.

(C) Relative mRNA expression of SHH-targeted genes in P6 GNPs 3 days after infection with sh-Ctrl or sh-*Atoh1* lentiviruses. Student's *t* test. *: $p < 0.05$, **: $p < 0.01$; ***: $p < 0.001$; $n = 4$ for *Ptch1*, $n = 3$ for *Ccnd1*, *Gli1* and *Mycn*. Data are represented as mean \pm SEM.

(D) Immunostaining for primary cilia in cultured P6 GNPs from wild-type mice infected with retroviruses encoding MSCV-I-GFP (left two panels) or MSCV-Atoh1-I-GFP (right two panels) in the presence of SHH for 2 days. Arrows indicate cells with intact cilia while arrowheads indicate centrioles without primary cilia. Green: GFP, white: Arl13b, red: γ -tubulin. Scale bar: 10 μ m. Bar graph shows the percentage of ciliated cells in each group. Student's *t* test. *: $p < 0.05$;

$n = 4$; 1200 cells counted per experiment. Data are represented as mean \pm SEM.

(E) Cerebella were electroporated with control shRNA (sh-Ctrl, left two panels, $n = 3$ animals) or *Atoh1* shRNA (sh-*Atoh1*, right two panels, $n = 4$ animals) for 36 hrs; around 500 electroporated cells were counted. Arrows indicate the primary cilia by Ift88 (white) and γ -tubulin (red) immunostaining in GFP+ cells while arrowheads indicate centrioles without Ift88 signal. Scale bar: 10 μ m. Bar graph displays the percentage of Ift88+ / GFP+ GNPs in each group. Student's *t* test. ***: $p < 0.001$. Data are represented as mean \pm SEM.

(F) Primary cilia in cerebella electroporated with pCIG2 (left two panels) or pCIG2-Atoh1 (right two panels) for 2 days. Arrows indicate presence of the primary cilium in GFP+ cells. Green: GFP, white: Arl13b, red: γ -tubulin. Scale bar: 10 μ m. Bar graph shows the percentage of ciliated GNPs in each group.

Student's *t* test: **: $p < 0.01$; $n = 3$ for pCIG2, $n = 4$ for pCIG2-Atoh1; around 500 cells were counted.

Data are represented as mean \pm SEM.

(G) Primary cilia in murine SHH MB cells obtained from the *Ptch1*^{+/-} MB mouse model. SHH MB cells were infected with retroviruses encoding RFP (MSCV-I-RFP, left panel) or Atoh1 and RFP (MSCV-Atoh1-I-RFP, right panel) in culture for 72 hrs. Red: RFP, white: Arl13b. Scale bar: 10 μ m.

Quantification in the bar graph reveals the percentage of ciliated SHH MB cells in each condition.

Student's *t* test. ***: $p < 0.001$; $n = 3$; 500 cells counted per experiment. Data are represented as mean \pm SEM.

Supplemental Figure 3

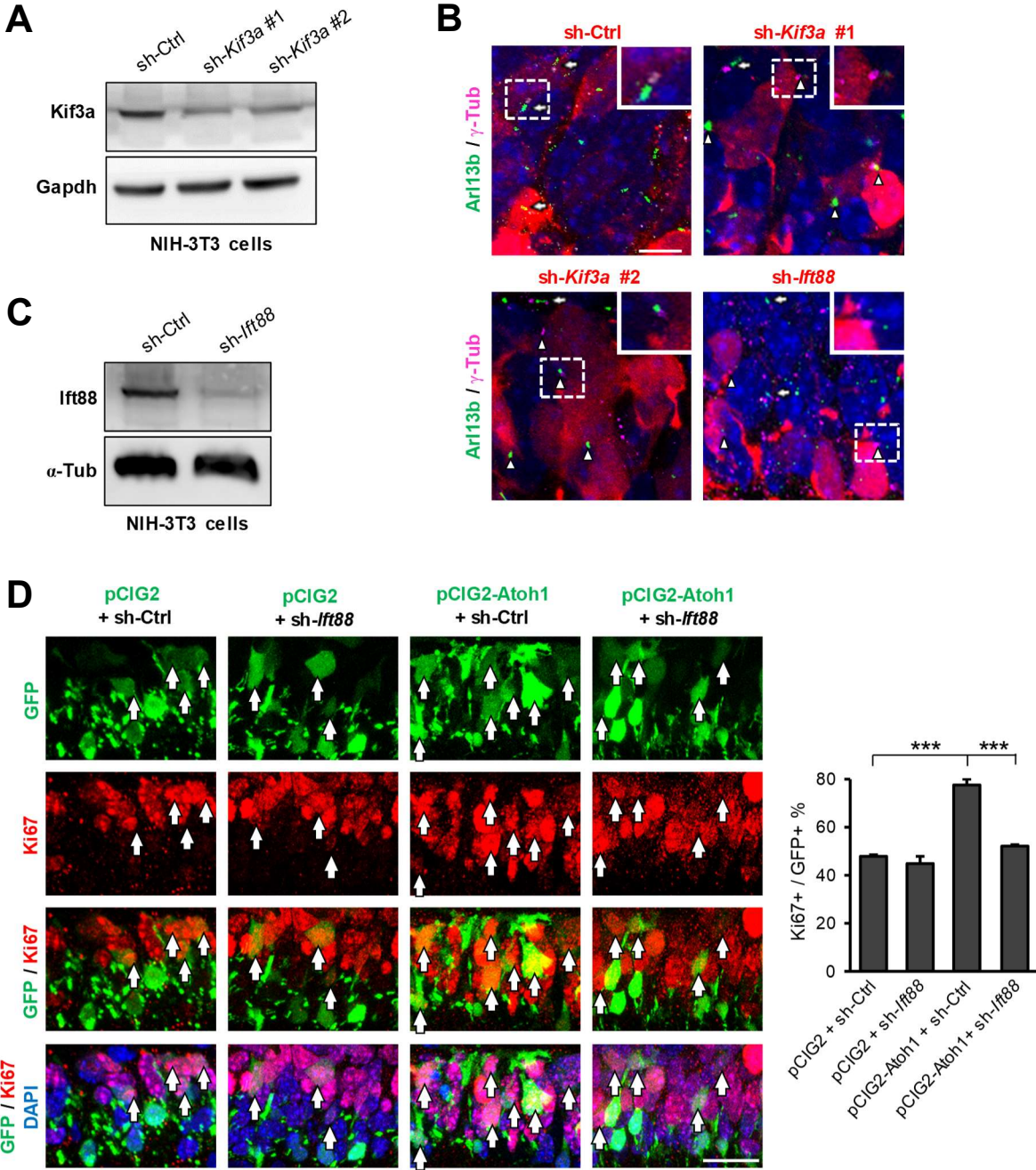


Figure S3. Knockdown of *Kif3a* and *Ifi88* and their effects on cell cycle and primary cilia in GNPs (Related to Figure 3)

(A) Lysates from NIH-3T3 cells transfected with plasmids encoding sh-Ctrl or sh-*Kif3a* (#1 and #2) were analyzed by immunoblotting. Protein lysates were analyzed using anti-*Kif3a* and anti-*Gapdh* antibodies.

(B) Wild-type cerebella were electroporated with a plasmid control (sh-Ctrl) or three independent vectors encoding for shRNA against *Kif3a* (sh-*Kif3a* #1 and #2) and *Ift88* (sh-*Ift88*). Arrowheads show distortion of primary cilia in sh-*Kif3a* and sh-*Ift88* electroporated cells, while the adjacent non-electroporated or sh-Ctrl electroporated cells possess a normal primary cilium (white arrows). Dashed squares are enlarged on the top-right of each image. Red: electroporated cells, green: Arl13b, magenta: γ -tubulin, blue: DAPI. Scale bar: 5 μ m.

(C) Lysates from NIH-3T3 cells infected with lentiviruses encoding sh-Ctrl or sh-*Ift88* were analyzed by immunoblotting. Protein lysates were analyzed by anti-*Ift88* and anti- α -tubulin antibodies.

(D) Proliferation status of GNPs overexpressing *Atoh1* (pCIG2-*Atoh1*) or control (pCIG2) in combination with sh-*Ift88* in cerebella 36 hrs after electroporation at P6. Arrows indicate the proliferating GNPs (Ki67+, red) in electroporated cells (GFP). Blue: DAPI. Scale bar: 10 μ m. Bar graph represents the percentage of Ki67+ cells in each group of GFP+ cells. Two-way ANOVA, $p=0.001$. Post-hoc: Bonferroni test. ***: $p<0.001$; $n = 3$ animals for each group; around 600 electroporated cells were counted. Data are represented as mean \pm SEM.

Supplemental Figure 4

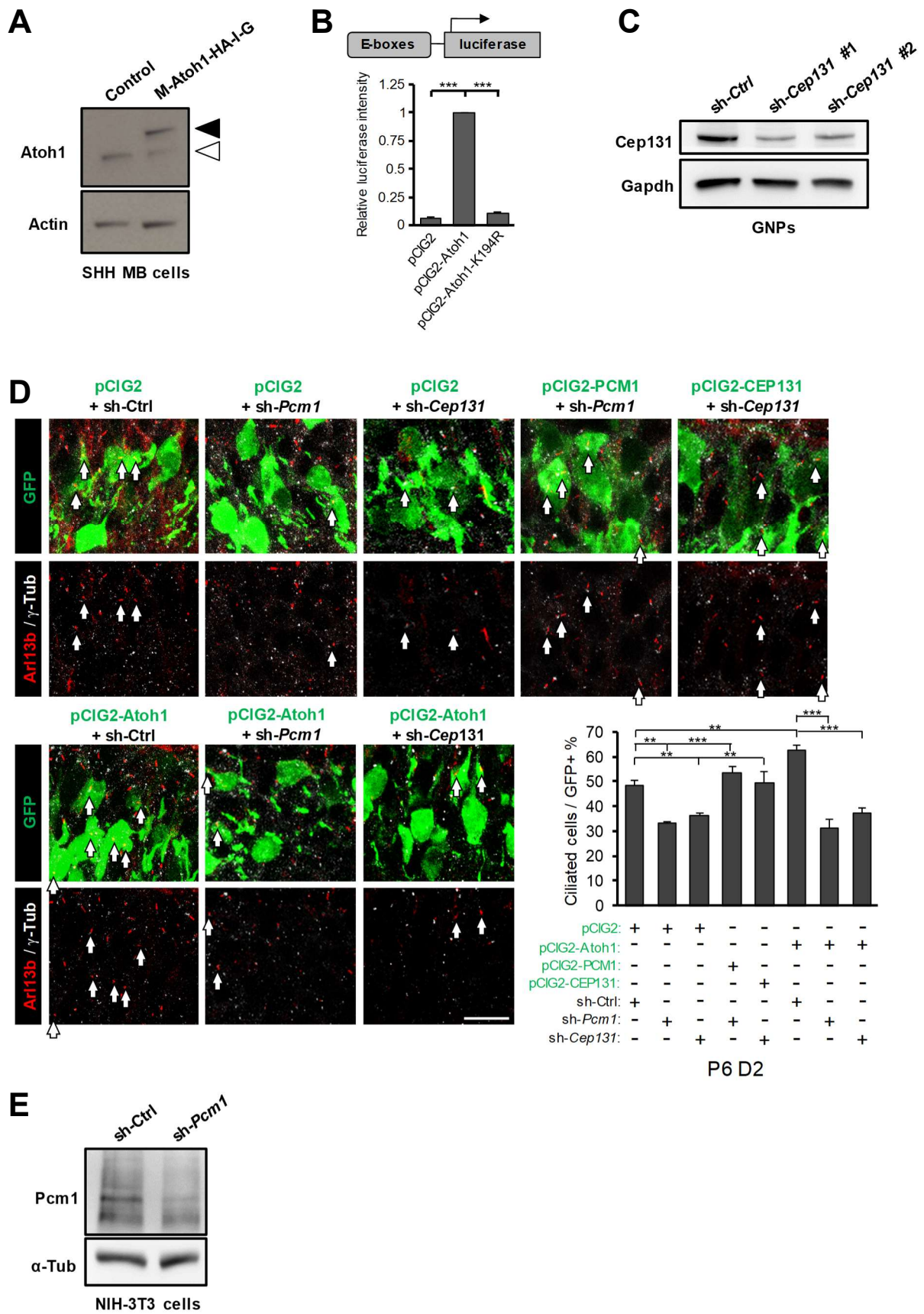


Figure S4. Additional data for the Atoh1 ChIP-qPCR, *Cep131*-reporter assay and effects of Cep131 and Pcm1 knockdown on primary cilia *in vivo* (Related to Figure 5 and 6)

(A) Atoh1 expression in SHH-MB cells used for the ChIP-qPCR in Figure 5B. Mouse SHH MB cells were infected with retroviruses encoding Atoh1-HA and GFP (M-Atoh1-HA-I-G) and subsequently FACS-sorted for GFP expression. Whole cell lysates of sorted SHH MB cells and control non-infected cells were analyzed by immunoblotting with antibodies against Atoh1 and Actin. The white arrowhead points to the endogenous Atoh1 in contrast to the black one, indicating the HA-tagged exogenous Atoh1.

(B) Atoh1 K194R mutant is transcriptionally silent. Bar graph represents the comparison between empty vector, wild-type Atoh1, and Atoh1 K194R mutant for the transcriptional activity in HEK293T cells through a luciferase reporter assay where the luciferase expression is controlled by a multimerized E-box containing upstream sequence. One-way ANOVA, $p < 0.001$. Post-hoc: Bonferroni test. ***: $p < 0.001$; $n = 3$. Data are represented as mean \pm SEM.

(C) Cultured P6 GNPs were infected with lentiviruses encoding sh-Ctrl or sh-*Cep131* (#1 and #2) for 2 days and whole cell lysates were immunoblotted using anti-Cep131 and anti-Gapdh antibodies.

(D) Effects of Pcm1 or Cep131 knockdown on the presence of primary cilia in GNPs electroporated with pCIG2 or pCIG2-Atoh1 *in vivo*. P6 cerebella were electroporated with indicated plasmids for 2 days (P6 D2). Cep131 silencing was achieved by sh-*Cep131* #1 in (C). Arrows indicate primary cilia in GFP+ cells. Green: electroporated cells, Red: Arl13b, White: γ -tubulin. Scale bar: 10 μ m. Bar graph represents the percentage of cells with primary cilia in each group of GFP+ cells. Two-way ANOVA, $p < 0.001$. Post-hoc: Tukey HSD test. **: $p < 0.01$, ***: $p < 0.001$; animal number: $n = 3$ for each groups; around 300 electroporated cells were counted in each group. Data are represented as mean \pm SEM.

(E) Lysates from NIH-3T3 cells transfected with plasmids encoding sh-Ctrl or sh-*Pcm1* were analyzed by immunoblotting. To achieve stable cell lines, cells were selected with puromycin (2 μ g/ml) after transfection. Protein lysates were immunoblotted with anti-Pcm1 and anti- α -tubulin antibodies.

Supplemental Figure 5

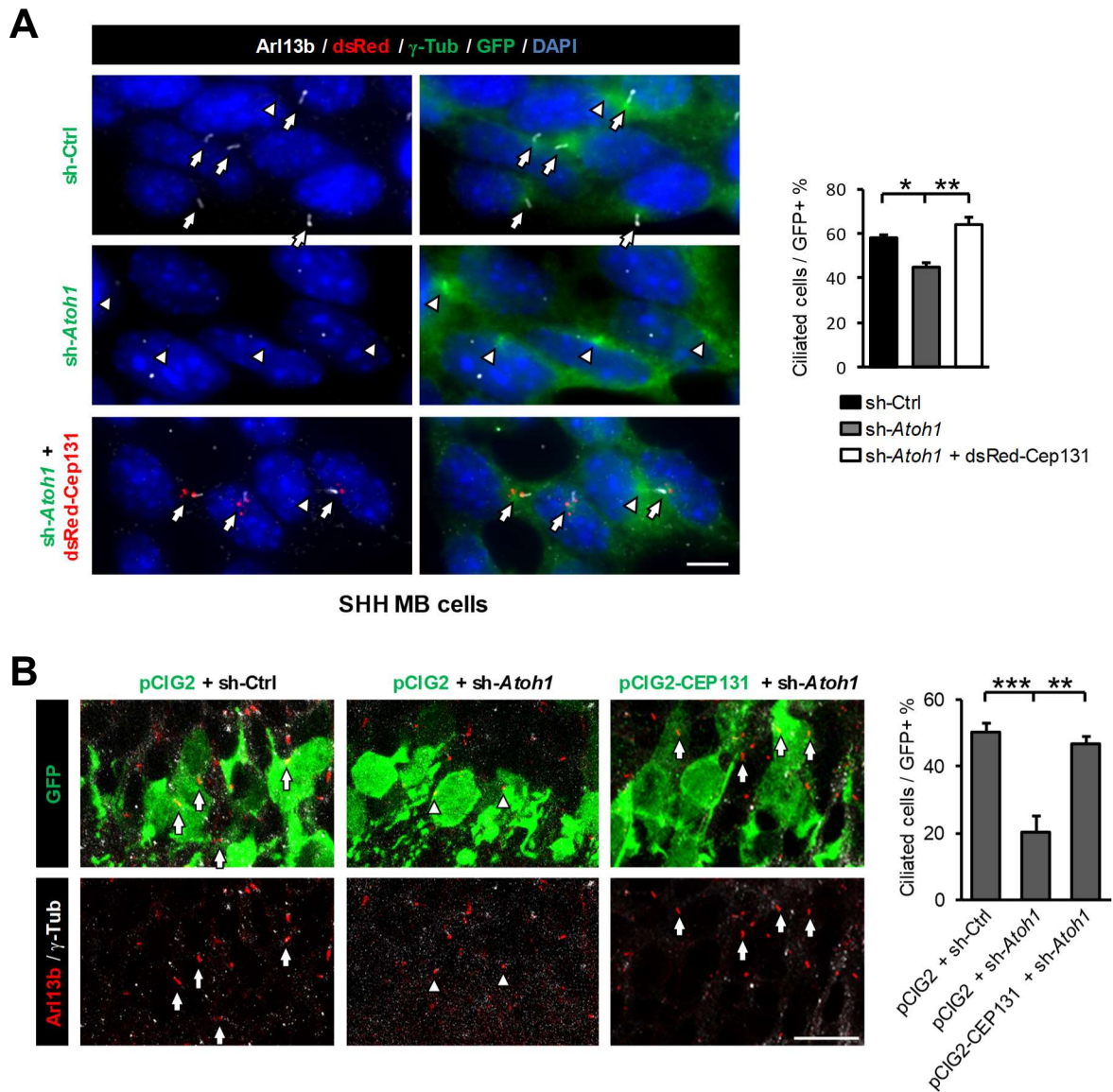


Figure S5. Cep131 acts downstream of Atoh1 for ciliogenesis in SHH MB cells and in GNPs *in vivo*
(Related to Figure 6)

(A) Rescue effect of Cep131 on primary cilia upon *Atoh1* knockdown in SHH MB cells. Primary cultures of SHH MB cells derived from *Ptch1*^{+/-} mice were infected with indicated combinations of lentiviruses (sh-Ctrl, sh-*Atoh1* and dsRed-Cep131) and immunostained 3 days later. Arrows indicate fully formed primary cilia in contrast to absent primary cilia (arrowheads). Green: GFP and γ -tubulin, Red: dsRed-Cep131, White: Arl13b, Blue: DAPI. Scale bar: 5 μ m. Bar graph represents the percentage

of ciliated SHH MB cells among those GFP+ or GFP+/dsRed-Cep131+. One-way ANOVA, $p < 0.01$. Post-hoc: Tukey HSD test. *: $p < 0.05$, **: $p < 0.01$; $n = 3$; around 600 cells counted per condition. Data are represented as mean \pm SEM.

(B) Rescue effect of Cep131 on primary cilia presence upon *Atoh1* knockdown *in vivo*. P6 cerebella were electroporated with indicated plasmids for 2 days. Arrows indicate the presence of a primary cilium in GFP+ cells, while arrowheads indicate defective cilia. Green: electroporated cells, Red: Arl13b, White: γ -tubulin. Scale bar: 10 μ m. Bar graph represents the percentage of cells with primary cilia in each group of GFP+ cells. One-way ANOVA, $p < 0.001$. Post-hoc: Bonferroni test. **: $p < 0.01$, ***: $p < 0.001$; animal number: $n = 4$ for pCIG2 + sh-Ctrl and pCIG2-CEP131 + sh-*Atoh1*, $n = 3$ for pCIG2 + sh-*Atoh1*; around 800 electroporated cells were counted. Data are represented as mean \pm SEM.

Supplemental Figure 6

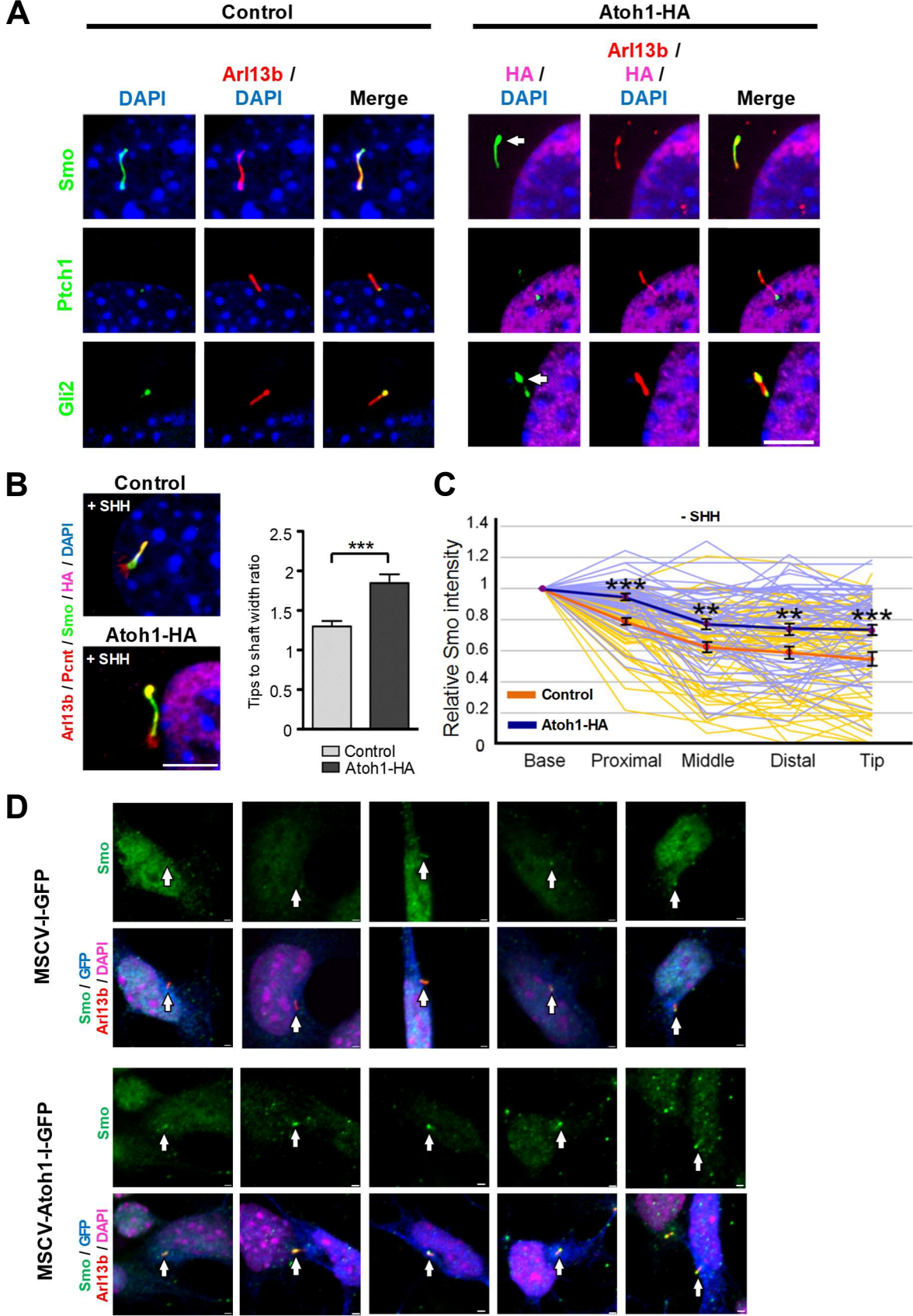


Figure S6. Distribution of SHH signaling components in NIH-3T3 cells and GNP (Related to Figure 7)

(A) NIH-3T3 cells were co-transfected with either control or Atoh1-HA constructs along with plasmids encoding Smo (green), Ptch1 (green), or Gli2 (green) and cultured in the presence of SHH, following with immunostaining by anti-Arl13b (red), anti-HA (magenta), and DAPI. A bulge (white arrow) can be detected at the ciliary tip upon Atoh1 expression in either Smo-labeled or Gli2-labeled primary cilium. Scale bar: 5 μ m.

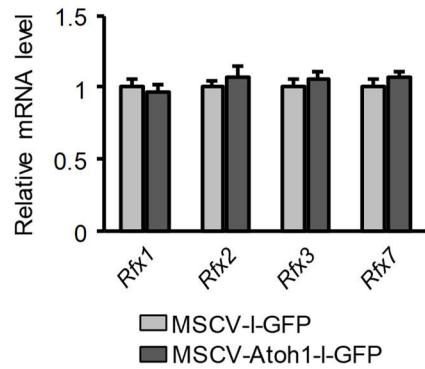
(B) NIH-3T3 cells, cultured in presence of SHH, were co-transfected with either control or Atoh1-HA constructs along with plasmids encoding Smo (green) and finally immunostained for primary cilia (Arl13b, red), centrioles (Pcnt, red), and Atoh1 (HA, magenta). Blue: DAPI. Scale bar: 1 μ m. Bar graph shows relative width of the primary cilium tip to its shaft. Student's *t* test. ***: $p < 0.001$; $n = 43$ for Atoh1, $n = 40$ for control cells. Data are represented as mean \pm SEM.

(C) Graph represents the relative Smo intensity along the primary cilium shaft normalized to its base for individual NIH-3T3 cells. Cells were treated as in (B) in the absence of SHH (Control: yellow lines, $n = 59$; Atoh1-HA: light blue lines, $n = 60$). The average of Smo intensity is shown in thick lines (Control: Orange; Atoh1-HA: Blue). Student's *t* test. **: $p < 0.01$, ***: $p < 0.001$. Data are represented as mean \pm SEM.

(D) Extended images related to Figure 7C show endogenous Smo (green) within the primary cilium in control GNP and Atoh1-overexpressing GNP upon SHH activation. Scale bar: 1 μ m.

Supplemental Figure 7

A



B

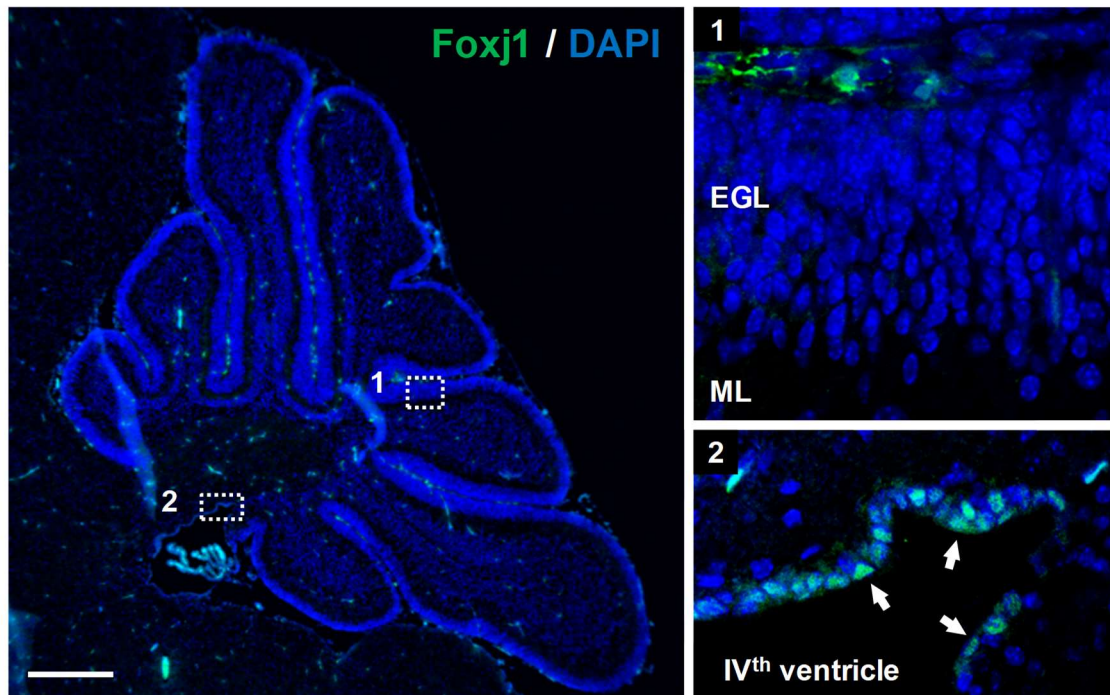


Figure S7. Investigation of potential transcriptional targets of Atoh1 in the cerebellum implicated in ciliogenesis (Related to Figure 4)

(A) The expression level of the ciliogenesis transcription factors *Rfx1*, *Rfx2*, *Rfx3* and *Rfx7* in cultured GNPs infected with either MSCV-I-GFP or MSCV-Atoh1-I-GFP for two days was assessed by RT-qPCR. Student's *t* test, $n=3$. Data are represented as mean \pm SEM.

(B) Cerebellar section of a P6 wild-type mouse immunostained with anti-Foxj1 (green) antibodies. Cropped regions (dashed squares) are enlarged at the right, zooming on the cerebellar EGL and ML (1) and on the ependymal lining of the IVth ventricle (2) where arrows indicate presence of Foxj1+ cells, as previously described (Jacquet et al., 2009). Blue: DAPI. Scale bar: 500 μ m.

Supplemental Table 1

Gene	RNA-seq <i>Atoh1^{null}</i> vs wild type		Atoh1 ChIP-seq peaks	
	<i>p</i> value	Fold change	Genomic coordinates (NCBI37/mm9)	Locus
<i>Sipa1l2</i>	3.37E-19	0.60	chr8: 127943282-127943608	intron (20/20)
<i>Baiap2</i>	3.53E-09	0.56	chr11: 119801434-119801698	-2.7 kb from TSS
			chr11: 119813760-119813937	intron (1/13)
			chr11: 119843629-119843893	intron (6/13)
			chr11: 119849941-119850238	intron (6/13)
			chr11: 119852522-119852941	intron (6/13)
<i>Ahi1</i>	1.75E-07	1.59	chr10: 20710249-20710404	intron (15/23)
<i>Ccdc85c</i>	9.10E-06	0.55	chr12: 109446944-109447226	intron (3/5)
			chr12: 109458826-109459033	intron (2/5)
			chr12: 109459597-109459962	intron (2/5)
			chr12: 109465294-109465476	intron (1/5)
			chr12: 109470220-109470600	intron (1/5)
			chr12: 109479079-109480146	intron (1/5)
			chr12: 109480528-109480875	intron (1/5)
			chr12: 109497952-109498283	intron (1/5)
			chr12: 109516557-109516738	-3.3 kb from TSS
<i>Cep131</i>	4.23E-05	0.65	chr11: 119925694-119925965	exon (26/26)
<i>Mtap7d1</i>	6.32E-04	0.66	chr4: 125936417-125936619	-3.0 kb from TSS
<i>Dvl3</i>	4.00E-03	0.68	chr6: 120529805-120530547	intron (13/14)

Table S1. List of genes in Figures 4C and 4D with information relative to the RNA-seq and the Atoh1 ChIP-seq, published by Klisch et al. (2011) (Related to Figure 4)

Supplemental Table 2

Materials	Target sequence	Vector	Reference
sh-<i>Atoh1</i> #2	CCGACAAGAAGCTGTCCAAA	pLVTHM (Addgene #12247)	Wiznerowicz and Trono, 2003
sh-<i>Atoh1</i> #5	CATCTACATCAACGCCTTGT		
sh-<i>Cep131</i> #1	GCTGTGGACTTGAGTCTGATT	pLKO	
sh-<i>Cep131</i> #2	CGCTAACAACAGGAGCAACAA	pLKO	
sh-<i>Kif3a</i> #1	ATATTGGGCCAGCAGATTATA	pRNAT-U6.1/Neo	
sh-<i>Kif3a</i> #2	ATAGGAGAATGGCAGCT	pRNAT-U6.1/Neo	Tsai <i>et al.</i> , 2010
sh-<i>Ift88</i>	GCCCTCAGATAGAAAGACCAA	pLKO	
sh-<i>Pcm1</i>	GAGGGTAACTAACGCTAT TTC	pLKO	

Tabel S2. List of sh-RNAs applied for gene interference studies (Related to STAR Methods)

Supplemental Table 3

Gene	Nucleotide Sequence		Reference
<i>Atoh1</i>	Forward	CCCTAACAGCGATGATGGCA	
	Reverse	TCTCCGTCACCTTCTGTGGGA	
<i>Cep131 #1</i>	Forward	AGATCCGAAAAGGCCGAGAC	
	Reverse	CACGCTTCACACGGCTCTC	
<i>Cep131 #2</i>	Forward	ACTCCTGAAGGCAGTCCAGA	Hall <i>et al.</i> , 2013
	Reverse	CGTCCATGACTGGTTGACCT	
<i>Cep290</i>	Forward	GAACTCCAGCTTCTTAGATTAGCC	
	Reverse	TCAGCTCTGGTTTGGTCCTTG	
<i>Ofd1</i>	Forward	CCAGCAGAGACAGGAAGAATCAA	
	Reverse	CCTGGAGAACTTTCATCCTTGTC	
<i>Pcm1 #1</i>	Forward	TGAAGTCTGCTCAGGAAACG	Kubo <i>et al.</i> , 2008
	Reverse	GCGGCAAATCCTCAACTTC	
<i>Pcm1 #2</i>	Forward	AGTTGAGGATTTGCCGCTCA	
	Reverse	GGCTCCCAGTGTTCAGGTT	
<i>Bbs4</i>	Forward	GCCATCAACTTCAGCCAAA	
	Reverse	CACTTATCCAGGCGAACAGC	
<i>For20</i>	Forward	CTCCAGATGGAGCCCAGAAT	
	Reverse	GTCATCGTCAGGTCTTCTGC	
<i>Talpid3</i>	Forward	TGGAACGTTATGTGGCTCCT	
	Reverse	GGACGCAGGAGGACTTTCTA	
<i>Mtap7d1</i>	Forward	GCTGAAAGGGACAAGCGAAT	
	Reverse	CGGCTTCCTCTTTCTGCTTC	

Gene	Nucleotide Sequence		Reference
<i>Sipa1L2</i>	Forward	GCTGCTTCCATACATGCCAA	
	Reverse	CTCCAACACTGTAGCACACG	
<i>Baiap2</i>	Forward	AGCCAAGGGAGTAAGAACCC	
	Reverse	TTGTAGCCGTCAGACACGTA	
<i>Ahi1</i>	Forward	GGGACACGTACGTCAAAGTG	
	Reverse	TCCGCAGGTCCATAATCCTC	
<i>Ccdc85c</i>	Forward	CGCCATGAAGGTTCTGGAAG	
	Reverse	GACCACGTTGCACATCTCTC	
<i>Dvl3</i>	Forward	ACGCCTGATGAGAAGACACA	
	Reverse	CCACAATGGAGATGCCCAAG	
<i>Rfx1</i>	Forward	CCAGTTCACGTTGCTCAAGA	
	Reverse	CCGGGTACTGGTAGGTGCTA	
<i>Rfx2</i>	Forward	AGGTCATCCAGACCAAGGTG	
	Reverse	TGAGGTCACTCAGCATCTGG	
<i>Rfx3</i>	Forward	AGATTCTCATCCCCGACGTC	
	Reverse	CCAGGTGATTGAGCGATGTG	
<i>Rfx7</i>	Forward	GATGGGTTGGAAGGAGTTGA	
	Reverse	GCCATTGACTTGGTGCCTAT	
<i>Ptch1</i>	Forward	CTTCGCTCTGGAGCAGAT	
	Reverse	GAGGAGACCCACAACCAA	
<i>Ccnd1</i>	Forward	CCGGCCCGAGGAGCT	Forget <i>et al.</i> , 2014
	Reverse	ATGGCGGCCAGGTTCC	
<i>Gli1</i>	Forward	GCTTGGATGAAGGACCTTGTG	
	Reverse	GCTGATCCAGCCTAAGGTTCTC	

Gene	Nucleotide Sequence		Reference
<i>Mycn</i>	Forward	GTGTCTGTTCCAGCTACTGC	
	Reverse	CATCTTCCTCCTGCTCATC	
<i>Tbp</i>	Forward	ACATCTCAGCAACCCACACA	
	Reverse	GGGGTCATAGGAGTCATTGG	
<i>M18S</i>	Forward	TTCGAACGTCTGCCCTATCAA	
	Reverse	ATGGTAGGCACGGCGACTA	

Table S3. List of primers for RT-qPCR (Related to STAR Methods)

Supplemental Table 4

Locus	Nucleotide Sequence		Amplified region in the genome (Assembly NCBI37/mm9)
<i>Cep131</i> 3' region	Forward	CACGCCCAACACAGTAGAGA	chr11: 119925703-119925852
	Reverse	CAGCAGCTGGTGTGTGAGAG	
<i>Atoh1</i> enhancer	Forward	GAGCTTTCTGCGGTACCATC	chr6: 64677582-64678055
	Reverse	CAGTTTGGGCTTTCTTCGTC	
<i>Gli2</i> enhancer	Forward	GCTGCCTCAGAGGAGAAATG	chr1: 120813307-120813453
	Reverse	ATGAGGCAATGCCAGTCTCT	
<i>Cep131</i> intron #21	Forward	CAGCTCCGAGAGCTCTGTTT	chr11: 119926980-119927814
	Reverse	CCTGCCTTTAGCTCCACAGT	
<i>Cep131</i> intron #7	Forward	CCCTGACTAGAAGGGCTGTG	chr11: 119935343-119936741
	Reverse	CTTGGTGCTTCTCTGGATGG	
<i>Pde6g</i> promoter	Forward	ACTGGTTGTAGGGCTGTGCT	chr11: 120314800-120315223
	Reverse	TGCTGACATTTCTCAGTGG	
<i>Rab37</i> promoter	Forward	TTACCAACCTGCCTTTCCTG	chr11: 114951860-114952810
	Reverse	AGTGGTGGCTGAGGTTTTTG	

Table S4. List of primers for ChIP-qPCR (Related to STAR Methods)

Discussion

D.1 Highlights of our findings and take-home messages

Our results support a model in which *Atoh1* functions as a key permissive factor for GNP's post-natal proliferation. In an environment constantly enriched of SHH like the EGL, the expression of *Atoh1* works as a variable that dictates whether GNP's should respond to SHH and divide or, conversely, stop to respond to it and terminally differentiate. This role of *Atoh1* is mainly achieved through the regulation of primary cilia, the GNP's antennae required to transduce the SHH signaling cascade. Both formation of primary cilia and signaling functions are positively orchestrated by *Atoh1* (**Figure 2** and **Figure 7**). Through this way, *Atoh1* maintains post-natal GNP's capable of assembling primary cilia, hence keeping them into a SHH-driven proliferation competent state over time. *Atoh1* downregulation caused by developmentally programmed intracellular or extracellular cues, compromises both formation and functions of primary cilia, making GNP's unable to transduce proliferative signals anymore. Under these conditions, GNP's are left with no option than exiting the cell cycle to terminally differentiate under the influence of local determinants.

With our experiments we show that enforced expression of *Atoh1* *in vivo* counteracts the natural occurring *Atoh1* downregulation, and it is sufficient to maintain GNP's in proliferation by actively sustaining ciliogenesis in these cells (**Figure 1**, **Figure 2** and **Figure 3**).

Mechanistically, we also demonstrate that *Atoh1* controls ciliogenesis by directly regulating the expression of *Cep131* through binding of a regulatory element located in the 3' region of *Cep131* locus (**Figure 5**). *Cep131* encodes for a key component of CS, large pericentrosomal protein complexes involved in ciliogenesis. By regulating the abundance of *Cep131*, *Atoh1* shapes the CS landscape of the cell (**Figure 4** and **Figure 6**). *Cep131* in GNP's is indeed essential for CS integrity, as its depletion either via direct *Cep131* silencing or via *Atoh1* downregulation perturbs the organization of these tiny organelles around the centrosome (**Figure 4** and **Figure 6**). Equipped with such a defective pool of CS, GNP's become unable to sustain the ciliogenesis program.

Importantly, re-establishing the proper CS organization by ectopically expressing *Cep131* in *Atoh1*-depleted cells is sufficient to restore ciliogenesis, indicating that *Atoh1* ultimately controls primary cilia formation in GNP's by regulating *Cep131* expression (**Figure 6**).

Interestingly, the *Atoh1*-*Cep131*-ciliogenesis pathway that we here identify is also active in the context of *Ptch1* loss-of-function-driven mouse SHH-MB. Such data indicate that *Atoh1* strikingly conserves its normal ciliogenesis functions also in transformed GNP's, further confirming the role of *Atoh1* as a lineage dependency master regulator in SHH-MB (**Figure 2** and **Figure S5**).

The following paragraphs are meant to further extend the topics covered in the DISCUSSION section of the paper, highlighting some aspects that could not be presented due to editorial space constraints.

D.2 Atoh1 may control cell cycle and timing of neurogenesis, by regulating ciliogenesis

During CNS development, NPCs undergo phases of expansion to generate the adequate number of neurons, before to terminally differentiate. Balancing proliferation and differentiation therefore becomes essential for the proper development of a neural tissue, as both reduced and excessive neurogenesis may result into detrimental outcomes.

In the last twenty years, cell cycle regulation, in particular its duration (or length), has emerged as an important determinant for governing this balance (Hardwick et al., 2015). NPCs are known to slow down their cell cycle when they approach the time of terminal differentiation, and this is predominantly achieved by lengthening the G1 phase, (Calegari et al., 2005; Hardwick et al., 2015). Genetic or pharmacological manipulations altering G1 progression in NPCs enhance differentiation rate when the G1 phase is lengthened and increase proliferation when it is shortened (Calegari and Huttner, 2003; Hardwick et al., 2015; Lange et al., 2009). This led to the hypothesis that the G1 phase works as a fundamental crossroad for integrating proliferative *versus* differentiation stimuli: the more it takes for a cell to reach the cell cycle restriction point and be committed for cycling, the more it is likely that differentiation determinants accumulate enough to drive cell cycle exit and neurogenesis (Calegari and Huttner, 2003).

In proliferative ciliated cells, cell cycle progression is tightly linked with ciliogenesis. Primary cilia must be continuously assembled and disassembled because the centrosome needs to be dismissed from its axoneme-nucleating activity to organize the mitotic spindle during mitosis. GNPs are no exception, and show a similar behavior during cell cycle progression, as marked by the absence of primary cilia in mitotic cells and in a fraction of S/G2 cells (data not shown). We are however unaware about the precise kinetics of ciliary formation and ciliary disassembly in cycling GNPs in relations with the phases of the cell cycle. Such characterization would require targeted experiments mostly based on cell cultures synchronization, an approach that is unfortunately incompatible with the labile GNPs primary cultures. Nevertheless, it is very likely that such kinetics resembles those described for many other cell types, that is assembly of the

cilium in early G1 phase, followed by disassembly at the G1/S transition and/or before mitotic entry (Pugacheva et al., 2007; Wang et al., 2013).

Under this assumption, we propose a model to explain how Atoh1 could orchestrate GNs neurogenesis, by regulating ciliogenesis and G1 phase length. Upon entry in the G0/G1 phase GNPs that express Atoh1 also stably express Cep131, thereby are equipped with all the components required to reorganize CS around the centrosome (mind that CS are dispersed during mitosis). The so-well assembled CS may sustain the growth of the primary cilium by regulating various aspects of ciliogenesis, including vesicle trafficking via proper Rab8 centrosomal recruitment, BBSome assembly, and IFT formation (**Figure XIX**). Once assembled and fully functional, primary cilia enable GNPs to transduce SHH, which is present in the EGL. The abundant expression of the SHH targets Mycn and D-type cyclins rapidly drive GNPs toward the cell cycle restriction point, after which GNPs become committed to divide. Such process is repeated several times (a GNP can divide up to 2000 times (Espinosa and Luo, 2008)) and lasts as long as Atoh1 expression is maintained elevated enough.

Indeed, since early in post-natal days a number of intracellular and extracellular cues will begin to progressively deplete Atoh1 from GNPs until its complete disappearance. At the onset of such mechanisms, Cep131 expression will consequently decrease, leaving GNPs in the early G1 phase to perhaps assemble less functional copies of CS. Reduced inputs from CS, conceivably leads to delayed and slower assembly of primary cilia, and possibly a reduced functionality reflected by lower SHH signaling levels (as discussed in the next paragraph and shown in **Figure 7** and **Figure S2**). As a result, the accumulation of Mycn and D-type cyclins over the threshold required to transit the cell cycle restriction point will be much delayed in time. Overall, according to our model, (i) the slower or even failed ciliary assembly in early G1 and (ii) the delayed accumulation of pro-proliferative factors both converge at lengthening the G1 phase, therefore massively exposing GNPs to differentiation cues that will inevitably cause cell cycle exit.

On the same line, we speculate that when Atoh1 is overexpressed, either experimentally or during SHH-MB formation, the G1 phase of GNPs will be markedly shortened, therefore leading to delayed differentiation (**Figure 1**).

Although technically challenging, it would be interesting to test this model by monitoring at least the duration of the G1 phase in GNPs upon Atoh1 manipulation. Live cell imaging tracking of cell cycle progression or EdU/BrdU dual labeling could be suitable systems to gain insights into cell cycle length and progression in GNPs (Harris et al., 2018; Sakaue-Sawano et al., 2008).

Therefore, we postulate that by controlling ciliogenesis Atoh1 could balance proliferation and differentiation in post-natal GNP by ultimately governing the length of G1 phase, which has been proposed to be an important determinant for neurogenesis in the developing CNS.

D.3 Possible consequences of loss or gain of Cep131 on centrosome duplication

One important event occurring during the cell cycle is the duplication of the centrosome, which is functional during mitosis for segregating the sister chromatids and also for cytokinesis. Centrosome duplication begins approximately at the onset of S phase and terminates in G2 and mutations or deregulated expression of centrosomal proteins implicated in this process may result in formation of extra centrosomes (centrosome amplification) (Firat-Karalar and Stearns, 2014). When aberrantly equipped with additional centrosomes, mitotic cells normally fail at organizing proper mitotic spindles and consequently undergo chromosome segregation errors that eventually result in genomic instability (Krämer et al., 2002).

Interestingly, Cep131 on CS has been implicated in centrosome replication by permitting the recruitment of Cep152 at the duplicating centrioles (Kodani et al., 2015). In addition, Cep131 itself also resides at the centrosome distal tip, where its abundance is finely modulated by specific E3-ubiquitin ligases and deubiquitinating enzymes (Han et al., 2019; Staples et al., 2012). Importantly adequate concentrations of centrosomal Cep131 seem critical for proper centrosome biogenesis, as both silencing and overexpression of Cep131 may result into centrosome amplification and genomic instability (Han et al., 2019; Kim et al., 2019a; Staples et al., 2012).

In our work we did not explore the effects of Cep131 depletion on GNP centrosome duplication. However, being the downregulation of Cep131 in GNP a natural, developmentally regulated process, it is very unlikely that such reduction might lead to aberrant centrosome biogenesis and genomic aberrations. Indeed, it is possible that during the last cell cycles of a GNP, Cep131 levels are reduced due to progressive downregulation of Atoh1, but remain high enough to direct correct centrosome duplication. Conceivably, the minimal amount of Cep131 sufficient for sustaining ciliogenesis may be anyway higher compared to the amount required for centrosome duplication. Therefore, in a system like GNP where Cep131 expression is predicted to progressively decrease, failure in ciliogenesis and consequent cell cycle exit might happen much before than any possible centrosome duplication defect.

Conversely, such situation could be different when Atoh1 is overexpressed, as in SHH-MB. The enhanced expression of Cep131 over the physiological levels, may this time promote

centrosome amplification, contributing to the genomic instability that typically characterizes and drives tumorigenesis (Levine et al., 2017). Elevated expression of Cep131 and association with tumor growth or bad prognosis was reported in breast, liver and colon cancer (Han et al., 2019; Kim et al., 2019a; Liu et al., 2017). Moreover, targeting Cep131 has been proposed as a potential cancer treatment in combination with other chemotherapies (Kim et al., 2019b). Interestingly, although also the knockdown of *Cep131* in immortalized cell lines caused genomic instability, *Cep131* deletion or downregulation is very rarely found in cancer, indicating that it may not act as an oncogenic driving event (Denu et al., 2019; Staples et al., 2012).

D.4 Role of CS in neurogenesis and consequences of their absence in post mitotic GNs

Our results provide further evidence of the key role of CS in neurogenesis. Indeed, previous reports indicated that repression of *Pcm1* and loss of CS integrity in embryonic basal cortical NPCs leads to enhanced neurogenesis at the expense of proliferation and self-renewal (Ge et al., 2010; Zhang et al., 2016). This was attributed to a general disruption of centrosome functions, which led to defective interkinetic nuclear migration, an essential requirement for maintenance of the basal cortical progenitor pool (Ge et al., 2010).

In the case of GNPs in the EGL, interkinetic nuclear migration does not occur; however, *Pcm1* and CS are utilized in GNPs for producing primary cilia, which are required for maintaining them into proliferation. Thus, although regulating different aspects of centrosome biology, CS seem to conserve a similar role in inhibiting neurogenesis also in cerebellar neurons.

What appears surprising is that CS, immunostained with both *Pcm1* and *Cep131* in the developing P6 cerebellum, do not just disappear upon cell cycle exit, but remain undetectable also in those GNs of the iEGL approaching to undergo their final radial migration through the immature ML (**Figure 4**).

During neuron migration, the nucleus represents the largest cargo to displace and it is caged by arrays of microtubules emanating from the centrosome. Normally, the centrosome precedes the nucleus in the leading process, where it provides a cue for the forward pulling force on the nucleus transmitted through the microtubules (Solecki et al., 2004; Tsai and Gleeson, 2005). Therefore, the microtubule anchoring properties of the centrosome seem essential during neuron migration. If CS are generally required for ensuring the centrosome with these functions (paragraph **I.5.3.1**), how can GNs migrate without integral CS?

One potential answer could be simply that CS in migrating GNs are not required for the centrosome to organize the microtubule network. Microtubules anchoring factors as Ninein or SSX2IP, which in some cell lines were shown to depend on CS for their centrosomal localization, could reach the centrosome via alternative pathways in GNs.

Another explanation comes from a study showing that the microtubule cage that surrounds the nucleus of migrating GNs surprisingly appears disengaged from the centrosome. According to these data, the centrosome does not seem to relay to the nucleus the pulling force coming from the leading process, as instead it happens in migrating cortical neurons (Umeshima et al., 2007). Whatever the mechanism, it appears clear that CS are required in GNs for their SHH-dependent post-natal expansion, but not at later stages of development.

D.5 Contribution of Atoh1 to SHH signaling

Most of the pathways and the components required for building up primary cilia, including vesicular trafficking (e.g. Rabin8-Rab8 GTPases) and IFT proteins (e.g. BBSome, kinesin-2, IFT proteins), are then also utilized to fulfill mature primary cilia functions, as signaling. In this context, CS play a pivotal role, by shuttling, sequestering and storing key mediators of both of these two facets of primary cilia biology. Motivated by this knowledge, we sought to explore if Atoh1 could also regulate SHH signaling relay through the primary cilium, besides just sustaining ciliogenesis.

Our results in the simpler model NIH-3T3 cells report that Atoh1 overexpression enhances the ciliary accumulation of Smo and Gli2 upon SHH stimulation (**Figure S6**). This effect is so pronounced that a bulge containing the two proteins appears at the tip of most primary cilia. Notably, such bulges resemble those displayed by primary cilia defective for retrograde IFT trains assembly or motility, which are therefore unable to export material. However, in those cases, also cilia-mediated signaling is typically disrupted. Conversely, we show that Atoh1-overexpressing NIH-3T3 (potently) still respond to SHH, thereby ruling out any evident deleterious effect of ciliary bulges on SHH signaling (**Figure S6**). We therefore propose that such swelling of the ciliary tip might just reflect an artifact due to overexpression of tagged Smo and Gli2. Despite similarly redistributing in the cilium in response to SHH, overexpressed tagged Smo and Gli2 may not indeed faithfully recapitulate the trafficking of their endogenous counterparts.

Nevertheless, an effect of Atoh1 in their ciliary transport is clear, as also supported by immunostaining of endogenous Smo at the primary cilia of cultured GNPs (**Figure 7**). Here

also, *Atoh1* overexpression is associated with increased Smo accumulation at the cilium, in presence of SHH.

Once again, it must be noticed that neither the ciliary accumulation of endogenous Smo always necessarily reflects downstream pathway activation (Rohatgi et al., 2009). Indeed, inactive Smo is known to continuously transit through the primary cilium and eventually it can also accumulate in response to drugs (e.g. cyclopamine) or IFT manipulation, but in all cases it remains inactive and unable to downstream signaling. However, in our experimental setting, *Atoh1* overexpression enhances the SHH-mediated transcription of target genes as *Ptch1*, *Gli1*, *Mycn*, *Ccnd1* and *Ccnd2*, indicating that the observed additional Smo at the cilium corresponds to its active form, capable of activating Gli (**Figure XXI**).

The exact mechanism controlled by *Atoh1* to promote Smo shuttling in the cilium was not deeply investigated, however it could likely rely on CS regulation as well, given their prominent role in orchestrating ciliary functions, including the SHH signaling (Lopes et al., 2011; Odabasi et al., 2019). For instance, properly assembled CS may promote efficient stoichiometric formation of the BBSome, which has been implicated in the ciliary transport of Smo (Chamling et al., 2014; Kim et al., 2004; Zhang et al., 2012b). They could also regulate the assembly of IFT particles, important for Smo and Gli trafficking, by controlling the recruitment of Ift88 at the ciliary base (Singla et al., 2010); depletion of CS was indeed recently shown to reduce Ift88 levels in the cilium (Odabasi et al., 2019).

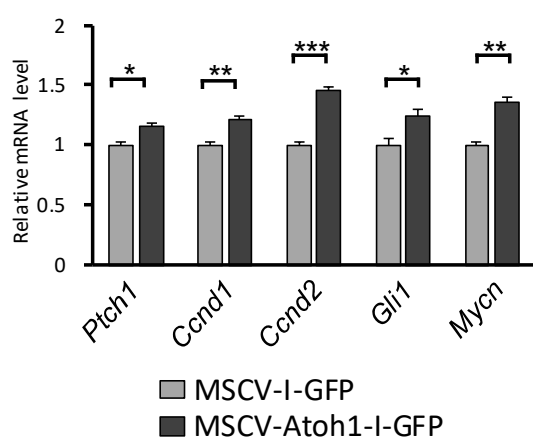


Figure XXI. Expression of SHH target genes upon *Atoh1* overexpression in GNPs. Relative mRNA expression of a panel of SHH-target genes in primary GNPs infected with indicated retroviruses and cultured in presence of SHH for 72hrs. Expression was measured via RT-qPCR. Student's *t* test. *: $p < 0.05$, **: $p < 0.01$; ***: $p < 0.001$; $n = 3$. Data are represented as mean \pm SEM.

Additionally, CS may gate the recruitment of intracellular Smo-containing vesicles at the ciliary base, by regulating the abundance and the activity of Rab8 at the basal body (Kim et al., 2004). In conclusion we speculate that by maintaining a functional pool of CS around the basal body, Atoh1 not only grants GNPs the appropriate tools for properly building up primary cilia, but also ensures cilia with the means for efficiently transducing the SHH signaling.

D.6 Atoh1 collaborates with the SHH pathway at multiple steps.

That Atoh1 maintained GNPs competent to respond to SHH was already known since previous studies (Ayrault et al., 2010; Flora et al., 2009). For long this activity of Atoh1 was attributed to its ability to regulate *Gli2* expression in both GNPs and SHH-MB, hence providing cells with the main transcriptional mediator of the SHH pro-proliferative program (Flora et al., 2009). Indeed, among the Gli factors, only Gli2 seems exclusively required for proper expansion of GNPs pool, while Gli1 and Gli3 seem overall dispensable (Blaess et al., 2008; Corrales et al., 2004). In addition, a recent work reported that Atoh1 seems to share a large part of its transcriptional targets with Gli2 and that the co-occurrence of Atoh1 and Gli2 at the same *cis*-regulative regions synergistically activates downstream genes (Yin et al., 2019). Therefore, by regulating multiple aspects of Gli2 functions, Atoh1 collaborates at shaping the SHH response in SHH-activated GNPs.

Our finding that Atoh1 controls ciliogenesis in GNPs adds up a novel key node in the Atoh1-SHH interplay. Importantly, we demonstrate that *in vivo* overexpression of Atoh1 alone is not sufficient to sustain GNPs responsiveness to SHH when primary cilia are ablated or dysfunctional (**Figure 3**). This result suggests that Atoh1-overexpressing GNPs, although likely maintaining elevated Gli2 expression in virtue of the Atoh1-Gli2 axis, require a functional primary cilium for the proper generation of the Gli2^A form. Supposedly, Gli2^(FL) expression alone in GNPs is not sufficient to drive proliferation, if Gli2 is not SHH-dependently activated through the primary cilium. This hypothesis is also corroborated by failure of Atoh1 overexpression alone to drive GNPs proliferation in absence of SHH (Ayrault et al., 2010).

Therefore, by regulating the SHH signaling at multiple levels, namely (i) expression of Gli2, (ii) maintenance of primary cilia and (iii) synergy with Gli2 in targets activation, Atoh1 robustly sustains GNPs proliferative response to SHH. When such network is combined with the ability of the SHH signaling to stabilize Atoh1 protein by impeding its proteasomal degradation (Forget et al., 2014), then a positive feedback loop appears (**Figure XXII**). Such loop is critical

for sustaining the SHH-dependent expansion of GNPs in the post-natal cerebellum, as well as the proliferation of SHH-MB cells.

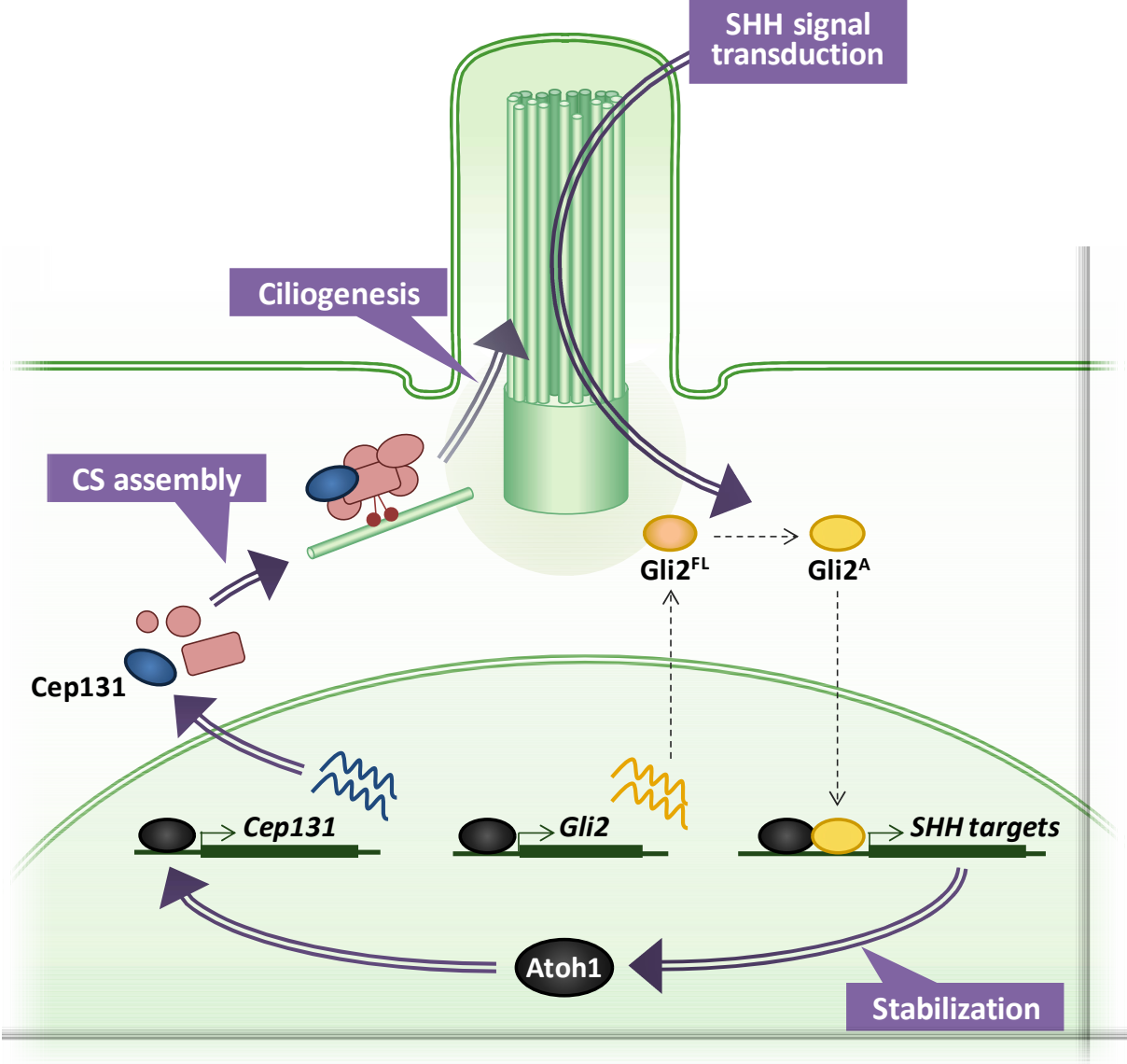


Figure XXII. Positive feedback loop between Atoh1 and SHH in GNPs or SHH-MB cells. Atoh1 (black ovals) in GNPs and in SHH-MB cells positively regulates the expression of both Cep131 (blue ovals) and Gli2 (yellow ovals). Cep131 is crucial for correctly assembling CS around the centrosome. Well organized CS sustain the formation of a functional primary cilium, through which the SHH signaling can be transduced. SHH promotes the formation of the activator form of Gli2 (Gli2^A) from the full-length form (Gli2^{FL}). Gli2^A enters in the nucleus where it activates SHH target genes, hence promoting cell proliferation. In addition, Atoh1 collaborates with Gli2 for the expression of a large panel of common targets. As the SHH signaling protects Atoh1 from proteasomal degradation, a positive feedback loop is closed (represented by all the purple arrows).

D.7 Dual and opposite roles of *Atoh1* in GNs development

Class II-bHLH proneural transcription factors promote neurogenesis in the developing nervous system. Hence their accumulation and activation in NPCs typically push these cells to exit the cell cycle and differentiate to neurons (Imayoshi and Kageyama, 2014). Accordingly, *Atoh1* expression and activity in progenitor cells of different tissues induce them to abandon the progenitor phenotype and undertake a certain differentiation fate. This is the case of sensory HCs in the inner ear, D1 neurons in the spinal cord, but also the case of non-neuronal cells as the secretory lineage of the intestine. Coherently with these functions, *Atoh1* is typically downregulated in colorectal cancer, where through promoting differentiation of tumor cells, it works as a tumor suppressor gene (Leow et al., 2004).

Therefore, *Atoh1* activity is generally associated with cell cycle withdrawal and consequent cell differentiation.

Consistently, it is also widely accepted that in the developing mouse cerebellum, from E12.5 onwards, *Atoh1* is involved in committing uRL progenitors to the GN lineage (perhaps in collaboration with other transcription factors, as *Zic1*) and for governing subsequent phases of their developmental program, as migration to the EGL and terminal maturation to GNs. Indeed, KO or overexpression of *Atoh1* in uRL progenitors respectively cause blockade of GNs formation or premature expression of differentiation markers (Ben-Arie et al., 1997; Gazit et al., 2004; Helms et al., 2001; Kawauchi and Saito, 2008) (paragraph **I.6.3.1**).

However, after lineage commitment and migration to the EGL, GNPs still express *Atoh1* and undergo a second phase of proliferation, which is SHH-dependent. Quite surprisingly considering the typical functions of proneural factors, we and others have shown that *Atoh1* also promotes proliferation of GNPs by maintaining their sensitivity to SHH, at least through regulation of *Cep131* and *Gli2* expression (Ayrault et al., 2010; Flora et al., 2009; Forget et al., 2014). In addition, by essentially using the same mechanisms, *Atoh1* also sustains SHH-MB cells expansion, hence becoming critical for the growth of this tumor (Ayrault et al., 2010; Flora et al., 2009).

How can *Atoh1* actively promote opposite processes as differentiation and proliferation in the same cell lineage? The answer perhaps relies on the differential accumulation rate between the proliferation and differentiation determinants controlled by *Atoh1*. This different kinetics of expression may be functionally translated into distinct, non-overlapping, sequential phases of proliferation and differentiation during GNs development.

After its expression onset in uRL precursors, *Atoh1* initiates its transcriptional program by downstream activating genes involved in pan-neuronal differentiation and GN identity specification, perhaps also regulating genes required for the migration of GNPs to the EGL (Gazit et al., 2004; Kawauchi and Saito, 2008). Interestingly, by this stage GNPs are already ciliated, express *Gli2* and can potentially respond to SHH, although such response will begin only after E17.5, when PCs initiate to secrete the mitogen (Corrales et al., 2004; Shimada et al., 2018). Therefore, although direct experimental evidence is missing, it is likely that *Atoh1* not only commits uRL progenitors to migrate and differentiate to GNs, but also prepares them for their imminent expansion phase in the EGL, equipping them with the machineries required to transduce SHH. Once reached the EGL, SHH fuels GNPs proliferation, and the continued expression of *Atoh1* and its pro-proliferative targets (e.g. *Cep131*, *Gli2*, *E2f1*...) sustain such response (our results; Flora et al., 2009; Klisch et al., 2011). However, at the same time, *Atoh1* also continues to regulate the expression of neuronal differentiation genes (e.g. *Neurod1*, *Nhlh1/2*, *Sema6a*, components of the Notch1 pathway) that progressively accumulate into proliferating GNPs gradually conferring differentiation competence. Once accumulated enough, such differentiation determinants may eventually take over proliferation factors (perhaps also downregulating *Atoh1*, as *Neurod1* does), consequently inducing terminal cell cycle exit and differentiation.

Importantly, such model is in accordance with several observations of ours and others. Klisch and colleagues (2011) found that cKO of *Atoh1* in early post-natal GNPs (P0) blocks their differentiation and migration to the IGL; in contrast, *Atoh1* loss in P5 GNPs does not disturb subsequent phases of their development. The easiest explanation is that perhaps by P0 GNPs have not accumulated enough *Atoh1*-dependent differentiation determinants to complete their maturation to GNs in absence of *Atoh1*, while at P5 they are already fully proficient for this transition.

In our experiments, *in vivo* overexpression of *Atoh1* (via pCIG2-*Atoh1* electroporation) in P6 GNPs prolongs their stay into a cycling state, supposedly by counteracting the progressive physiological downregulation of endogenous *Atoh1*. Hence, genes as *Cep131* and *Gli2* may remain highly expressed and sustain proliferation of GNPs for a few additional cell cycles (**Figure 1**). However, although *Atoh1* levels remain high, the differentiation determinants, many of them under the control of *Atoh1* itself, will eventually take over, inevitably inducing cell cycle exit (**Figure 1**).

This model is also compatible with the role of Atoh1 in SHH-MB. SHH-MB originates from GNP aberrantly activated by SHH, which acquire the ability to partially escape from tumor-suppressing programs as cell cycle exit or senescence (Ayrault et al., 2009; Tamayo-Orrego et al., 2016; Uziel et al., 2006). It is known that cycling SHH-MB cells closely recapitulate GNPs in active proliferation, as also confirmed by recent single-cell transcriptome analysis (Hovestadt et al., 2019). Hence, Shh-MB cells likely resemble GNPs "fixed" in a state in which Atoh1 is actively engaged at sustaining proliferation. Overexpression of Atoh1 in a context in which GNPs/SHH-MB cells are poorly able to arrest their expansion (e.g. inactivation of TP53 or p16^{Ink4a} functions) can result only into enhanced proliferation due to accumulation of Atoh1-dependent proliferative factors.

Notably, the general developmental model described above does not keep into account all the possible (and unknown) subtle modifications of Atoh1 activity that could occur during GNs development. Such variables may include regulation of Atoh1 nuclear abundance, transcriptional activity and chromatin occupancy. For instance, changes of Atoh1 phosphorylation status or changes in the availability of binding partners represent mechanisms potentially able to modify the targetome of Atoh1 during GNs development. Moreover, other temporally regulated non-cell autonomous cues (e.g. signaling molecules, ECM ligands) may add up to Atoh1 in regulating the expression of both proliferation and differentiation determinants.

Hence, by orchestrating the functions of Atoh1 and its downstream targets, all these additional modules may participate in the generation of a complex developmental program that finally ensures proper balance between sequential phases of cell proliferation and differentiation.

Bibliography

- Adams, K.A., Maida, J.M., Golden, J.A., and Riddle, R.D. (2000). The transcription factor Lmx1b maintains Wnt1 expression within the isthmic organizer. *Dev. Camb. Engl.* *127*, 1857–1867.
- Akazawa, C., Ishibashi, M., Shimizu, C., Nakanishi, S., and Kageyama, R. (1995). A mammalian helix-loop-helix factor structurally related to the product of *Drosophila* proneural gene *atonal* is a positive transcriptional regulator expressed in the developing nervous system. *J. Biol. Chem.* *270*, 8730–8738.
- Alcantara, S., Ruiz, M., De Castro, F., Soriano, E., and Sotelo, C. (2000). Netrin 1 acts as an attractive or as a repulsive cue for distinct migrating neurons during the development of the cerebellar system. *Development* *127*, 1359.
- Alder, J., Cho, N.K., and Hatten, M.E. (1996). Embryonic precursor cells from the rhombic lip are specified to a cerebellar granule neuron identity. *Neuron* *17*, 389–399.
- Alder, J., Lee, K.J., Jessell, T.M., and Hatten, M.E. (1999). Generation of cerebellar granule neurons in vivo by transplantation of BMP-treated neural progenitor cells. *Nat. Neurosci.* *2*, 535–540.
- Ali, F., Hindley, C., McDowell, G., Deibler, R., Jones, A., Kirschner, M., Guillemot, F., and Philpott, A. (2011). Cell cycle-regulated multi-site phosphorylation of Neurogenin 2 coordinates cell cycling with differentiation during neurogenesis. *Dev. Camb. Engl.* *138*, 4267–4277.
- Álvarez-Rodríguez, R., Barzi, M., Berenguer, J., and Pons, S. (2007). Bone Morphogenetic Protein 2 Opposes Shh-mediated Proliferation in Cerebellar Granule Cells through a TIEG-1-based Regulation of Nmyc. *J. Biol. Chem.* *282*, 37170–37180.
- Angley, C., Kumar, M., Dinsio, K.J., Hall, A.K., and Siegel, R.E. (2003). Signaling by Bone Morphogenetic Proteins and Smad1 Modulates the Postnatal Differentiation of Cerebellar Cells. *J. Neurosci.* *23*, 260.
- Anne, S.L., Govek, E.-E., Ayrault, O., Kim, J.H., Zhu, X., Murphy, D.A., Van Aelst, L., Roussel, M.F., and Hatten, M.E. (2013). WNT3 inhibits cerebellar granule neuron progenitor proliferation and medulloblastoma formation via MAPK activation. *PLoS One* *8*, e81769.
- Anvarian, Z., Mykytyn, K., Mukhopadhyay, S., Pedersen, L.B., and Christensen, S.T. (2019). Cellular signalling by primary cilia in development, organ function and disease. *Nat. Rev. Nephrol.* *15*, 199–219.
- Aragaki, M., Tsuchiya, K., Okamoto, R., Yoshioka, S., Nakamura, T., Sakamoto, N., Kanai, T., and Watanabe, M. (2008). Proteasomal degradation of Atoh1 by aberrant Wnt signaling maintains the undifferentiated state of colon cancer. *Biochem. Biophys. Res. Commun.* *368*, 923–929.
- Araujo, A.P.B., Ribeiro, M.E.O.B., Ricci, R., Torquato, R.J., Toma, L., and Porcionatto, M.A. (2010). Glial cells modulate heparan sulfate proteoglycan (HSPG) expression by neuronal precursors during early postnatal cerebellar development. *Int. J. Dev. Neurosci. Off. J. Int. Soc. Dev. Neurosci.* *28*, 611–620.
- Archer, T.C., Ehrenberger, T., Mundt, F., Gold, M.P., Krug, K., Mah, C.K., Mahoney, E.L., Daniel, C.J., LeNail, A., Ramamoorthy, D., et al. (2018). Proteomics, Post-translational Modifications, and Integrative Analyses Reveal Molecular Heterogeneity within Medulloblastoma Subgroups. *Cancer Cell* *34*, 396–410.e8.

- Aruga, J., Yokota, N., Hashimoto, M., Furuichi, T., Fukuda, M., and Mikoshiba, K. (1994). A Novel Zinc Finger Protein, Zic, Is Involved in Neurogenesis, Especially in the Cell Lineage of Cerebellar Granule Cells. *J. Neurochem.* *63*, 1880–1890.
- Asano, M., and Gruss, P. (1992). Pax-5 is expressed at the midbrain-hindbrain boundary during mouse development. *Mech. Dev.* *39*, 29–39.
- Asante, D., Stevenson, N.L., and Stephens, D.J. (2014). Subunit composition of the human cytoplasmic dynein-2 complex. *J. Cell Sci.* *127*, 4774–4787.
- Ayrault, O., Zindy, F., Rehg, J., Sherr, C.J., and Roussel, M.F. (2009). Two Tumor Suppressors, p27Kip1 and Patched-1, Collaborate to Prevent Medulloblastoma. *Mol. Cancer Res.* *7*, 33–40.
- Ayrault, O., Zhao, H., Zindy, F., Qu, C., Sherr, C.J., and Roussel, M.F. (2010). Atoh1 inhibits neuronal differentiation and collaborates with Gli1 to generate medulloblastoma-initiating cells. *Cancer Res.* *70*, 5618–5627.
- Bai, R.-Y., Staedtke, V., Lidov, H.G., Eberhart, C.G., and Riggins, G.J. (2012). OTX2 represses myogenic and neuronal differentiation in medulloblastoma cells. *Cancer Res.* *72*, 5988–6001.
- Baker, N.E., and Brown, N.L. (2018). All in the family: proneural bHLH genes and neuronal diversity. *Development* *145*, dev159426.
- Balczon, R., Bao, L., and Zimmer, W.E. (1994). PCM-1, A 228-kD centrosome autoantigen with a distinct cell cycle distribution. *J. Cell Biol.* *124*, 783–793.
- Bansal, L.R., Belair, J., Cummings, D., and Zuccoli, G. (2015). Late-onset radiation-induced vasculopathy and stroke in a child with medulloblastoma. *J. Child Neurol.* *30*, 800–802.
- Barakat, M.T., Humke, E.W., and Scott, M.P. (2013). Kif3a is necessary for initiation and maintenance of medulloblastoma. *Carcinogenesis* *34*, 1382–1392.
- Bay, S.N., Long, A.B., and Caspary, T. (2018). Disruption of the ciliary GTPase Arl13b suppresses Sonic hedgehog overactivation and inhibits medulloblastoma formation. *Proc. Natl. Acad. Sci.* *115*, 1570–1575.
- Beachy, P.A., Karhadkar, S.S., and Berman, D.M. (2004). Tissue repair and stem cell renewal in carcinogenesis. *Nature* *432*, 324–331.
- Ben-Arie, N., Bellen, H.J., Armstrong, D.L., McCall, A.E., Gordadze, P.R., Guo, Q., Matzuk, M.M., and Zoghbi, H.Y. (1997). Math1 is essential for genesis of cerebellar granule neurons. *Nature* *390*, 169.
- Ben-Arie, N., Hassan, B.A., Bermingham, N.A., Malicki, D.M., Armstrong, D., Matzuk, M., Bellen, H.J., and Zoghbi, H.Y. (2000). Functional conservation of atonal and Math1 in the CNS and PNS. *Dev. Camb. Engl.* *127*, 1039–1048.
- Benmerah, A. (2013). The ciliary pocket. *Curr. Opin. Cell Biol.* *25*, 78–84.
- Berberi, N.F., Johnson, A.D., Lewis, J.S., Askwith, C.C., and Mykityn, K. (2008). Identification of ciliary localization sequences within the third intracellular loop of G protein-coupled receptors. *Mol. Biol. Cell* *19*, 1540–1547.

- Berman, D.M., Karhadkar, S.S., Hallahan, A.R., Pritchard, J.I., Eberhart, C.G., Watkins, D.N., Chen, J.K., Cooper, M.K., Taipale, J., Olson, J.M., et al. (2002). Medulloblastoma Growth Inhibition by Hedgehog Pathway Blockade. *Science* 297, 1559–1561.
- Bermingham, N.A., Hassan, B.A., Price, S.D., Vollrath, M.A., Ben-Arie, N., Eatock, R.A., Bellen, H.J., Lysakowski, A., and Zoghbi, H.Y. (1999). Math1: An Essential Gene for the Generation of Inner Ear Hair Cells. *Science* 284, 1837–1841.
- Bermingham, N.A., Hassan, B.A., Wang, V.Y., Fernandez, M., Banfi, S., Bellen, H.J., Fritsch, B., and Zoghbi, H.Y. (2001). Proprioceptor Pathway Development Is Dependent on MATH1. *Neuron* 30, 411–422.
- Bernhard, W., and de Harven, E. (1960). L'ultrastructure du centriole et d'autres éléments de l'appareil achromatique. In *Verhandlungen Band II / Biologisch-Medizinischer Teil*, W. Bargmann, D. Peters, and C. Wolpers, eds. (Springer Berlin Heidelberg), pp. 217–227.
- Bertrand, N., Castro, D.S., and Guillemot, F. (2002). Proneural genes and the specification of neural cell types. *Nat. Rev. Neurosci.* 3, 517.
- Bhatia, N., Thiyagarajan, S., Elcheva, I., Saleem, M., Dlugosz, A., Mukhtar, H., and Spiegelman, V.S. (2006). Gli2 Is Targeted for Ubiquitination and Degradation by β -TrCP Ubiquitin Ligase. *J. Biol. Chem.* 281, 19320–19326.
- Blacque, O.E., Reardon, M.J., Li, C., McCarthy, J., Mahjoub, M.R., Ansley, S.J., Badano, J.L., Mah, A.K., Beales, P.L., Davidson, W.S., et al. (2004). Loss of *C. elegans* BBS-7 and BBS-8 protein function results in cilia defects and compromised intraflagellar transport. *Genes Dev.* 18, 1630–1642.
- Blacque, O.E., Scheidel, N., and Kuhns, S. (2017). Rab GTPases in cilium formation and function. *Small GTPases* 9, 76–94.
- Blaess, S., Graus-Porta, D., Belvindrah, R., Radakovits, R., Pons, S., Littlewood-Evans, A., Senften, M., Guo, H., Li, Y., Miner, J.H., et al. (2004). β 1-Integrins Are Critical for Cerebellar Granule Cell Precursor Proliferation. *J. Neurosci. Off. J. Soc. Neurosci.* 24, 3402–3412.
- Blaess, S., Stephen, D., and Joyner, A.L. (2008). Gli3 coordinates three-dimensional patterning and growth of the tectum and cerebellum by integrating Shh and Fgf8 signaling. *Dev. Camb. Engl.* 135, 2093–2103.
- Bloch-Gallego, E., Ezan, F., Tessier-Lavigne, M., and Sotelo, C. (1999). Floor plate and netrin-1 are involved in the migration and survival of inferior olivary neurons. *J. Neurosci. Off. J. Soc. Neurosci.* 19, 4407–4420.
- Borghesani, P.R., Peyrin, J.M., Klein, R., Rubin, J., Carter, A.R., Schwartz, P.M., Luster, A., Corfas, G., and Segal, R.A. (2002). BDNF stimulates migration of cerebellar granule cells. *Dev. Camb. Engl.* 129, 1435–1442.
- Borowska, A., and Józwiak, J. (2016). Medulloblastoma: molecular pathways and histopathological classification. *Arch. Med. Sci. AMS* 12, 659–666.
- Bossuyt, W., Kazanjian, A., De Geest, N., Kelst, S.V., Hertogh, G.D., Geboes, K., Boivin, G.P., Luciani, J., Fuks, F., Chuah, M., et al. (2009). Atonal homolog 1 Is a Tumor Suppressor Gene. *PLoS Biol.* 7.

Brazelton, W.J., Amundsen, C.D., Silflow, C.D., and Lefebvre, P.A. (2001). The *bld1* mutation identifies the *Chlamydomonas osm-6* homolog as a gene required for flagellar assembly. *Curr. Biol.* **11**, 1591–1594.

Briggs, K.J., Corcoran-Schwartz, I.M., Zhang, W., Harcke, T., Devereux, W.L., Baylin, S.B., Eberhart, C.G., and Watkins, D.N. (2008). Cooperation between the *Hic1* and *Ptch1* tumor suppressors in medulloblastoma. *Genes Dev.* **22**, 770–785.

Briscoe, J., Chen, Y., Jessell, T.M., and Struhl, G. (2001). A hedgehog-insensitive form of patched provides evidence for direct long-range morphogen activity of sonic hedgehog in the neural tube. *Mol. Cell* **7**, 1279–1291.

Brooks, E.R., and Wallingford, J.B. (2014). Multiciliated Cells. *Curr. Biol.* **24**, R973–R982.

Brown, J.M., Cochran, D.A., Craige, B., Kubo, T., and Witman, G.B. (2015). Assembly of IFT trains at the ciliary base depends on IFT74. *Curr. Biol.* **25**, 1583–1593.

Brown, N.J., Marjanović, M., Lüders, J., Stracker, T.H., and Costanzo, V. (2013). *Cep63* and *Cep152* Cooperate to Ensure Centriole Duplication. *PLOS ONE* **8**, e69986.

Buckner, R.L. (2013). The cerebellum and cognitive function: 25 years of insight from anatomy and neuroimaging. *Neuron* **80**, 807–815.

Buglino, J.A., and Resh, M.D. (2012). Palmitoylation of Hedgehog Proteins. *Vitam. Horm.* **88**, 229–252.

Bunt, J., Hasselt, N.E., Zwijnenburg, D.A., Hamdi, M., Koster, J., Versteeg, R., and Kool, M. (2012). *OTX2* directly activates cell cycle genes and inhibits differentiation in medulloblastoma cells. *Int. J. Cancer* **131**, E21–32.

Buonamici, S., Williams, J., Morrissey, M., Wang, A., Guo, R., Vattay, A., Hsiao, K., Yuan, J., Green, J., Ospina, B., et al. (2010). Interfering with Resistance to Smoothed Antagonists by Inhibition of the PI3K Pathway in Medulloblastoma. *Sci. Transl. Med.* **2**, 51ra70.

Burke, R., Nellen, D., Bellotto, M., Hafen, E., Senti, K.A., Dickson, B.J., and Basler, K. (1999). Dispatched, a novel sterol-sensing domain protein dedicated to the release of cholesterol-modified hedgehog from signaling cells. *Cell* **99**, 803–815.

Byrne, E.F.X., Sircar, R., Miller, P.S., Hedger, G., Luchetti, G., Nachtergaele, S., Tully, M.D., Mydock-McGrane, L., Covey, D.F., Rambo, R.P., et al. (2016). Structural basis of Smoothed regulation by its extracellular domains. *Nature* **535**, 517–522.

Čajánek, L., Glatter, T., and Nigg, E.A. (2015). The E3 ubiquitin ligase *Mib1* regulates *Plk4* and centriole biogenesis. *J. Cell Sci.* **128**, 1674–1682.

Calegari, F., and Huttner, W.B. (2003). An inhibition of cyclin-dependent kinases that lengthens, but does not arrest, neuroepithelial cell cycle induces premature neurogenesis. *J. Cell Sci.* **116**, 4947–4955.

Calegari, F., Haubensak, W., Haffner, C., and Huttner, W.B. (2005). Selective lengthening of the cell cycle in the neurogenic subpopulation of neural progenitor cells during mouse brain development. *J. Neurosci. Off. J. Soc. Neurosci.* **25**, 6533–6538.

- Canettieri, G., Di Marcotullio, L., Greco, A., Coni, S., Antonucci, L., Infante, P., Pietrosanti, L., De Smaele, E., Ferretti, E., Miele, E., et al. (2010). Histone deacetylase and Cullin3–REN^{KCTD11} ubiquitin ligase interplay regulates Hedgehog signalling through Gli acetylation. *Nat. Cell Biol.* *12*, 132–142.
- Caparrós-Martín, J.A., Valencia, M., Reytor, E., Pacheco, M., Fernandez, M., Perez-Aytes, A., Gean, E., Lapunzina, P., Peters, H., Goodship, J.A., et al. (2013). The ciliary Evc/Evc2 complex interacts with Smo and controls Hedgehog pathway activity in chondrocytes by regulating Sufu/Gli3 dissociation and Gli3 trafficking in primary cilia. *Hum. Mol. Genet.* *22*, 124–139.
- Castro, D.S., Martynoga, B., Parras, C., Ramesh, V., Pacary, E., Johnston, C., Drechsel, D., Lebel-Potter, M., Garcia, L.G., Hunt, C., et al. (2011). A novel function of the proneural factor *Ascl1* in progenitor proliferation identified by genome-wide characterization of its targets. *Genes Dev.* *25*, 930–945.
- Cavalli, F.M.G., Remke, M., Rampasek, L., Peacock, J., Shih, D.J.H., Luu, B., Garzia, L., Torchia, J., Nor, C., Morrissy, A.S., et al. (2017). Intertumoral Heterogeneity within Medulloblastoma Subgroups. *Cancer Cell* *31*, 737-754.e6.
- de Chadarévian, J.P., Vekemans, M., and Bernstein, M. (1985). Fanconi's anemia, medulloblastoma, Wilms' tumor, horseshoe kidney, and gonadal dysgenesis. *Arch. Pathol. Lab. Med.* *109*, 367–369.
- Chamling, X., Seo, S., Searby, C.C., Kim, G., Slusarski, D.C., and Sheffield, V.C. (2014). The centriolar satellite protein AZI1 interacts with BBS4 and regulates ciliary trafficking of the BBSome. *PLoS Genet.* *10*, e1004083.
- Chan, J.A., Balasubramanian, S., Witt, R.M., Nazemi, K.J., Choi, Y., Pazyra-Murphy, M.F., Walsh, C.O., Thompson, M., and Segal, R.A. (2009). Proteoglycan interactions with Sonic Hedgehog specify mitogenic responses. *Nat. Neurosci.* *12*, 409–417.
- Charron, F., Stein, E., Jeong, J., McMahon, A.P., and Tessier-Lavigne, M. (2003). The Morphogen Sonic Hedgehog Is an Axonal Chemoattractant that Collaborates with Netrin-1 in Midline Axon Guidance. *Cell* *113*, 11–23.
- Chaya, T., Omori, Y., Kuwahara, R., and Furukawa, T. (2014). ICK is essential for cell type-specific ciliogenesis and the regulation of ciliary transport. *EMBO J.* *33*, 1227–1242.
- Chen, J.K., Taipale, J., Cooper, M.K., and Beachy, P.A. (2002a). Inhibition of Hedgehog signaling by direct binding of cyclopamine to Smoothened. *Genes Dev.* *16*, 2743–2748.
- Chen, J.K., Taipale, J., Young, K.E., Maiti, T., and Beachy, P.A. (2002b). Small molecule modulation of Smoothened activity. *Proc. Natl. Acad. Sci. U. S. A.* *99*, 14071–14076.
- Chen, M.-H., Li, Y.-J., Kawakami, T., Xu, S.-M., and Chuang, P.-T. (2004). Palmitoylation is required for the production of a soluble multimeric Hedgehog protein complex and long-range signaling in vertebrates. *Genes Dev.* *18*, 641–659.
- Chen, Y., Li, S., Tong, C., Zhao, Y., Wang, B., Liu, Y., Jia, J., and Jiang, J. (2010). G protein-coupled receptor kinase 2 promotes high-level Hedgehog signaling by regulating the active state of Smo through kinase-dependent and kinase-independent mechanisms in *Drosophila*. *Genes Dev.* *24*, 2054–2067.

Chen, Y., Sasai, N., Ma, G., Yue, T., Jia, J., Briscoe, J., and Jiang, J. (2011). Sonic Hedgehog Dependent Phosphorylation by CK1 α and GRK2 Is Required for Ciliary Accumulation and Activation of Smoothened. *PLoS Biol.* *9*.

Cheng, Y.-F., Tong, M., and Edge, A.S.B. (2016). Destabilization of Atoh1 by E3 Ubiquitin Ligase Huwe1 and Casein Kinase 1 Is Essential for Normal Sensory Hair Cell Development. *J. Biol. Chem.* *291*, 21096–21109.

Chi, C.L., Martinez, S., Wurst, W., and Martin, G.R. (2003). The isthmic organizer signal FGF8 is required for cell survival in the prospective midbrain and cerebellum. *Dev. Camb. Engl.* *130*, 2633–2644.

Chih, B., Liu, P., Chinn, Y., Chalouni, C., Komuves, L.G., Hass, P.E., Sandoval, W., and Peterson, A.S. (2011). A ciliopathy complex at the transition zone protects the cilia as a privileged membrane domain. *Nat. Cell Biol.* *14*, 61–72.

Chizhikov, V.V., and Millen, K.J. (2004). Control of roof plate formation by Lmx1a in the developing spinal cord. *Development* *131*, 2693–2705.

Chizhikov, V.V., Lindgren, A.G., Currle, D.S., Rose, M.F., Monuki, E.S., and Millen, K.J. (2006). The roof plate regulates cerebellar cell-type specification and proliferation. *Development* *133*, 2793–2804.

Chizhikov, V.V., Davenport, J., Zhang, Q., Shih, E.K., Cabello, O.A., Fuchs, J.L., Yoder, B.K., and Millen, K.J. (2007). Cilia Proteins Control Cerebellar Morphogenesis by Promoting Expansion of the Granule Progenitor Pool. *J. Neurosci.* *27*, 9780–9789.

Chizhikov, V.V., Lindgren, A.G., Mishima, Y., Roberts, R.W., Aldinger, K.A., Miesegaes, G.R., Currle, D.S., Monuki, E.S., and Millen, K.J. (2010). Lmx1a regulates fates and location of cells originating from the cerebellar rhombic lip and telencephalic cortical hem. *Proc. Natl. Acad. Sci.* *107*, 10725–10730.

Cho, Y.-J., Tsherniak, A., Tamayo, P., Santagata, S., Ligon, A., Greulich, H., Berhoukim, R., Amani, V., Goumnerova, L., Eberhart, C.G., et al. (2011). Integrative genomic analysis of medulloblastoma identifies a molecular subgroup that drives poor clinical outcome. *J. Clin. Oncol. Off. J. Am. Soc. Clin. Oncol.* *29*, 1424–1430.

Choksi, S.P., Lauter, G., Swoboda, P., and Roy, S. (2014). Switching on cilia: transcriptional networks regulating ciliogenesis. *Development* *141*, 1427–1441.

Chonko, K.T., Jahan, I., Stone, J., Wright, M.C., Fujiyama, T., Hoshino, M., Fritzsich, B., and Maricich, S.M. (2013). Atoh1 directs hair cell differentiation and survival in the late embryonic mouse inner ear. *Dev. Biol.* *381*, 401–410.

Ciemerych, M.A., Kenney, A.M., Sicinska, E., Kalaszczynska, I., Bronson, R.T., Rowitch, D.H., Gardner, H., and Sicinski, P. (2002). Development of mice expressing a single D-type cyclin. *Genes Dev.* *16*, 3277–3289.

Clifford, S.C., Lusher, M.E., Lindsey, J.C., Langdon, J.A., Gilbertson, R.J., Straughton, D., and Ellison, D.W. (2006). Wnt/Wingless Pathway Activation and Chromosome 6 Loss Characterise a Distinct Molecular Sub-Group of Medulloblastomas Associated with a Favourable Prognosis. *Cell Cycle* *5*, 2666–2670.

- Cohen, S.B. (1982). Familial polyposis coli and its extracolonic manifestations. *J. Med. Genet.* *19*, 193–203.
- Conkar, D., Culfa, E., Odabasi, E., Rauniyar, N., Yates, J.R., and Firat-Karalar, E.N. (2017). The centriolar satellite protein CCDC66 interacts with CEP290 and functions in cilium formation and trafficking. *J. Cell Sci.* *130*, 1450–1462.
- Cooper, M.K., Wassif, C.A., Krakowiak, P.A., Taipale, J., Gong, R., Kelley, R.I., Porter, F.D., and Beachy, P.A. (2003). A defective response to Hedgehog signaling in disorders of cholesterol biosynthesis. *Nat. Genet.* *33*, 508–513.
- Corcoran, R.B., and Scott, M.P. (2006). Oxysterols stimulate Sonic hedgehog signal transduction and proliferation of medulloblastoma cells. *Proc. Natl. Acad. Sci.* *103*, 8408–8413.
- Corcoran, R.B., Raveh, T., Barakat, M.T., Lee, E.Y., and Scott, M.P. (2008). Insulin-like Growth Factor 2 is Required for Progression to Advanced Medulloblastoma in patched1 Heterozygous Mice. *Cancer Res.* *68*, 8788–8795.
- Corrales, J.D., Rocco, G.L., Blaess, S., Guo, Q., and Joyner, A.L. (2004). Spatial pattern of sonic hedgehog signaling through Gli genes during cerebellum development. *Development* *131*, 5581–5590.
- Corrales, J.D., Blaess, S., Mahoney, E.M., and Joyner, A.L. (2006). The level of sonic hedgehog signaling regulates the complexity of cerebellar foliation. *Dev. Camb. Engl.* *133*, 1811–1821.
- Crossley, P.H., and Martin, G.R. (1995). The mouse *Fgf8* gene encodes a family of polypeptides and is expressed in regions that direct outgrowth and patterning in the developing embryo. *Dev. Camb. Engl.* *121*, 439–451.
- Dahmane, N., and Ruiz-i-Altaba, A. (1999). Sonic hedgehog regulates the growth and patterning of the cerebellum. *Development* *126*, 3089.
- Dammermann, A., and Merdes, A. (2002). Assembly of centrosomal proteins and microtubule organization depends on PCM-1. *J. Cell Biol.* *159*, 255–266.
- Darnell, D., and Gilbert, S.F. (2017). *Neuroembryology*. Wiley Interdiscip. Rev. Dev. Biol. *6*.
- Dassule, H.R., Lewis, P., Bei, M., Maas, R., and McMahon, A.P. (2000). Sonic hedgehog regulates growth and morphogenesis of the tooth. *Dev. Camb. Engl.* *127*, 4775–4785.
- Davis, C.A., and Joyner, A.L. (1988). Expression patterns of the homeo box-containing genes *En-1* and *En-2* and the proto-oncogene *int-1* diverge during mouse development. *Genes Dev.* *2*, 1736–1744.
- Deane, J.A., Cole, D.G., Seeley, E.S., Diener, D.R., and Rosenbaum, J.L. (2001). Localization of intraflagellar transport protein IFT52 identifies basal body transitional fibers as the docking site for IFT particles. *Curr. Biol. CB* *11*, 1586–1590.
- Del Cerro, M.P., and Snider, R.S. (1972). Studies on the developing cerebellum. II. The ultrastructure of the external granular layer. *J. Comp. Neurol.* *144*, 131–164.
- Denu, R.A., Sass, M.M., Johnson, J.M., Potts, G.K., Choudhary, A., Coon, J.J., and Burkard, M.E. (2019). Polo-like kinase 4 maintains centriolar satellite integrity by phosphorylation of centrosomal protein 131 (CEP131). *J. Biol. Chem.* jbc.RA118.004867.

- Deshpande, I., Liang, J., Hedeem, D., Roberts, K.J., Zhang, Y., Ha, B., Latorraca, N.R., Faust, B., Dror, R.O., Beachy, P.A., et al. (2019). Smoothened stimulation by membrane sterols drives Hedgehog pathway activity. *Nature* *571*, 284–288.
- Di Marcotullio, L., Ferretti, E., De Smaele, E., Argenti, B., Mincione, C., Zazzeroni, F., Gallo, R., Masuelli, L., Napolitano, M., Maroder, M., et al. (2004). REN(KCTD11) is a suppressor of Hedgehog signaling and is deleted in human medulloblastoma. *Proc. Natl. Acad. Sci. U. S. A.* *101*, 10833–10838.
- Di Marcotullio, L., Ferretti, E., Greco, A., De Smaele, E., Po, A., Sico, M.A., Alimandi, M., Giannini, G., Maroder, M., Screpanti, I., et al. (2006a). Numb is a suppressor of Hedgehog signalling and targets Gli1 for Itch-dependent ubiquitination. *Nat. Cell Biol.* *8*, 1415–1423.
- Di Marcotullio, L., Ferretti, E., Greco, A., De Smaele, E., Po, A., Sico, M.A., Alimandi, M., Giannini, G., Maroder, M., Screpanti, I., et al. (2006b). Numb is a suppressor of Hedgehog signalling and targets Gli1 for Itch-dependent ubiquitination. *Nat. Cell Biol.* *8*, 1415–1423.
- Di Marcotullio, L., Greco, A., Mazzà, D., Canettieri, G., Pietrosanti, L., Infante, P., Coni, S., Moretti, M., De Smaele, E., Ferretti, E., et al. (2011). Numb activates the E3 ligase Itch to control Gli1 function through a novel degradation signal. *Oncogene* *30*, 65–76.
- Di Pietro, C., Marazziti, D., La Sala, G., Abbaszadeh, Z., Golini, E., Matteoni, R., and Tocchini-Valentini, G.P. (2017). Primary Cilia in the Murine Cerebellum and in Mutant Models of Medulloblastoma. *Cell. Mol. Neurobiol.* *37*, 145–154.
- Dijkgraaf, G.J.P., Aliche, B., Weinmann, L., Januario, T., West, K., Modrusan, Z., Burdick, D., Goldsmith, R., Robarge, K., Sutherlin, D., et al. (2011). Small molecule inhibition of GDC-0449 refractory smoothened mutants and downstream mechanisms of drug resistance. *Cancer Res.* *71*, 435–444.
- Dishinger, J.F., Kee, H.L., Jenkins, P.M., Fan, S., Hurd, T.W., Hammond, J.W., Truong, Y.N.-T., Margolis, B., Martens, J.R., and Verhey, K.J. (2010). Ciliary entry of the kinesin-2 motor KIF17 is regulated by importin- β 2 and RanGTP. *Nat. Cell Biol.* *12*, 703–710.
- Douanne, T., André-Grégoire, G., Thys, A., Trillet, K., Gavard, J., and Bidère, N. (2019). CYLD Regulates Centriolar Satellites Proteostasis by Counteracting the E3 Ligase MIB1. *Cell Rep.* *27*, 1657-1665.e4.
- Dudek, H., Datta, S.R., Franke, T.F., Birnbaum, M.J., Yao, R., Cooper, G.M., Segal, R.A., Kaplan, D.R., and Greenberg, M.E. (1997). Regulation of Neuronal Survival by the Serine-Threonine Protein Kinase Akt. *Science* *275*, 661–665.
- Duval, N., Daubas, P., Carbon, C.B. de, Cloment, C.S., Tinevez, J.-Y., Lopes, M., Ribes, V., and Robert, B. (2014). Msx1 and Msx2 act as essential activators of Atoh1 expression in the murine spinal cord. *Development* *141*, 1726–1736.
- Dwyer, J.R., Sever, N., Carlson, M., Nelson, S.F., Beachy, P.A., and Parhami, F. (2007). Oxysterols Are Novel Activators of the Hedgehog Signaling Pathway in Pluripotent Mesenchymal Cells. *J. Biol. Chem.* *282*, 8959–8968.
- Eberhart, C.G., Cohen, K.J., Tihan, T., Goldthwaite, P.T., and Burger, P.C. (2003). Medulloblastomas with systemic metastases: evaluation of tumor histopathology and clinical behavior in 23 patients. *J. Pediatr. Hematol. Oncol.* *25*, 198–203.

- Ebert, P.J., Timmer, J.R., Nakada, Y., Helms, A.W., Parab, P.B., Liu, Y., Hunsaker, T.L., and Johnson, J.E. (2003). Zic1 represses Math1 expression via interactions with the Math1 enhancer and modulation of Math1 autoregulation. *Development* 130, 1949–1959.
- Echelard, Y., Epstein, D.J., St-Jacques, B., Shen, L., Mohler, J., McMahon, J.A., and McMahon, A.P. (1993). Sonic hedgehog, a member of a family of putative signaling molecules, is implicated in the regulation of CNS polarity. *Cell* 75, 1417–1430.
- Eddison, M., Toole, L., Bell, E., and Wingate, R.J.T. (2004). Segmental identity and cerebellar granule cell induction in rhombomere 1. *BMC Biol.* 2, 14.
- Egeberg, D.L., Lethan, M., Manguso, R., Schneider, L., Awan, A., Jørgensen, T.S., Byskov, A.G., Pedersen, L.B., and Christensen, S.T. (2012). Primary cilia and aberrant cell signaling in epithelial ovarian cancer. *Cilia* 1, 15.
- Ellison, D.W. (2010). Childhood medulloblastoma: novel approaches to the classification of a heterogeneous disease. *Acta Neuropathol. (Berl.)* 120, 305–316.
- Ellison, D.W., Onilude, O.E., Lindsey, J.C., Lusher, M.E., Weston, C.L., Taylor, R.E., Pearson, A.D., Clifford, S.C., and United Kingdom Children’s Cancer Study Group Brain Tumour Committee (2005). beta-Catenin status predicts a favorable outcome in childhood medulloblastoma: the United Kingdom Children’s Cancer Study Group Brain Tumour Committee. *J. Clin. Oncol. Off. J. Am. Soc. Clin. Oncol.* 23, 7951–7957.
- Endoh-Yamagami, S., Evangelista, M., Wilson, D., Wen, X., Theunissen, J.-W., Phamluong, K., Davis, M., Scales, S.J., Solloway, M.J., de Sauvage, F.J., et al. (2009). The Mammalian Cos2 Homolog Kif7 Plays an Essential Role in Modulating Hh Signal Transduction during Development. *Curr. Biol.* 19, 1320–1326.
- Engel, B.D., Ishikawa, H., Wemmer, K.A., Geimer, S., Wakabayashi, K., Hirono, M., Craige, B., Pazour, G.J., Witman, G.B., Kamiya, R., et al. (2012). The role of retrograde intraflagellar transport in flagellar assembly, maintenance, and function. *J. Cell Biol.* 199, 151–167.
- Englund, C., Kowalczyk, T., Daza, R.A.M., Dagan, A., Lau, C., Rose, M.F., and Hevner, R.F. (2006). Unipolar Brush Cells of the Cerebellum Are Produced in the Rhombic Lip and Migrate through Developing White Matter. *J. Neurosci.* 26, 9184–9195.
- Espinosa, J.S., and Luo, L. (2008). Timing Neurogenesis and Differentiation. *J. Neurosci. Off. J. Soc. Neurosci.* 28, 2301–2312.
- Fan, X., Mikolaenko, I., Elhassan, I., Ni, X., Wang, Y., Ball, D., Brat, D.J., Perry, A., and Eberhart, C.G. (2004). Notch1 and notch2 have opposite effects on embryonal brain tumor growth. *Cancer Res.* 64, 7787–7793.
- Farwell, J.R., and Flannery, J.T. (1987). Adult occurrence of medulloblastoma. *Acta Neurochir. (Wien)* 86, 1–5.
- Fernandes, M., Antoine, M., and Hébert, J.M. (2012). SMAD4 is essential for generating subtypes of neurons during cerebellar development. *Dev. Biol.* 365, 82–90.

- Fernandez-L, A., Northcott, P.A., Dalton, J., Fraga, C., Ellison, D., Angers, S., Taylor, M.D., and Kenney, A.M. (2009). YAP1 is amplified and up-regulated in hedgehog-associated medulloblastomas and mediates Sonic hedgehog-driven neural precursor proliferation. *Genes Dev.* *23*, 2729–2741.
- Ferrante, M.I., Zullo, A., Barra, A., Bimonte, S., Messaddeq, N., Studer, M., Dollé, P., and Franco, B. (2006). Oral-facial-digital type I protein is required for primary cilia formation and left-right axis specification. *Nat. Genet.* *38*, 112–117.
- Firat-Karalar, E.N., Rauniyar, N., Yates, J.R., and Stearns, T. (2014). Proximity Interactions among Centrosome Components Identify Regulators of Centriole Duplication. *Curr. Biol.* *24*, 664–670.
- Fisch, C., and Dupuis-Williams, P. (2011). Ultrastructure of cilia and flagella - back to the future! *Biol. Cell* *103*, 249–270.
- Firat-Karalar, E.N., and Stearns, T. (2014). The centriole duplication cycle. *Philos. Trans. R. Soc. B Biol. Sci.* *369*.
- Flora, A., Klisch, T.J., Schuster, G., and Zoghbi, H.Y. (2009). Deletion of Atoh1 Disrupts Sonic Hedgehog Signaling in the Developing Cerebellum and Prevents Medulloblastoma. *Science* *326*, 1424.
- Florio, M., Leto, K., Muzio, L., Tinterri, A., Badaloni, A., Croci, L., Zordan, P., Barili, V., Albieri, I., Guillemot, F., et al. (2012). Neurogenin 2 regulates progenitor cell-cycle progression and Purkinje cell dendritogenesis in cerebellar development. *Dev. Camb. Engl.* *139*, 2308–2320.
- Follit, J.A., Tuft, R.A., Fogarty, K.E., and Pazour, G.J. (2006). The Intraflagellar Transport Protein IFT20 Is Associated with the Golgi Complex and Is Required for Cilia Assembly. *Mol. Biol. Cell* *17*, 3781–3792.
- Forget, A., Bihannic, L., Cigna, S.M., Lefevre, C., Remke, M., Barnat, M., Dodier, S., Shirvani, H., Mercier, A., Mensah, A., et al. (2014). Shh signaling protects Atoh1 from degradation mediated by the E3 ubiquitin ligase Huwe1 in neural precursors. *Dev. Cell* *29*, 649–661.
- Forget, A., Martignetti, L., Puget, S., Calzone, L., Brabetz, S., Picard, D., Montagud, A., Liva, S., Sta, A., Dingli, F., et al. (2018). Aberrant ERBB4-SRC Signaling as a Hallmark of Group 4 Medulloblastoma Revealed by Integrative Phosphoproteomic Profiling. *Cancer Cell* *34*, 379-395.e7.
- Frank-Kamenetsky, M., Zhang, X.M., Bottega, S., Guicherit, O., Wichterle, H., Dudek, H., Bumcrot, D., Wang, F.Y., Jones, S., Shulok, J., et al. (2002). Small-molecule modulators of Hedgehog signaling: identification and characterization of Smoothed agonists and antagonists. *J. Biol.* *1*, 10.
- Gajjar, A., Chintagumpala, M., Ashley, D., Kellie, S., Kun, L.E., Merchant, T.E., Woo, S., Wheeler, G., Ahern, V., Krasin, M.J., et al. (2006). Risk-adapted craniospinal radiotherapy followed by high-dose chemotherapy and stem-cell rescue in children with newly diagnosed medulloblastoma (St Jude Medulloblastoma-96): long-term results from a prospective, multicentre trial. *Lancet Oncol.* *7*, 813–820.
- Gallet, A., Ruel, L., Staccini-Lavenant, L., and Théron, P.P. (2006). Cholesterol modification is necessary for controlled planar long-range activity of Hedgehog in *Drosophila* epithelia. *Development* *133*, 407–418.

- Gallo, R., Zazzeroni, F., Alesse, E., Mincione, C., Borello, U., Buanne, P., D'Eugenio, R., Mackay, A.R., Argenti, B., Gradini, R., et al. (2002). REN: a novel, developmentally regulated gene that promotes neural cell differentiation. *J. Cell Biol.* *158*, 731–740.
- Gao, W.-Q., Heintz, N., and Hatten, M.E. (1991). Cerebellar granule cell neurogenesis is regulated by cell-cell interactions in vitro. *Neuron* *6*, 705–715.
- Garancher, A., Lin, C.Y., Morabito, M., Richer, W., Rocques, N., Larcher, M., Bihannic, L., Smith, K., Miquel, C., Leboucher, S., et al. (2018). NRL and CRX Define Photoreceptor Identity and Reveal Subgroup-Specific Dependencies in Medulloblastoma. *Cancer Cell* *33*, 435-449.e6.
- Garcia-Gonzalo, F.R., and Reiter, J.F. (2012). Scoring a backstage pass: mechanisms of ciliogenesis and ciliary access. *J. Cell Biol.* *197*, 697–709.
- Garcia-Gonzalo, F.R., Corbit, K.C., Simerol-Piquer, M.S., Ramaswami, G., Otto, E.A., Noriega, T.R., Seol, A.D., Robinson, J.F., Bennett, C.L., Josifova, D.J., et al. (2011). A transition zone complex regulates mammalian ciliogenesis and ciliary membrane composition. *Nat. Genet.* *43*, 776–784.
- Garzia, L., Kijima, N., Morrissy, A.S., De Antonellis, P., Guerreiro-Stucklin, A., Holgado, B.L., Wu, X., Wang, X., Parsons, M., Zayne, K., et al. (2018). A Hematogenous Route for Medulloblastoma Leptomeningeal Metastases. *Cell* *172*, 1050-1062.e14.
- Gavalas, A., Davenne, M., Lumsden, A., Chambon, P., and Rijli, F.M. (1997). Role of Hoxa-2 in axon pathfinding and rostral hindbrain patterning. *Dev. Camb. Engl.* *124*, 3693–3702.
- Gazit, R., Krizhanovsky, V., and Ben-Arie, N. (2004). Math1 controls cerebellar granule cell differentiation by regulating multiple components of the Notch signaling pathway. *Development* *131*, 903–913.
- Ge, X., Frank, C.L., Calderon de Anda, F., and Tsai, L.-H. (2010). Hook3 interacts with PCM1 to regulate pericentriolar material assembly and the timing of neurogenesis. *Neuron* *65*, 191–203.
- Geerts, W.J.C., Vocking, K., Schoonen, N., Haarbosch, L., van Donselaar, E.G., Regan-Klapisz, E., and Post, J.A. (2011). Cobblestone HUVECs: A human model system for studying primary ciliogenesis. *J. Struct. Biol.* *176*, 350–359.
- Genovesi, L.A., Ng, C.G., Davis, M.J., Remke, M., Taylor, M.D., Adams, D.J., Rust, A.G., Ward, J.M., Ban, K.H., Jenkins, N.A., et al. (2013). Sleeping Beauty mutagenesis in a mouse medulloblastoma model defines networks that discriminate between human molecular subgroups. *Proc. Natl. Acad. Sci.* *110*, E4325–E4334.
- Gheiratmand, L., Coyaud, E., Gupta, G.D., Laurent, E.M., Hasegan, M., Prosser, S.L., Gonçalves, J., Raught, B., and Pelletier, L. (2019). Spatial and proteomic profiling reveals centrosome-independent features of centriolar satellites. *EMBO J.*
- Ghossoub, R., Molla-Herman, A., Bastin, P., and Benmerah, A. (2011). The ciliary pocket: a once-forgotten membrane domain at the base of cilia. *Biol. Cell* *103*, 131–144.
- Gibbons, I.R., and Rowe, A.J. (1965). Dynein: A Protein with Adenosine Triphosphatase Activity from Cilia. *Science* *149*, 424.

Gibson, P., Tong, Y., Robinson, G., Thompson, M.C., Currie, D.S., Eden, C., Kranenburg, T.A., Hogg, T., Poppleton, H., Martin, J., et al. (2010). Subtypes of medulloblastoma have distinct developmental origins. *Nature* 468, 1095–1099.

Gilthorpe, J.D., Papantoniou, E.-K., Chédotal, A., Lumsden, A., and Wingate, R.J.T. (2002). The migration of cerebellar rhombic lip derivatives. *Development* 129, 4719–4728.

Gilula, N.B., and Satir, P. (1972). THE CILIARY NECKLACE: A Ciliary Membrane Specialization. *J. Cell Biol.* 53, 494–509.

Giordana, M.T., Schiffer, P., Lanotte, M., Girardi, P., and Chio, A. (1999). Epidemiology of adult medulloblastoma. *Int. J. Cancer* 80, 689–692.

Goodrich, L.V., Milenković, L., Higgins, K.M., and Scott, M.P. (1997). Altered neural cell fates and medulloblastoma in mouse patched mutants. *Science* 277, 1109–1113.

Gowan, K., Helms, A.W., Hunsaker, T.L., Collisson, T., Ebert, P.J., Odom, R., and Johnson, J.E. (2001). Crossinhibitory Activities of Ngn1 and Math1 Allow Specification of Distinct Dorsal Interneurons. *Neuron* 31, 219–232.

Graser, S., Stierhof, Y.-D., Lavoie, S.B., Gassner, O.S., Lamla, S., Le Clech, M., and Nigg, E.A. (2007). Cep164, a novel centriole appendage protein required for primary cilium formation. *J. Cell Biol.* 179, 321.

Grausam, K.B., Dooyema, S.D.R., Bihannic, L., Premathilake, H., Morrissy, A.S., Forget, A., Schaefer, A.M., Gundelach, J.H., Macura, S., Maher, D.M., et al. (2017). ATOH1 Promotes Leptomeningeal Dissemination and Metastasis of Sonic Hedgehog Subgroup Medulloblastomas. *Cancer Res.* 77, 3766–3777.

Guo, C., Qiu, H.-Y., Huang, Y., Chen, H., Yang, R.-Q., Chen, S.-D., Johnson, R.L., Chen, Z.-F., and Ding, Y.-Q. (2007). Lmx1b is essential for Fgf8 and Wnt1 expression in the isthmus organizer during tectum and cerebellum development in mice. *Dev. Camb. Engl.* 134, 317–325.

Gupta, G.D., Coyaud, É., Gonçalves, J., Mojarad, B.A., Liu, Y., Wu, Q., Gheiratmand, L., Comartin, D., Tkach, J.M., Cheung, S.W.T., et al. (2015). A Dynamic Protein Interaction Landscape of the Human Centrosome-Cilium Interface. *Cell* 163, 1484–1499.

Hahn, H., Wicking, C., Zaphiropoulos, P.G., Gailani, M.R., Shanley, S., Chidambaram, A., Vorechovsky, I., Holmberg, E., Uden, A.B., Gillies, S., et al. (1996). Mutations of the human homolog of *Drosophila* patched in the nevoid basal cell carcinoma syndrome. *Cell* 85, 841–851.

Hahn, H., Wojnowski, L., Specht, K., Kappler, R., Calzada-Wack, J., Potter, D., Zimmer, A., Müller, U., Samson, E., Quintanilla-Martinez, L., et al. (2000). Patched target Igf2 is indispensable for the formation of medulloblastoma and rhabdomyosarcoma. *J. Biol. Chem.* 275, 28341–28344.

Hallahan, A.R., Pritchard, J.I., Hansen, S., Benson, M., Stoeck, J., Hatton, B.A., Russell, T.L., Ellenbogen, R.G., Bernstein, I.D., Beachy, P.A., et al. (2004). The SmoA1 Mouse Model Reveals That Notch Signaling Is Critical for the Growth and Survival of Sonic Hedgehog-Induced Medulloblastomas. *Cancer Res.* 64, 7794–7800.

Han, K.-J., Wu, Z., Pearson, C.G., Peng, J., Song, K., and Liu, C.-W. (2019). Deubiquitylase USP9X maintains centriolar satellite integrity by stabilizing pericentriolar material 1 protein. *J. Cell Sci.* 132.

- Han, Y.-G., Kim, H.J., Dlugosz, A.A., Ellison, D.W., Gilbertson, R.J., and Alvarez-Buylla, A. (2009). Dual and opposing roles of primary cilia in medulloblastoma development. *Nat. Med.* *15*, 1062–1065.
- Hanaway, J. (1967). Formation and differentiation of the external granular layer of the chick cerebellum. *J. Comp. Neurol.* *131*, 1–14.
- Hardwick, L.J.A., Ali, F.R., Azzarelli, R., and Philpott, A. (2015). Cell cycle regulation of proliferation versus differentiation in the central nervous system. *Cell Tissue Res.* *359*, 187–200.
- Harris, L., Zalucki, O., and Piper, M. (2018). BrdU/EdU dual labeling to determine the cell-cycle dynamics of defined cellular subpopulations. *J. Mol. Histol.* *49*, 229–234.
- Hartmann, W., Koch, A., Brune, H., Waha, A., Schüller, U., Dani, I., Denkhaus, D., Langmann, W., Bode, U., Wiestler, O.D., et al. (2005). Insulin-like growth factor II is involved in the proliferation control of medulloblastoma and its cerebellar precursor cells. *Am. J. Pathol.* *166*, 1153–1162.
- Hatten, M.E., and Heintz, N. (1995). Mechanisms of neural patterning and specification in the developing cerebellum. *Annu. Rev. Neurosci.* *18*, 385–408.
- Helms, A.W., and Johnson, J.E. (1998). Progenitors of dorsal commissural interneurons are defined by MATH1 expression. *Development* *125*, 919–928.
- Helms, A.W., Abney, A.L., Ben-Arie, N., Zoghbi, H.Y., and Johnson, J.E. (2000). Autoregulation and multiple enhancers control Math1 expression in the developing nervous system. *Development* *127*, 1185–1196.
- Helms, A.W., Gowan, K., Abney, A., Savage, T., and Johnson, J.E. (2001). Overexpression of MATH1 Disrupts the Coordination of Neural Differentiation in Cerebellum Development. *Mol. Cell. Neurosci.* *17*, 671–682.
- Herculano-Houzel, S. (2010). Coordinated Scaling of Cortical and Cerebellar Numbers of Neurons. *Front. Neuroanat.* *4*.
- Hill, P., Wang, B., and Rüther, U. (2007). The molecular basis of Pallister Hall associated polydactyly. *Hum. Mol. Genet.* *16*, 2089–2096.
- Hill, R.M., Kuijper, S., Lindsey, J.C., Petrie, K., Schwalbe, E.C., Barker, K., Boulton, J.K.R., Williamson, D., Ahmad, Z., Hallsworth, A., et al. (2015). Combined MYC and P53 defects emerge at medulloblastoma relapse and define rapidly progressive, therapeutically targetable disease. *Cancer Cell* *27*, 72–84.
- Hoang-Minh, L.B., Deleyrolle, L.P., Nakamura, N.S., Parker, A.K., Martuscello, R.T., Reynolds, B.A., and Sarkisian, M.R. (2016). PCM1 Depletion Inhibits Glioblastoma Cell Ciliogenesis and Increases Cell Death and Sensitivity to Temozolomide. *Transl. Oncol.* *9*, 392–402.
- Hori, A., and Toda, T. (2017). Regulation of centriolar satellite integrity and its physiology. *Cell. Mol. Life Sci. CMLS* *74*, 213–229.
- Hori, A., Ikebe, C., Tada, M., and Toda, T. (2014). Msd1/SSX2IP-dependent microtubule anchorage ensures spindle orientation and primary cilia formation. *EMBO Rep.* *15*, 175–184.
- Hori, A., Barnouin, K., Snijders, A.P., and Toda, T. (2016). A non-canonical function of Plk4 in centriolar satellite integrity and ciliogenesis through PCM1 phosphorylation. *EMBO Rep.* *17*, 326–337.

- Hoshino, M., Nakamura, S., Mori, K., Kawauchi, T., Terao, M., Nishimura, Y.V., Fukuda, A., Fuse, T., Matsuo, N., Sone, M., et al. (2005). Ptf1a, a bHLH transcriptional gene, defines GABAergic neuronal fates in cerebellum. *Neuron* 47, 201–213.
- Hovestadt, V., Smith, K.S., Bihannic, L., Filbin, M.G., Shaw, M.L., Baumgartner, A., DeWitt, J.C., Groves, A., Mayr, L., Weisman, H.R., et al. (2019). Resolving medulloblastoma cellular architecture by single-cell genomics. *Nature* 1.
- Huang, D., Wang, Y., Tang, J., and Luo, S. (2018a). Molecular mechanisms of suppressor of fused in regulating the hedgehog signalling pathway. *Oncol. Lett.* 15, 6077–6086.
- Huang, N., Xia, Y., Zhang, D., Wang, S., Bao, Y., He, R., Teng, J., and Chen, J. (2017). Hierarchical assembly of centriole subdistal appendages via centrosome binding proteins CCDC120 and CCDC68. *Nat. Commun.* 8, 15057.
- Huang, P., Zheng, S., Wierbowski, B.M., Kim, Y., Nedelcu, D., Aravena, L., Liu, J., Kruse, A.C., and Salic, A. (2018b). The structural basis of Smoothed activation in Hedgehog signaling. *Cell* 174, 312–324.e16.
- Huangfu, D., Liu, A., Rakeman, A.S., Murcia, N.S., Niswander, L., and Anderson, K.V. (2003). Hedgehog signalling in the mouse requires intraflagellar transport proteins. *Nature* 426, 83–87.
- Huard, J.M., Forster, C.C., Carter, M.L., Sicinski, P., and Ross, M.E. (1999). Cerebellar histogenesis is disturbed in mice lacking cyclin D2. *Development* 126, 1927–1935.
- Humke, E.W., Dorn, K.V., Milenkovic, L., Scott, M.P., and Rohatgi, R. (2010). The output of Hedgehog signaling is controlled by the dynamic association between Suppressor of Fused and the Gli proteins. *Genes Dev.* 24, 670–682.
- Ibi, M., Zou, P., Inoko, A., Shiromizu, T., Matsuyama, M., Hayashi, Y., Enomoto, M., Mori, D., Hirotsune, S., Kiyono, T., et al. (2011). Trichoplein controls microtubule anchoring at the centrosome by binding to Odf2 and ninein. *J. Cell Sci.* 124, 857.
- Imayoshi, I., and Kageyama, R. (2014). bHLH Factors in Self-Renewal, Multipotency, and Fate Choice of Neural Progenitor Cells. *Neuron* 82, 9–23.
- Infante, P., Faedda, R., Bernardi, F., Bufalieri, F., Severini, L.L., Alfonsi, R., Mazzà, D., Siler, M., Coni, S., Po, A., et al. (2018). Itch/ β -arrestin2-dependent non-proteolytic ubiquitylation of SuFu controls Hedgehog signalling and medulloblastoma tumorigenesis. *Nat. Commun.* 9, 976.
- Inoue, F., Kurokawa, D., Takahashi, M., and Aizawa, S. (2012). Gbx2 Directly Restricts Otx2 Expression to Forebrain and Midbrain, Competing with Class III POU Factors. *Mol. Cell. Biol.* 32, 2618–2627.
- Insinna, C., Pathak, N., Perkins, B., Drummond, I., and Besharse, J.C. (2008). The homodimeric kinesin, Kif17, is essential for vertebrate photoreceptor sensory outer segment development. *Dev. Biol.* 316, 160–170.
- Insinna, C., Humby, M., Sedmak, T., Wolfrum, U., and Besharse, J.C. (2009). Different Roles For KIF17 and Kinesin II In Photoreceptor Development and Maintenance. *Dev. Dyn. Off. Publ. Am. Assoc. Anat.* 238, 2211–2222.

Ishikawa, H., and Marshall, W.F. (2017). Intraflagellar Transport and Ciliary Dynamics. *Cold Spring Harb. Perspect. Biol.* 9.

Ishikawa, H., Kubo, A., Tsukita, S., and Tsukita, S. (2005). Odf2-deficient mother centrioles lack distal/subdistal appendages and the ability to generate primary cilia. *Nat. Cell Biol.* 7, 517–524.

Ito, M. (2006). Cerebellar circuitry as a neuronal machine. *Prog. Neurobiol.* 78, 272–303.

Ito, M. (2013). Error detection and representation in the olivo-cerebellar system. *Front. Neural Circuits* 7.

Jahan, I., Pan, N., Kersigo, J., and Fritzscht, B. (2010). Neurod1 suppresses hair cell differentiation in ear ganglia and regulates hair cell subtype development in the cochlea. *PLoS One* 5, e11661.

Jakab, R.L., and Hátori, J. (1988). Quantitative morphology and synaptology of cerebellar glomeruli in the rat. *Anat. Embryol. (Berl.)* 179, 81–88.

Jenkins, P.M., Hurd, T.W., Zhang, L., McEwen, D.P., Brown, R.L., Margolis, B., Verhey, K.J., and Martens, J.R. (2006). Ciliary targeting of olfactory CNG channels requires the CNGB1b subunit and the kinesin-2 motor protein, KIF17. *Curr. Biol. CB* 16, 1211–1216.

Jenks, A.D., Vyse, S., Wong, J.P., Kostaras, E., Keller, D., Burgoyne, T., Shoemark, A., Tsalikis, A., de la Roche, M., Michaelis, M., et al. (2018). Primary Cilia Mediate Diverse Kinase Inhibitor Resistance Mechanisms in Cancer. *Cell Rep.* 23, 3042–3055.

Jessell, T.M. (2000). Neuronal specification in the spinal cord: inductive signals and transcriptional codes. *Nat. Rev. Genet.* 1, 20–29.

Jia, J., Tong, C., Wang, B., Luo, L., and Jiang, J. (2004). Hedgehog signalling activity of Smoothed requires phosphorylation by protein kinase A and casein kinase I. *Nature* 432, 1045–1050.

Jia, J., Zhang, L., Zhang, Q., Tong, C., Wang, B., Hou, F., Amanai, K., and Jiang, J. (2005). Phosphorylation by double-time/CKIepsilon and CKIalpha targets cubitus interruptus for Slimb/beta-TRCP-mediated proteolytic processing. *Dev. Cell* 9, 819–830.

Jiang, Y., Kumada, T., Cameron, D.B., and Komuro, H. (2008). Cerebellar granule cell migration and the effects of alcohol. *Dev. Neurosci.* 30, 7–23.

Jin, H., White, S.R., Shida, T., Schulz, S., Aguiar, M., Gygi, S.P., Bazan, J.F., and Nachury, M.V. (2010). The conserved Bardet-Biedl syndrome proteins assemble a coat that traffics membrane proteins to cilia. *Cell* 141, 1208–1219.

Johnson, R.L., Milenkovic, L., and Scott, M.P. (2000). In vivo functions of the patched protein: requirement of the C terminus for target gene inactivation but not Hedgehog sequestration. *Mol. Cell* 6, 467–478.

Johnston, D.L., Keene, D., Kostova, M., Strother, D., Lafay-Cousin, L., Fryer, C., Scheinemann, K., Carret, A.-S., Fleming, A., Percy, V., et al. (2014). Incidence of medulloblastoma in Canadian children. *J. Neurooncol.* 120, 575–579.

Jonassen, J.A., San Agustin, J., Follit, J.A., and Pazour, G.J. (2008). Deletion of IFT20 in the mouse kidney causes misorientation of the mitotic spindle and cystic kidney disease. *J. Cell Biol.* 183, 377–384.

Jones, D.T., Jäger, N., Kool, M., Zichner, T., Hutter, B., Sultan, M., Cho, Y.-J., Pugh, T.J., Hovestadt, V., Stütz, A.M., et al. (2012). ICGC PedBrain: Dissecting the genomic complexity underlying medulloblastoma. *Nature* 488, 100–105.

Julian, E., Hallahan, A.R., and Wainwright, B.J. (2010). RBP-J is not required for granule neuron progenitor development and medulloblastoma initiated by Hedgehog pathway activation in the external germinal layer. *Neural Develop.* 5, 27.

Kaplan, O.I., Doroquez, D.B., Cevik, S., Bowie, R.V., Clarke, L., Sanders, A.A.W.M., Kida, K., Rappoport, J.Z., Sengupta, P., and Blacque, O.E. (2012). Endocytosis genes facilitate protein and membrane transport in *C. elegans* sensory cilia. *Curr. Biol. CB* 22, 451–460.

Kawauchi, D., and Saito, T. (2008). Transcriptional cascade from Math1 to Mbh1 and Mbh2 is required for cerebellar granule cell differentiation. *Dev. Biol.* 322, 345–354.

Kawauchi, D., Robinson, G., Uziel, T., Gibson, P., Rehg, J., Gao, C., Finkelstein, D., Qu, C., Pounds, S., Ellison, D.W., et al. (2012). A mouse model of the most aggressive subgroup of human medulloblastoma. *Cancer Cell* 21, 168–180.

Kawauchi, D., Ogg, R.J., Liu, L., Shih, D.J.H., Finkelstein, D., Murphy, B.L., Rehg, J.E., Korshunov, A., Calabrese, C., Zindy, F., et al. (2017). Novel MYC-driven medulloblastoma models from multiple embryonic cerebellar cells. *Oncogene* 36, 5231–5242.

Keady, B.T., Samtani, R., Tobita, K., Tsuchya, M., San Agustin, J.T., Follit, J.A., Jonassen, J.A., Subramanian, R., Lo, C.W., and Pazour, G.J. (2012). IFT25 links the signal-dependent movement of Hedgehog components to intraflagellar transport. *Dev. Cell* 22, 940–951.

Kee, H.L., Dishinger, J.F., Lynne Blasius, T., Liu, C.-J., Margolis, B., and Verhey, K.J. (2012). A size-exclusion permeability barrier and nucleoporins characterize a ciliary pore complex that regulates transport into cilia. *Nat. Cell Biol.* 14, 431–437.

Kenney, A.M., and Rowitch, D.H. (2000). Sonic hedgehog promotes G(1) cyclin expression and sustained cell cycle progression in mammalian neuronal precursors. *Mol. Cell. Biol.* 20, 9055–9067.

Kenney, A.M., Cole, M.D., and Rowitch, D.H. (2003). Nmyc upregulation by sonic hedgehog signaling promotes proliferation in developing cerebellar granule neuron precursors. *Dev. Camb. Engl.* 130, 15–28.

Kenney, A.M., Widlund, H.R., and Rowitch, D.H. (2004). Hedgehog and PI-3 kinase signaling converge on Nmyc1 to promote cell cycle progression in cerebellar neuronal precursors. *Dev. Camb. Engl.* 131, 217–228.

Kervarrec, T., Samimi, M., Guyétant, S., Sarma, B., Chéret, J., Blanchard, E., Berthon, P., Schrama, D., Houben, R., and Touzé, A. (2019). Histogenesis of Merkel Cell Carcinoma: A Comprehensive Review. *Front. Oncol.* 9.

Keynes, R., and Krumlauf, R. (1994). Hox genes and regionalization of the nervous system. *Annu. Rev. Neurosci.* 17, 109–132.

Khanna, V., Achey, R.L., Ostrom, Q.T., Block-Beach, H., Kruchko, C., Barnholtz-Sloan, J.S., and de Blank, P.M. (2017). Incidence and survival trends for medulloblastomas in the United States from 2001 to 2013. *J. Neurooncol.* 135, 433–441.

- Kim, K., and Rhee, K. (2011). The pericentriolar satellite protein CEP90 is crucial for integrity of the mitotic spindle pole. *J. Cell Sci.* *124*, 338–347.
- Kim, D.H., Ahn, J.S., Han, H.J., Kim, H.-M., Hwang, J., Lee, K.H., Cha-Molstad, H., Ryoo, I.-J., Jang, J.-H., Ko, S.-K., et al. (2019a). Cep131 overexpression promotes centrosome amplification and colon cancer progression by regulating Plk4 stability. *Cell Death Dis.* *10*, 1–16.
- Kim, D.H., Kim, H.-M., Huong, P.T.T., Han, H.-J., Hwang, J., Cha-Molstad, H., Lee, K.H., Ryoo, I.-J., Kim, K.E., Huh, Y.H., et al. (2019b). Enhanced anticancer effects of a methylation inhibitor by inhibiting a novel DNMT1 target, CEP 131, in cervical cancer. *BMB Rep.* *52*, 342–347.
- Kim, J., Krishnaswami, S.R., and Gleeson, J.G. (2008). CEP290 interacts with the centriolar satellite component PCM-1 and is required for Rab8 localization to the primary cilium. *Hum. Mol. Genet.* *17*, 3796–3805.
- Kim, J., Kato, M., and Beachy, P.A. (2009). Gli2 trafficking links Hedgehog-dependent activation of Smoothened in the primary cilium to transcriptional activation in the nucleus. *Proc. Natl. Acad. Sci.* *106*, 21666–21671.
- Kim, J., Aftab, B.T., Tang, J.Y., Kim, D., Lee, A.H., Rezaee, M., Kim, J., Chen, B., King, E.M., Borodovsky, A., et al. (2013). Itraconazole and arsenic trioxide inhibit Hedgehog pathway activation and tumor growth associated with acquired resistance to smoothened antagonists. *Cancer Cell* *23*, 23–34.
- Kim, J., Hsia, E.Y.C., Brigui, A., Plessis, A., Beachy, P.A., and Zheng, X. (2015a). The role of ciliary trafficking in Hedgehog receptor signaling. *Sci. Signal.* *8*, ra55.
- Kim, J.C., Badano, J.L., Sibold, S., Esmail, M.A., Hill, J., Hoskins, B.E., Leitch, C.C., Venner, K., Ansley, S.J., Ross, A.J., et al. (2004). The Bardet-Biedl protein BBS4 targets cargo to the pericentriolar region and is required for microtubule anchoring and cell cycle progression. *Nat. Genet.* *36*, 462.
- Kim, S., Lee, K., Choi, J.-H., Ringstad, N., and Dynlacht, B.D. (2015b). Nek2 activation of Kif24 ensures cilium disassembly during the cell cycle. *Nat. Commun.* *6*, 8087.
- Kinzler, K.W., and Vogelstein, B. (1990). The GLI gene encodes a nuclear protein which binds specific sequences in the human genome. *Mol. Cell. Biol.* *10*, 634–642.
- Kinzler, K.W., Ruppert, J.M., Bigner, S.H., and Vogelstein, B. (1988). The GLI gene is a member of the Kruppel family of zinc finger proteins. *Nature* *332*, 371–374.
- Kise, Y., Morinaka, A., Teglund, S., and Miki, H. (2009). Sufu recruits GSK3beta for efficient processing of Gli3. *Biochem. Biophys. Res. Commun.* *387*, 569–574.
- Klein, A.-L., Zilian, O., Suter, U., and Taylor, V. (2004). Murine numb regulates granule cell maturation in the cerebellum. *Dev. Biol.* *266*, 161–177.
- Klein, R.S., Rubin, J.B., Gibson, H.D., DeHaan, E.N., Alvarez-Hernandez, X., Segal, R.A., and Luster, A.D. (2001). SDF-1 α induces chemotaxis and enhances Sonic hedgehog-induced proliferation of cerebellar granule cells. *Development* *128*, 1971–1981.
- Klinger, M., Wang, W., Kuhns, S., Bärenz, F., Dräger-Meurer, S., Pereira, G., and Gruss, O.J. (2014). The novel centriolar satellite protein SSX2IP targets Cep290 to the ciliary transition zone. *Mol. Biol. Cell* *25*, 495–507.

- Klisch, T.J., Xi, Y., Flora, A., Wang, L., Li, W., and Zoghbi, H.Y. (2011). In vivo Atoh1 targetome reveals how a proneural transcription factor regulates cerebellar development. *Proc. Natl. Acad. Sci.* *108*, 3288.
- Knoepfler, P.S., Cheng, P.F., and Eisenman, R.N. (2002). N-myc is essential during neurogenesis for the rapid expansion of progenitor cell populations and the inhibition of neuronal differentiation. *Genes Dev.* *16*, 2699–2712.
- Kobayashi, T., Tsang, W.Y., Li, J., Lane, W., and Dynlacht, B.D. (2011). Centriolar kinesin Kif24 interacts with CP110 to remodel microtubules and regulate ciliogenesis. *Cell* *145*, 914–925.
- Kobayashi, T., Kim, S., Lin, Y.-C., Inoue, T., and Dynlacht, B.D. (2014). The CP110-interacting proteins Talpid3 and Cep290 play overlapping and distinct roles in cilia assembly. *J. Cell Biol.* *204*, 215–229.
- Kobilka, B.K. (2007). G Protein Coupled Receptor Structure and Activation. *Biochim. Biophys. Acta* *1768*, 794–807.
- Kodani, A., Tonthat, V., Wu, B., and Sütterlin, C. (2010). Par6 α Interacts with the Dynactin Subunit p150Glued and Is a Critical Regulator of Centrosomal Protein Recruitment. *Mol. Biol. Cell* *21*, 3376–3385.
- Kodani, A., Yu, T.W., Johnson, J.R., Jayaraman, D., Johnson, T.L., Al-Gazali, L., Sztriha, L., Partlow, J.N., Kim, H., Krup, A.L., et al. (2015). Centriolar satellites assemble centrosomal microcephaly proteins to recruit CDK2 and promote centriole duplication. *ELife* *4*, e07519.
- Komuro, H., and Rakic, P. (1992). Selective role of N-type calcium channels in neuronal migration. *Science* *257*, 806–809.
- Komuro, H., and Rakic, P. (1993). Modulation of neuronal migration by NMDA receptors. *Science* *260*, 95–97.
- Komuro, H., and Rakic, P. (1995). Dynamics of granule cell migration: a confocal microscopic study in acute cerebellar slice preparations. *J. Neurosci. Off. J. Soc. Neurosci.* *15*, 1110–1120.
- Komuro, H., and Rakic, P. (1996). Intracellular Ca²⁺ fluctuations modulate the rate of neuronal migration. *Neuron* *17*, 275–285.
- Komuro, H., and Rakic, P. (1998). Distinct modes of neuronal migration in different domains of developing cerebellar cortex. *J. Neurosci. Off. J. Soc. Neurosci.* *18*, 1478–1490.
- Komuro, H., Yacubova, E., Yacubova, E., and Rakic, P. (2001). Mode and tempo of tangential cell migration in the cerebellar external granular layer. *J. Neurosci. Off. J. Soc. Neurosci.* *21*, 527–540.
- Kong, J.H., Siebold, C., and Rohatgi, R. (2019). Biochemical mechanisms of vertebrate hedgehog signaling. *Development* *146*, dev166892.
- Kool, M., Koster, J., Bunt, J., Hasselt, N.E., Lakeman, A., Sluis, P. van, Troost, D., Meeteren, N.S., Caron, H.N., Cloos, J., et al. (2008). Integrated Genomics Identifies Five Medulloblastoma Subtypes with Distinct Genetic Profiles, Pathway Signatures and Clinicopathological Features. *PLOS ONE* *3*, e3088.
- Kool, M., Korshunov, A., Remke, M., Jones, D.T.W., Schlanstein, M., Northcott, P.A., Cho, Y.-J., Koster, J., Schouten-van Meeteren, A., van Vuurden, D., et al. (2012). Molecular subgroups of

medulloblastoma: an international meta-analysis of transcriptome, genetic aberrations, and clinical data of WNT, SHH, Group 3, and Group 4 medulloblastomas. *Acta Neuropathol. (Berl.)* **123**, 473–484.

Kool, M., Jones, D.T.W., Jäger, N., Northcott, P.A., Pugh, T.J., Hovestadt, V., Piro, R.M., Esparza, L.A., Markant, S.L., Remke, M., et al. (2014). Genome sequencing of SHH medulloblastoma predicts genotype-related response to smoothed inhibition. *Cancer Cell* **25**, 393–405.

Kortmann, R.D., Kühl, J., Timmermann, B., Mittler, U., Urban, C., Budach, V., Richter, E., Willich, N., Flentje, M., Berthold, F., et al. (2000). Postoperative neoadjuvant chemotherapy before radiotherapy as compared to immediate radiotherapy followed by maintenance chemotherapy in the treatment of medulloblastoma in childhood: results of the German prospective randomized trial HIT '91. *Int. J. Radiat. Oncol. Biol. Phys.* **46**, 269–279.

Kovacs, J.J., Whalen, E.J., Liu, R., Xiao, K., Kim, J., Chen, M., Wang, J., Chen, W., and Lefkowitz, R.J. (2008). β -Arrestin-Mediated Localization of Smoothed to the Primary Cilium. *Science* **320**, 1777–1781.

Kozminski, K.G., Johnson, K.A., Forscher, P., and Rosenbaum, J.L. (1993). A motility in the eukaryotic flagellum unrelated to flagellar beating. *Proc. Natl. Acad. Sci. U. S. A.* **90**, 5519–5523.

Kozminski, K.G., Beech, P.L., and Rosenbaum, J.L. (1995). The *Chlamydomonas* kinesin-like protein FLA10 is involved in motility associated with the flagellar membrane. *J. Cell Biol.* **131**, 1517–1527.

Krämer, A., Neben, K., and Ho, A.D. (2002). Centrosome replication, genomic instability and cancer. *Leukemia* **16**, 767–775.

Kubo, A., and Tsukita, S. (2003). Non-membranous granular organelle consisting of PCM-1: subcellular distribution and cell-cycle-dependent assembly/disassembly. *J. Cell Sci.* **116**, 919–928.

Kubo, A., Sasaki, H., Yuba-Kubo, A., Tsukita, S., and Shiina, N. (1999). Centriolar satellites: molecular characterization, ATP-dependent movement toward centrioles and possible involvement in ciliogenesis. *J. Cell Biol.* **147**, 969–980.

Kumada, T., and Komuro, H. (2004). Completion of neuronal migration regulated by loss of Ca(2+) transients. *Proc. Natl. Acad. Sci. U. S. A.* **101**, 8479–8484.

Kumada, T., Jiang, Y., Cameron, D.B., and Komuro, H. (2007). How does alcohol impair neuronal migration? *J. Neurosci. Res.* **85**, 465–470.

Lai Wing Sun, K., Correia, J.P., and Kennedy, T.E. (2011). Netrins: versatile extracellular cues with diverse functions. *Dev. Camb. Engl.* **138**, 2153–2169.

Lainé, J., and Axelrad, H. (1994). The candelabrum cell: a new interneuron in the cerebellar cortex. *J. Comp. Neurol.* **339**, 159–173.

Lanford, P.J., Lan, Y., Jiang, R., Lindsell, C., Weinmaster, G., Gridley, T., and Kelley, M.W. (1999). Notch signalling pathway mediates hair cell development in mammalian cochlea. *Nat. Genet.* **21**, 289–292.

Lange, C., Huttner, W.B., and Calegari, F. (2009). Cdk4/cyclinD1 overexpression in neural stem cells shortens G1, delays neurogenesis, and promotes the generation and expansion of basal progenitors. *Cell Stem Cell* **5**, 320–331.

- Lasorella, A., Stegmüller, J., Guardavaccaro, D., Liu, G., Carro, M.S., Rothschild, G., Torre-Ubieta, L. de la, Pagano, M., Bonni, A., and Iavarone, A. (2006). Degradation of Id2 by the anaphase-promoting complex couples cell cycle exit and axonal growth. *Nature* *442*, 471–474.
- Lehtreck, K.F. (2015). IFT-cargo interactions and protein transport in cilia. *Trends Biochem. Sci.* *40*, 765–778.
- Lehtreck, K.-F., Johnson, E.C., Sakai, T., Cochran, D., Ballif, B.A., Rush, J., Pazour, G.J., Ikebe, M., and Witman, G.B. (2009). The *Chlamydomonas reinhardtii* BBSome is an IFT cargo required for export of specific signaling proteins from flagella. *J. Cell Biol.* *187*, 1117–1132.
- Lehtreck, K.F., Brown, J.M., Sampaio, J.L., Craft, J.M., Shevchenko, A., Evans, J.E., and Witman, G.B. (2013). Cycling of the signaling protein phospholipase D through cilia requires the BBSome only for the export phase. *J. Cell Biol.* *201*, 249–261.
- Lee, J.Y., and Stearns, T. (2013). FOP Is a Centriolar Satellite Protein Involved in Ciliogenesis. *PLoS ONE* *8*.
- Lee, J.J., Ekker, S.C., von Kessler, D.P., Porter, J.A., Sun, B.I., and Beachy, P.A. (1994). Autoproteolysis in hedgehog protein biogenesis. *Science* *266*, 1528–1537.
- Lee, K.J., Mendelsohn, M., and Jessell, T.M. (1998). Neuronal patterning by BMPs: a requirement for GDF7 in the generation of a discrete class of commissural interneurons in the mouse spinal cord. *Genes Dev.* *12*, 3394–3407.
- Lee, S., Jeong, H.-S., and Cho, H.-H. (2017). *Atoh1* as a Coordinator of Sensory Hair Cell Development and Regeneration in the Cochlea. *Chonnam Med. J.* *53*, 37–46.
- Lee, Y., Miller, H.L., Jensen, P., Hernan, R., Connelly, M., Wetmore, C., Zindy, F., Roussel, M.F., Curran, T., Gilbertson, R.J., et al. (2003). A Molecular Fingerprint for Medulloblastoma. *Cancer Res.* *63*, 5428–5437.
- Lee, Y., Kawagoe, R., Sasai, K., Li, Y., Russell, H.R., Curran, T., and McKinnon, P.J. (2007). Loss of suppressor-of-fused function promotes tumorigenesis. *Oncogene* *26*, 6442–6447.
- Leow, C.C., Romero, M.S., Ross, S., Polakis, P., and Gao, W.-Q. (2004). *Hath1*, Down-Regulated in Colon Adenocarcinomas, Inhibits Proliferation and Tumorigenesis of Colon Cancer Cells. *Cancer Res.* *64*, 6050–6057.
- Leto, K., Carletti, B., Williams, I.M., Magrassi, L., and Rossi, F. (2006). Different types of cerebellar GABAergic interneurons originate from a common pool of multipotent progenitor cells. *J. Neurosci. Off. J. Soc. Neurosci.* *26*, 11682–11694.
- Leung, C., Lingbeek, M., Shakhova, O., Liu, J., Tanger, E., Saremaslani, P., Van Lohuizen, M., and Marino, S. (2004). *Bmi1* is essential for cerebellar development and is overexpressed in human medulloblastomas. *Nature* *428*, 337–341.
- Levine, M.S., Bakker, B., Boeckx, B., Moyett, J., Lu, J., Vitre, B., Spierings, D.C., Lansdorp, P.M., Cleveland, D.W., Lambrechts, D., et al. (2017). Centrosome Amplification Is Sufficient to Promote Spontaneous Tumorigenesis in Mammals. *Dev. Cell* *40*, 313-322.e5.

- Lewis, P.M., Dunn, M.P., McMahon, J.A., Logan, M., Martin, J.F., St-Jacques, B., and McMahon, A.P. (2001). Cholesterol modification of sonic hedgehog is required for long-range signaling activity and effective modulation of signaling by Ptc1. *Cell* *105*, 599–612.
- Lewis, P.M., Gritli-Linde, A., Smeyne, R., Kottmann, A., and McMahon, A.P. (2004). Sonic hedgehog signaling is required for expansion of granule neuron precursors and patterning of the mouse cerebellum. *Dev. Biol.* *270*, 393–410.
- Li, L., Grausam, K.B., Wang, J., Lun, M.P., Ohli, J., Lidov, H.G.W., Calicchio, M.L., Zeng, E., Salisbury, J.L., Wechsler-Reya, R.J., et al. (2016). Sonic Hedgehog promotes proliferation of Notch-dependent monociliated choroid plexus tumour cells. *Nat. Cell Biol.* *18*, 418–430.
- Li, X., Song, N., Liu, L., Liu, X., Ding, X., Song, X., Yang, S., Shan, L., Zhou, X., Su, D., et al. (2017). USP9X regulates centrosome duplication and promotes breast carcinogenesis. *Nat. Commun.* *8*, 14866.
- Li, Y., Zhang, H., Litingtung, Y., and Chiang, C. (2006). Cholesterol modification restricts the spread of Shh gradient in the limb bud. *Proc. Natl. Acad. Sci. U. S. A.* *103*, 6548–6553.
- Liang, Y., Pang, Y., Wu, Q., Hu, Z., Han, X., Xu, Y., Deng, H., and Pan, J. (2014). FLA8/KIF3B phosphorylation regulates kinesin-II interaction with IFT-B to control IFT entry and turnaround. *Dev. Cell* *30*, 585–597.
- Liem, K.F., He, M., Ocbina, P.J.R., and Anderson, K.V. (2009). Mouse Kif7/Costal2 is a cilia-associated protein that regulates Sonic hedgehog signaling. *Proc. Natl. Acad. Sci. U. S. A.* *106*, 13377–13382.
- Liem, K.F., Ashe, A., He, M., Satir, P., Moran, J., Beier, D., Wicking, C., and Anderson, K.V. (2012). The IFT-A complex regulates Shh signaling through cilia structure and membrane protein trafficking. *J. Cell Biol.* *197*, 789–800.
- Liew, G.M., Ye, F., Nager, A.R., Murphy, J.P., Lee, J.S., Aguiar, M., Breslow, D.K., Gygi, S.P., and Nachury, M.V. (2014). The intraflagellar transport protein IFT27 promotes BBSome exit from cilia through the GTPase ARL6/BBS3. *Dev. Cell* *31*, 265–278.
- Lin, X., and Bulleit, R.F. (1997). Insulin-like growth factor I (IGF-I) is a critical trophic factor for developing cerebellar granule cells. *Dev. Brain Res.* *99*, 234–242.
- Lin, Y.-C., Niewiadomski, P., Lin, B., Nakamura, H., Phua, S.C., Jiao, J., Levchenko, A., Inoue, T., Rohatgi, R., and Inoue, T. (2013). Chemically inducible diffusion trap at cilia reveals molecular sieve-like barrier. *Nat. Chem. Biol.* *9*, 437–443.
- Lin, Z., Li, S., Sheng, H., Cai, M., Ma, L.Y.S., Hu, L., Xu, S., Yu, L.S., and Zhang, N. (2016). Suppression of GLI sensitizes medulloblastoma cells to mitochondria-mediated apoptosis. *J. Cancer Res. Clin. Oncol.* *142*, 2469–2478.
- Lindemann, C.B., and Lesich, K.A. (2010). Flagellar and ciliary beating: the proven and the possible. *J. Cell Sci.* *123*, 519.
- Liu, A., Losos, K., and Joyner, A.L. (1999). FGF8 can activate Gbx2 and transform regions of the rostral mouse brain into a hindbrain fate. *Dev. Camb. Engl.* *126*, 4827–4838.
- Liu, A., Wang, B., and Niswander, L.A. (2005). Mouse intraflagellar transport proteins regulate both the activator and repressor functions of Gli transcription factors. *Dev. Camb. Engl.* *132*, 3103–3111.

- Liu, H., Kiseleva, A.A., and Golemis, E.A. (2018). Ciliary signaling in cancer. *Nat. Rev. Cancer* *18*, 511–524.
- Liu, X.-H., Yang, Y.-F., Fang, H.-Y., Wang, X.-H., Zhang, M.-F., and Wu, D.-C. (2017). CEP131 indicates poor prognosis and promotes cell proliferation and migration in hepatocellular carcinoma. *Int. J. Biochem. Cell Biol.* *90*, 1–8.
- Lo, Y.-H., Chung, E., Li, Z., Wan, Y.-W., Mahe, M.M., Chen, M.-S., Noah, T.K., Bell, K.N., Yalamanchili, H.K., Klisch, T.J., et al. (2016). Transcriptional Regulation by ATOH1 and its Target SPDEF in the Intestine. *Cell. Mol. Gastroenterol. Hepatol.* *3*, 51–71.
- Loktev, A.V., Zhang, Q., Beck, J.S., Searby, C.C., Scheetz, T.E., Bazan, J.F., Slusarski, D.C., Sheffield, V.C., Jackson, P.K., and Nachury, M.V. (2008). A BBSome subunit links ciliogenesis, microtubule stability, and acetylation. *Dev. Cell* *15*, 854–865.
- Long, J., Li, B., Rodriguez-Blanco, J., Pastori, C., Volmar, C.-H., Wahlestedt, C., Capobianco, A., Bai, F., Pei, X.-H., Ayad, N.G., et al. (2014). The BET Bromodomain Inhibitor I-BET151 Acts Downstream of Smoothed Protein to Abrogate the Growth of Hedgehog Protein-driven Cancers. *J. Biol. Chem.* *289*, 35494–35502.
- Lopes, C.A.M., Prosser, S.L., Romio, L., Hirst, R.A., O’Callaghan, C., Woolf, A.S., and Fry, A.M. (2011). Centriolar satellites are assembly points for proteins implicated in human ciliopathies, including oral-facial-digital syndrome 1. *J. Cell Sci.* *124*, 600–612.
- Louis, D.N., Perry, A., Reifenberger, G., von Deimling, A., Figarella-Branger, D., Cavenee, W.K., Ohgaki, H., Wiestler, O.D., Kleihues, P., and Ellison, D.W. (2016). The 2016 World Health Organization Classification of Tumors of the Central Nervous System: a summary. *Acta Neuropathol. (Berl.)* *131*, 803–820.
- Lu, Q., Sun, E.E., Klein, R.S., and Flanagan, J.G. (2001). Ephrin-B Reverse Signaling Is Mediated by a Novel PDZ-RGS Protein and Selectively Inhibits G Protein–Coupled Chemoattraction. *Cell* *105*, 69–79.
- Ma, M., Wu, W., Li, Q., Li, J., Sheng, Z., Shi, J., Zhang, M., Yang, H., Wang, Z., Sun, R., et al. (2015). N-myc is a key switch regulating the proliferation cycle of postnatal cerebellar granule cell progenitors. *Sci. Rep.* *5*, 12740.
- Ma, Y.-C., Song, M.-R., Park, J.P., Henry Ho, H.-Y., Hu, L., Kurtev, M.V., Zieg, J., Ma, Q., Pfaff, S.L., and Greenberg, M.E. (2008). Regulation of Motor Neuron Specification by Phosphorylation of Neurogenin 2. *Neuron* *58*, 65–77.
- MacDonald, T.J., Aguilera, D., and Castellino, R.C. (2014). The rationale for targeted therapies in medulloblastoma. *Neuro-Oncol.* *16*, 9–20.
- Machold, R., and Fishell, G. (2005). Math1 is expressed in temporally discrete pools of cerebellar rhombic-lip neural progenitors. *Neuron* *48*, 17–24.
- Machold, R.P., Kittell, D.J., and Fishell, G.J. (2007). Antagonism between Notch and bone morphogenetic protein receptor signaling regulates neurogenesis in the cerebellar rhombic lip. *Neural Develop.* *2*, 5.

- Macûrek, L., Lindqvist, A., Lim, D., Lampson, M.A., Klompaker, R., Freire, R., Clouin, C., Taylor, S.S., Yaffe, M.B., and Medema, R.H. (2008). Polo-like kinase-1 is activated by aurora A to promote checkpoint recovery. *Nature* *455*, 119–123.
- Malicki, J., and Avidor-Reiss, T. (2014). From the cytoplasm into the cilium: Bon voyage. *Organogenesis* *10*, 138–157.
- Manni, E., and Petrosini, L. (2004). A century of cerebellar somatotopy: a debated representation. *Nat. Rev. Neurosci.* *5*, 241–249.
- Mao, J., Ligon, K.L., Rakhlin, E.Y., Thayer, S.P., Bronson, R.T., Rowitch, D., and McMahon, A.P. (2006). A novel somatic mouse model to survey tumorigenic potential applied to the Hedgehog pathway. *Cancer Res.* *66*, 10171–10178.
- Maricich, S.M., and Herrup, K. (1999). Pax-2 expression defines a subset of GABAergic interneurons and their precursors in the developing murine cerebellum. *J. Neurobiol.* *41*, 281–294.
- Marigo, V., Davey, R.A., Zuo, Y., Cunningham, J.M., and Tabin, C.J. (1996). Biochemical evidence that Patched is the Hedgehog receptor. *Nature* *384*, 176.
- Marillat, V., Cases, O., Nguyen-Ba-Charvet, K.T., Tessier-Lavigne, M., Sotelo, C., and Chédotal, A. (2002). Spatiotemporal expression patterns of slit and robo genes in the rat brain. *J. Comp. Neurol.* *442*, 130–155.
- Marin, F., and Puellas, L. (1994). Patterning of the embryonic avian midbrain after experimental inversions: a polarizing activity from the isthmus. *Dev. Biol.* *163*, 19–37.
- Martin, A.M., Raabe, E., Eberhart, C., and Cohen, K.J. (2014). Management of Pediatric and Adult Patients with Medulloblastoma. *Curr. Treat. Options Oncol.* *15*, 581–594.
- Martinez, S., Wassef, M., and Alvarado-Mallart, R.M. (1991). Induction of a mesencephalic phenotype in the 2-day-old chick prosencephalon is preceded by the early expression of the homeobox gene *en*. *Neuron* *6*, 971–981.
- Martínez, S., Marín, F., Nieto, M.A., and Puellas, L. (1995). Induction of ectopic engrailed expression and fate change in avian rhombomeres: intersegmental boundaries as barriers. *Mech. Dev.* *51*, 289–303.
- Martinez, S., Crossley, P.H., Cobos, I., Rubenstein, J.L., and Martin, G.R. (1999). FGF8 induces formation of an ectopic isthmus organizer and isthmocerebellar development via a repressive effect on *Otx2* expression. *Dev. Camb. Engl.* *126*, 1189–1200.
- Martinez, S., Andreu, A., Mecklenburg, N., and Echevarria, D. (2013). Cellular and molecular basis of cerebellar development. *Front. Neuroanat.* *7*.
- Marzban, H., Del Bigio, M.R., Alizadeh, J., Ghavami, S., Zachariah, R.M., and Rastegar, M. (2015). Cellular commitment in the developing cerebellum. *Front. Cell. Neurosci.* *8*.
- Massari, M.E., and Murre, C. (2000). Helix-Loop-Helix Proteins: Regulators of Transcription in Eucaryotic Organisms. *Mol. Cell. Biol.* *20*, 429–440.
- Matsunaga, E., Katahira, T., and Nakamura, H. (2002). Role of *Lmx1b* and *Wnt1* in mesencephalon and metencephalon development. *Dev. Camb. Engl.* *129*, 5269–5277.

- Mazelova, J., Astuto-Gribble, L., Inoue, H., Tam, B.M., Schonteich, E., Prekeris, R., Moritz, O.L., Randazzo, P.A., and Deretic, D. (2009). Ciliary targeting motif VxPx directs assembly of a trafficking module through Arf4. *EMBO J.* *28*, 183–192.
- McCleary-Wheeler, A.L. (2014). From Normal Development to Disease: The Biochemistry and Regulation of GLI2. *Med. Epigenetics* *2*, 1–19.
- McMahon, A.P., and Bradley, A. (1990). The Wnt-1 (int-1) proto-oncogene is required for development of a large region of the mouse brain. *Cell* *62*, 1073–1085.
- Merchant, T.E., Kun, L.E., Krasin, M.J., Wallace, D., Chintagumpala, M.M., Woo, S.Y., Ashley, D.M., Sexton, M., Kellie, S.J., Ahern, V., et al. (2008). Multi-institution prospective trial of reduced-dose craniospinal irradiation (23.4 Gy) followed by conformal posterior fossa (36 Gy) and primary site irradiation (55.8 Gy) and dose-intensive chemotherapy for average-risk medulloblastoma. *Int. J. Radiat. Oncol. Biol. Phys.* *70*, 782–787.
- Miale, I.L., and Sidman, R.L. (1961). An autoradiographic analysis of histogenesis in the mouse cerebellum. *Exp. Neurol.* *4*, 277–296.
- Mills, J., Niewmierzycka, A., Oloumi, A., Rico, B., St-Arnaud, R., Mackenzie, I.R., Mawji, N.M., Wilson, J., Reichardt, L.F., and Dedhar, S. (2006). Critical role of integrin-linked kinase in granule cell precursor proliferation and cerebellar development. *J. Neurosci. Off. J. Soc. Neurosci.* *26*, 830–840.
- Mirvis, M., Stearns, T., and James Nelson, W. (2018). Cilium structure, assembly, and disassembly regulated by the cytoskeleton. *Biochem. J.* *475*, 2329.
- Miyazawa, K., Himi, T., Garcia, V., Yamagishi, H., Sato, S., and Ishizaki, Y. (2000). A role for p27/Kip1 in the control of cerebellar granule cell precursor proliferation. *J. Neurosci. Off. J. Soc. Neurosci.* *20*, 5756–5763.
- Mizutani, K., Yoon, K., Dang, L., Tokunaga, A., and Gaiano, N. (2007). Differential Notch signalling distinguishes neural stem cells from intermediate progenitors. *Nature* *449*, 351–355.
- Molla-Herman, A., Ghossoub, R., Blisnick, T., Meunier, A., Serres, C., Silbermann, F., Emmerson, C., Romeo, K., Bourdoncle, P., Schmitt, A., et al. (2010). The ciliary pocket: an endocytic membrane domain at the base of primary and motile cilia. *J. Cell Sci.* *123*, 1785–1795.
- Morrissy, A.S., Garzia, L., Shih, D.J.H., Zuyderduyn, S., Huang, X., Skowron, P., Remke, M., Cavalli, F.M.G., Ramaswamy, V., Lindsay, P.E., et al. (2016). Divergent clonal selection dominates medulloblastoma at recurrence. *Nature* *529*, 351–357.
- Mourão, A., Nager, A.R., Nachury, M.V., and Lorentzen, E. (2014). Structural basis for membrane targeting of the BBSome by ARL6. *Nat. Struct. Mol. Biol.* *21*, 1035–1041.
- Moxon-Emre, I., Bouffet, E., Taylor, M.D., Laperriere, N., Scantlebury, N., Law, N., Spiegler, B.J., Malkin, D., Janzen, L., and Mabbott, D. (2014). Impact of craniospinal dose, boost volume, and neurologic complications on intellectual outcome in patients with medulloblastoma. *J. Clin. Oncol. Off. J. Am. Soc. Clin. Oncol.* *32*, 1760–1768.
- Mueller, J., Perrone, C.A., Bower, R., Cole, D.G., and Porter, M.E. (2004). The FLA3 KAP Subunit Is Required for Localization of Kinesin-2 to the Site of Flagellar Assembly and Processive Anterograde Intraflagellar Transport. *Mol. Biol. Cell* *16*, 1341–1354.

- Mukhopadhyay, S., and Rohatgi, R. (2014). G-protein—coupled receptors, hedgehog signaling and primary cilia. *Semin. Cell Dev. Biol.* *0*, 63–72.
- Mukhopadhyay, S., Wen, X., Ratti, N., Loktev, A., Rangell, L., Scales, S.J., and Jackson, P.K. (2013). The ciliary G-protein-coupled receptor Gpr161 negatively regulates the Sonic hedgehog pathway via cAMP signaling. *Cell* *152*, 210–223.
- Murre, C., McCaw, P.S., Vaessin, H., Caudy, M., Jan, L.Y., Jan, Y.N., Cabrera, C.V., Buskin, J.N., Hauschka, S.D., and Lassar, A.B. (1989). Interactions between heterologous helix-loop-helix proteins generate complexes that bind specifically to a common DNA sequence. *Cell* *58*, 537–544.
- Mykytyn, K., and Sheffield, V.C. (2004). Establishing a connection between cilia and Bardet-Biedl Syndrome. *Trends Mol. Med.* *10*, 106–109.
- Nachury, M.V., Loktev, A.V., Zhang, Q., Westlake, C.J., Peränen, J., Merdes, A., Slusarski, D.C., Scheller, R.H., Bazan, J.F., Sheffield, V.C., et al. (2007). A core complex of BBS proteins cooperates with the GTPase Rab8 to promote ciliary membrane biogenesis. *Cell* *129*, 1201–1213.
- Nakashima, K., Umeshima, H., and Kengaku, M. (2015). Cerebellar granule cells are predominantly generated by terminal symmetric divisions of granule cell precursors: Division of Granule Cell Precursors. *Dev. Dyn.* *244*, 748–758.
- Niewiadomski, P., Kong, J.H., Ahrends, R., Ma, Y., Humke, E.W., Khan, S., Teruel, M.N., Novitch, B.G., and Rohatgi, R. (2014). Gli protein activity is controlled by multi-site phosphorylation in vertebrate Hedgehog signaling. *Cell Rep.* *6*, 168–181.
- Niewiadomski, P., Niedziółka, S.M., Markiewicz, Ł., Uśpieński, T., Baran, B., and Chojnowska, K. (2019). Gli Proteins: Regulation in Development and Cancer. *Cells* *8*.
- Nigg, E.A., and Stearns, T. (2011). The centrosome cycle: Centriole biogenesis, duplication and inherent asymmetries. *Nat. Cell Biol.* *13*, 1154–1160.
- Noah, T.K., Kazanjian, A., Whitsett, J., and Shroyer, N.F. (2010). SAM Pointed Domain ETS Factor (SPDEF) regulates terminal differentiation and maturation of intestinal goblet cells. *Exp. Cell Res.* *316*, 452–465.
- Nonaka, S., Tanaka, Y., Okada, Y., Takeda, S., Harada, A., Kanai, Y., Kido, M., and Hirokawa, N. (1998). Randomization of left-right asymmetry due to loss of nodal cilia generating leftward flow of extraembryonic fluid in mice lacking KIF3B motor protein. *Cell* *95*, 829–837.
- Northcott, P.A., Korshunov, A., Witt, H., Hielscher, T., Eberhart, C.G., Mack, S., Bouffet, E., Clifford, S.C., Hawkins, C.E., French, P., et al. (2010). Medulloblastoma Comprises Four Distinct Molecular Variants. *J. Clin. Oncol.* *29*, 1408–1414.
- Northcott, P.A., Hielscher, T., Dubuc, A., Mack, S., Shih, D., Remke, M., Al-Halabi, H., Albrecht, S., Jabado, N., Eberhart, C.G., et al. (2011). Pediatric and adult sonic hedgehog medulloblastomas are clinically and molecularly distinct. *Acta Neuropathol. (Berl.)* *122*, 231–240.
- Northcott, P.A., Shih, D.J.H., Peacock, J., Garzia, L., Sorana Morrissy, A., Zichner, T., Stütz, A.M., Korshunov, A., Reimand, J., Schumacher, S.E., et al. (2012). Subgroup-specific structural variation across 1,000 medulloblastoma genomes. *Nature* *488*, 49–56.

- Northcott, P.A., Lee, C., Zichner, T., Stütz, A.M., Erkek, S., Kawauchi, D., Shih, D.J.H., Hovestadt, V., Zapatka, M., Sturm, D., et al. (2014). Enhancer hijacking activates GFI1 family oncogenes in medulloblastoma. *Nature* 511, 428–434.
- Northcott, P.A., Buchhalter, I., Morrissy, A.S., Hovestadt, V., Weischenfeldt, J., Ehrenberger, T., Gröbner, S., Segura-Wang, M., Zichner, T., Rudneva, V.A., et al. (2017). The whole-genome landscape of medulloblastoma subtypes. *Nature* 547, 311–317.
- Northcott, P.A., Robinson, G.W., Kratz, C.P., Mabbott, D.J., Pomeroy, S.L., Clifford, S.C., Rutkowski, S., Ellison, D.W., Malkin, D., Taylor, M.D., et al. (2019). Medulloblastoma. *Nat. Rev. Dis. Primer* 5, 1–20.
- Nüsslein-Volhard, C., and Wieschaus, E. (1980). Mutations affecting segment number and polarity in *Drosophila*. *Nature* 287, 795–801.
- Odabasi, E., Gul, S., Kavakli, I.H., and Firat-Karalar, E.N. (2019). Centriolar satellites are required for efficient ciliogenesis and ciliary content regulation. *EMBO Rep.* 20, e47723.
- Ogden, S.K., Fei, D.L., Schilling, N.S., Ahmed, Y.F., Hwa, J., and Robbins, D.J. (2008). G protein Galphai functions immediately downstream of Smoothed in Hedgehog signalling. *Nature* 456, 967–970.
- Ohyama, T., Nores, W.L., Murphy, M., and Mauk, M.D. (2003). What the cerebellum computes. *Trends Neurosci.* 26, 222–227.
- Okano-Uchida, T., Himi, T., Komiya, Y., and Ishizaki, Y. (2004). Cerebellar granule cell precursors can differentiate into astroglial cells. *Proc. Natl. Acad. Sci.* 101, 1211–1216.
- Oliver, T.G., Read, T.A., Kessler, J.D., Mehmeti, A., Wells, J.F., Huynh, T.T.T., Lin, S.M., and Wechsler-Reya, R.J. (2005). Loss of patched and disruption of granule cell development in a pre-neoplastic stage of medulloblastoma. *Development* 132, 2425–2439.
- Ostrom, Q.T., Gittleman, H., Truitt, G., Boscia, A., Kruchko, C., and Barnholtz-Sloan, J.S. (2018). CBTRUS Statistical Report: Primary Brain and Other Central Nervous System Tumors Diagnosed in the United States in 2011–2015. *Neuro-Oncol.* 20, iv1–iv86.
- Ou, Y.Y., Mack, G.J., Zhang, M., and Rattner, J.B. (2002). CEP110 and ninein are located in a specific domain of the centrosome associated with centrosome maturation. *J. Cell Sci.* 115, 1825.
- Owa, T., Taya, S., Miyashita, S., Yamashita, M., Adachi, T., Yamada, K., Yokoyama, M., Aida, S., Nishioka, T., Inoue, Y.U., et al. (2018). Meis1 Coordinates Cerebellar Granule Cell Development by Regulating Pax6 Transcription, BMP Signaling and Atoh1 Degradation. *J. Neurosci.* 38, 1277.
- Packer, R.J., Zhou, T., Holmes, E., Vezina, G., and Gajjar, A. (2013). Survival and secondary tumors in children with medulloblastoma receiving radiotherapy and adjuvant chemotherapy: results of Children’s Oncology Group trial A9961. *Neuro-Oncol.* 15, 97–103.
- Pal, K., Hwang, S., Somatilaka, B., Badgandi, H., Jackson, P.K., DeFea, K., and Mukhopadhyay, S. (2016). Smoothed determines β -arrestin-mediated removal of the G protein-coupled receptor Gpr161 from the primary cilium. *J. Cell Biol.* 212, 861–875.
- Pala, R., Alomari, N., and Nauli, S.M. (2017). Primary Cilium-Dependent Signaling Mechanisms. *Int. J. Mol. Sci.* 18.

- Pan, N., Jahan, I., Lee, J.E., and Fritsch, B. (2009). Defects in the cerebella of conditional Neurod1 null mice correlate with effective Tg(Atoh1-cre) recombination and granule cell requirements for Neurod1 for differentiation. *Cell Tissue Res.* 337, 407–428.
- Pan, N., Jahan, I., Kersigo, J., Kopecky, B., Santi, P., Johnson, S., Schmitz, H., and Fritsch, B. (2011). Conditional deletion of Atoh1 using Pax2-Cre results in viable mice without differentiated cochlear hair cells that have lost most of the organ of Corti. *Hear. Res.* 275, 66–80.
- Pan, Y., Bai, C.B., Joyner, A.L., and Wang, B. (2006). Sonic hedgehog Signaling Regulates Gli2 Transcriptional Activity by Suppressing Its Processing and Degradation. *Mol. Cell. Biol.* 26, 3365–3377.
- Pazour, G.J., Wilkerson, C.G., and Witman, G.B. (1998). A dynein light chain is essential for the retrograde particle movement of intraflagellar transport (IFT). *J. Cell Biol.* 141, 979–992.
- Pazour, G.J., Dickert, B.L., and Witman, G.B. (1999). The DHC1b (DHC2) isoform of cytoplasmic dynein is required for flagellar assembly. *J. Cell Biol.* 144, 473–481.
- Pazour, G.J., Dickert, B.L., Vucica, Y., Seeley, E.S., Rosenbaum, J.L., Witman, G.B., and Cole, D.G. (2000). Chlamydomonas IFT88 and Its Mouse Homologue, Polycystic Kidney Disease Gene Tg737, Are Required for Assembly of Cilia and Flagella. *J. Cell Biol.* 151, 709–718.
- Pazzaglia, S., Mancuso, M., Atkinson, M.J., Tanori, M., Rebessi, S., Majo, V.D., Covelli, V., Hahn, H., and Saran, A. (2002). High incidence of medulloblastoma following X-ray-irradiation of newborn Ptc1 heterozygous mice. *Oncogene* 21, 7580–7584.
- Pazzaglia, S., Tanori, M., Mancuso, M., Gessi, M., Pasquali, E., Leonardi, S., Oliva, M.A., Rebessi, S., Majo, V.D., Covelli, V., et al. (2006). Two-hit model for progression of medulloblastoma preneoplasia in Patched heterozygous mice. *Oncogene* 25, 5575–5580.
- Pedersen, L.B., and Rosenbaum, J.L. (2008). Intraflagellar transport (IFT) role in ciliary assembly, resorption and signalling. *Curr. Top. Dev. Biol.* 85, 23–61.
- Pedersen, L.B., Miller, M.S., Geimer, S., Leitch, J.M., Rosenbaum, J.L., and Cole, D.G. (2005). Chlamydomonas IFT172 is encoded by FLA11, interacts with CrEB1, and regulates IFT at the flagellar tip. *Curr. Biol. CB* 15, 262–266.
- Pei, Y., Moore, C.E., Wang, J., Tewari, A.K., Eroshkin, A., Cho, Y.-J., Witt, H., Korshunov, A., Read, T.-A., Sun, J.L., et al. (2012). An Animal Model of MYC-Driven Medulloblastoma. *Cancer Cell* 21, 155–167.
- Peignon, G., Durand, A., Cacheux, W., Ayrault, O., Terris, B., Laurent-Puig, P., Shroyer, N.F., Seuning, I.V., Honjo, T., Perret, C., et al. (2011). Complex interplay between β -catenin signalling and Notch effectors in intestinal tumorigenesis. *Gut* 60, 166–176.
- Penas, C., Govek, E.-E., Fang, Y., Ramachandran, V., Daniel, M., Wang, W., Maloof, M.E., Rahaim, R.J., Bibian, M., Kawauchi, D., et al. (2015). Casein Kinase 1 δ Is an APC/CCdh1 Substrate that Regulates Cerebellar Granule Cell Neurogenesis. *Cell Rep.* 11, 249–260.
- Pepinsky, R.B., Zeng, C., Wen, D., Rayhorn, P., Baker, D.P., Williams, K.P., Bixler, S.A., Ambrose, C.M., Garber, E.A., Miatkowski, K., et al. (1998). Identification of a palmitic acid-modified form of human Sonic hedgehog. *J. Biol. Chem.* 273, 14037–14045.

- Perreault, S., Ramaswamy, V., Achrol, A.S., Chao, K., Liu, T.T., Shih, D., Remke, M., Schubert, S., Bouffet, E., Fisher, P.G., et al. (2014). MRI Surrogates for Molecular Subgroups of Medulloblastoma. *AJNR Am. J. Neuroradiol.* 35, 1263–1269.
- Pietsch, T., Waha, A., Koch, A., Kraus, J., Albrecht, S., Tonn, J., Sörensen, N., Berthold, F., Henk, B., Schmandt, N., et al. (1997). Medulloblastomas of the desmoplastic variant carry mutations of the human homologue of *Drosophila patched*. *Cancer Res.* 57, 2085–2088.
- Pizer, B., Donachie, P.H.J., Robinson, K., Taylor, R.E., Michalski, A., Punt, J., Ellison, D.W., and Picton, S. (2011). Treatment of recurrent central nervous system primitive neuroectodermal tumours in children and adolescents: results of a Children’s Cancer and Leukaemia Group study. *Eur. J. Cancer Oxf. Engl.* 1990 47, 1389–1397.
- Plotnikova, O.V., Pugacheva, E.N., and Golemis, E.A. (2009). Primary Cilia and the Cell Cycle. *Methods Cell Biol.* 94, 137–160.
- Pomeroy, S.L., Tamayo, P., Gaasenbeek, M., Sturla, L.M., Angelo, M., McLaughlin, M.E., Kim, J.Y.H., Goumnerova, L.C., Black, P.M., Lau, C., et al. (2002). Prediction of central nervous system embryonal tumour outcome based on gene expression. *Nature* 415, 436–442.
- Pons, S., Trejo, J.L., Martínez-Morales, J.R., and Martí, E. (2001). Vitronectin regulates Sonic hedgehog activity during cerebellum development through CREB phosphorylation. *Dev. Camb. Engl.* 128, 1481–1492.
- Porter, J.A., von Kessler, D.P., Ekker, S.C., Young, K.E., Lee, J.J., Moses, K., and Beachy, P.A. (1995). The product of hedgehog autoproteolytic cleavage active in local and long-range signalling. *Nature* 374, 363–366.
- Porter, J.A., Young, K.E., and Beachy, P.A. (1996). Cholesterol modification of hedgehog signaling proteins in animal development. *Science* 274, 255–259.
- Pöschl, J., Stark, S., Neumann, P., Gröbner, S., Kawauchi, D., Jones, D.T.W., Northcott, P.A., Lichter, P., Pfister, S.M., Kool, M., et al. (2014). Genomic and transcriptomic analyses match medulloblastoma mouse models to their human counterparts. *Acta Neuropathol. (Berl.)* 128, 123–136.
- Prevo, B., Mangeol, P., Oswald, F., Scholey, J.M., and Peterman, E.J.G. (2015). Functional differentiation of cooperating kinesin-2 motors orchestrates cargo import and transport in *C. elegans* cilia. *Nat. Cell Biol.* 17, 1536–1545.
- Przyborski, S.A., Knowles, B.B., and Ackerman, S.L. (1998). Embryonic phenotype of *Unc5h3* mutant mice suggests chemorepulsion during the formation of the rostral cerebellar boundary. *Development* 125, 41.
- Pugacheva, E.N., Jablonski, S.A., Hartman, T.R., Henske, E.P., and Golemis, E.A. (2007). HEF1-dependent Aurora A activation induces disassembly of the primary cilium. *Cell* 129, 1351–1363.
- Pugh, T.J., Weeraratne, S.D., Archer, T.C., Pomeranz Krummel, D.A., Auclair, D., Bochicchio, J., Carneiro, M.O., Carter, S.L., Cibulskis, K., Erlich, R.L., et al. (2012). Medulloblastoma exome sequencing uncovers subtype-specific somatic mutations. *Nature* 488, 106–110.

Qin, L., Wine-Lee, L., Ahn, K.J., and Crenshaw, E.B. (2006). Genetic analyses demonstrate that bone morphogenetic protein signaling is required for embryonic cerebellar development. *J. Neurosci. Off. J. Soc. Neurosci.* *26*, 1896–1905.

Quan, X.-J., Yuan, L., Tiberi, L., Claeys, A., De Geest, N., Yan, J., van der Kant, R., Xie, W.R., Klisch, T.J., Shymkowitz, J., et al. (2016). Post-translational Control of the Temporal Dynamics of Transcription Factor Activity Regulates Neurogenesis. *Cell* *164*, 460–475.

Quarantotti, V., Chen, J.-X., Tischer, J., Gonzalez Tejedro, C., Papachristou, E.K., D'Santos, C.S., Kilmartin, J.V., Miller, M.L., and Gergely, F. (2019). Centriolar satellites are acentriolar assemblies of centrosomal proteins. *EMBO J.*

Raffel, C., Jenkins, R.B., Frederick, L., Hebrink, D., Alderete, B., Fults, D.W., and James, C.D. (1997). Sporadic medulloblastomas contain PTCH mutations. *Cancer Res.* *57*, 842–845.

Rahimi-Balaei, M., Bergen, H., Kong, J., and Marzban, H. (2018). Neuronal Migration During Development of the Cerebellum. *Front. Cell. Neurosci.* *12*.

Rakic, P. (1971). Neuron-glia relationship during granule cell migration in developing cerebellar cortex. A Golgi and electronmicroscopic study in Macacus Rhesus. *J. Comp. Neurol.* *141*, 283–312.

Ramaswamy, V., and Taylor, M.D. (2017). Medulloblastoma: From Myth to Molecular. *J. Clin. Oncol. Off. J. Am. Soc. Clin. Oncol.* *35*, 2355–2363.

Ramaswamy, V., Remke, M., Bouffet, E., Faria, C.C., Perreault, S., Cho, Y.-J., Shih, D.J., Luu, B., Dubuc, A.M., Northcott, P.A., et al. (2013). Recurrence patterns across medulloblastoma subgroups: an integrated clinical and molecular analysis. *Lancet Oncol.* *14*, 1200–1207.

Ramaswamy, V., Remke, M., Bouffet, E., Bailey, S., Clifford, S.C., Doz, F., Kool, M., Dufour, C., Vassal, G., Milde, T., et al. (2016). Risk stratification of childhood medulloblastoma in the molecular era: The Current Consensus. *Acta Neuropathol. (Berl.)* *131*, 821–831.

Ramnani, N. (2012). Frontal Lobe and Posterior Parietal Contributions to the Cortico-cerebellar System. *The Cerebellum* *11*, 366–383.

Rausch, T., Jones, D.T.W., Zapatka, M., Stütz, A.M., Zichner, T., Weischenfeldt, J., Jäger, N., Remke, M., Shih, D., Northcott, P.A., et al. (2012). Genome Sequencing of Pediatric Medulloblastoma Links Catastrophic DNA Rearrangements with TP53 Mutations. *Cell* *148*, 59–71.

Reiter, J.F., and Leroux, M.R. (2017). Genes and molecular pathways underpinning ciliopathies. *Nat. Rev. Mol. Cell Biol.* *18*, 533–547.

Remke, M., Ramaswamy, V., Peacock, J., Shih, D.J.H., Koelsche, C., Northcott, P.A., Hill, N., Cavalli, F.M.G., Kool, M., Wang, X., et al. (2013). TERT promoter mutations are highly recurrent in SHH subgroup medulloblastoma. *Acta Neuropathol. (Berl.)* *126*, 917–929.

Riddle, R.D., Johnson, R.L., Laufer, E., and Tabin, C. (1993). Sonic hedgehog mediates the polarizing activity of the ZPA. *Cell* *75*, 1401–1416.

Rieger, S., Senghaas, N., Walch, A., and Köster, R.W. (2009). Cadherin-2 controls directional chain migration of cerebellar granule neurons. *PLoS Biol.* *7*, e1000240.

- Rios, I., Alvarez-Rodríguez, R., Martí, E., and Pons, S. (2004). Bmp2 antagonizes sonic hedgehog-mediated proliferation of cerebellar granule neurones through Smad5 signalling. *Development* 131, 3159.
- Robarge, K.D., Brunton, S.A., Castanedo, G.M., Cui, Y., Dina, M.S., Goldsmith, R., Gould, S.E., Guichert, O., Gunzner, J.L., Halladay, J., et al. (2009). GDC-0449-a potent inhibitor of the hedgehog pathway. *Bioorg. Med. Chem. Lett.* 19, 5576–5581.
- Robertson, P.L., Muraszko, K.M., Holmes, E.J., Sposto, R., Packer, R.J., Gajjar, A., Dias, M.S., Allen, J.C., and Children's Oncology Group (2006). Incidence and severity of postoperative cerebellar mutism syndrome in children with medulloblastoma: a prospective study by the Children's Oncology Group. *J. Neurosurg.* 105, 444–451.
- Robinson, G., Parker, M., Kranenburg, T.A., Lu, C., Chen, X., Ding, L., Phoenix, T.N., Hedlund, E., Wei, L., Zhu, X., et al. (2012). Novel mutations target distinct subgroups of medulloblastoma. *Nature* 488, 43–48.
- Robinson, G.W., Orr, B.A., Wu, G., Gururangan, S., Lin, T., Qaddoumi, I., Packer, R.J., Goldman, S., Prados, M.D., Desjardins, A., et al. (2015). Vismodegib Exerts Targeted Efficacy Against Recurrent Sonic Hedgehog-Subgroup Medulloblastoma: Results From Phase II Pediatric Brain Tumor Consortium Studies PBTC-025B and PBTC-032. *J. Clin. Oncol.* 33, 2646–2654.
- Rocamora, N., García-Ladona, F.J., Palacios, J.M., and Mengod, G. (1993). Differential expression of brain-derived neurotrophic factor, neurotrophin-3, and low-affinity nerve growth factor receptor during the postnatal development of the rat cerebellar system. *Brain Res. Mol. Brain Res.* 17, 1–8.
- Rodriguez, C.I., and Dymecki, S.M. (2000). Origin of the precerebellar system. *Neuron* 27, 475–486.
- Rohatgi, R., and Snell, W.J. (2010). The ciliary membrane. *Curr. Opin. Cell Biol.* 22, 541–546.
- Rohatgi, R., Milenkovic, L., Corcoran, R.B., and Scott, M.P. (2009). Hedgehog signal transduction by Smoothed: pharmacologic evidence for a 2-step activation process. *Proc. Natl. Acad. Sci. U. S. A.* 106, 3196–3201.
- Roostaei, T., Nazeri, A., Sahraian, M.A., and Minagar, A. (2014). The human cerebellum: a review of physiologic neuroanatomy. *Neurol. Clin.* 32, 859–869.
- Rose, M.F., Ahmad, K.A., Thaller, C., and Zoghbi, H.Y. (2009a). Excitatory neurons of the proprioceptive, interoceptive, and arousal hindbrain networks share a developmental requirement for Math1. *Proc. Natl. Acad. Sci. U. S. A.* 106, 22462–22467.
- Rose, M.F., Ren, J., Ahmad, K.A., Chao, H.-T., Klisch, T.J., Flora, A., Greer, J.J., and Zoghbi, H.Y. (2009b). Math1 is essential for the development of hindbrain neurons critical for perinatal breathing. *Neuron* 64, 341–354.
- Rowitch, D.H., and McMahon, A.P. (1995). Pax-2 expression in the murine neural plate precedes and encompasses the expression domains of Wnt-1 and En-1. *Mech. Dev.* 52, 3–8.
- Rubin, J.B., Choi, Y., and Segal, R.A. (2002). Cerebellar proteoglycans regulate sonic hedgehog responses during development. *Development* 129, 2223–2232.

- Rudin, C.M., Hann, C.L., Laterra, J., Yauch, R.L., Callahan, C.A., Fu, L., Holcomb, T., Stinson, J., Gould, S.E., Coleman, B., et al. (2009). Treatment of medulloblastoma with hedgehog pathway inhibitor GDC-0449. *N. Engl. J. Med.* *361*, 1173–1178.
- Ryder, E.F., and Cepko, C.L. (1994). Migration patterns of clonally related granule cells and their progenitors in the developing chick cerebellum. *Neuron* *12*, 1011–1028.
- Sakaue-Sawano, A., Kurokawa, H., Morimura, T., Hanyu, A., Hama, H., Osawa, H., Kashiwagi, S., Fukami, K., Miyata, T., Miyoshi, H., et al. (2008). Visualizing spatiotemporal dynamics of multicellular cell-cycle progression. *Cell* *132*, 487–498.
- Salsano, E., Pollo, B., Eoli, M., Giordana, M.T., and Finocchiaro, G. (2004). Expression of MATH1, a marker of cerebellar granule cell progenitors, identifies different medulloblastoma sub-types. *Neurosci. Lett.* *370*, 180–185.
- Sang, L., Miller, J.J., Corbit, K.C., Giles, R.H., Brauer, M.J., Otto, E.A., Baye, L.M., Wen, X., Scales, S.J., Kwong, M., et al. (2011). Mapping the NPHP-JBTS-MKS protein network reveals ciliopathy disease genes and pathways. *Cell* *145*, 513–528.
- Santamaria, A., Wang, B., Elowe, S., Malik, R., Zhang, F., Bauer, M., Schmidt, A., Silljé, H.H.W., Körner, R., and Nigg, E.A. (2011). The Plk1-dependent Phosphoproteome of the Early Mitotic Spindle. *Mol. Cell. Proteomics MCP* *10*.
- Schüller, U., Zhao, Q., Godinho, S.A., Heine, V.M., Medema, R.H., Pellman, D., and Rowitch, D.H. (2007). Forkhead Transcription Factor FoxM1 Regulates Mitotic Entry and Prevents Spindle Defects in Cerebellar Granule Neuron Precursors. *Mol. Cell. Biol.* *27*, 8259.
- Schüller, U., Heine, V.M., Mao, J., Kho, A.T., Dillon, A.K., Han, Y.-G., Huillard, E., Sun, T., Ligon, A.H., Qian, Y., et al. (2008). Acquisition of granule neuron precursor identity is a critical determinant of progenitor cell competence to form Shh-induced medulloblastoma. *Cancer Cell* *14*, 123–134.
- Schuermans, C., Armant, O., Nieto, M., Stenman, J.M., Britz, O., Klenin, N., Brown, C., Langevin, L.-M., Seibt, J., Tang, H., et al. (2004). Sequential phases of cortical specification involve Neurogenin-dependent and -independent pathways. *EMBO J.* *23*, 2892–2902.
- Schwalbe, E.C., Lindsey, J.C., Nakjang, S., Crosier, S., Smith, A.J., Hicks, D., Rafiee, G., Hill, R.M., Iliasova, A., Stone, T., et al. (2017). Novel molecular subgroups for clinical classification and outcome prediction in childhood medulloblastoma: a cohort study. *Lancet Oncol.* *18*, 958–971.
- Sedjāi, F., Acquaviva, C., Chevrier, V., Chauvin, J.-P., Coppin, E., Aouane, A., Coulier, F., Tolun, A., Pierres, M., Birnbaum, D., et al. (2010). Control of ciliogenesis by FOR20, a novel centrosome and pericentriolar satellite protein. *J. Cell Sci.* *123*, 2391–2401.
- Segal, R.A., Takahashi, H., and McKay, R.D. (1992). Changes in neurotrophin responsiveness during the development of cerebellar granule neurons. *Neuron* *9*, 1041–1052.
- Sekerková, G., Ilijic, E., and Mugnaini, E. (2004). Time of origin of unipolar brush cells in the rat cerebellum as observed by prenatal bromodeoxyuridine labeling. *Neuroscience* *127*, 845–858.
- Serafini, T., Colamarino, S.A., Leonardo, E.D., Wang, H., Beddington, R., Skarnes, W.C., and Tessier-Lavigne, M. (1996). Netrin-1 is required for commissural axon guidance in the developing vertebrate nervous system. *Cell* *87*, 1001–1014.

- Sharma, T., Schwalbe, E.C., Williamson, D., Sill, M., Hovestadt, V., Mynarek, M., Rutkowski, S., Robinson, G.W., Gajjar, A., Cavalli, F., et al. (2019). Second-generation molecular subgrouping of medulloblastoma: an international meta-analysis of Group 3 and Group 4 subtypes. *Acta Neuropathol. (Berl.)* 138, 309–326.
- Shimada, I.S., Hwang, S.-H., Somatilaka, B.N., Wang, X., Skowron, P., Kim, J., Kim, M., Shelton, J.M., Rajaram, V., Xuan, Z., et al. (2018). Basal Suppression of the Sonic Hedgehog Pathway by the G-Protein-Coupled Receptor Gpr161 Restricts Medulloblastoma Pathogenesis. *Cell Rep.* 22, 1169–1184.
- Shroyer, N.F., Wallis, D., Venken, K.J.T., Bellen, H.J., and Zoghbi, H.Y. (2005). Gfi1 functions downstream of Math1 to control intestinal secretory cell subtype allocation and differentiation. *Genes Dev.* 19, 2412–2417.
- Sillitoe, R.V., and Joyner, A.L. (2007). Morphology, molecular codes, and circuitry produce the three-dimensional complexity of the cerebellum. *Annu. Rev. Cell Dev. Biol.* 23, 549–577.
- Simeone, A. (2000). Positioning the isthmic organizer where Otx2 and Gbx2 meet. *Trends Genet. TIG* 16, 237–240.
- Simeone, A., Acampora, D., Gulisano, M., Stornaiuolo, A., and Boncinelli, E. (1992). Nested expression domains of four homeobox genes in developing rostral brain. *Nature* 358, 687–690.
- Singla, V., Romaguera-Ros, M., Garcia-Verdugo, J.M., and Reiter, J.F. (2010). Ofd1, a human disease gene, regulates the length and distal structure of centrioles. *Dev. Cell* 18, 410–424.
- Sjostrom, S.K., Finn, G., Hahn, W.C., Rowitch, D.H., and Kenney, A.M. (2005). The Cdk1 Complex Plays a Prime Role in Regulating N-Myc Phosphorylation and Turnover in Neural Precursors. *Dev. Cell* 9, 327–338.
- Smeyne, R.J., Chu, T., Lewin, A., Bian, F., Sanlioglu, S., S-Crisman, S., Kunsch, C., Lira, S.A., and Oberdick, J. (1995). Local control of granule cell generation by cerebellar Purkinje cells. *Mol. Cell. Neurosci.* 6, 230–251.
- Smith, M.J., Beetz, C., Williams, S.G., Bhaskar, S.S., O’Sullivan, J., Anderson, B., Daly, S.B., Urquhart, J.E., Bholah, Z., Oudit, D., et al. (2014). Germline mutations in SUFU cause Gorlin syndrome-associated childhood medulloblastoma and redefine the risk associated with PTCH1 mutations. *J. Clin. Oncol. Off. J. Am. Soc. Clin. Oncol.* 32, 4155–4161.
- Solecki, D.J., Liu, X.L., Tomoda, T., Fang, Y., and Hatten, M.E. (2001). Activated Notch2 signaling inhibits differentiation of cerebellar granule neuron precursors by maintaining proliferation. *Neuron* 31, 557–568.
- Solecki, D.J., Model, L., Gaetz, J., Kapoor, T.M., and Hatten, M.E. (2004). Par6 α signaling controls glial-guided neuronal migration. *Nat. Neurosci.* 7, 1195.
- Sorokin, S. (1962). Centrioles and the Formation of Rudimentary Cilia by Fibroblasts and Smooth Muscle Cells. *J. Cell Biol.* 15, 363–377.
- Spassky, N., Han, Y.-G., Aguilar, A., Strehl, L., Besse, L., Laclef, C., Ros, M.R., Garcia-Verdugo, J.M., and Alvarez-Buylla, A. (2008). Primary Cilia are required for cerebellar development and Shh-dependent expansion of progenitor pool. *Dev. Biol.* 317, 246–259.

- Spektor, A., Tsang, W.Y., Khoo, D., and Dynlacht, B.D. (2007). Cep97 and CP110 suppress a cilia assembly program. *Cell* 130, 678–690.
- Staples, C.J., Myers, K.N., Beveridge, R.D.D., Patil, A.A., Lee, A.J.X., Swanton, C., Howell, M., Boulton, S.J., and Collis, S.J. (2012). The centriolar satellite protein Cep131 is important for genome stability. *J. Cell Sci.* 125, 4770–4779.
- Stegmüller, J., Konishi, Y., Huynh, M.A., Yuan, Z., Dibacco, S., and Bonni, A. (2006). Cell-intrinsic regulation of axonal morphogenesis by the Cdh1-APC target SnoN. *Neuron* 50, 389–400.
- Stegmüller, J., Huynh, M.A., Yuan, Z., Konishi, Y., and Bonni, A. (2008). TGFbeta-Smad2 signaling regulates the Cdh1-APC/SnoN pathway of axonal morphogenesis. *J. Neurosci. Off. J. Soc. Neurosci.* 28, 1961–1969.
- Stepanek, L., and Pigino, G. (2016). Microtubule doublets are double-track railways for intraflagellar transport trains. *Science* 352, 721–724.
- Stiles, J., and Jernigan, T.L. (2010). The Basics of Brain Development. *Neuropsychol. Rev.* 20, 327–348.
- Stilling, B. (1864). *Untersuchungen über den Bau des kleinen Gehirns des Menschen* (Kay).
- Stowe, T.R., Wilkinson, C.J., Iqbal, A., and Stearns, T. (2012). The centriolar satellite proteins Cep72 and Cep290 interact and are required for recruitment of BBS proteins to the cilium. *Mol. Biol. Cell* 23, 3322–3335.
- Strutt, H., Thomas, C., Nakano, Y., Stark, D., Neave, B., Taylor, A.M., and Ingham, P.W. (2001). Mutations in the sterol-sensing domain of Patched suggest a role for vesicular trafficking in Smoothened regulation. *Curr. Biol.* 11, 608–613.
- Subkhankulova, T., Zhang, X., Leung, C., and Marino, S. (2010). Bmi1 directly represses p21Waf1/Cip1 in Shh-induced proliferation of cerebellar granule cell progenitors. *Mol. Cell. Neurosci.* 45, 151–162.
- Sudarov, A., Turnbull, R.K., Kim, E.J., Lebel-Potter, M., Guillemot, F., and Joyner, A.L. (2011). Ascl1 genetics reveals insights into cerebellum local circuit assembly. *J. Neurosci. Off. J. Soc. Neurosci.* 31, 11055–11069.
- Suspitsin, E.N., and Imyanitov, E.N. (2016). Bardet-Biedl Syndrome. *Mol. Syndromol.* 7, 62–71.
- Taipale, J., Chen, J.K., Cooper, M.K., Wang, B., Mann, R.K., Milenkovic, L., Scott, M.P., and Beachy, P.A. (2000). Effects of oncogenic mutations in Smoothened and Patched can be reversed by cyclopamine. *Nature* 406, 1005–1009.
- Taipale, J., Cooper, M.K., Maiti, T., and Beachy, P.A. (2002). Patched acts catalytically to suppress the activity of Smoothened. *Nature* 418, 892–897.
- Takahashi, H., and Liu, F.-C. (2006). Genetic Patterning of the mammalian telencephalon by morphogenetic molecules and transcription factors. *Birth Defects Res. Part C Embryo Today Rev.* 78, 256–266.
- Takeda, S., Yonekawa, Y., Tanaka, Y., Okada, Y., Nonaka, S., and Hirokawa, N. (1999). Left-Right Asymmetry and Kinesin Superfamily Protein KIF3A: New Insights in Determination of Laterality and Mesoderm Induction by *kif3A*^{-/-} Mice Analysis. *J. Cell Biol.* 145, 825–836.

- Tam, B.M., Moritz, O.L., Hurd, L.B., and Papermaster, D.S. (2000). Identification of an outer segment targeting signal in the COOH terminus of rhodopsin using transgenic *Xenopus laevis*. *J. Cell Biol.* *151*, 1369–1380.
- Tamayo-Orrego, L., Wu, C.-L., Bouchard, N., Khedher, A., Swikert, S.M., Remke, M., Skowron, P., Taylor, M.D., and Charron, F. (2016). Evasion of Cell Senescence Leads to Medulloblastoma Progression. *Cell Rep.* *14*, 2925–2937.
- Tang, Y., Gholamin, S., Schubert, S., Willardson, M.I., Lee, A., Bandopadhyay, P., Bergthold, G., Masoud, S., Nguyen, B., Vue, N., et al. (2014). Epigenetic targeting of Hedgehog pathway transcriptional output through BET bromodomain inhibition. *Nat. Med.* *20*, 732–740.
- Tang, Z., Lin, M.G., Stowe, T.R., Chen, S., Zhu, M., Stearns, T., Franco, B., and Zhong, Q. (2013). Autophagy Promotes Primary Ciliogenesis by Removing OFD1 from Centriolar Satellites. *Nature* *502*, 254–257.
- Tanos, B.E., Yang, H.-J., Soni, R., Wang, W.-J., Macaluso, F.P., Asara, J.M., and Tsou, M.-F.B. (2013). Centriole distal appendages promote membrane docking, leading to cilia initiation. *Genes Dev.* *27*, 163–168.
- Tao, Y., Black, I.B., and DiCicco-Bloom, E. (1996). Neurogenesis in neonatal rat brain is regulated by peripheral injection of basic fibroblast growth factor (bFGF). *J. Comp. Neurol.* *376*, 653–663.
- Taylor, M.D., Liu, L., Raffel, C., Hui, C., Mainprize, T.G., Zhang, X., Agatep, R., Chiappa, S., Gao, L., Lowrance, A., et al. (2002). Mutations in *SUFU* predispose to medulloblastoma. *Nat. Genet.* *31*, 306–310.
- Taylor, M.D., Northcott, P.A., Korshunov, A., Remke, M., Cho, Y.-J., Clifford, S.C., Eberhart, C.G., Parsons, D.W., Rutkowski, S., Gajjar, A., et al. (2012). Molecular subgroups of medulloblastoma: the current consensus. *Acta Neuropathol. (Berl.)* *123*, 465–472.
- Teglund, S., and Toftgård, R. (2010). Hedgehog beyond medulloblastoma and basal cell carcinoma. *Biochim. Biophys. Acta BBA - Rev. Cancer* *1805*, 181–208.
- Teo, W.-Y., Shen, J., Su, J.M.F., Yu, A., Wang, J., Chow, W.-Y., Li, X., Jones, J., Dauser, R., Whitehead, W., et al. (2013). Implications of tumor location on subtypes of medulloblastoma. *Pediatr. Blood Cancer* *60*, 1408–1410.
- Thomas, A., and Noël, G. (2019). Medulloblastoma: optimizing care with a multidisciplinary approach. *J. Multidiscip. Healthc.* *12*, 335–347.
- Thompson, M.C., Fuller, C., Hogg, T.L., Dalton, J., Finkelstein, D., Lau, C.C., Chintagumpala, M., Adesina, A., Ashley, D.M., Kellie, S.J., et al. (2006). Genomics identifies medulloblastoma subgroups that are enriched for specific genetic alterations. *J. Clin. Oncol. Off. J. Am. Soc. Clin. Oncol.* *24*, 1924–1931.
- Tollenaere, M.A.X., Mailand, N., and Bekker-Jensen, S. (2015). Centriolar satellites: key mediators of centrosome functions. *Cell. Mol. Life Sci. CMLS* *72*, 11–23.
- Tong, K.K., and Kwan, K.M. (2013). Common partner Smad-independent canonical bone morphogenetic protein signaling in the specification process of the anterior rhombic lip during cerebellum development. *Mol. Cell. Biol.* *33*, 1925–1937.

- Tong, K.K., Ma, T.C., and Kwan, K.M. (2015). BMP/Smad signaling and embryonic cerebellum development: stem cell specification and heterogeneity of anterior rhombic lip. *Dev. Growth Differ.* *57*, 121–134.
- Torroja, C., Gorfinkiel, N., and Guerrero, I. (2004). Patched controls the Hedgehog gradient by endocytosis in a dynamin-dependent manner, but this internalization does not play a major role in signal transduction. *Dev. Camb. Engl.* *131*, 2395–2408.
- Torroja, C., Gorfinkiel, N., and Guerrero, I. (2005). Mechanisms of Hedgehog gradient formation and interpretation. *J. Neurobiol.* *64*, 334–356.
- Tsai, L.-H., and Gleeson, J.G. (2005). Nucleokinesis in neuronal migration. *Neuron* *46*, 383–388.
- Tsao, C.-C., and Gorovsky, M.A. (2008). Tetrahymena IFT122A is not essential for cilia assembly but plays a role in returning IFT proteins from the ciliary tip to the cell body. *J. Cell Sci.* *121*, 428–436.
- Tukachinsky, H., Lopez, L.V., and Salic, A. (2010). A mechanism for vertebrate Hedgehog signaling: recruitment to cilia and dissociation of SuFu–Gli protein complexes. *J. Cell Biol.* *191*, 415–428.
- Umeshima, H., Hirano, T., and Kengaku, M. (2007). Microtubule-based nuclear movement occurs independently of centrosome positioning in migrating neurons. *Proc. Natl. Acad. Sci.* *104*, 16182–16187.
- Urbán, N., Berg, D.L.C. van den, Forget, A., Andersen, J., Demmers, J.A.A., Hunt, C., Ayrault, O., and Guillemot, F. (2016). Return to quiescence of mouse neural stem cells by degradation of a proactivation protein. *Science* *353*, 292–295.
- Uziel, T., Zindy, F., Xie, S., Lee, Y., Forget, A., Magdaleno, S., Rehg, J.E., Calabrese, C., Solecki, D., Eberhart, C.G., et al. (2005). The tumor suppressors Ink4c and p53 collaborate independently with Patched to suppress medulloblastoma formation. *Genes Dev.* *19*, 2656–2667.
- Uziel, T., Zindy, F., Sherr, C.J., and Roussel, M.F. (2006). The CDK inhibitor p18Ink4c is a tumor suppressor in medulloblastoma. *Cell Cycle Georget. Tex* *5*, 363–365.
- Van Keymeulen, A., Mascré, G., Youseff, K.K., Harel, I., Michaux, C., De Geest, N., Szpalski, C., Achouri, Y., Bloch, W., Hassan, B.A., et al. (2009). Epidermal progenitors give rise to Merkel cells during embryonic development and adult homeostasis. *J. Cell Biol.* *187*, 91–100.
- VanDussen, K.L., and Samuelson, L.C. (2010). Mouse atonal homolog 1 directs intestinal progenitors to secretory cell rather than absorptive cell fate. *Dev. Biol.* *346*, 215–223.
- Veleri, S., Manjunath, S.H., Fariss, R.N., May-Simera, H., Brooks, M., Foskett, T.A., Gao, C., Longo, T.A., Liu, P., Nagashima, K., et al. (2014). Ciliopathy-associated gene Cc2d2a promotes assembly of subdistal appendages on the mother centriole during cilia biogenesis. *Nat. Commun.* *5*, 4207.
- Villumsen, B.H., Danielsen, J.R., Povlsen, L., Sylvestersen, K.B., Merdes, A., Beli, P., Yang, Y.-G., Choudhary, C., Nielsen, M.L., Mailand, N., et al. (2013). A new cellular stress response that triggers centriolar satellite reorganization and ciliogenesis. *EMBO J.* *32*, 3029–3040.
- Vladoiu, M.C., El-Hamamy, I., Donovan, L.K., Farooq, H., Holgado, B.L., Sundaravadanam, Y., Ramaswamy, V., Hendrikse, L.D., Kumar, S., Mack, S.C., et al. (2019). Childhood cerebellar tumours mirror conserved fetal transcriptional programs. *Nature* *572*, 67–73.

- Voogd, J., and Glickstein, M. (1998). The anatomy of the cerebellum. *Trends Neurosci.* *21*, 370–375.
- Vorechovský, I., Tingby, O., Hartman, M., Strömberg, B., Nister, M., Collins, V.P., and Toftgård, R. (1997). Somatic mutations in the human homologue of *Drosophila* patched in primitive neuroectodermal tumours. *Oncogene* *15*, 361.
- Vosper, J.M.D., Fiore-Herich, C.S., Horan, I., Wilson, K., Wise, H., and Philpott, A. (2007). Regulation of neurogenin stability by ubiquitin-mediated proteolysis. *Biochem. J.* *407*, 277–284.
- Waha, A., Waha, A., Koch, A., Meyer-Puttlitz, B., Weggen, S., Sörensen, N., Tonn, J.C., Albrecht, S., Goodyer, C.G., Berthold, F., et al. (2003). Epigenetic Silencing of the HIC-1 Gene in Human Medulloblastomas. *J. Neuropathol. Exp. Neurol.* *62*, 1192–1201.
- Wallace, V.A. (1999). Purkinje-cell-derived Sonic hedgehog regulates granule neuron precursor cell proliferation in the developing mouse cerebellum. *Curr. Biol. CB* *9*, 445–448.
- Wallace, K., Liu, T.-H., and Vaessin, H. (2000). The pan-neural bHLH proteins DEADPAN and ASENSE regulate mitotic activity and cdk inhibitor dacapo expression in the *Drosophila* larval optic lobes. *Genesis* *26*, 77–85.
- Wang, L.-H., and Baker, N.E. (2015). E-proteins and ID-proteins: Helix-loop-helix partners in development and disease. *Dev. Cell* *35*, 269–280.
- Wang, B., Fallon, J.F., and Beachy, P.A. (2000). Hedgehog-Regulated Processing of Gli3 Produces an Anterior/Posterior Repressor Gradient in the Developing Vertebrate Limb. *Cell* *100*, 423–434.
- Wang, C., Pan, Y., and Wang, B. (2010). Suppressor of fused and Spop regulate the stability, processing and function of Gli2 and Gli3 full-length activators but not their repressors. *Dev. Camb. Engl.* *137*, 2001–2009.
- Wang, G., Chen, Q., Zhang, X., Zhang, B., Zhuo, X., Liu, J., Jiang, Q., and Zhang, C. (2013). PCM1 recruits Plk1 to the pericentriolar matrix to promote primary cilia disassembly before mitotic entry. *J. Cell Sci.* *126*, 1355–1365.
- Wang, L., Lee, K., Malonis, R., Sanchez, I., and Dynlacht, B.D. (2016). Tethering of an E3 ligase by PCM1 regulates the abundance of centrosomal KIAA0586/Talpid3 and promotes ciliogenesis. *ELife* *5*.
- Wang, V.Y., Hassan, B.A., Bellen, H.J., and Zoghbi, H.Y. (2002). *Drosophila* atonal Fully Rescues the Phenotype of Math1 Null Mice: New Functions Evolve in New Cellular Contexts. *Curr. Biol.* *12*, 1611–1616.
- Wang, V.Y., Rose, M.F., and Zoghbi, H.Y. (2005). Math1 expression redefines the rhombic lip derivatives and reveals novel lineages within the brainstem and cerebellum. *Neuron* *48*, 31–43.
- Wang, X., Dubuc, A.M., Ramaswamy, V., Mack, S., Gendoo, D.M.A., Remke, M., Wu, X., Garzia, L., Luu, B., Cavalli, F., et al. (2015). Medulloblastoma subgroups remain stable across primary and metastatic compartments. *Acta Neuropathol. (Berl.)* *129*, 449–457.
- Wassarman, K.M., Lewandoski, M., Campbell, K., Joyner, A.L., Rubenstein, J.L., Martinez, S., and Martin, G.R. (1997). Specification of the anterior hindbrain and establishment of a normal mid/hindbrain organizer is dependent on Gbx2 gene function. *Dev. Camb. Engl.* *124*, 2923–2934.

- Waszak, S.M., Northcott, P.A., Buchhalter, I., Robinson, G.W., Sutter, C., Groebner, S., Grund, K.B., Brugières, L., Jones, D.T.W., Pajtler, K.W., et al. (2018). Spectrum and prevalence of genetic predisposition in medulloblastoma: a retrospective genetic study and prospective validation in a clinical trial cohort. *Lancet Oncol.* *19*, 785–798.
- Wechsler-Reya, R.J., and Scott, M.P. (1999). Control of Neuronal Precursor Proliferation in the Cerebellum by Sonic Hedgehog. *Neuron* *22*, 103–114.
- Wei, Q., Zhang, Y., Li, Y., Zhang, Q., Ling, K., and Hu, J. (2012). The BBSome controls IFT assembly and turnaround in cilia. *Nat. Cell Biol.* *14*, 950–957.
- Wei, Q., Xu, Q., Zhang, Y., Li, Y., Zhang, Q., Hu, Z., Harris, P.C., Torres, V.E., Ling, K., and Hu, J. (2013). Transition fibre protein FBF1 is required for the ciliary entry of assembled intraflagellar transport complexes. *Nat. Commun.* *4*, 2750.
- Wen, X., Lai, C.K., Evangelista, M., Hongo, J.-A., de Sauvage, F.J., and Scales, S.J. (2010). Kinetics of Hedgehog-Dependent Full-Length Gli3 Accumulation in Primary Cilia and Subsequent Degradation. *Mol. Cell. Biol.* *30*, 1910–1922.
- Wetmore, C., Eberhart, D.E., and Curran, T. (2001). Loss of p53 but not ARF accelerates medulloblastoma in mice heterozygous for patched. *Cancer Res.* *61*, 513–516.
- Weyer, A., and Schilling, K. (2003). Developmental and cell type-specific expression of the neuronal marker NeuN in the murine cerebellum. *J. Neurosci. Res.* *73*, 400–409.
- Wheway, G., Nazlamova, L., and Hancock, J.T. (2018). Signaling through the Primary Cilium. *Front. Cell Dev. Biol.* *6*.
- Wingate, R.J. (2001). The rhombic lip and early cerebellar development. *Curr. Opin. Neurobiol.* *11*, 82–88.
- Wingate, R.J., and Hatten, M.E. (1999). The role of the rhombic lip in avian cerebellum development. *Dev. Camb. Engl.* *126*, 4395–4404.
- Wong, S.Y., Seol, A.D., So, P.-L., Ermilov, A.N., Bichakjian, C.K., Epstein Jr, E.H., Dlugosz, A.A., and Reiter, J.F. (2009). Primary cilia can both mediate and suppress Hedgehog pathway-dependent tumorigenesis. *Nat. Med.* *15*, 1055–1061.
- Woods, C., Montcouquiol, M., and Kelley, M.W. (2004). Math1 regulates development of the sensory epithelium in the mammalian cochlea. *Nat. Neurosci.* *7*, 1310–1318.
- Wright, M.C., Reed-Geaghan, E.G., Bolock, A.M., Fujiyama, T., Hoshino, M., and Maricich, S.M. (2015). Unipotent, Atoh1+ progenitors maintain the Merkel cell population in embryonic and adult mice. *J. Cell Biol.* *208*, 367–379.
- Wu, X., Northcott, P.A., Dubuc, A., Dupuy, A.J., Shih, D.J.H., Witt, H., Croul, S., Bouffet, E., Fults, D.W., Eberhart, C.G., et al. (2012). Clonal selection drives genetic divergence of metastatic medulloblastoma. *Nature* *482*, 529–533.
- Wurst, W., and Bally-Cuif, L. (2001a). Neural plate patterning: upstream and downstream of the isthmus organizer. *Nat. Rev. Neurosci.* *2*, 99–108.

- Wurst, W., and Bally-Cuif, L. (2001b). Neural plate patterning: Upstream and downstream of the isthmus organizer. *Nat. Rev. Neurosci.* *2*, 99–108.
- Yamada, M., Seto, Y., Taya, S., Owa, T., Inoue, Y.U., Inoue, T., Kawaguchi, Y., Nabeshima, Y.-I., and Hoshino, M. (2014). Specification of spatial identities of cerebellar neuron progenitors by *ptf1a* and *atoh1* for proper production of GABAergic and glutamatergic neurons. *J. Neurosci. Off. J. Soc. Neurosci.* *34*, 4786–4800.
- Yang, C., Chen, W., Chen, Y., and Jiang, J. (2012). Smoothed transduces Hedgehog signal by forming a complex with *Evc/Evc2*. *Cell Res.* *22*, 1593–1604.
- Yang, Q., Bermingham, N.A., Finegold, M.J., and Zoghbi, H.Y. (2001). Requirement of *Math1* for Secretory Cell Lineage Commitment in the Mouse Intestine. *Science* *294*, 2155–2158.
- Yang, Z.-J., Ellis, T., Markant, S.L., Read, T.-A., Kessler, J.D., Bourbonoulas, M., Schüller, U., Machold, R., Fishell, G., Rowitch, D.H., et al. (2008). Medulloblastoma can be initiated by deletion of *Patched* in lineage-restricted progenitors or stem cells. *Cancer Cell* *14*, 135–145.
- Yauch, R.L., Dijkgraaf, G.J.P., Alicke, B., Januario, T., Ahn, C.P., Holcomb, T., Pujara, K., Stinson, J., Callahan, C.A., Tang, T., et al. (2009). Smoothed Mutation Confers Resistance to a Hedgehog Pathway Inhibitor in Medulloblastoma. *Science* *326*, 572–574.
- Ye, F., Breslow, D.K., Koslover, E.F., Spakowitz, A.J., Nelson, W.J., and Nachury, M.V. (2013). Single molecule imaging reveals a major role for diffusion in the exploration of ciliary space by signaling receptors. *ELife* *2*, e00654.
- Ye, P., Xing, Y., Dai, Z., and D’Ercole, A.J. (1996). In vivo actions of insulin-like growth factor-I (IGF-I) on cerebellum development in transgenic mice: evidence that IGF-I increases proliferation of granule cell progenitors. *Dev. Brain Res.* *95*, 44–54.
- Ye, W., Bouchard, M., Stone, D., Liu, X., Vella, F., Lee, J., Nakamura, H., Ang, S.L., Busslinger, M., and Rosenthal, A. (2001). Distinct regulators control the expression of the mid-hindbrain organizer signal *FGF8*. *Nat. Neurosci.* *4*, 1175–1181.
- Yeung, J., Ha, T.J., Swanson, D.J., Choi, K., Tong, Y., and Goldowitz, D. (2014). *Wls* Provides a New Compartmental View of the Rhombic Lip in Mouse Cerebellar Development. *J. Neurosci.* *34*, 12527–12537.
- Yeung, J., Ha, T.J., Swanson, D.J., and Goldowitz, D. (2016). A Novel and Multivalent Role of *Pax6* in Cerebellar Development. *J. Neurosci.* *36*, 9057–9069.
- Yin, W.-C., Satkunendran, T., Mo, R., Morrissy, S., Zhang, X., Huang, E.S., Uusküla-Reimand, L., Hou, H., Son, J.E., Liu, W., et al. (2019). Dual Regulatory Functions of *SUFU* and Targetome of *GLI2* in SHH Subgroup Medulloblastoma. *Dev. Cell* *48*, 167-183.e5.
- Yokota, N., Aruga, J., Takai, S., Yamada, K., Hamazaki, M., Iwase, T., Sugimura, H., and Mikoshiba, K. (1996). Predominant expression of human *zic* in cerebellar granule cell lineage and medulloblastoma. *Cancer Res.* *56*, 377–383.
- Yoshimura, S., Egerer, J., Fuchs, E., Haas, A.K., and Barr, F.A. (2007). Functional dissection of Rab GTPases involved in primary cilium formation. *J. Cell Biol.* *178*, 363–369.

- Yuan, W., Zhou, L., Chen, J.H., Wu, J.Y., Rao, Y., and Ornitz, D.M. (1999). The mouse SLIT family: secreted ligands for ROBO expressed in patterns that suggest a role in morphogenesis and axon guidance. *Dev. Biol.* *212*, 290–306.
- Yung, A.R., Druckenbrod, N.R., Cloutier, J.-F., Wu, Z., Tessier-Lavigne, M., and Goodrich, L.V. (2018). Netrin-1 Confines Rhombic Lip-Derived Neurons to the CNS. *Cell Rep.* *22*, 1666–1680.
- Zhang, L., and Goldman, J.E. (1996a). Developmental fates and migratory pathways of dividing progenitors in the postnatal rat cerebellum. *J. Comp. Neurol.* *370*, 536–550.
- Zhang, L., and Goldman, J.E. (1996b). Generation of cerebellar interneurons from dividing progenitors in white matter. *Neuron* *16*, 47–54.
- Zhang, L., He, X., Liu, X., Zhang, F., Huang, L.F., Potter, A.S., Xu, L., Zhou, W., Zheng, T., Luo, Z., et al. (2019). Single-Cell Transcriptomics in Medulloblastoma Reveals Tumor-Initiating Progenitors and Oncogenic Cascades during Tumorigenesis and Relapse. *Cancer Cell*.
- Zhang, Q., Yu, D., Seo, S., Stone, E.M., and Sheffield, V.C. (2012a). Intrinsic protein-protein interaction-mediated and chaperonin-assisted sequential assembly of stable bardet-biedl syndrome protein complex, the BBSome. *J. Biol. Chem.* *287*, 20625–20635.
- Zhang, Q., Seo, S., Bugge, K., Stone, E.M., and Sheffield, V.C. (2012b). BBS proteins interact genetically with the IFT pathway to influence SHH-related phenotypes. *Hum. Mol. Genet.* *21*, 1945–1953.
- Zhang, W., Kim, P.J., Chen, Z., Lokman, H., Qiu, L., Zhang, K., Rozen, S.G., Tan, E.K., Je, H.S., and Zeng, L. (2016). MiRNA-128 regulates the proliferation and neurogenesis of neural precursors by targeting PCM1 in the developing cortex. *ELife* *5*.
- Zhao, H., Ayrault, O., Zindy, F., Kim, J.-H., and Roussel, M.F. (2008). Post-transcriptional down-regulation of Atoh1/Math1 by bone morphogenic proteins suppresses medulloblastoma development. *Genes Dev.* *22*, 722–727.
- Zhao, Y., Tong, C., and Jiang, J. (2007). Hedgehog regulates smoothed activity by inducing a conformational switch. *Nature* *450*, 252–258.
- Zhao, Z., Lee, R.T.H., Pusapati, G.V., Iyu, A., Rohatgi, R., and Ingham, P.W. (2016). An essential role for Grk2 in Hedgehog signalling downstream of Smoothed. *EMBO Rep.* *17*, 739–752.
- Zheng, J.L., and Gao, W.Q. (2000). Overexpression of Math1 induces robust production of extra hair cells in postnatal rat inner ears. *Nat. Neurosci.* *3*, 580–586.
- Zhou, P., Porcionatto, M., Pilapil, M., Chen, Y., Choi, Y., Talias, K.F., Bikoff, J.B., Hong, E.J., Greenberg, M.E., and Segal, R.A. (2007). Polarized signaling endosomes coordinate BDNF-induced chemotaxis of cerebellar precursors. *Neuron* *55*, 53–68.
- Zhu, Y., Yu, T., Zhang, X.-C., Nagasawa, T., Wu, J.Y., and Rao, Y. (2002). Role of the chemokine SDF-1 as the meningeal attractant for embryonic cerebellar neurons. *Nat. Neurosci.* *5*, 719–720.
- Zhukova, N., Ramaswamy, V., Remke, M., Pfaff, E., Shih, D.J.H., Martin, D.C., Castelo-Branco, P., Baskin, B., Ray, P.N., Bouffet, E., et al. (2013). Subgroup-specific prognostic implications of TP53 mutation in medulloblastoma. *J. Clin. Oncol. Off. J. Am. Soc. Clin. Oncol.* *31*, 2927–2935.

Zhulya, O., Nieuwenhuis, E., Liu, Y.C., Angers, S., and Hui, C. (2015). Ptch2 shares overlapping functions with Ptch1 in Smo regulation and limb development. *Dev. Biol.* 397, 191–202.

Zindy, F., Uziel, T., Ayrault, O., Calabrese, C., Valentine, M., Rehg, J.E., Gilbertson, R.J., Sherr, C.J., and Roussel, M.F. (2007). Genetic alterations in mouse medulloblastomas and generation of tumors de novo from primary cerebellar granule neuron precursors. *Cancer Res.* 67, 2676–2684.

Zine, A., and de Ribaupierre, F. (2002). Notch/Notch ligands and Math1 expression patterns in the organ of Corti of wild-type and Hes1 and Hes5 mutant mice. *Hear. Res.* 170, 22–31.

Zine, A., Aubert, A., Qiu, J., Therianos, S., Guillemot, F., Kageyama, R., and de Ribaupierre, F. (2001). Hes1 and Hes5 activities are required for the normal development of the hair cells in the mammalian inner ear. *J. Neurosci. Off. J. Soc. Neurosci.* 21, 4712–4720.

Zingg, D., Debbache, J., Peña-Hernández, R., Antunes, A.T., Schaefer, S.M., Cheng, P.F., Zimmerli, D., Haeusel, J., Calçada, R.R., Tuncer, E., et al. (2018). EZH2-Mediated Primary Cilium Deconstruction Drives Metastatic Melanoma Formation. *Cancer Cell* 34, 69-84.e14.

Zong, H., Espinosa, J.S., Su, H.H., Muzumdar, M.D., and Luo, L. (2005). Mosaic analysis with double markers in mice. *Cell* 121, 479–492.

Annex

Résumé en Français

Le développement du cervelet nécessite des étapes de prolifération, de migration et de différenciation cellulaires très articulées et finement coordonnées. Ces processus sont bien résumés par l'histogenèse des neurones granulaires, petits neurones glutamatergiques situés dans le cortex cérébelleux qui représentent la plus grande population neuronale de l'ensemble du cerveau.

Au cours du développement post-natal du cervelet, les cellules progénitrices unipotentes qui génèrent les neurones granulaires (appelés progéniteurs des neurones granulaires, PNG) sont situées à la surface du cervelet dans une région appelée couche granulaire externe (CGE).

Dans la CGE, les PNG connaissent une importante phase de prolifération qui atteindra son apogée vers le jour post-natal (P) 6 et s'arrêtera complètement vers la fin de la troisième semaine après la naissance, lorsque tous les PNG auront progressivement quitté le cycle cellulaire. Une fois devenus post-mitotiques, les PNG se déplacent sous les PNG en cours de prolifération et commencent à migrer d'abord tangentiellement, donc parallèlement à la surface du cervelet, et puis radialement vers l'intérieur du cervelet. Cette dernière migration radiale amènera les PNG à leur destination finale dans le cortex cérébelleux, la couche granulaire interne (CGI), où ils achèveront leur maturation en neurones granulaires.

La prolifération des PNG dans la CGE est activée par le morphogène Sonic Hedgehog (Shh), qui est sécrété par les cellules de Purkinje, un autre type de neurones cérébelleux situés sous la CGE. La transduction du signal Shh conduit à l'expression de gènes pro-prolifératifs tels que *Mycn* ou *Ccdn1* et *Ccdn2* qui permettent à la cellule d'entrer dans le cycle cellulaire.

La transduction du signal Shh a lieu à travers une structure cellulaire dédiée, le cil primaire. Le cil principal est une structure semblable à une antenne qui dépasse de la cellule; il est constitué d'un axonème de microtubules qui se forme à partir d'un corps basal qui n'est autre que le centriole maternel centrosome. L'axonème est ensuite entouré d'une partie spécialisée de la membrane plasmique appelée membrane ciliaire.

Les PNG ont un cil primaire et, comme preuve de son importance, diverses études ont montré l'impossibilité de former un cil primaire lorsque, par exemple, des gènes essentiels à la ciliogenèse sont supprimés, empêchant les PNG de transduire Shh et de proliférer en conséquence. Une observation très intéressante est que le cil primaire semble être

définitivement absorbé lorsque les PNG se différencient. Ainsi, la présence d'un cil primaire apparaît comme un phénomène fortement régulé lors du développement des neurones granulaires.

Enfin, il est important de noter que la prolifération dérégulée des PNG provoquée par une signalisation Shh activée de manière aberrante peut conduire à la formation d'une tumeur cérébrale agressive appelé Shh-médulloblastome (Shh-MB) qui touche principalement les enfants. Les thérapies actuelles, qui consistent principalement en une résection chirurgicale de la tumeur, suivie d'une combinaison de radiothérapie et de chimiothérapie, permettent à plus de 70% des patients de survivre, mais au prix de dommages collatéraux très graves qui réduisent considérablement leur qualité de vie. Par conséquent, la recherche de nouvelles thérapies ciblées visant à éliminer les cellules cancéreuses et à réduire la morbidité envers les tissus sains est un objectif extrêmement important.

À partir de toutes ces considérations, il est très intéressant et important d'étudier la nature des mécanismes cellulaires et moléculaires qui régulent l'équilibre entre prolifération et différenciation des PNG. Puisque le cil principal est si important pour la prolifération des PNG (mais aussi des cellules Shh-MB) en réponse à la signalisation Shh, notre objectif est de comprendre comment la présence et les fonctions de cet organelle cellulaire sont régulées pendant le développement de neurones granulaires.

Un régulateur essentiel pour la formation et l'expansion des PNG est le facteur de transcription proneural de type basique hélice-boucle-hélice Atoh1.

Au cours de la période postnatale, Atoh1 est exprimé exclusivement dans les PNG en prolifération active dans la CGE, tandis que son expression est inhibée lorsque ces cellules quittent le cycle cellulaire.

De plus, Atoh1 est souvent surexprimé dans les Shh-MB, où son activité est essentielle à la formation et à l'expansion de cette tumeur. Plusieurs publications ont montré que l'une des fonctions clés d'Atoh1 dans les PNG de la CGE est de maintenir ces cellules dans un état compétent à Shh. En d'autres termes, l'expression (ou la surexpression) de Atoh1 dans les PNG ne favorise pas la prolifération *per se*, mais permet aux cellules de répondre fortement à Shh, inhibant ou retardant efficacement leur différenciation.

Les mécanismes contrôlés par Atoh1 pour orchestrer cet état de compétence à Shh dans les PNG sont toutefois peu connus à ce jour.

Etant donné qu'Atoh1 et le cil primaire ne sont présents que sur les PNG en prolifération active et que ces cellules ont besoin des ces deux composants pour la transduction du signal de Shh, nous nous sommes demandé s'il existait une relation possible entre Atoh1 et le cil primaire.

De ce fait, avec notre travail, nous montrons que l'expression de Atoh1 est remarquablement corrélée à la présence du cil primaire dans les PNG, les deux étant limités aux progéniteurs proliférant dans la CGE.

En utilisant l'électroporation *in vivo*, des lignées de souris transgéniques et des cultures primaires de PNG transduites par lentivirus, nous montrons que la perte d'Atoh1 par les PNG entraîne une diminution de la ciliogenèse et une activation réduite des gènes cibles du Shh. En revanche, la surexpression de Atoh1 dans les PNG *in vitro* et *in vivo* augmente la fraction de PNG ciliée. Il est important de noter que la réduction de la ciliogenèse observée après la perte de Atoh1 est un événement qui se produit avant d'observer une diminution significatif de la prolifération des PNG. Cela indique que la rétraction des cils ne se produit pas à la suite d'une sortie prématurée du cycle cellulaire.

Inversement, la surexpression de Atoh1 *in vitro* et *in vivo* maintient de manière aberrante les cils primaires sur les PNG, qui restent sensibles à Shh et retardent leur différenciation.

En particulier, la suppression des cils primaires des PNG *in vivo* par l'inactivation génétique de gènes impliqués dans la ciliogenèse (par exemple, *Kif3a* ou *Ift88*) empêche le maintien des PNG en prolifération par la surexpression de Atoh1. Ce fait indique qu'Atoh1 favorise l'expansion des PNG en maintenant la présence du cil primaire et préservant ainsi leur capacité à répondre aux stimuli mitogéniques de Shh. En fait, la surexpression de Atoh1 ne favorise pas seulement le maintien des cils primaires sur les PNG, mais également ses fonctions de signalisation, comme indiqué par une réponse transcriptionnelle accrue à Shh et une plus grande accumulation de composants de la voie de Shh (par exemple Smoothened) sur le cil.

La formation d'un cil primaire est un processus complexe qui nécessite le recrutement pondéré de divers composants (protéines et vésicules intracellulaires) au niveau du corps basal et la mise en place d'un transport intraflagellaire qui déplace les protéines ciliaires de la base du cil à la pointe et inversement. Les satellites centriolaires (SC) jouent un rôle essentiel dans tous ces processus. Les SC sont de grands complexes protéiques, assemblés sur une protéine d'échafaudage appelée Pericentriolar material 1 (Pcm1), qui orbite autour du centrosome attaché au réseau de microtubules par des dynéines. La destruction ou la dispersion dans le cytoplasme du SC dans diverses lignées cellulaires, mais également dans les PNG, empêche les

cellules de former un cil primaire. Cette perte d'organisation des SC autour du centrosome peut être obtenue en perdant des composants essentiels à leur stabilité ou à leur localisation.

Grâce à des expériences de microscopie, nous avons constaté que la présence des SC, bien assemblés autour du centrosome, est très fortement corrélée à l'expression de *Atoh1* dans les PNG de la CGE. En effet, l'inactivation génique d'*Atoh1* dans les PNG *in vitro* ne provoque pas seulement des défauts de ciliogenèse, mais provoque également la dispersion des SC dans le cytoplasme. Nous avons donc émis l'hypothèse que *Atoh1* pourrait contrôler la ciliogenèse chez les PNG en régulant la bonne intégrité ou la localisation des SC.

Dans le but de rechercher des cibles transcriptionnelles potentielles d'*Atoh1* capable d'expliquer ce phénotype au niveau des SC, nous avons croisé des données publiées d'expression génique du cervelet de souris knock-out pour *Atoh1* avec des données de ChIP-seq (Chromatine immunoprécipitation-sequencing) d'*Atoh1* et avec une liste de gènes connus pour être impliqués dans la régulation des SC. Parmi les gènes résultant de cette analyse, nous avons trouvé Centrosomal protein of 131 kDa (*Cep131*), qui est un composant essentiel des SC.

Nous avons donc procédé à la validation de *Cep131* en tant que cible transcriptionnelle réelle de *Atoh1*. Les données d'expression géniques et protéiques issues de la perte ou la surexpression d'*Atoh1* combinées à des essais de gène rapporteur et des expériences d'immunoprécipitation de la chromatine montrent que *Cep131* est bien une cible d'*Atoh1* dans les PNG. En particulier, *Atoh1* se lie à des séquences régulatrices situées à l'extrémité 3' du locus génomique *Cep131*, à partir duquel il est capable de trans-activer l'expression de *Cep131*. Fait très important, l'extinction génique de *Cep131* provoque la dispersion des SC dans les PNG et empêche la formation d'un cil primaire *in vivo* et *in vitro*, en récapitulant les phénotypes observés à la suite de la perte de *Atoh1*.

De plus, l'expression ectopique de *Cep131* dans les PNG, dans lesquels *Atoh1* a été inactivé, rétablit non seulement la position correcte des SC, mais également, par conséquent, la capacité de reformer un cil primaire *in vitro* et *in vivo*.

Ces données indiquent que *Atoh1* régule la ciliogenèse dans les PNG à travers l'expression de *Cep131*, ce qui permet la formation et le fonctionnement correct de SC.

Fait intéressant, nous démontrons en outre que cette voie *Atoh1*-SC-cil primaire-*Shh* qui contrôle la prolifération des PNG est également conservée dans le contexte des *Shh*-MB.

Ces données révèlent un mécanisme par lequel la ciliogenèse est régulée dans des progéniteurs de neurones, offrant de nouvelles informations sur le processus complexe de la neurogenèse cérébelleuse et de la pathogenèse de *Shh*-MB.

Titre : Contrôle de la ciliogenèse des progéniteurs des neurones du cervelet

Mots clés : Cervelet, Médulloblastome, Atoh1, Cil Primaire, Cep131, Sonic Hedgehog

Résumé : Pendant le développement du cervelet, les progéniteurs des neurones granulaires (PNG) nécessitent la présence du cil primaire pour proliférer en réponse à Sonic Hedgehog (SHH). En effet, la prolifération dérégulée des PNGs peut conduire à la formation d'une tumeur pédiatrique maligne appelée SHH-médulloblastome (MB), de ce fait comprendre comment le cil primaire est régulé dans les PNGs est crucial.

Nous montrons que le facteur de transcription Atoh1 contrôle la présence du cil primaire dans les PNGs *in vitro* et *in vivo*. En particulier, la suppression du cil primaire par l'inactivation génétique de gènes impliqués dans la ciliogenèse (par exemple, *Kif3a* ou *Ift88*) empêche Atoh1 de maintenir les PNGs en prolifération, ce qui indique qu'Atoh1 favorise l'expansion des PNGs en maintenant la présence du cil primaire. D'un point de vue moléculaire, Atoh1 contrôle la formation du cil primaire en régulant le bon positionnement peri-centrosomal des satellites centriolaires (SC), complexes protéiques essentiels

pour la ciliogenèse. L'inactivation de Atoh1 dans les PNGs perturbe en effet la distribution subcellulaire des SCs, altérant ainsi inévitablement la ciliogenèse. Cette nouvelle fonction de Atoh1 est gouvernée par la régulation transcriptionnelle directe d'un composant clé des SCs, Cep131. L'expression ectopique de Cep131 dans les PNGs restaure les effets liés à l'inactivation d'Atoh1, rétablissant la localisation correcte du SC et comme conséquence la présence d'un cil primaire.

De plus, nous avons montré que cette voie Atoh1-SC-cil primaire-SHH contrôlant la prolifération des PNGs est également conservée dans le contexte du SHH-MB, où Atoh1 est surexprimée et essentielle pour sa formation et sa maintenance.

Ces données révèlent un mécanisme par lequel la ciliogenèse est régulée dans des progéniteurs de neurones, offrant de nouvelles informations sur la neurogenèse dans le cervelet et sur la pathogenèse du SHH-MB.

Title: Ciliogenesis control mechanisms in cerebellar neuron progenitors

Keywords: Cerebellum, Medulloblastoma, Atoh1, Primary Cilium, Cep131, Sonic Hedgehog

Abstract: Cerebellar granule neuron progenitors (GNPs) require the primary cilium to proliferate in response to Sonic Hedgehog (SHH) during cerebellar development. As aberrant proliferation of GNPs may lead to SHH-type medulloblastoma (SHH-MB), a pediatric brain tumor, understanding which mechanisms control ciliogenesis in GNPs represents a major interest in the field. Here, we show that the proneural bHLH transcription factor Atoh1 controls the presence of primary cilia in GNPs both *in vitro* and *in vivo*, thus maintaining GNPs responsive to the mitogenic effects of SHH. Indeed, loss of primary cilia induced via knockdown of specific ciliary components (e.g. *Kif3a* and *Ift88*) abolishes the ability of Atoh1 to keep GNPs in proliferation *in vivo*. Mechanistically, Atoh1 controls ciliogenesis by regulating the proper peri-centrosomal clustering of centriolar satellites (CS), large multiprotein complexes working as essential machineries for ciliogenesis.

Knockdown of *Atoh1* in GNPs perturbs CS subcellular distribution, leading to impairment of ciliogenesis. Luciferase reporter assays and chromatin immunoprecipitation experiments indicate that Atoh1 can directly regulate the expression of Cep131, a key CS core component. Importantly, ectopic expression of Cep131 in GNPs depleted of Atoh1, is sufficient to restore proper CS localization and consequent primary cilia formation, indicating that the Atoh1-Cep131-CS axis is responsible for ciliogenesis in GNPs.

In addition, we further demonstrated that these functions of Atoh1 are also conserved in the context of SHH-MB, where Atoh1 is typically overexpressed and acts as a lineage-dependent transcription factor. These data reveal a mechanism whereby ciliogenesis is regulated in neuron progenitors providing novel insights into cerebellar neurogenesis and pathogenesis of SHH-MB.

